frontiers | Research Topics

Novel molecular mechanisms and clinical strategies in solid tumor recurrence and metastasis: From bench to bedside

Edited by
Zheng Wang, Yanfeng Liu, Hangcheng Fu
and Yonglong Zhang

Published in
Frontiers in Medicine
Frontiers in Oncology

ISSN 1664-8714
ISBN 978-2-8325-4506-5
DOI 10.3389/978-2-8325-4506-5

About Frontiers

Frontiers is more than just an open access publisher of scholarly articles: it is a pioneering approach to the world of academia, radically improving the way scholarly research is managed. The grand vision of Frontiers is a world where all people have an equal opportunity to seek, share and generate knowledge. Frontiers provides immediate and permanent online open access to all its publications, but this alone is not enough to realize our grand goals.

Frontiers journal series

The Frontiers journal series is a multi-tier and interdisciplinary set of open-access, online journals, promising a paradigm shift from the current review, selection and dissemination processes in academic publishing. All Frontiers journals are driven by researchers for researchers; therefore, they constitute a service to the scholarly community. At the same time, the *Frontiers journal series* operates on a revolutionary invention, the tiered publishing system, initially addressing specific communities of scholars, and gradually climbing up to broader public understanding, thus serving the interests of the lay society, too.

Dedication to quality

Each Frontiers article is a landmark of the highest quality, thanks to genuinely collaborative interactions between authors and review editors, who include some of the world's best academicians. Research must be certified by peers before entering a stream of knowledge that may eventually reach the public - and shape society; therefore, Frontiers only applies the most rigorous and unbiased reviews. Frontiers revolutionizes research publishing by freely delivering the most outstanding research, evaluated with no bias from both the academic and social point of view. By applying the most advanced information technologies, Frontiers is catapulting scholarly publishing into a new generation.

What are Frontiers Research Topics?

Frontiers Research Topics are very popular trademarks of the *Frontiers journals series*: they are collections of at least ten articles, all centered on a particular subject. With their unique mix of varied contributions from Original Research to Review Articles, Frontiers Research Topics unify the most influential researchers, the latest key findings and historical advances in a hot research area.

Find out more on how to host your own Frontiers Research Topic or contribute to one as an author by contacting the Frontiers editorial office: frontiersin.org/about/contact

Novel molecular mechanisms and clinical strategies in solid tumor recurrence and metastasis: From bench to bedside

Topic editors

Zheng Wang — Shanghai Jiao Tong University, China
Yanfeng Liu — Shanghai Jiao Tong University, China
Hangcheng Fu — University of Louisville, United States
Yonglong Zhang — Shanghai Jiao Tong University, China

Citation

Wang, Z., Liu, Y., Fu, H., Zhang, Y., eds. (2024). *Novel molecular mechanisms and clinical strategies in solid tumor recurrence and metastasis: From bench to bedside*. Lausanne: Frontiers Media SA. doi: 10.3389/978-2-8325-4506-5

Table of contents

frontiers | Frontiers in Medicine

TYPE Editorial
PUBLISHED 13 February 2024
DOI 10.3389/fmed.2024.1364666

OPEN ACCESS

EDITED AND REVIEWED BY
Alice Chen,
Consultant, Potomac, MD, United States

*CORRESPONDENCE
Hangcheng Fu
✉ fuhangcheng.fdt@hotmail.com

RECEIVED 02 January 2024
ACCEPTED 30 January 2024
PUBLISHED 13 February 2024

CITATION
Fu H (2024) Editorial: Novel molecular mechanisms and clinical strategies in solid tumor recurrence and metastasis: from bench to bedside. *Front. Med.* 11:1364666. doi: 10.3389/fmed.2024.1364666

Editorial: Novel molecular mechanisms and clinical strategies in solid tumor recurrence and metastasis: from bench to bedside

Hangcheng Fu*

Department of Urology, University of Louisville School of Medicine, Louisville, KY, United States

KEYWORDS

renal cell carcinoma, solid tumor, oligometastase, breast cancer, molecular marker

Editorial on the Research Topic
Novel molecular mechanisms and clinical strategies in solid tumor recurrence and metastasis: from bench to bedside

In the realm of oncology, the pursuit of understanding and treating various forms of cancer continually evolves, bringing to light novel insights and therapeutic strategies. Recent studies in the fields of breast cancer, renal cell carcinoma (RCC), and small cell lung cancer (SCLC) exemplify this progress, highlighting the importance of interdisciplinary research and personalized treatment approaches.

Deciphering molecular mechanisms of acute kidney injury in RCC

The study by Wang et al., "*Identification of AKI Signatures and Classification Patterns in ccRCC Based on Machine Learning*," ventures into the intricate relationship between Acute Kidney Injury (AKI) and clear cell renal cell carcinoma (ccRCC). Previous study revealed that compromised CKD after nephrectomy was associated with worsening overall survival however the group of patients are of great heterogeneity (1). Utilizing public databases and machine learning algorithms, the research identifies seven novel AKI biomarkers. These biomarkers not only aid in early AKI detection but also distinguish between two subtypes of ccRCC with different prognoses and immune characteristics. This study underscores the power of machine learning in unraveling complex biological relationships, offering a significant leap in personalized cancer treatment. It can help us to better understanding the mechanism behind the renal cell carcinoma pathology and AKI induced CKD.

Advancing SCLC treatment with combined therapies in solid tumors

In the realm of lung cancer, the study "*Efficacy and Safety of Immune Checkpoint Inhibitors Combined with Chemotherapy as First-line Treatment for Extensive-stage Small Cell Lung Cancer*" is a meta-analysis based on mixed-effect models (Zheng et al.). It shows that combining immune checkpoint inhibitors (ICIs) with chemotherapy significantly

prolongs survival in patients with extensive-stage SCLC. This combination, however, does not markedly improve the objective response rate or disease control rate and raises the incidence of immune-related adverse events. These findings spotlight the need for a nuanced understanding of treatment benefits vs. risks, informing clinical decision-making in SCLC management.

Radiotherapy in oligometastases: a paradigm shift

Kao et al. shifts the focus to a less explored area in cancer treatment—oligometastases. They defined <5 metastatic lesions in the radiology finding as oligometastases. The study reports encouraging outcomes from comprehensive involved site radiotherapy, often in combination with systemic therapy. With a significant proportion of patients achieving long-term remissions and high rates of local control, the study advocates for a potential paradigm shift in treating metastatic cancers. It also highlights the predominance of distant failures, suggesting a tailored approach to managing minimal residual disease.

Breast cancer: a molecular culprit

In breast cancer research, the study "*Association Between Endocrine Therapy and Cognitive Decline in Breast Cancer Based on Propensity Score Matching*" by Yin et al. addresses a crucial aspect of cancer treatment—the balance between therapeutic efficacy and side effects. The research reveals a concerning association between prolonged endocrine therapy in breast cancer patients and cognitive impairment. By utilizing propensity score matching, the study ensures a rigorous evaluation of this relationship, adding a crucial dimension to patient care in breast cancer treatment.

In addition, Lian et al. delves into the molecular intricacies of breast cancer. The over-expression of SLC31A1, a gene associated with copper transport and cuproptosis, is linked to poor prognosis and increased immune cell infiltration in breast cancer. This study not only opens new avenues in understanding breast cancer progression but also posits SLC31A1 as a potential target for novel therapeutic strategies. Miao et al. highlights the role of the DYNLT1 gene in breast cancer. This study demonstrates that DYNLT1 is overexpressed in breast cancer and is associated with poor relapse-free survival. It further explores the mechanisms by which DYNLT1 influences tumor cell proliferation and metastasis, offering new insights into potential targets for therapy and prognostication in breast cancer.

Future perspectives

These studies collectively signify a monumental shift in cancer research. They emphasize the importance of integrating findings from molecular biology, machine learning, and epidemiology into clinical practice. The challenge ahead lies in translating these insights into tangible benefits for patients, balancing treatment efficacy with quality of life.

Moreover, these studies underscore the importance of considering the holistic impact of cancer treatment. From cognitive effects in breast cancer patients undergoing endocrine therapy to the challenges of managing adverse events in SCLC treatment, a patient-centric approach is paramount.

As cancer research continues to advance, a multidisciplinary approach becomes increasingly vital. The integration of data science, molecular biology, and patient-centered clinical research holds the key to unraveling the complexities of cancer. The future of oncology lies in the ability to personalize treatment, minimize side effects, and improve overall patient outcomes.

Author contributions

HF: Writing—original draft, Writing—review & editing.

Funding

The author(s) declare that no financial support was received for the research, authorship, and/or publication of this article.

Conflict of interest

The author declares that the research was conducted in the absence of any commercial or financial relationships that could be construed as a potential conflict of interest.

Publisher's note

References

1. Wu J, Suk-Ouichai C, Dong W, Antonio EC, Derweesh IH, Lane BR, et al. Analysis of survival for patients with chronic kidney disease primarily related to renal cancer surgery. *BJU Int*. (2018) 121:93–100. doi: 10.1111/bju.13994

frontiers | Frontiers in Medicine

TYPE Original Research
PUBLISHED 26 January 2023
DOI 10.3389/fmed.2023.1132287

OPEN ACCESS

EDITED BY
Zheng Wang,
Shanghai Jiao Tong University, China

REVIEWED BY
Hangcheng Fu,
University of Louisville, United States
Renhong Huang,
Shanghai Jiao Tong University, China

*CORRESPONDENCE
Jingjing Wu
✉ jswjj520@163.com
Hongfeng Chen
✉ fenhong674chen@yeah.net

†These authors have contributed equally to this work

SPECIALTY SECTION
This article was submitted to Precision Medicine, a section of the journal Frontiers in Medicine

RECEIVED 27 December 2022
ACCEPTED 13 January 2023
PUBLISHED 26 January 2023

CITATION
Yin Y, Jin L, Chu M, Zhou Y, Tu S, Cheng Y, Ye M, Wu J and Chen H (2023) Association between endocrine therapy and cognitive decline in breast cancer based on propensity score matching.
Front. Med. 10:1132287.
doi: 10.3389/fmed.2023.1132287

Association between endocrine therapy and cognitive decline in breast cancer based on propensity score matching

Yulian Yin†, Lan Jin†, Meiling Chu†, Yue Zhou, Siyuan Tu, Yifan Cheng, Meina Ye, Jingjing Wu* and Hongfeng Chen*

Longhua Hospital Shanghai University of Traditional Chinese Medicine, Shanghai, China

Purpose: To study the *status quo* of the cognitive function of the breast cancer patients with (who went through) the endocrine therapy by the epidemiological investigation, analyze the key factor of the cognition impairment and explore the impact of the endocrine therapy time on the cognition decline after using Propensity Score Matching to balance the covariates.

Methods: In this study, the epidemiological questionnaire information was collected from 226 female breast cancer endocrine treatment patients who visited the Breast Clinic of Longhua Hospital Affiliated to Shanghai University of Chinese Medicine from November 2020 to February 2022, and the results of the overall cognitive function, the function test of each cognitive domain, the patient's self-cognition, quality of life, and emotional status evaluation of the patients. In this study, according to the principle of random matching, the nearest matching method with a matching tolerance of 0.2 and a matching ratio of 1:2 was used for orientation score matching. After the covariant such as age, BMI, and duration of education were balanced, the effects of the duration of endocrine therapy on the overall cognitive function and the functions of each cognitive domain were analyzed.

Results: In 226 cases of female breast cancer patients (who went through) the endocrine therapy, the propensity score matching was performed, ultimately, 99 were ruled out, successful matched ones were 49 of the cognition-decline group and 78 of the standard group. With age, education time, BMI and other covariates balanced, the endocrine therapy duration was the risk factor of the cognition impairment ($P < 0.05$, OR = 1.296, 95% CI = 1.008–1.665), with the extension of endocrine treatment time, there was a rising risk of the cognition impairment (LLA statistic = 5.872, $P < 0.05$). The cognitive domain scores in the cognition-decline group were lower than the standard group ($P < 0.05$), but there was a difference in self-report cognition.

Conclusion: The endocrine therapy duration was the risk factor for the cognition impairment of the breast cancer patients, and with prolonged endocrine treatment, there was a rising (an increasing) risk for the cognition impairment.

KEYWORDS

breast cancer, endocrine therapy, cognitive function, association, propensity score matching

Introduction

According to the statistics of the International Agency for Research on Cancer, in 2020, female breast cancer ranked first in the incidence of malignant tumors in the world, accounting for 11.7% of all new cases of malignant tumors (1). There were 416,371 new cases of breast cancer in China, accounting for 19.9% of the total number of new female cancers, and ranking first in the incidence of female cancers in China. With the increasing level of diagnosis and treatment of breast cancer, the five-year survival rate has reached 90% (2). About 70% of patients with breast cancer are hormone receptor positive (3). Endocrine therapy is a special and long-term treatment that needs to be received by hormone receptor positive breast cancer patients. To receive endocrine therapy for 5–10 years is currently recognized as the first-line plan to prevent tumor recurrence and prolong the survival time of patients. In view of the high incidence and relatively high survival rate of breast cancer, the quality of life of patients has become a close concern. According to the statistics of some scholars, the common symptoms of breast cancer patients receiving endocrine therapy include climacteric symptoms, bone-related adverse events, lymphedema, fatigue, depression, sleep disorders and cognitive impairment, among which the related research on cognitive impairment is rare (4). Endocrine therapy for breast cancer is an anti-tumor regimen targeting the resistance to estrogen, which is able to protect the nervous system and plays an important role in improving the cognitive function and memory ability of women (5). All of the above have suggested the possibility of cognitive impairment in breast cancer patients receiving endocrine therapy, but the relationship between the two is still unclear (6). In this study, we used the propensity score matching method to balance various variables that differ between the cognitive decline and the normal in endocrine patients with breast cancer, making the duration of endocrine treatment the only test variable to assess the impact of the duration of endocrine treatment on cognitive function.

Study design

This study is a prospective interventional single-center study. The subjects of this study were breast cancer patients who were treated in the first department of breast cancer clinic of Longhua Hospital affiliated to Shanghai University of Traditional Chinese Medicine from November 2020 to February 2022. A schematic diagram of the research flowchart is shown in **Figure 1**.

The Medical Ethics Committee of Longhua Hospital affiliated to Shanghai University of Traditional Chinese Medicine approved this research. Written informed consent was obtained from all individual participants included in the study. The clinical trial registration number is ChiCTR2200057785.

Participant

All participants met the 2020 Guidelines for Diagnosis and Treatment of Breast Cancer by the Chinese Society of Clinical Oncology (CSCO) (7), and were clearly diagnosed with breast cancer based on basic and molecular pathology. Inclusion criteria: (1) Patients were diagnosed with breast cancer, and the immunohistochemical examination of postoperative pathology showed positive ER and/or PR. (2) Endocrine therapy lasting for three months or more, including selective hormone receptor modulators, and/or aromatase inhibitors, and/or ovarian castration. (3) Female patients aged 30–55 years old (including 30 and 55 years old). Whisenant et al. (4) have enough visual, auditory, and cultural degree, can read and write simple sentences. (4) Individual oral communication can be conducted and blood tests can be completed with coordination. (5) Understand and voluntarily participate in project research and sign informed consent form. Exclusion criteria: (1) Patients were under treatment for breast cancer recurrence and/or metastasis. (2) Selective hormone receptor modulators, and/or aromatase inhibitors, and/or ovarian castration have been used before breast cancer. (3) The cerebrovascular diseases or neurodegenerative diseases that affect cognitive function, such as vascular dementia, Alzheimer's disease, and frontotemporal dementia, are confirmed. (4) Anxiety, depression, schizophrenia and other mental disorders were confirmed by the specialized hospital.

Materials and methods

Observation indexes

1) Overall cognitive function scale: Montreal Cognitive Assessment (MoCA).

2) Sub-cognitive domain function scale(memory, language ability, attention, visual space and execution function):

① Memory test scale: Auditory verb learn test-Huashan version (AVLT-H).

② Language ability test scale: Verbal fluency test (VFT).

③ Attention test scale: Digital span test (DST).

④ Visual space and executive ability test scale: Trail Making Test (TMT-A, TMT-B) and clock-drawing test (CDT).

3) Self-rating cognitive scale: Functional Assessment of Cancer Therapy-Cognitive Function (FACT-cog) (8). The FACT-cog scale consists of four factor scales, namely, perceived cognitive impairments (CogPCI), perceived cognitive abilities (CogPCA), and others' comments. Co goal) and the impact of cognitive changes on quality of life (CogQOL).

4) Examination indicators: Serum Estradiol (E2) and Follicle-stimulating Hormone (FSH); Test time point: the test was performed on the third day of the first menstrual cycle of patients without menopause before or after the investigation; Patients who have already stopped menstruating are tested before investigation or within 1 week after investigation.

Correction and matching of samples

Previously, we completed the overall cognitive function evaluation of 226 patients using convenient sampling. The score of MoCA scale <26 was judged as overall cognitive function decline, and a total of 75 patients (33.19%) were included. We compared the basic information of the subjects with normal cognitive function (normal group) and those with decreased overall cognitive function (decline group) in the overall sample, and found that there were statistical differences in age, educational duration and BMI of the two groups of people, as shown in **Appendix Table 1**, which might mask the effect of the duration of endocrine therapy on cognitive function.

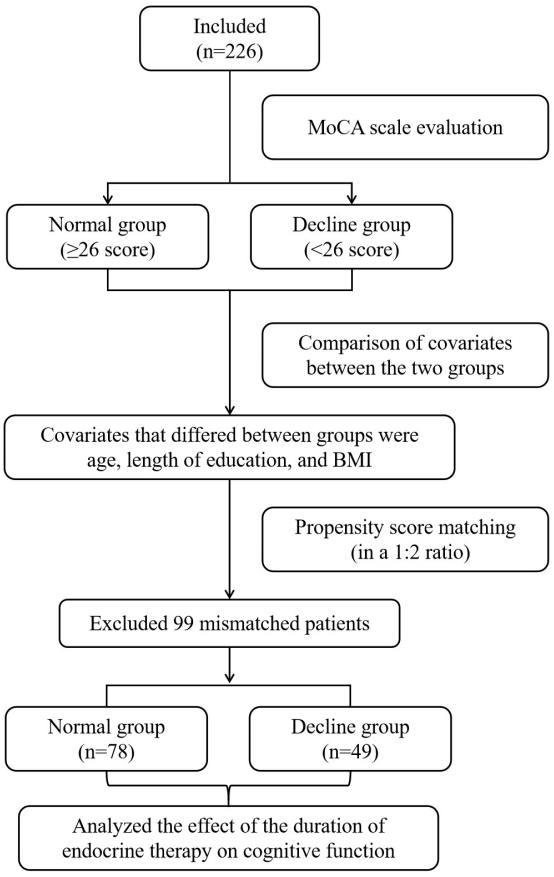

FIGURE 1
Schematic diagram of the research flowchart.

Therefore, we included the patient's age, BMI, and educational duration in the covariates for tendency score matching, and used PSM extension of SPSS 22.0 software for tendency score matching, so that the factors of uneven distribution between groups were balanced.

In this study, based on the principle of random matching, the closest matching method with the matching tolerance (Caliper) of 0.2 and the matching ratio of 1:2 between two groups of samples was used for orientation score matching. After 99 mismatched cases were excluded, 78 cases in the normal group and 49 cases in the decline group were successfully matched. The statistical value of L1 measure after matching is 0.724, which is less than 0.781 before matching. There is no variable | d | d| >0.25, which indicates that the matching is good and all the matched variables are balanced. The absolute values of the standard differences in age, BMI and educational duration after matching decreased from 48.6, 37.7, and 103.8% before matching to 2.2, 2.4, and 3.1% after matching, respectively, all less than 10%, suggesting that the inter-group balance was good after matching, as shown in **Figure 2**.

Quality control

The investigator strictly followed the inclusion and exclusion criteria of clinical trial protocol to select the appropriate subjects and conducted the investigation and data entry as required. To reduce the random error caused by different researchers in the scale investigation, all scale investigations for subjects were conducted by the investigating doctor himself/herself, and the data of subjects were sequenced and numbered according to the time sequence of completing the investigation. Other researchers regularly examined the subject's data, checked whether the case report form was correctly filled, whether there were omissions, signatures, and dates, and so on, and fed back the problems to the investigating doctor for correction after they found them.

Data management

Within 1 week after the completion of the investigation, all the data in the case report form were entered into the Excel table relevant to this study, and 20% of the data were extracted for manual verification again. Any error entered was corrected based on the original data.

Statistical methods

Statistical analysis was performed using SPSS 22.0 software. All tests were bilateral, and the test level was $\alpha = 0.05$. The level of statistical significance was set at $P < 0.05$. Descriptive statistics were performed for each variable. First, normality test was performed for measurement data. The results were expressed as mean standard deviation ($\bar{x}$ s) for normal distribution, such as age and BMI. If the data did not follow the normal distribution, the results were expressed as median and quartile $M(P_{25}, P_{75})$, such as menarche age. Independent sample t test was used to test the difference between the two groups of variables that were in accordance with the normal distribution and with uniform variance, such as the age of the two groups after matching, and Wilcoxon rank sum test was used for the rest, such as the duration of endocrine treatment in the two groups. The enumeration data or classified variables were expressed as frequency and percentage. For example, the number of patients with or without family history of cancer and the classification of endocrine protocol were included. The difference between the two groups of variables was examined by χ^2 test or Fisher exact probability method.

The OR value and 95% confidence interval of the risk relationship between the duration of endocrine treatment and the cognitive decline of endocrine treatment patients were calculated by conditional logistic regression analysis. The Linear-by-Linear Association test (LLA) (9) was used to analyze the trend relationship between the duration of endocrine therapy and the risk of cognitive decline.

Results

Patient characteristics

After matching, the covariates such as age, education duration, BMI, tumor family history, basic disease, and medication history, pregnancy duration, lactation duration, menopausal status, menarche age, tumor treatment (chemotherapy, radiotherapy, targeted therapy, endocrine medication type), emotional state (SAS and SDS), quality of life, and TCM symptom score of the normal group and the declined group were balanced and comparable, as shown in Appendix Table 1.

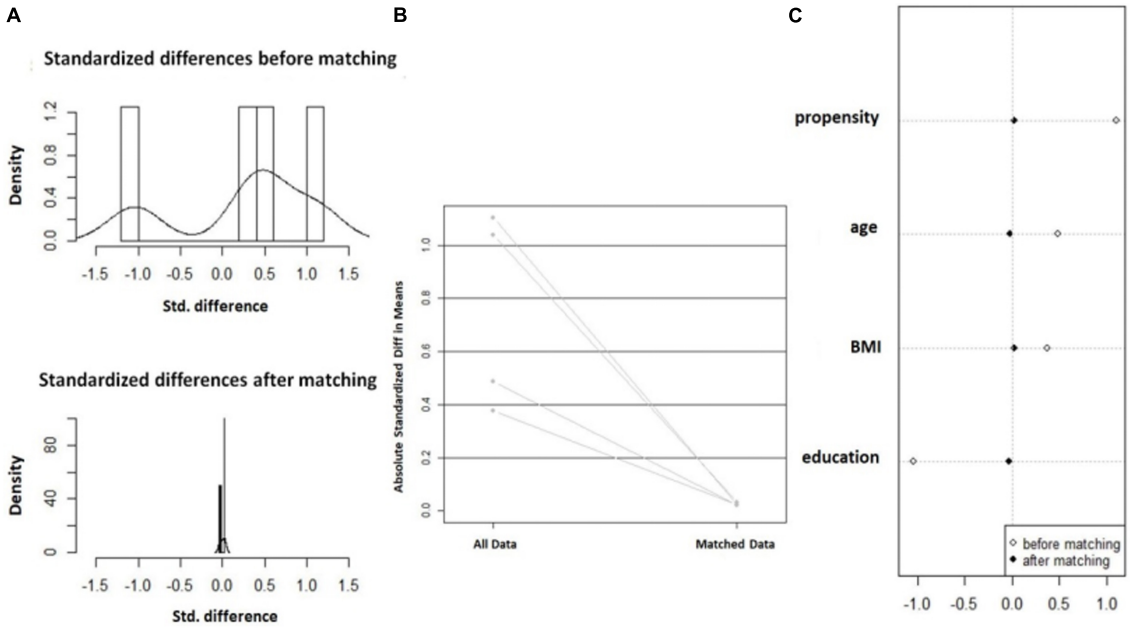

FIGURE 2
Balance change diagram before and after orientation score matching. **(A)** Histogram of SD; **(B)** Standardized mean difference line diagram; and **(C)** Scatter plot of single variable SD.

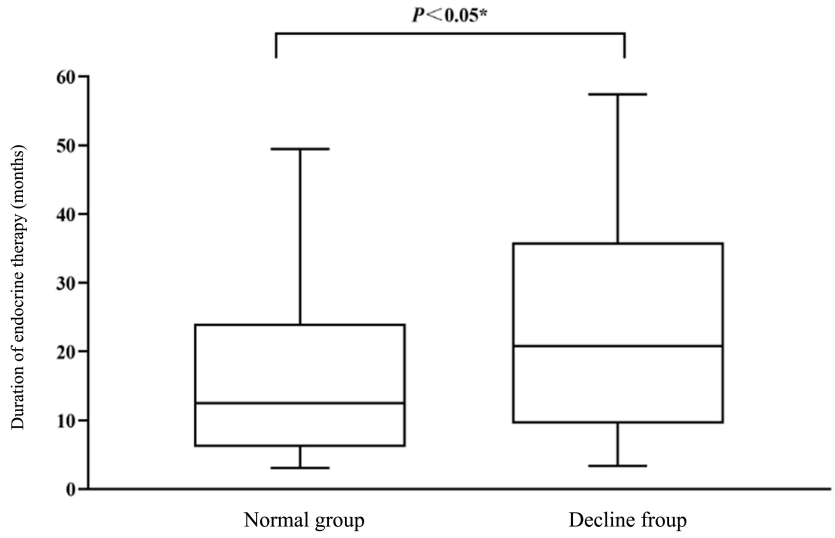

FIGURE 3
Comparison of endocrine therapy duration (months) between normal group and declining group.

Correlation between duration of endocrine therapy and overall cognitive decline

After normality test, the duration of endocrine treatment did not follow the normal distribution. The duration of endocrine treatment in the descending group was 20.77(9.52, 35.88) months, which was significantly higher than that of 12.5(6.09, 24.07) months in the normal group. The statistical value $z = -2.434$ and $P = 0.015 < 0.05$ by non-parametric test were obtained, and the difference was statistically significant, as shown in Figure 3.

The duration of endocrine treatment was divided into six groups and conditional logistic regression analysis was performed. The negative double likelihood pair value after the formal inclusion of the variable was 87.084, which was less than the negative double likelihood pair value of the invalid model was 91.445, suggesting that the effect of the model with the included variable was better than that of the invalid model. Moreover, $\chi^2 = 4.290$ and $P = 0.038$ indicated that the conditional Logistic regression was statistically significant. The results of conditional logistic regression analysis showed that the duration of endocrine treatment was positively correlated with the overall cognitive decline. The duration of endocrine treatment was a risk factor for the overall cognitive

TABLE 1 Comparison of duration of endocrine treatment in normal and decline groups.

Endocrine treatment duration/Month	Normal group, n = 78(%)	Decline group, n = 49(%)
3−6	19(24.36)	6(12.25)
6−12	18(23.08)	10(20.41)
12−24	22(28.21)	12(24.49)
24−36	10(12.82)	9(18.37)
36−48	6(7.69)	7(14.28)
48−60	3(3.84)	5(10.20)
Statistic	Wald $\chi^2 = 4.104$, $P = 0.043$*	
OR(95%CI)	1.296(1.008−1.665)	

*Stands for statistical difference.

decline ($P < 0.05$, OR = 1.296, 95% CI = 1.008−1.665), as shown in Table 1. At the same time, the results of the LLA trend test suggested that the risk of overall cognitive decline increased with the prolongation of endocrine therapy (LLA statistic = 5.872, $P = 0.015 < 0.05$).

Comparison of sub-cognitive domain functions (memory, language ability, attention, visual space, and executive function) between the two groups

As shown in Table 2, the scores of short time, short delay memory, long delay memory, and memory and recognition after cue presentation in the decline group were lower than those of the normal group. In the language function module, we used the 60−s word fluency test, which was based on the 15−s cutoff score. The word output and total score of patients in the decline group were lower than those in the normal group for 15 s. In the DST of reactive attention level, the anteroposterior, inversion and total scores of the decline group were lower than those of the normal group. In the Visual Space and Executive Function evaluation module, the TMT and CDT test scores were lower in the decline group than in the normal group.

TABLE 2 Comparison of sub-cognitive domain function between normal group and decline group.

	Item	Normal group	Decline group	Statistic	P-value
Memory module; AVLT-H	AVLT short-term memory	21.85 ± 3.26	18.27 ± 3.32	T = −5.987	0.000
	AVLT short delay recall	8(7, 10)	6(5, 8)	Z = −5.245	0.000
	AVLT long delay recall	8(6, 9)	6(5, 8)	Z = −4.843	0.000
	AVLT cued recall	8(7, 10)	6(5, 8)	Z = −4.243	0.000
	AVLT recognition	11(10, 12)	10(9, 11)	Z = −2.801	0.005
language ability; VFT	VFT	20.6 ± 4.54	16.78 ± 3.53	T = −5.021	0.000
	VFT-1st	10(9, 12)	9(8, 10)	Z = −2.357	0.018
	VFT-2nd	5(3, 6)	3(2, 5)	Z = −3.478	0.001
	VFT-3rd	3(1, 4)	2(1, 3)	Z = −2.828	0.005
	VFT-4th	3(2, 3.25)	2(1, 3)	Z = −2.411	0.016
Attention module; DST	Forward Digit Span	12(10, 13)	10(7.5, 12)	Z = −3.691	0.000
	Backward Digit Span	8(6, 10.25)	7.22 ± 2.49	Z = −2.669	0.008
	Total Score	19.5(17, 2.25)	17.04 ± 4.45	Z = −3.568	0.000
Visual space and Executive ability module; TMT-A TMT-B CDT	TMT-A	32.32 ± 8.18	37(31, 42)	Z = −5.245	0.000
	TMT-B	72.5(60, 95.25)	97(72.5, 131.5)	Z = −3.472	0.001
	TMT interference*	40(25.75, 65.25)	62(41, 9)	Z = −2.908	0.004
	CDT	10(8, 10)	7(6.5, 9.5)	Z = −4.591	0.000
Self-rating cognitive module; FACT-cog	CogPCI	59.6 ± 14.28	63(53.5, 69)	Z = −0.513	0.608
	CogPCA	21.53 ± 7.45	22(16, 27)	Z = −0.404	0.686
	CogOth	16(14, 16)	16(14, 16)	Z = −0.501	0.616
	CogQOL	14(11.75, 16)	14(11, 16)	Z = −0.961	0.337
	FACT-cog	109.5 ± 22.16	113(92.5, 123)	Z = −0.528	0.598

*The TMT-B completion time minus the TMT-A completion time is the TMT interference amount.

TABLE 3 Comparison of E_2 (pg/ml) and FSH (IU/L) values between the normal group and the decline group.

	E_2	FSH
Normal group	10.08(6.06, 28.81)	10.36(5.82, 28.79)
Decline group	10.08(10.08, 22.17)	13.58(6.33, 25.02)
Statistic	Z = −0.809, P = 0.418	Z = −0.461, P = 0.645

There was no statistical difference in the subjective evaluation of cognitive function between the two groups.

Comparison of serum estradiol and follicle stimulating hormone levels between the two groups

There was no statistical difference in serum estradiol and follicle-stimulating hormone levels between the normal group and the decline group, as shown in **Table 3**.

Discussion

The concept of tendency scoring was first proposed by statistical experts Rosenbaum and Rubin in 1983 (10), and the theoretical basis and dimension reduction process of tendency scoring were elaborated in detail. It is a powerful tool to deal with the confounding bias in observational studies and has a wide application prospect (11). Among them, Propensity Score Matching (PSM) is the most commonly used one, which matches the individuals with the same or similar propensity scores in the treatment group and the control group in 1:1 or 1:n to make the covariates of the two groups in a balanced state. The processing effect is estimated based on the matched data sets, which has the advantage of ensuring the objectivity of the study (12). Moreover, when the sample size is 200, the relative bias of the propensity score matching is the smallest (13).

Huang et al. (14) used PSM to match the rehabilitation patients after a tibial plateau operation in two groups and concluded that comprehensive rehabilitation treatment with traditional Chinese medicine could improve the rehabilitation efficacy of tibial plateau fracture within six months after the operation. Wang et al. (15) used PSM to balance the inter-group covariates to explore the correlation between serum scandium level and oral cancer risk, and they believed that serum scandium level had a negative correlation with oral cancer risk. PSM is also applied to relevant research on breast cancer. Sun (16) matched the PSM of postmenopausal HR-positive breast cancer patients receiving new adjuvant endocrine therapy with those receiving postoperative adjuvant endocrine therapy, to explore the efficacy and prognosis of postmenopausal HR-positive breast cancer patients receiving new adjuvant endocrine therapy. It was considered that the five-year disease-free survival and total survival of postmenopausal breast cancer patients receiving pre-operative new adjuvant endocrine therapy or post-operative adjuvant endocrine therapy were the same.

In this study, we also used PSM to balance the covariates except for the duration of endocrine therapy to explore the effect of the duration of endocrine therapy on the cognitive function of patients with breast cancer treated by endocrine therapy. We matched the overall cases and found that there was no difference in the self-cognition scores of patients after matching between the two groups with normal or decreased overall cognitive function, and the effects of personal characteristics such as age, educational level, and BMI on the self-cognition of subjects were controlled. The results showed that the duration of endocrine therapy was a risk factor for overall cognitive decline, and with of prolonged endocrine therapy, the risk of overall cognitive decline in breast cancer patients receiving endocrine therapy also increased.

With the changes in clinical practice guidelines for breast cancer, there have been two major changes in endocrine therapy for HR-positive breast cancer patients. First, endocrine drugs are continuously developed and marketed. At first, TAM is the main therapeutic drug, and AIs are later used as the first-line drug for postmenopausal breast cancer patients. The second major change is the extension of treatment time, which ranges from two to three years at first to five to eight years and then to 10 years (17). It is generally believed that extended endocrine therapy can reduce the risk of recurrence and metastasis of breast cancer. At the same time, long-term use of endocrine therapy can cause a series of side effects, such as endometrial lesions, venous thrombosis, and osteoporosis (18, 19), which have been widely reported. At present, some scholars have paid attention to the fact that endocrine therapy may affect the cognitive function of breast cancer patients to a certain extent. Chen et al. (20) focused on detecting the effect of TAM on the executive attention of breast cancer patients and found that patients taking TAM had poorer executive function than patients not taking TAM and healthy people. Liao et al. (21) conducted a case-control trial to explore the association between TAM and Alzheimer's disease. They compared breast cancer patients over 65 years old with AD and breast cancer patients without any dementia-related diseases and analyzed TAM as the main exposure factor. They found that compared with patients who did not use TAM, patients who had used TAM had an OR value of 3.09 for AD. However, the researchers finally believed that the use of TAM might be a survival effect rather than a toxicity effect to increase the risk of AD. Therefore, the relationship between endocrine therapy and cognitive impairment in breast cancer needs further investigation. In our study, breast cancer patients who have received endocrine therapy for five years are taken as the research object. The research results show that the duration of endocrine therapy is a risk factor for cognitive decline. That is to say, the overall cognitive function of patients tends to decrease with the prolongation of endocrine therapy.

The comparison of the overall decreased cognitive function with that of normal patients in each cognitive domain revealed that patients with overall decreased cognitive function had a certain decrease in the ability scores in each cognitive domain, that is, the prolongation of endocrine therapy not only affected the overall cognition of patients but also caused adverse effects on patients in each cognitive domain dimension. For example, patients with decreased overall cognitive function showed decreased memory in all dimensions (short time, short delay, long delay, clues, and recognition memory). For the influence on language function, the result of the original 60−s language function test can be shortened to 15 s, that is, the 15−s language function test can objectively detect the decline in the language function of patients. In the aspect of attention, DST can be directly used to test attention in the clinical process. The attention of patients in the overall cognitive decline group was lower than that in the normal group. However, the median DST of the two groups of patients was higher than the conventional standard 6 points

from the results, suggesting that the cognitive decline of female breast cancer patients aged 30−55 years old receiving endocrine therapy might not be mainly manifested as inattention, or the conventional standard 6 points for people over 60 years old used to evaluate female breast cancer patients aged 30−55 years old might overestimate their attention. From the TMT and CDT test results reflecting visual space and executive ability, the scores of patients in the decline group were lower than those of the normal group in both tests, but the median CDT of the decline group was higher than the conventional 6-point standard, suggesting that for patients with decreased cognitive function, visual space and executive ability should not be taken as the primary impaired cognitive domain.

At the same time, no statistical differences were observed in E_2 and FSH levels between the baseline-consistent groups. This may be related to the low levels of both E_2 and FSH in breast cancer patients after endocrine treatment, while the low levels cannot reflect their effects on cognitive function. It is also possible that the objectively detectable levels of E_2 and FSH in peripheral blood after endocrine treatment cannot reflect the overall situation of sex hormones in patients' bodies, and cannot reflect their effects on cognitive function.

It should be noted that regardless of whether the overall cognitive function of patients is decreased, there is the uncertainty of over-estimation or under-estimation for their cognitive function, and the results of self-evaluation cognition are not consistent with the measured cognition, which may be a major feature of patients with breast cancer treated by endocrine therapy. Therefore, in the clinical process, patients' judgment cannot be used as the standard to make clinical diagnoses and treatment decisions.

Conclusion

To sum up, our results still need a larger cohort dataset and more rigorous research evidence. However, according to the results of this study, prolonged endocrine therapy does have certain adverse effects on cognitive function. Although the current guidelines both in China and abroad advocate extending the duration of endocrine therapy, clinicians need to assess the proportion of risks and benefits in consideration of patients' conditions to make optimal clinical decisions. Meanwhile, some drugs, rehabilitation, and physical therapy may reduce the risk of cognitive decline caused by endocrine therapy, which of course also needs further research.

Data availability statement

The original contributions presented in this study are included in the article/supplementary material, further inquiries can be directed to the corresponding authors.

Ethics statement

The studies involving human participants were reviewed and approved by the Medical Ethics Committee of Longhua Hospital affiliated to Shanghai University of Traditional Chinese Medicine. Written informed consent for participation was not required for this study in accordance with the national legislation and the institutional requirements.

Author contributions

YY and LJ: conceptualization, formal analysis, data curation, and visualization. LJ: writing—original draft. YY and MC: validation, visualization, writing—review and editing. MY: methodology. YZ, ST, and YC: investigation, validation, and data curation. JW and HC: supervision, project administration, and funding acquisition. All authors contributed to the article and approved the submitted version.

Funding

This study was supported by Shanghai Science and Technology Innovation Action Plan (21Y11923000) and Clinical Research Project of Shanghai Municipal Health Committee (20204Y0167).

Conflict of interest

The authors declare that the research was conducted in the absence of any commercial or financial relationships that could be construed as a potential conflict of interest.

Publisher's note

References

1. Sung H, Ferlay J, Siegel R, Laversanne M, Soerjomataram I, Jemal A, et al. Global cancer statistics 2020: GLOBOCAN estimates of incidence and mortality worldwide for 36 cancers in 185 countries. *CA Cancer J Clin.* (2021) 71:209–49. doi: 10.3322/caac.21660

2. Allemani C, Matsuda T, Di Carlo V, Harewood R, Matz M, Nikšić M, et al. Global surveillance of trends in cancer survival 2000-14 (CONCORD-3): analysis of individual records for 37 513 025 patients diagnosed with one of 18 cancers from 322 population-based registries in 71 countries. *Lancet.* (2018) 391:1023–75. doi: 10.1016/S0140-6736(17)33326-3

3. Howlader N, Altekruse S, Li C, Chen V, Clarke C, Ries L, et al. US incidence of breast cancer subtypes defined by joint hormone receptor and HER2 status. *J Natl Cancer Inst.* (2014) 106:dju055. doi: 10.1093/jnci/dju055

4. Whisenant M, Williams L, Mendoza T, Cleeland C, Chen T, Fisch M, et al. Identification of breast cancer survivors with high symptom burden. *Cancer Nurs.* (2022) 45:253–61. doi: 10.1097/NCC.0000000000001019

5. Duarte A, Hrynchak M, Gonçalves I, Quintela T, Santos C. Sex hormone decline and amyloid β synthesis, transport and clearance in the brain. *J Neuroendocrinol.* (2016) 28:2587. doi: 10.1111/jne.12432

6. Biro E, Kahan Z, Kalman J, Rusz O, Pakaski M, Irinyi T, et al. Cognitive functioning and psychological well-being in breast cancer patients on endocrine therapy. *In Vivo.* (2019) 33:1381–92. doi: 10.21873/invivo.11615

7. Guidelines Working Committee of Chinese Society of Clinical Oncology. *Guidelines for diagnosis and treatment of breast cancer: 2020 edition [M]*. Beijing: People's Medical Publishing House (2020).

8. Li J, Gao W, Sun L, Bu Y, Cao F. The reliability and validity of Chinese version of cancer treatment function evaluation-cognitive function scale applied to breast cancer patients. *China J Pract Nurs.* (2015) 31:2554–6.

9. Huo J, Smith B, Giordano S, Reece G, Shih Y. Comparative study of Cochran-Armitage trend test and linear regression in trend analysis of epidemiological rate. *Chin J Epidemiol.* (2017) 38:684–7. doi: 10.1007/s10549-016-3832-x

10. Rosenbaum P, Rubin D. The central role of the propensity score in observational studies for causal effects. *Biometrika.* (1983) 70:41–55.

11. Elze M, Gregson J, Baber U, Williamson E, Sartori S, Mehran R, et al. Comparison of propensity score methods and covariate adjustment: evaluation in 4 cardiovascular studies. *J Am Coll Cardiol.* (2017) 69:345–57.

12. Badhiwala J, Karmur B, Wilson J. Propensity score matching: a powerful tool for analyzing observational nonrandomized data. *Clin Spine Surg.* (2021) 34:22–4. doi: 10.1097/BSD.0000000000001055

13. Valera M, Albert C, Marcos J, Larreategui Z, Bori L, Meseguer M. A propensity score-based, comparative study assessing humid and dry time-lapse incubation, with single-step medium, on embryo development and clinical outcomes. *Hum Reprod.* (2022) 37:1980–93. doi: 10.1093/humrep/deac165

14. Huang Y, Wang D, Lv W. Effects of treatment of traditional Chinese medicine on postoperative rehabilitation of tibial plateau fracture patients based on propensity score matching. *CJTCMP.* (2021) 36:4408–11.

15. Wang J, Lin J, Chen L, Chen Q, Lin L, Bao X, et al. Scandium and oral cancer: a case-control study based on propensity score matching. *J Environ Occup Med.* (2020) 37:421–6.

16. Sun R. *To investigate the prognosis of postmenopausal breast cancer patients with neoadjuvant endocrine therapy based on propensity score matching method[D]*. Changchun: Jilin University (2021).

17. Pudkasam S, Polman R, Pitcher M, Fisher M, Chinlumprasert N, Stojanovska L, et al. Physical activity and breast cancer survivors: importance of adherence, motivational interviewing and psychological health. *Maturitas.* (2018) 116:66–72.

18. Tjan-Heijnen V, van Hellemond I, Peer P, Swinkels A, Smorenburg C, van der Sangen M, et al. Extended adjuvant aromatase inhibition after sequential endocrine therapy (DATA): a randomised, phase 3 trial. *Lancet Oncol.* (2017) 18:1502–11. doi: 10.1016/S1470-2045(17)30600-9

19. Gnant M, Fitzal F, Rinnerthaler G, Steger G, Greil-Ressler S, Balic M, et al. Duration of adjuvant aromatase-inhibitor therapy in postmenopausal breast cancer. *N Engl J Med.* (2021) 385:395–405. doi: 10.1056/NEJMoa2104162

20. Chen X, Li J, Zhang J, He X, Zhu C, Zhang L, et al. Impairment of the executive attention network in premenopausal women with hormone receptor-positive breast cancer treated with tamoxifen. *Psychoneuroendocrinology.* (2017) 75:116–23. doi: 10.1016/j.psyneuen.2016.10.020

21. Liao K, Lin C, Lai S. Nationwide case-control study examining the association between tamoxifen use and Alzheimer's disease in aged women with breast cancer in Taiwan. *Front Pharmacol.* (2017) 5:612. doi: 10.3389/fphar.2017.00612

Appendix

APPENDIX TABLE A1 Balance comparisons of covariates between the normal group and the declining group after propensity score matching.

Variable		Before matching				After matching			
		Normal group(n = 151)	Decline group(n = 75)	Statistic	P	Normal group(n = 78)	Decline group(n = 49)	Statistic	P
Age		46(40, 49)	49(44, 52)	Z = −3.448	0.001*	46.42 ± 5.65	46.96 ± 5.79	T = 0.516	0.607
Length of education		15(13.50, 16)	9(8, 14)	Z = −6.967	0.000*	14(11, 16)	12.51 ± 3.83	Z = −1.329	0.184
BMI		21.67(20.32, 23.61)	22.97 ± 2.42	Z = −2.894	0.004*	22.69 ± 2.92	23.59(21.09, 25.17)	Z = −1.102	0.270
Family history of cancer	Yes No	71(47.02%) 80(52.98%)	31(41.33%) 44(58.67%)	χ^2 = 0.654	0.419	37(47.44%) 41(52.57%)	22(44.90%) 27(55.10%)	χ^2 = 0.078	0.780
Medication history	Yes No	23(15.23%) 128(84.77%)	13(17.33%) 62(82.67%)	χ^2 = 0.165	0.684	17(21.79%) 61(78.21%)	−8(16.33%) 41(83.67%)	χ^2 = 0.569	0.451
Number of pregnancies		2(1, 3)	2(2, 4)	Z = −1.575	0.115	2(2, 4)	2.5(2, 4)	Z = −0.791	0.429
Duration of lactation		16(6, 24)	18.83 ± 13.37	Z = −1.354	0.176	20(8, 24)	18.03 ± 14.31	Z = −0.811	0.417
Menopausal status	Yes No	14(9.27%) 137(90.73%)	14(18.67%) 61(81.33%)	χ^2 = 4.075	0.044*	11(14.10%) 67(85.90%)	8(16.33%) 41(83.67%)	χ^2 = 0.117	0.732
Menopausal age (postmenopausal)		48.50 ± 3.67	47.71 ± 2.53	T = −0.659	0.515	47.00 ± 2.73	49.45 ± 2.70	T = −1.950	0.068
Menarche age (premenopausal)		13(12, 14)	14(13, 15)	Z = −2.516	0.012*	14(13, 15)	14(13, 14)	Z = −0.045	0.964
Endocrine therapies	SERMs AIs OFS sequential therapy	61 11 60 24	27 11 26 6	χ^2 = 5.440	0.142	30 11 24 13	19 5 16 9	χ^2 = 0.448	0.930
Chemotherapy	Yes No	125(82.78%) 26(17.22%)	63(84%) 12(16%)	χ^2 = 0.053	0.818	63(80.77%) 15(19.23%)	41(83.67%) 8(16.33%)	χ^2 = 0.171	0.679
Number of radiotherapy		25(25, 30)	25(25, 26)	Z = −1.620	0.105	25(20, 30)	25(25, 27.75)	Z = −0.495	0.621
Targeted Therapy	Yes No	20(13.25%) 131(86.75%)	14(18.67%) 61(81.33%)	χ^2 = 1.152	0.283	11(14.10%) 67(85.90%)	7(14.29%) 42(85.71%)	χ^2 = 0.001	0.977
SAS		43.75(37.50, 48.75)	42.97 ± 9.62	Z = −0.891	0.373	42.5(37.5, 47.5)	42.5(38.13, 46.88)	Z = −0.446	0.655
SDS		44.59 ± 9.83	42.50(36.25, 51.25)	Z = −0.663	0.507	44.18 ± 11.1	42.5(37.5, 50.63)	Z = −0.295	0.768
FACT-B		107(94, 123)	108.60 ± 20.97	Z = −0.758	0.448	105.74 ± 19.91	107.82 ± 17.77	Z = −0.528	0.598

*Stands for statistical difference.

frontiers | Frontiers in Medicine

TYPE Original Research
PUBLISHED 04 April 2023
DOI 10.3389/fmed.2023.1167676

OPEN ACCESS

EDITED BY
Hangcheng Fu,
University of Louisville, United States

REVIEWED BY
Xiaoqing Wang,
Shanghai Jiao Tong University, China
Liang Chen,
Shenzhen Institute of Advanced Technology (CAS), China

*CORRESPONDENCE
Tianhao Zhou
✉ wwwzhou0809@163.com
Lei Wang
✉ Wang198111lei@126.com
Lijuan Zang
✉ Lou19941205@163.com

†These authors have contributed equally to this work

SPECIALTY SECTION
This article was submitted to Precision Medicine, a section of the journal Frontiers in Medicine

RECEIVED 16 February 2023
ACCEPTED 13 March 2023
PUBLISHED 04 April 2023

CITATION
Miao S, Ju G, Jiang C, Xue B, Zhao L, Zhang R, Diao H, Yu X, Zhang L, Pan X, Zhang H, Zang L, Wang L and Zhou T (2023) Identification of DYNLT1 associated with proliferation, relapse, and metastasis in breast cancer. *Front. Med.* 10:1167676. doi: 10.3389/fmed.2023.1167676

Identification of DYNLT1 associated with proliferation, relapse, and metastasis in breast cancer

Sen Miao[1†], Gaoda Ju[2†], Chonghua Jiang[3†], Bing Xue[1†], Lihua Zhao[1], Rui Zhang[1], Han Diao[1], Xingzhou Yu[1], Linlin Zhang[1], Xiaozao Pan[1], Hua Zhang[1], Lijuan Zang[4*], Lei Wang[5*] and Tianhao Zhou[6*]

[1]Department of Pathology, Affiliated Hospital of Jining Medical University, Jining, China, [2]Department of Medical Oncology, Key Laboratory of Carcinogenesis and Translational Research (Ministry of Education/Beijing), Peking University Cancer Hospital and Institute, Beijing, China, [3]Department of Neurosurgery, Affiliated Haikou Hospital of Xiangya Medical College, Central South University, Haikou, China, [4]Department of Pathology Center, Shanghai General Hospital, Shanghai Jiaotong University School of Medicine, Shanghai, China, [5]Department of Breast Surgery, Affiliated Hospital of Jining Medical University, Jining, China, [6]Department of Medical Oncology, Shanghai First People's Hospital, Shanghai Jiao Tong University School of Medicine, Shanghai, China

Background: Breast cancer (BC) is the most common malignant disease worldwide. Although the survival rate is improved in recent years, the prognosis is still bleak once recurrence and metastasis occur. It is vital to investigate more efficient biomarkers for predicting the metastasis and relapse of BC. DYNLT1 has been reported that participating in the progression of multiple cancers. However, there is still a lack of study about the correlation between DYNLT1 and BC.

Methods: In this study, we evaluated and validated the expression pattern and prognostic implication of DYNLT1 in BC with multiple public cohorts and BC tumor microarrays (TMAs) of paraffin-embedded tissues collected from the Affiliated Hospital of Jining Medical University. The response biomarkers for immune therapy, such as tumor mutational burden (TMB), between different DYNLT1 expression level BC samples were investigated using data from the TCGA-BRCA cohort utilizing public online tools. In addition, colony formation and transwell assay were conducted to verify the effects of DYNLT1 in BC cell line proliferation and invasion.

Results: The results demonstrated that DYNLT1 overexpressed in BC and predicted poor relapse-free survival in our own BC TMA cohort. In addition, DYNLT1 induced BC development by promoting MDA-MB-231 cell proliferation migration, and metastasis.

Conclusion: Altogether, our findings proposed that DYNLT1 could be a diagnostic and prognostic indicator in BC.

KEYWORDS

DYNLT1, breast cancer, biomarker, prognosis, immune checkpoint blocking therapy

1. Introduction

Breast carcinoma (BC) is the most common cancer in women and ranks the second leading cause of tumor-related death in women in the United States and in China (1, 2). According to the molecular pathological types, there are various therapeutic strategies for BC, such as surgical therapy, radiation therapy, chemotherapy, endocrine therapy, and targeted therapy (3). The response to treatment and prognosis of BC relies on molecular characteristics that have been well established, and the molecular type based on estrogen receptor (ER), progesterone receptor (PR), and human epidermal growth factor receptor-2 (HER-2) status shows excellent performance for guiding clinicians to select the optimal treatment for BC patients in the past few decades (4, 5). In addition, with the development of modern genomic and transcriptomic technologies, numerous gene markers are identified for predicting the response to treatment and prognosis of cancer (6, 7). The prognosis of BC is improved in the past few decades; however, there are still numerous women dying from BC, especially triple-negative breast cancer (TNBC), in the world. As a result, it is urgent to explore a more specific molecular target to direct the diagnosis and treatment of BC.

In this study, we identified that dynein light chain tctex type 1 (DYNLT1), a component of the cytoplasmic dynein 1 complex, may predict the prognosis of BC. DYNLT1 is responsible for the intracellular retrograde motility of vesicles and organelles along microtubules, binding to transport cargo, and is involved in apical cargo transport. It is reported that DYNLT1 plays an important role in many biological functions and diseases, such as Huntington's disease (8), fertilizing potential of human spermatozoa (9), migration of epidermal cells in hypoxia (10), autophagy lysosomal degradation (11), and several types of cancer. DYNLT1 has been reported to promote glioblastoma progression and is associated with tumor-node-metastasis (TNM) grade (12). In gastric cancer (GC), DYNLT1 takes part in the miR-15b-3p/Caspase-3/Caspase-9 signaling pathway to promote malignant transformation (13). However, it is still unclear whether DYNLT1 is related to BC.

In this study, we evaluated the mRNA expression of *DYNLT1* between BC and normal breast tissues from multiple public cohorts and validated the results at the protein level by immunohistochemistry (IHC) staining for DYNLT1 in 68 BC samples along with paired 55 adjacent normal breast specimens collected from the Affiliated Hospital of Jining Medical University. In addition, we observed that DYNLT1 affected the migratory and colony-forming abilities of BC cells *in vitro*. Furthermore, *in vivo* experiment was conducted to verify that DYNLT1 knockdown suppressed tumor growth and abolished distant metastasis. Therefore, we proposed that DYNLT1 may have the potential to become a promising diagnostic indicator and prognostic predictor of BC patients.

2. Methods and materials

2.1. Data acquisition

A total of four Gene Expression Omnibus (GEO) cohorts (GSE15852, GSE9309, GSE109169, and GSE53752) (14–17) were downloaded from the GEO website (https://www.ncbi.nlm.nih.gov/geo) for evaluating the mRNA expression of *DYNLT1* between BC and normal breast tissues.

2.2. GEPIA 2.0 database

The GEPIA 2.0 (http://gepia2.cancer-pku.cn/#index) database (18) was utilized to evaluate the mRNA expression of *DYNLT1* in pan cancers using data from The Cancer Genome Atlas (TCGA). In addition, GEPIA 2.0 was also utilized to evaluate the prognostic implication of *DYNLT1* in pan cancers.

2.3. Breast cancer gene-expression miner database

The Breast Cancer Gene-Expression Miner (http://bcgenex.centregauducheau.fr/BC-GEM/GEM-Accueil.php?js=1) database (19) was utilized to evaluate the mRNA expression of *DYNLT1* in subgroups of BC samples stratified based on multiple clinic-pathological features.

2.4. PrognoScan database

The PrognoScan (http://dna00.bio.kyutech.ac.jp/PrognoScan/index.html) database (20) was utilized to evaluate the prognostic implication of *DYNLT1* in cancer.

2.5. Protein–protein interaction analysis

DYNLT1 was inputted into the String (https://www.string-db.org/) database (21), and a PPI network was successfully outputted.

2.6. GO and KEGG analyses

DYNLT1 and its potential interacting proteins were utilized to perform gene ontology (GO) and Kyoto Encyclopedia of Genes and Genomes (KEGG) analyses by R software with the "clusterProfiler" package (22). Terms with a false discovery rate (FDR) of <0.05 were illustrated.

2.7. CAMOIP database

The CAMOIP (http://camoip.net/) database (23) was utilized to perform GSEA analysis, immune infiltration analysis, and immunogenicity analysis with data from TCGA-BRCA. Tumor mutational burden (TMB), neoantigen load, TGF-beta response score, tumor-infiltrating lymphocytes (TILs) regional fraction, and immune cells' infiltration ratio calculated by CIBERSORT were compared between DYNLT1 high and DYNLT1 low BC samples.

2.8. ciBorPortal database

The ciBorPortal (http://www.cbioportal.org/) database (24, 25) was utilized to perform mutational analysis with data from TCGA-BRCA (Firehose Legacy). Core DNA damage repair (DDR)-related genes and their corresponding pathways were extracted from a previous study (26), such as base excision repair (BER), nucleotide excision repair (NER), mismatch repair (MMR), Fanconi anemia (FA), homologous recombination (HR), non-homologous end joining (NHEJ), direct repair (DR), translesion synthesis (TLS), and damage sensor. A sample with pathway mutation means that at least one DDR-related gene in the pathway is mutated.

2.9. CancerSEA database

The CancerSEA (http://biocc.hrbmu.edu.cn/CancerSEA/home.jsp) database was utilized to evaluate the correlation of *DYNLT1* expression with 14 functional states of single BC cells (27) using data from the GSE75367 cohort (28).

2.10. Human BC specimens

A total of 68 BC samples paired with 55 normal breast tissues collected from the Affiliated Hospital of Jining Medical University were approved by the Ethics Committee of the Affiliated Hospital of Jining Medical University (approval number: 2021-08-C015). All participants provided written informed consent.

2.11. Cell culture

MDA-MB-231 and HEK 293T cells were cultured in the DMEM medium (Gibco) with 10% fetal bovine serum (FBS) (Gibco) and 1% penicillin–streptomycin (Gibco) at 37°C with 5% CO_2.

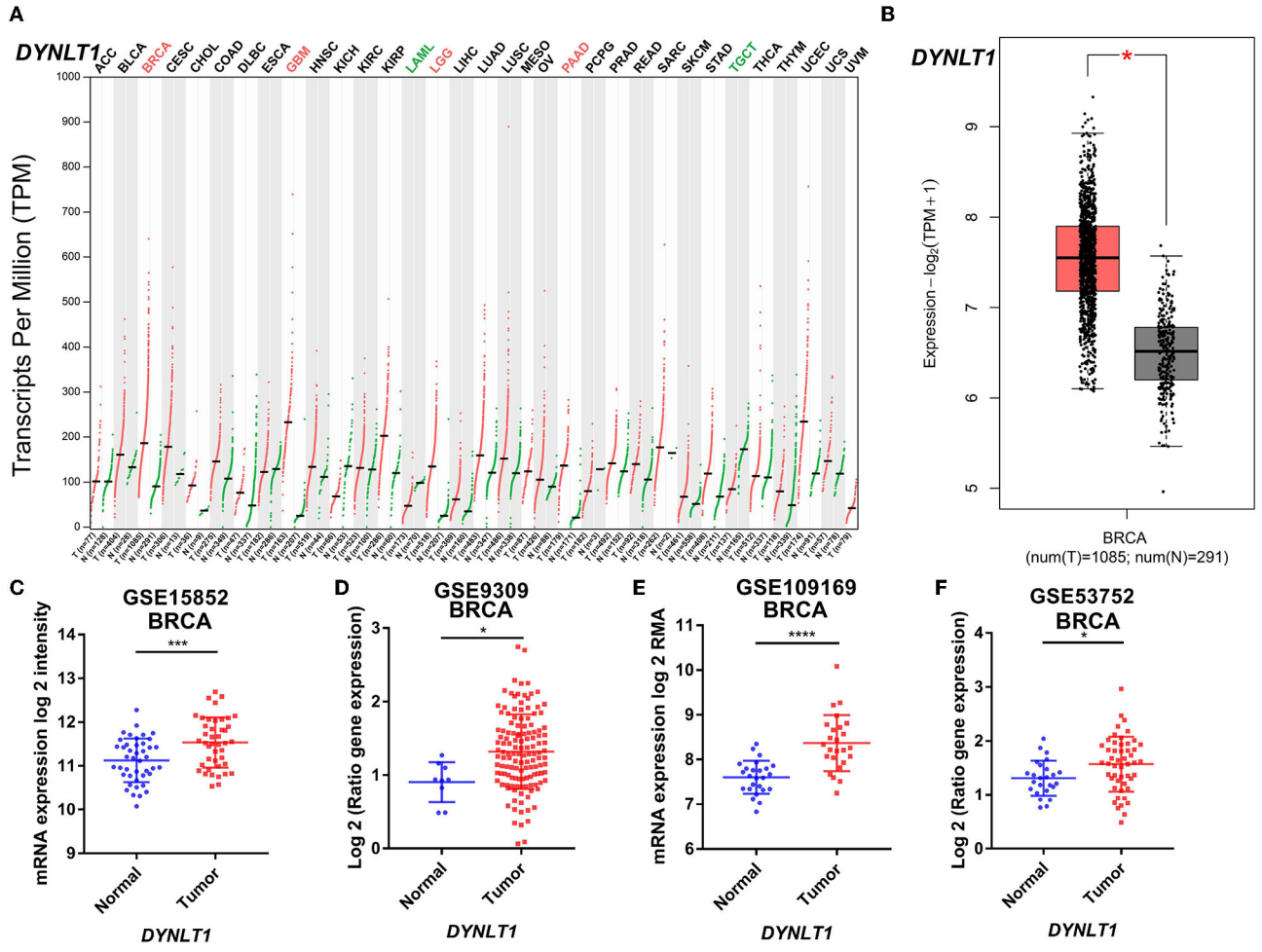

FIGURE 1
DYNLT1 mRNA expression was higher in BC tissues compared to normal breast tissues. **(A)** *DYNLT1* mRNA expression across 33 cancer types (TCGA). **(B)** *DYNLT1* mRNA expression between BC tissues and normal breast tissues in the TCGA-BRCA cohort. **(C)** *DYNLT1* mRNA expression between BC tissues and normal breast tissues in the GSE15852 cohort. **(D)** *DYNLT1* mRNA expression between BC tissues and normal breast tissues in the GSE9309 cohort. **(E)** *DYNLT1* mRNA expression between BC tissues and normal breast tissues in the GSE109169 cohort. **(F)** *DYNLT1* mRNA expression between BC tissues and normal breast tissues in the GSE53752 cohort. TCGA, The Cancer Genome Atlas; $^{*}P < 0.05$, $^{***}P < 0.001$, and $^{****}P < 0.0001$.

2.12. Western blotting

Cells were lysed by denatured buffer and quantified by the Pierce BCA protein assay (Thermo Scientific). The whole cell lysate protein was separated by SDS-PAGE, transferred to NC membranes (Millipore), blocked by no-fat milk, and then detected by primary antibody DYNLT1 (Proteintech, 11954-1-AP, 1:2000) and HRP-conjugated secondary antibody (Sigma), followed by being exposed to enhanced chemiluminescence (Vazyme). β-actin (Abclonal, AC026, 1:10000) was used as a loading control.

2.13. Plasmids and *Lentivirus* production

Annealing and ligation of the DYNLT1-knockdown shRNA were performed and inserted into the enzyme cut pLKO.1. The shDYNLT1 plasmids were then transinfected into HEK293T cells along with psPAX and pMD2.0G. Next, *Lentivirus* was collected to infect MDA-MB-231 cells. The primer sequences are shown as follows: DYNLT1-sh1-F: CCGGGAGGCTATAGAAAGCGCAATTCTCGAGAATTGCGCTTTCTATAGCCTCTTTTTG, DYNLT1-sh1-R: AATTCAAAAAGAGGCTATAGAAAGCGCAATTCTCGAGAATTGCGCTTTCTATAGCCTC; DYNLT1-sh2-F: CCGGCCACAAATGTAGTAGAACAAACTCGAGTTTGTTCTACTACATTTGTGGTTTTTTG, DYNLT1-sh2-R: AATTCAAAAAACCACAAATGTAGTAGAACAAACTCGAGTTTGTTCTACTACATTTGTGG.

2.14. IHC assay

Immunohistochemistry (IHC) staining for DYNLT1 (Proteintech, 11954-1-AP, 1:500) was operated by the standard IHC protocol as described earlier (29). The IHC score (values 0–12) was determined by multiplying the score for staining intensity with the score for the frequency of positive staining cells of DYNLT1. Staining intensity was defined as follows: (0) negative; (1) weak; (2) moderate; and (3) strong. The frequency of positive cells was defined as follows: <5%, 0; 5%−25%, 1; 26%−50%, 2; 51%−75%, 3; and more than 75%, 4 (30).

2.15. Colony-forming assay

MDA-MB-231 cells were seeded at a density of 200 cells per well in six-well plates. Single cells were cultured in DMEM with 10% FBS at 37°C with 5% CO_2 for 3 weeks. Colonies were fixed with 10% formalin and then stained with 0.1% crystal violet.

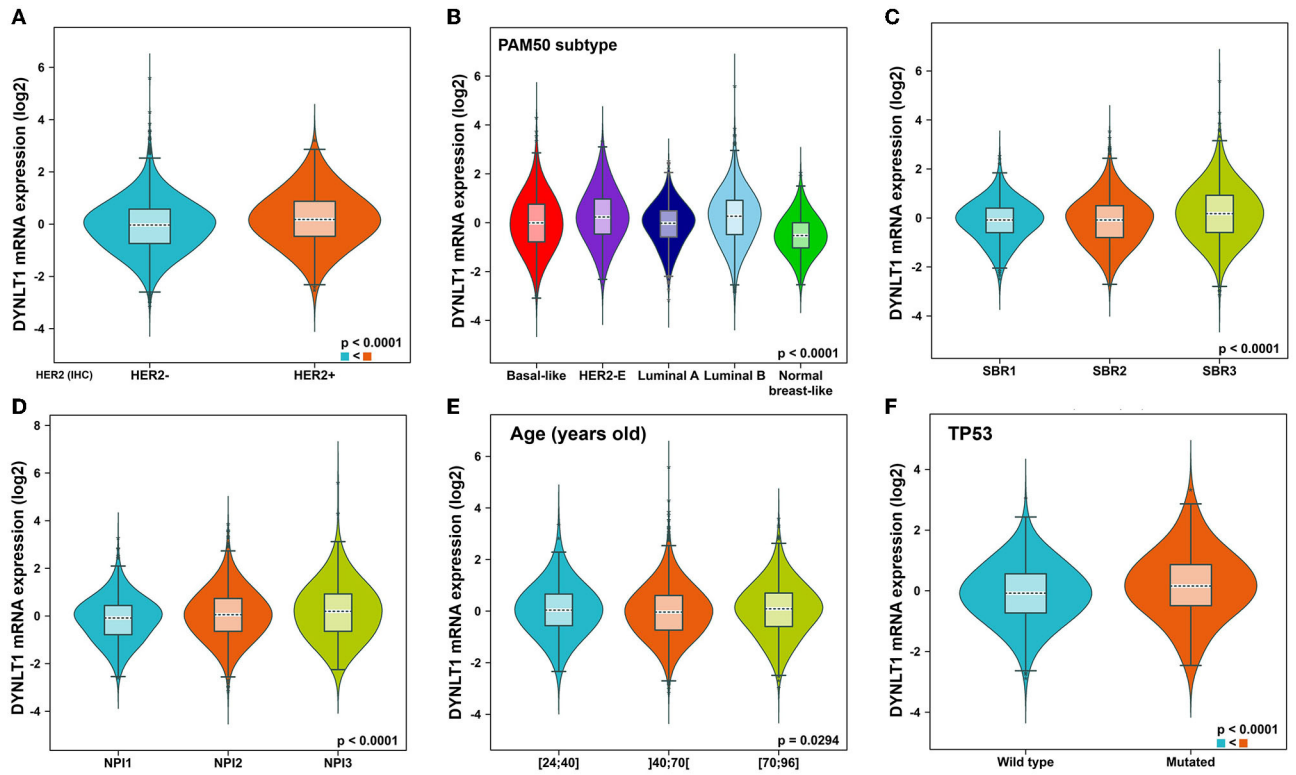

FIGURE 2
Subtype analysis of DYNLT1 mRNA expression based on clinic-pathological features of BC tissues. **(A)** Subtype analysis of DYNLT1 mRNA expression based on HER2 status. **(B)** Subtype analysis of DYNLT1 mRNA expression based on PAM50 subtype. **(C)** Subtype analysis of DYNLT1 mRNA expression based on SBR grade. **(D)** Subtype analysis of DYNLT1 mRNA expression based on NPI. **(E)** Subtype analysis of DYNLT1 mRNA expression based on age. **(F)** Subtype analysis of DYNLT1 mRNA expression based on TP53 mutant status. HER-2, human epidermal growth factor receptor-2; SBR, Scarff-Bloom-Richardson; NPI, Nottingham prognostic index.

2.16. Cell growth assay

Lentivirus-infected stable cells were seeded into 96-well plates and cultured in 10% FBS DMEM (2,000 cells per well, five parallel wells). Then, the cells were collected at different points in time, and the cell number in each well was counted by the CCK-8 reagent. The absorbance at 450 nm was employed to determine the number of viable cells.

2.17. Transwell assay

The migration assays and invasion assays were performed using a transwell chamber (Corning). A total of 2×10^4 cells per well were seeded into the upper chamber for the migration assays, while 5×10^4 cells per well were seeded into the upper chamber after matrigel was coagulated at 37°C for the invasion assays with serum-free medium, and the bottom of the chamber contained the DMEM medium with 10% FBS. Cells were fixed by 10% formalin and stained by 0.1% crystal violet after migration for 24 h. Migrated BC cells' pictures were captured by an inverted light microscope at ×100 magnification, and three random fields were counted.

2.18. Tumor models

Female SCID mice (6 weeks old) were purchased from the Shanghai Model organism. SCID mice were injected in the right lower breast fat pad with MDA-MB-231 cells knockdown DYNLT1 or vector shRNA control (1×10^6 cells per mouse). Tumor volume was measured every 7 days and calculated according to the formula as follows: volume = 0.5 × tumor length × width × width. Mice were generally sacrificed when tumors became necrotic or their volume reached 1,500 mm^3, recorded as death for the survival curve. The lung and the liver of dead mice were excised and fixed in formalin. Paraffin-embedded lungs were systematically sectioned and stained with hematoxylin and eosin (H&E) staining, and images were captured by Leica Aperio CS2.

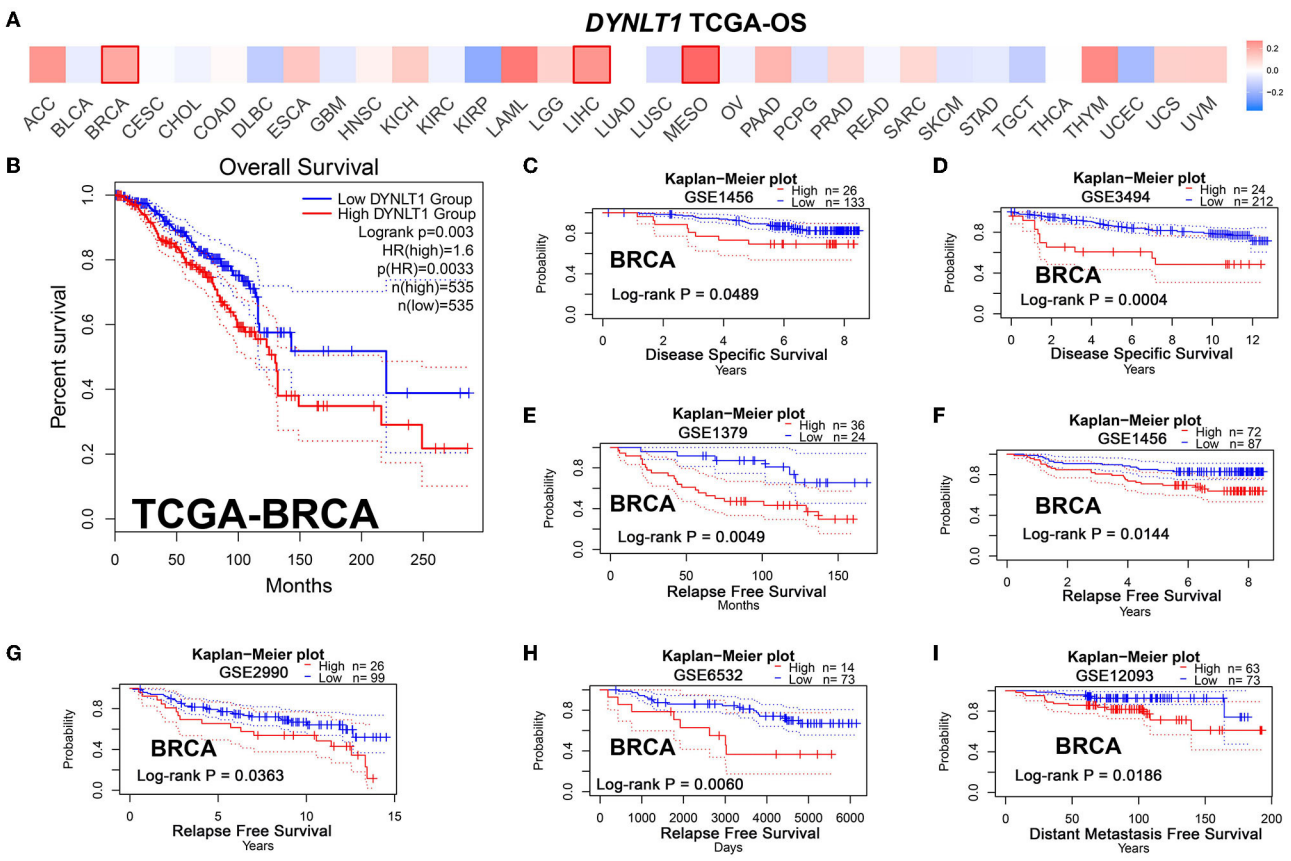

FIGURE 3
High DYNLT1 expression predicted poor survival in BC. **(A)** High expression predicted poor prognosis in BC, LGG, and LIHC in the GEPIA database. **(B)** High DYNLT1 expression predicted poor overall survival (OS) of BC patients in the TCGA-BRCA cohort. **(C, D)** High DYNLT1 expression predicted poor disease-specific survival (DSS) of BC patients in the GSE1456 cohort **(C)** and GSE3494 cohort **(D)**. **(E–H)** High DYNLT1 expression predicted poor relapse-free survival (RFS) of BC patients in the GSE1379 cohort **(E)**, GSE1456 cohort **(F)**, GSE2990 cohort **(G)**, and GSE6532 cohort **(H)**. **(I)** High DYNLT1 expression predicted poor distant metastasis-free survival (DMFS) of BC patients in the GSE12093 cohort.

2.19. Statistical analysis

Student's *t*-test and chi-square test were utilized to analyze the difference between the two groups. A *P*-value of <0.05 was considered statistically significant.

3. Results

3.1. DYNLT1 expression was higher in BC compared to normal breast tissues

First, we evaluated the mRNA expression of *DYNLT1* across 33 cancer types and paired normal samples with data from TCGA by the GEPIA database. Our results demonstrated that the mRNA expression of *DYNLT1* was higher in most types of cancer tissues compared with paired normal samples, such as BC, GBM, LGG, and PAAD (Figures 1A, B). Next, four GEO cohorts were utilized to validate the result that the mRNA expression of *DYNLT1* was higher in BC tissues compared to paired normal breast samples (Figures 1C–F). In addition, subgroup analysis of multiple clinic pathological features of BC samples in the Breast Cancer Gene-Expression Miner database showed that DYNLT1 expression is related to HER-2 status, PAM50-based intrinsic subtype, Scarff-Bloom-Richardson (SBR) grade, Nottingham prognostic index (NPI), and age and mutation status of TP53 (Figures 2A–F).

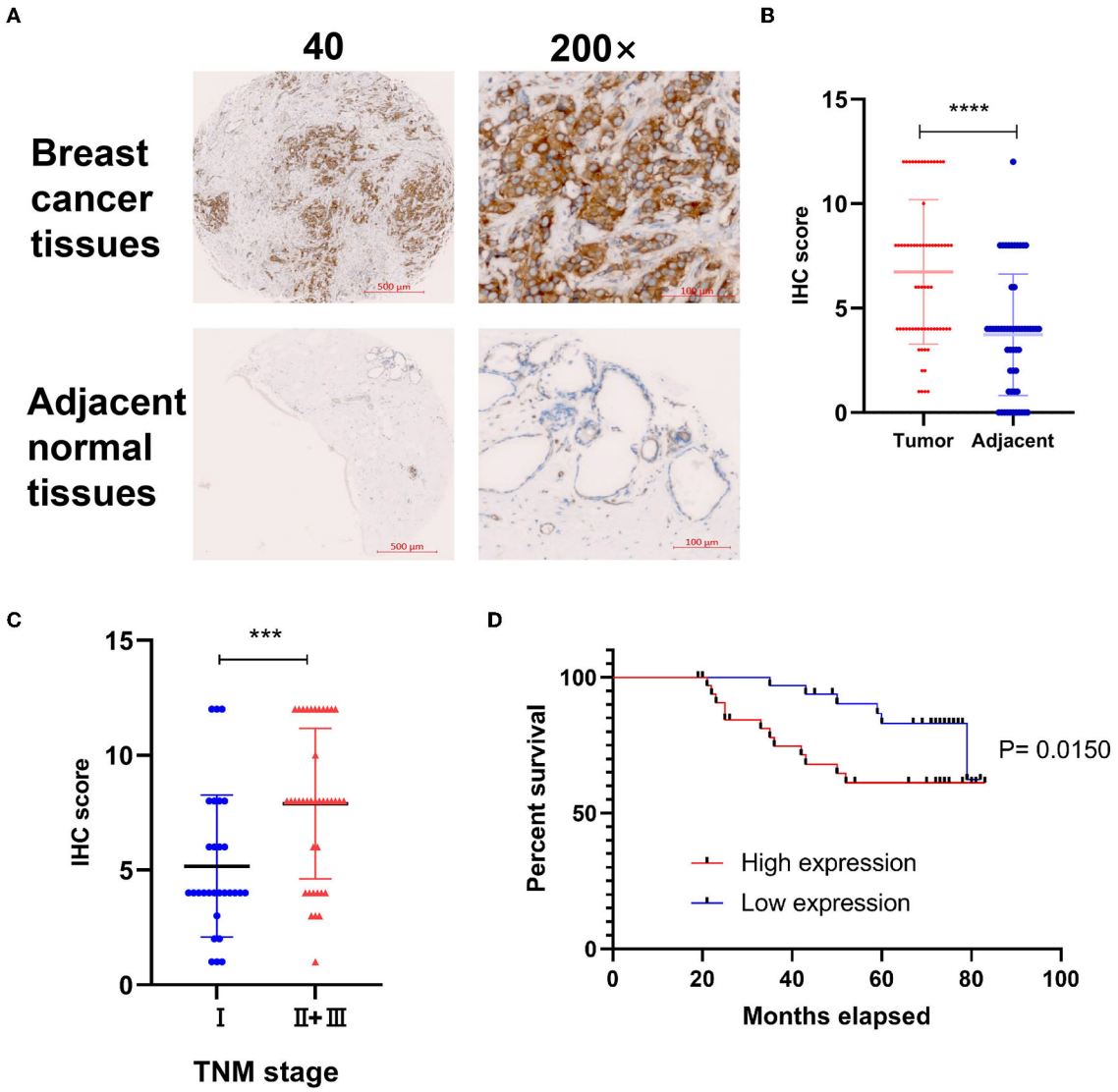

FIGURE 4
Validated the protein expression pattern and prognostic implication of DYNLT1 in BC. **(A)** Protein expression of DYNLT1 was higher in BC compared to normal breast tissues. **(B)** Scatter plot of TMED IHC score between BC and normal breast tissues. **(C)** Scatter plot of TMED IHC score between TNM stage I BC and TNM stage II+III BC tissues. **(D)** Kaplan–Meier analysis was utilized to compare the relapse-free survival between high DYNLT1 expression BC patients and low DYNLT1 expression BC patients. IHC, immunohistochemistry. ***$P < 0.001$ and ****$P < 0.0001$.

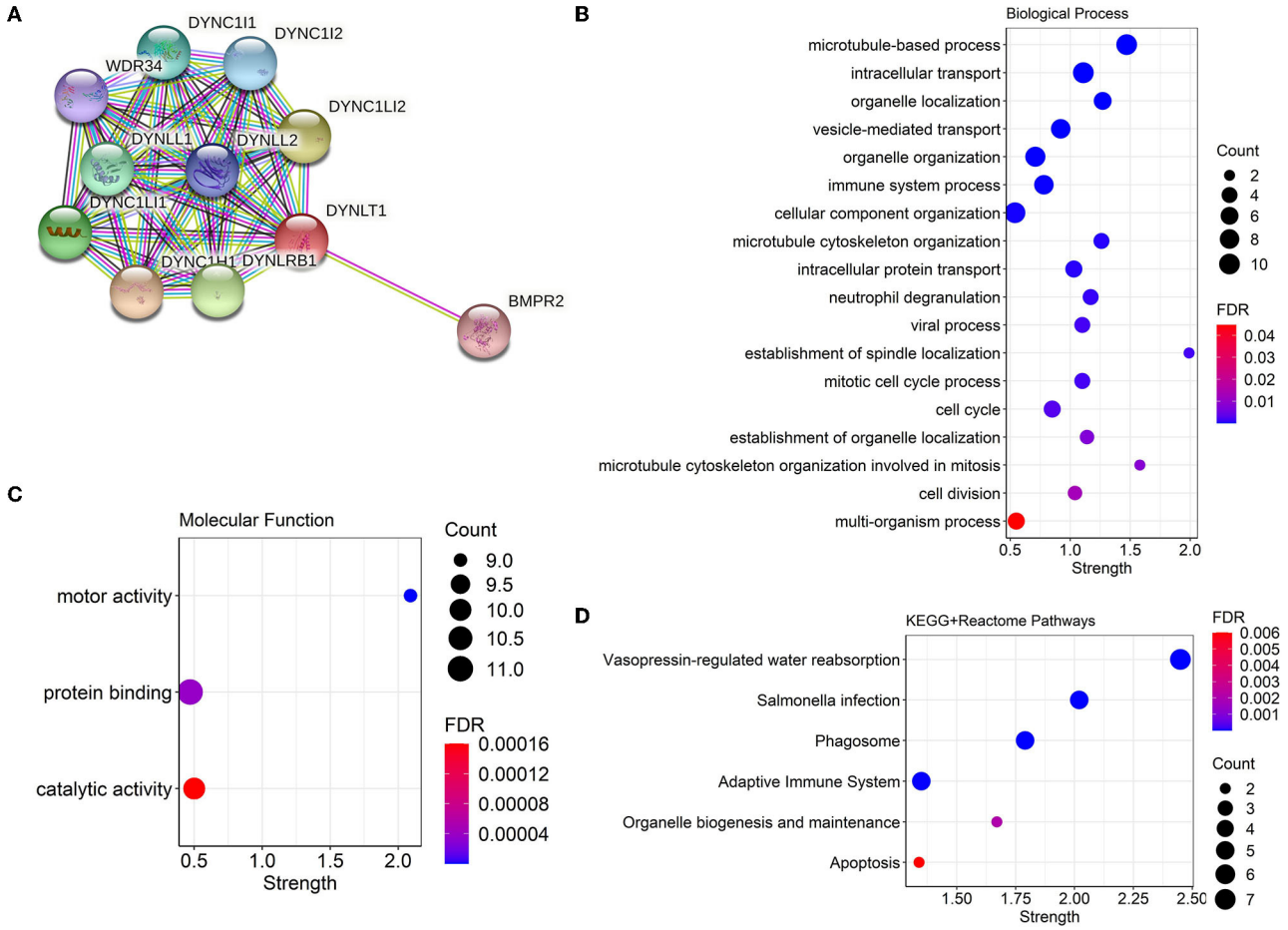

FIGURE 5
PPI network and functional annotation of DYNLT1. **(A)** PPI network based on DYNLT1. **(B, C)** Gene ontology enrichment analysis: biological process **(B)** and molecular function **(C)**. **(D)** KEGG pathway enrichment analysis. PPI, protein–protein network; GO, gene ontology; KEGG, kyoto encyclopedia of genes and genomes.

3.2. High expression of *DYNLT1* predicting poor overall relapse and distant metastasis-free survival of BC

First, we evaluated the prognostic implications of *DYNLT1* in 33 cancer types using data from TCGA by the GEPIA database. Our results demonstrated that *DYNLT1* was a significant ($P < 0.05$) risk factor for the prognosis of BC, MESO, and LIHC (Figures 3A, B). Furthermore, we validated the prognostic implication of *DYNLT1* in BC by the PrgnoScan database. Our results identified that high expression of *DYNLT1* predicted poor disease-specific survival (Figures 3C, D), relapse-free survival (Figures 3E–H), and distant metastasis-free survival (Figure 3I) in BC.

3.3. Validated the expression pattern and prognostic implication of BC by TMA

To explore the correlation of DYNLT1 and the characteristic of BC patients at the protein level, a BC TMA, containing 68 cancer tissues were used for IHC staining for DYNLT1. The results validated that DYNLT1 expressed significantly higher in BC tissues than in adjacent normal breast samples (Figures 4A, B). High expression of DYNLT1 was positively correlated with higher TNM stage (Figure 4C) and predicted poor relapse-free survival (RFS) with a log-rank *P*-value of <0.015 (Figure 4D).

3.4. PPI network and functional annotation of DYNLT1

We constructed a PPI network combining DYNLT1 and its potential interacting proteins by the String database. The result indicated that DYNLT1 may be capable of interacting with BMPR2, DYNC1H1, DYNC1I1, DYNC1I2, DYNC1LI1, DYNC1LI2, DYNLL1, DYNLL2, DYNLRB1, and WDR34 (Figure 5A). The gene ontology and pathway functional enrichment analyses of genes in this network demonstrated that these genes may involve

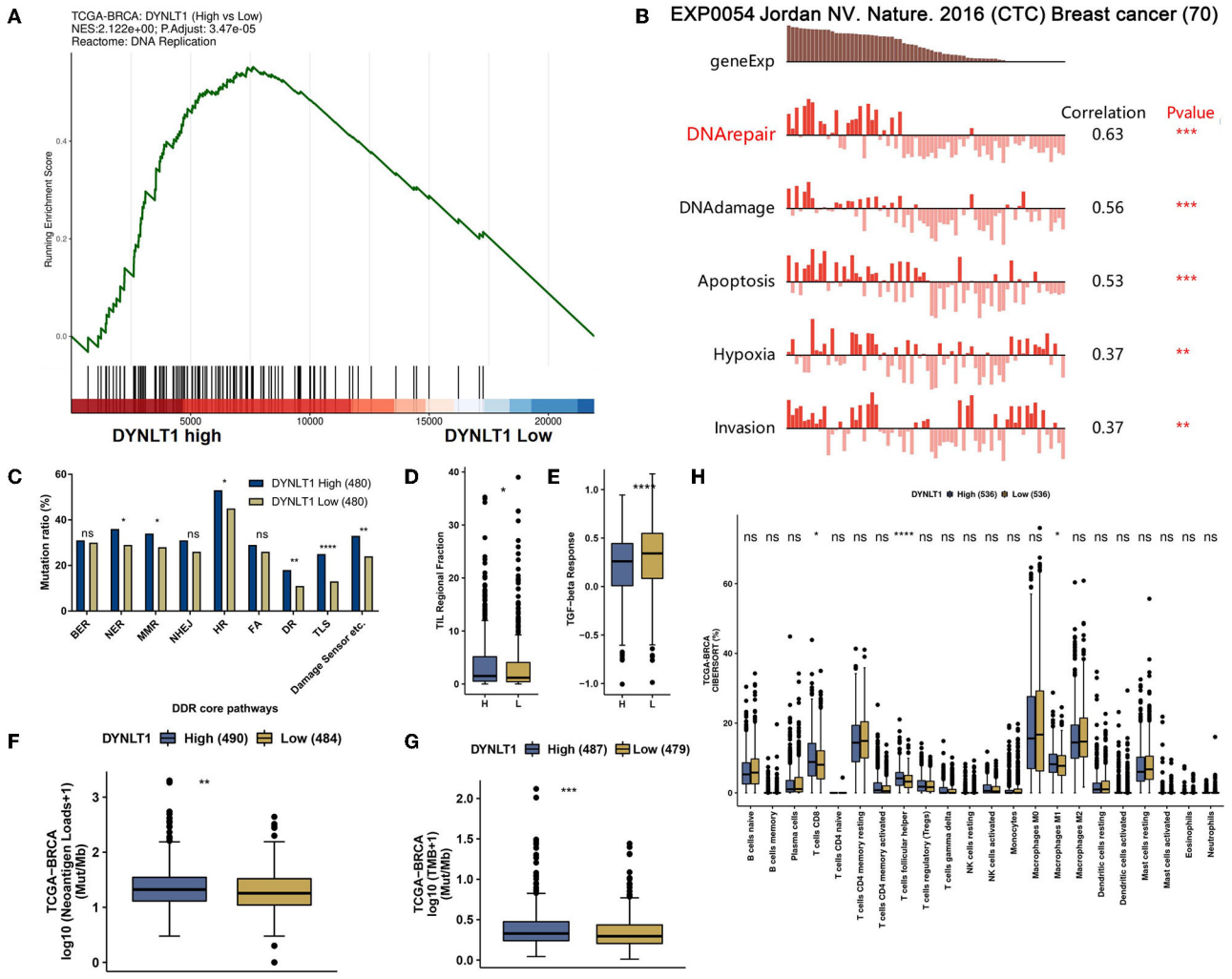

FIGURE 6
DYNLT1 may predict well overcome in immune checkpoint blocked therapy for patients with BC. **(A)** GSEA analysis showed that the DNA replication pathway was enriched in DYNLT1 High BC samples. **(B)** DTNLT1 mRNA expression was positively related to DNA damage, DNA repair, apoptosis, hypoxia, TILs, and invasion at the single BC cell level. **(C)** The DDR pathways' mutational ratio between DYNLT1 High and DYNLT1 Low BC samples. **(D)** The regional fraction between DYNLT1 High and DYNLT1 Low BC samples. **(E)** The TGF-beta response score between DYNLT1 High and DYNLT1 Low BC samples. **(F)** The neoantigen loads between DYNLT1 High and DYNLT1 Low BC samples. **(G)** The TMB between DYNLT1 High and DYNLT1 Low BC samples. **(H)** The infiltration ratio of immune cells between DYNLT1 High and DYNLT1 Low BC samples. TMB, tumor mutational burden; DDR, DNA damage repair; TILs, tumor-infiltrating lymphocytes; BER, base excision repair; NER, nucleotide excision repair; MMR, mismatch repair; FA, Fanconi anemia; HR, homologous recombination; NHEJ, non-homologous end joining; DR, direct repair; TLS, translesion synthesis; *$P < 0.05$; **$P < 0.01$; ***$P < 0.001$; and ****$P < 0.0001$.

in cell cycle, cell division, immune system process, vesicle-mediated transport, motor activity, protein binding, phagosome, adaptive immune system, and apoptosis (Figures 5B–D).

3.5. DYNLT1 as a predictive biomarker for immune checkpoint blocking therapy in patients with BC

Generally, a high DNA damage repair (DDR) mutational ratio, a high proportion of TMB, high neoantigen loads, high TILs regional fraction, and low TGF-beta response predict well overcome in ICB therapy for patients with cancer (31, 32). In our study, the results of GSEA analysis based on data from TCGA-BRCA showed that DNA replication (Figure 6A) pathways were enriched in DYNLT1 high BC samples. In addition, we found that DTNLT1 expression was positively related to DNA damage and DNA repair (Pearson's correlation > 0.3, $P < 0.05$) at the single cell level of BC by the CancerSEA database (Figure 6B). We found that BC patients in the DYNLT1 high group had higher levels of DDR mutational ratio (Figure 6C), TILs regional fraction (Figure 6D), and lower TGF-beta response (Figure 6E) compared to those in the DYNLT1 low group. Moreover, a high proportion of neoantigen loads (Figure 6F) and TMB (Figure 6G) was shown in the DYNLT1 high group, and the CIBERSORT analysis showed that BC samples in the DYNLT1

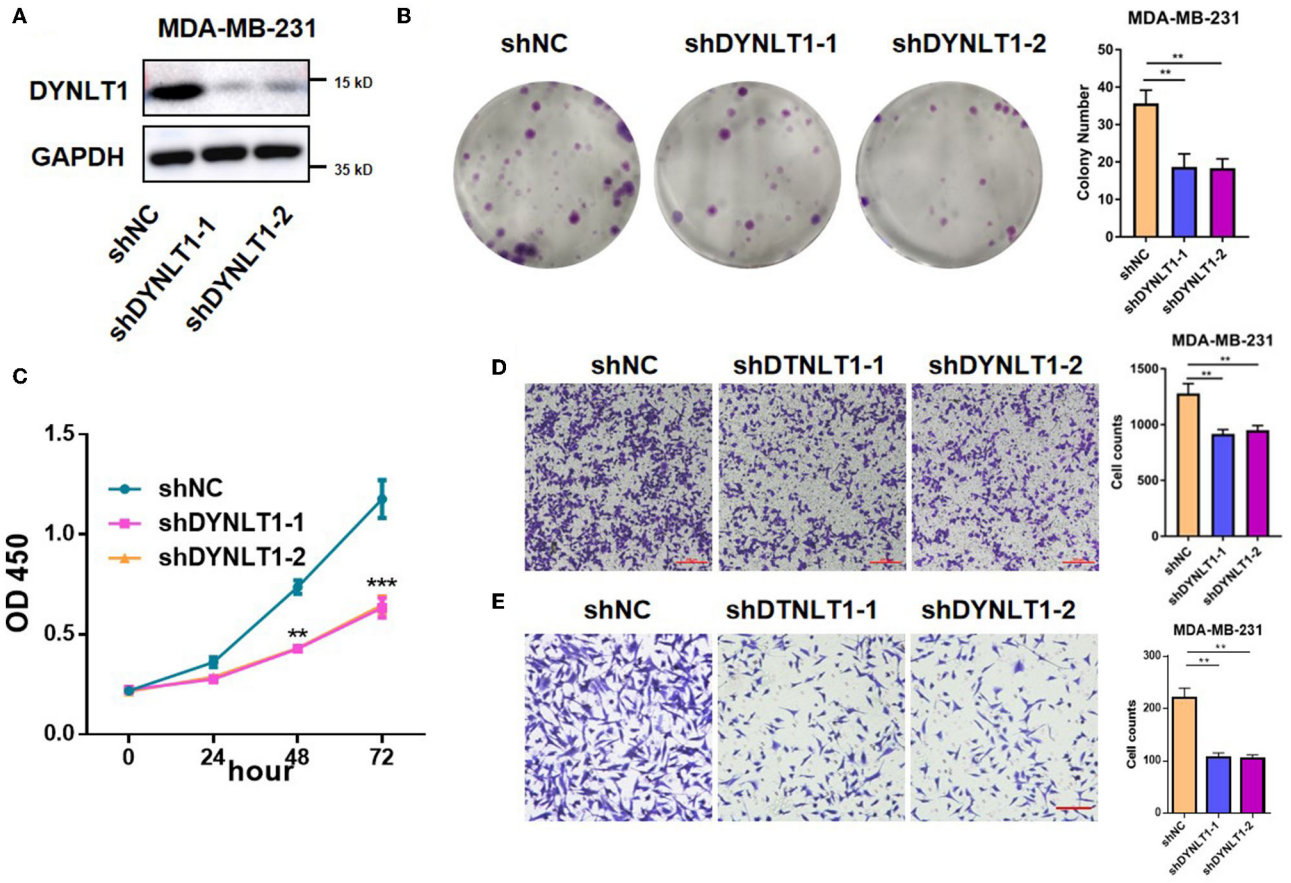

FIGURE 7
DYNLT1 knockdown inhibited MDA-MB-231 cells' colony formation and migration. **(A)** Knockdown expression of DYNLT1 in MDA-MB-231 cells. **(B)** DYNLT1 knockdown inhibited cell colony formation and histogram of colony numbers between the DYNLT1 knockdown group and control group. **(C)** CCK-8 assay of the DYNLT1 knockdown group and control group. **(D)** DYNLT1 knockdown inhibited cell migration and histogram of cell counts between the DYNLT1 knockdown group and control group. **(E)** DYNLT1 knockdown inhibited cell invasion and histogram of cell counts between the DYNLT1 knockdown group and the control group. Scale bar = 100 μm, ***$P < 0.001$, **$P < 0.01$.

high group had a higher infiltration ratio of CD8+ T cells and follicular helper T cells than those in the DYNLT1 low group (Figure 6H).

3.6. DYNLT1 knockdown suppressed the colony-forming, proliferation, migratory, and invasion abilities of BC cells

To explore the functional role of DYNLT1 in BC cells, *in vitro* experiments were conducted. First, MDA-MB-231-shDYNLT1 and MDA-MB-231-sh scramble (NC) stable cell lines were constructed successfully by lentiviral transduction (Figure 7A). Next, the results of the colony-forming assay and CCK-8 assays demonstrated that knockdown expression of DYNLT1 inhibited the colony formation and proliferation abilities in MDA-MB-231 cells (Figures 7B, C). Furthermore, a transwell assay was conducted to confirm that migration and invasion abilities were also attenuated with the DYNLT1 knockdown in MDA-MB-231 cells (Figures 7D, E).

3.7. Knockdown of DYNLT1 suppressed tumor growth and abolished the lung and liver metastasis *in vivo*

To determine the role of DYNLT1 *in vivo*, MDA-MB-231-shDYNLT1 and MDA-MB-231-shNC cells were injected into a mammary fat pad in severe combined immunodeficiency (SCID) female mice. Knockdown of DYNLT1 led to smaller tumor volume (Figures 8A, B) and poor survival (Figure 8C). The lung and the liver samples of sacrificed mice were formalin-fixed and paraffin-embedded, and HE stain was conducted to evaluate the distant metastasis. As expected, the knockdown of DYNLT1 prevented tumor cells from metastasizing to distant organs including the lung and the liver, which prolong the survival period of tumor-burden mice (Figures 8D, E).

4. Discussion

With the development of modern genomic/transcriptomic technologies and increasing public cancer genomic programs, such

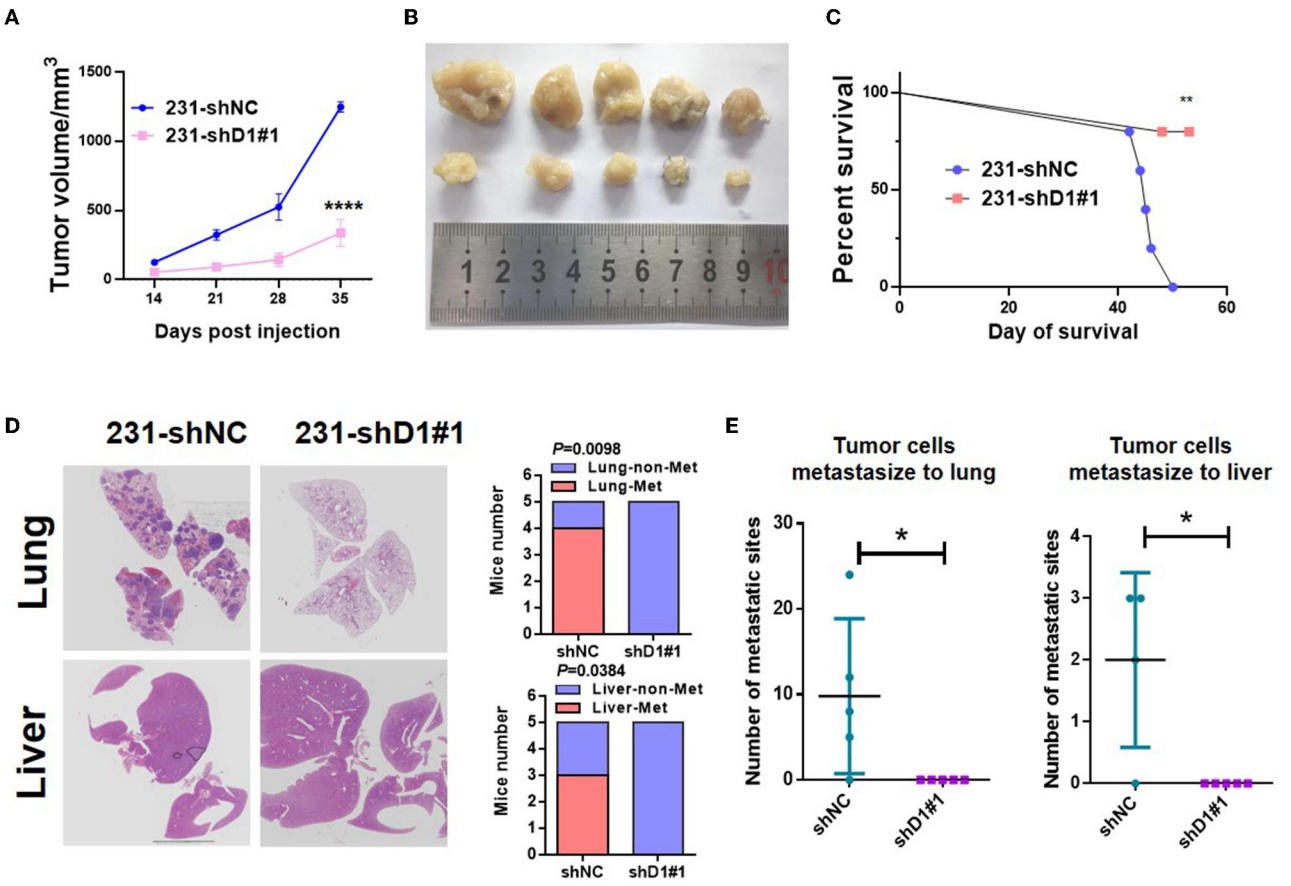

FIGURE 8
DYNLT1 knockdown suppressed tumor growth and abolished lung and liver metastasis *in vivo*. **(A)** DYNLT1 knockdown in MDA-MB-231 cells suppresses tumor growth in SCID mice. **(B)** Tumor samples were shown after mice were sacrificed. **(C)** Survival of SCID mice with MDA-MB-231-shNC tumor or MDA-MB-231-shDYNLT1#1 tumor. **(D)** Representative lung and liver HE staining of mice with MDA-MB-231-shNC tumor or MDA-MB-231-shDYNLT1#1 tumor (scale bar = 5 mm). **(E)** The number of tumor metastatic sites in the lung and the liver ($n = 5$ biological replicates). *$P < 0.05$, **$P < 0.01$, and ****$P < 0.0001$.

as TCGA and GEO, numerous biomarkers were identified for improving our ability to diagnose and treat cancer or utilized as predictors of prognosis and response to therapies in cancer. For example, DYNLT1 serving as a prognostic indicator for GBM patients has been reported (12). However, there is no report on whether DYNLT1 may act as a biomarker of BC.

In our study, we validated that DYNLT1 expression was higher in BC than normal breast tissues by integrated bioinformatics analysis using data from multiple public cohorts and ourselves BC and adjacent normal breast specimens. In addition, we demonstrated that high DYNLT1 expression meant a poor prognosis in BC, and DYNLT1 knockdown suppressed MDA-MB-231 cell migration and colony formation. Furthermore, in *in vivo* experiment, we found that DYNLT1 knockdown suppressed tumor growth and abolished distant metastasis. Mice with DYNLT1 knockdown tumor cells survived a longer period. However, there is still a limitation in our study. The molecular mechanism of how high DYNLT1 expression enhances BC cells' proliferative and invasive abilities remains unclear.

Abnormal proliferative and invasive abilities are the leading causes of progression and poor prognosis in BC. It has been reported that DYNLT1 promoted migration, invasion, and proliferation, and inhibited apoptosis of GC *via* the exo-miR-15b-3p/DYNLT1/Caspase-3/Caspase-9 pathway (13). Previous studies also found that DYNLT1 interacted with the tumor suppressor REIC/Dkk-3 which induced malignant cell death *via* modification of the Wnt signaling pathway (33, 34). In addition, Kawasaki et al. (35) demonstrated that REIC/Dkk-3 overexpression could induce multidrug-resistant BC cell line MCF-7 apoptosis *via* downregulating P-glycoprotein. Hence, a high expression of DYNLT1 can promote the progression of BC *via* interacting with REIC/Dkk-3.

Recent evidence indicates that a high proportion of TMB and loads of neoantigens predicted a good response for ICB therapy in many types of cancer (36, 37), and patients with high TILs and low TGF-beta response in tumor samples always carry a better prognostic significance in ICB treatment (38, 39). Our results showed that biomarkers representing an effective response to ICB treatment were always accompanied by DYNLT1 high expression in BC samples. Therefore, we inferred that DYNLT1 may be a response biomarker in ICB therapy for BC.

5. Conclusion

Our study first suggested that DYNLT1 may serve as a biomarker for diagnosing and ICB treating BC or a predictor for predicting the prognosis of BC.

Data availability statement

The raw data supporting the conclusions of this article will be made available by the authors, without undue reservation.

Ethics statement

The studies involving human participants were reviewed and approved by Ethics Committee of Affiliated Hospital of Jining Medical University (approval number: 2021-08-C015). The patients/participants provided their written informed consent to participate in this study. The animal study was reviewed and approved by the Ethics Committee of Affiliated Hospital of Jining Medical University, JNNL-202-DW-02.

Author contributions

SM, GJ, CJ, and BX performed the experiments and wrote the manuscript. LihZ, RZ, HD, XY, LinZ, XP, and HZ collected the BC sample and performed the experiments. LijZ, LW, and TZ supervised the project and provided funds for the whole project. All authors approved the final manuscript.

Funding

This study was funded by Lin He's Academician Workstation of New Medicine and Clinical Translation at Jining Medical University [JYHL2021 FMS08] and the Doctoral Research Fund of Affiliated Hospital of Jining Medical University [grant 2020-BS-007].

Conflict of interest

The authors declare that the research was conducted in the absence of any commercial or financial relationships that could be construed as a potential conflict of interest.

The reviewer XW declared a shared parent affiliation with the author TZ to the handling editor at the time of review.

Publisher's note

Supplementary material

The Supplementary Material for this article can be found online at: https://www.frontiersin.org/articles/10.3389/fmed.2023.1167676/full#supplementary-material

SUPPLEMENTARY TABLE 1
Clinical information of patients.

References

1. Siegel RL, Miller KD, Jemal A. Cancer statistics, 2020. *CA Cancer J Clin.* (2020) 70:145–64. doi: 10.3322/caac.21601

2. Chen W, Zheng R, Baade PD, Zhang S, Zeng H, Bray F, et al. Cancer statistics in China, 2015. *CA Cancer J Clin.* (2016) 66:115–32. doi: 10.3322/caac.21338

3. Furrukh M, Qureshi A. Treatment of breast cancer; review and updates. *J Ayub Med Coll Abbottabad.* (2018) 30:264–74.

4. Prat A, Pineda E, Adamo B, Galván P, Fernández A, Gaba L, et al. Clinical implications of the intrinsic molecular subtypes of breast cancer. *Breast.* (2015) 24:S26–35. doi: 10.1016/j.breast.2015.07.008

5. Huo D, Hu H, Rhie SK, Gamazon ER, Cherniack AD, Liu J, et al. Comparison of breast cancer molecular features and survival by African and European ancestry in the cancer genome atlas. *JAMA Oncol.* (2017) 3:1654–62. doi: 10.1001/jamaoncol.2017.0595

6. Tsang JYS, Tse GM. Molecular classification of breast cancer. *Adv Anat Pathol.* (2020) 27:27–35. doi: 10.1097/PAP.0000000000000232

7. Hammerl D, Smid M, Timmermans AM, Sleijfer S, Martens JWM, Debets R. Breast cancer genomics and immuno-oncological markers to guide immune therapies. *Semin Cancer Biol.* (2018) 52(Pt 2):178–88. doi: 10.1016/j.semcancer.2017.11.003

8. Rosseto SM, Alarcon TA, Rocha DMC, Ribeiro FM, Ferguson SSG, Martins-Silva C, et al. DYNLT1 gene expression is downregulated in whole blood of patients at different Huntington's disease stages. *Neurol Sci.* (2021) 42:1963–7. doi: 10.1007/s10072-020-04772-0

9. Elzeiny D, Monir R, El Sabakhawy K, Selim MK, Zalata A. Relationship between DYNLT1 and Beclin1 expression and the fertilising potential of human spermatozoa. *Andrologia.* (2019) 51:e13380. doi: 10.1111/and.13380

10. Chen X, Zhou X, Shi X, Xia X, Zhang Y, Fan D. MAP4 regulates Tctex-1 and promotes the migration of epidermal cells in hypoxia. *Exp Dermatol.* (2018) 27:1210–5. doi: 10.1111/exd.13763

11. Dong S, Zhang Y, Ming J, Zhang X, Li X, Xu J, et al. Tctex1 plays a key role in the α-synuclein autophagy lysosomal degradation pathway. *Neurosci Lett.* (2017) 661:90–5. doi: 10.1016/j.neulet.2017.09.050

12. Dumitru CA, Brouwer E, Stelzer T, Nocerino S, Rading S, Wilkens L, et al. Dynein light chain protein Tctex1: a novel prognostic marker and molecular mediator in glioblastoma. *Cancers.* (2021) 13:2624. doi: 10.3390/cancers13112624

13. Wei S, Peng L, Yang J, Sang H, Jin D, Li X, et al. Exosomal transfer of miR-15b-3p enhances tumorigenesis and malignant transformation through the DYNLT1/Caspase-3/Caspase-9 signaling pathway in gastric cancer. *J Exp Clin Cancer Res.* (2020) 39:32. doi: 10.1186/s13046-019-1511-6

14. Pau Ni IB, Zakaria Z, Muhammad R, Abdullah N, Ibrahim N, Aina Emran N, et al. Gene expression patterns distinguish breast carcinomas from normal breast tissues: the Malaysian context. *Pathol Res Pract.* (2010) 206:223–8. doi: 10.1016/j.prp.2009.11.006

15. Tsai C-A, Liu L-YD. Identifying gene set association enrichment using the coefficient of intrinsic dependence. *PLoS ONE.* (2013) 8:e58851. doi: 10.1371/journal.pone.0058851

16. Chang J-W, Kuo W-H, Lin C-M, Chen W-L, Chan S-H, Chiu M-F, et al. Wild-type p53 upregulates an early onset breast cancer-associated gene GAS7 to suppress metastasis *via* GAS7-CYFIP1-mediated signaling pathway. *Oncogene.* (2018) 37:4137–50. doi: 10.1038/s41388-018-0253-9

17. Kuo W-H, Chang Y-Y, Lai L-C, Tsai M-H, Hsiao CK, Chang K-J, et al. Molecular characteristics and metastasis predictor genes of triple-negative breast cancer: a clinical study of triple-negative breast carcinomas. *PLoS ONE.* (2012) 7:e45831. doi: 10.1371/journal.pone.0045831

18. Tang Z, Kang B, Li C, Chen T, Zhang Z. GEPIA2: an enhanced web server for large-scale expression profiling and interactive analysis. *Nucleic Acids Res.* (2019) 47:W556–W60. doi: 10.1093/nar/gkz430

19. Jézéquel P, Gouraud W, Ben Azzouz F, Guérin-Charbonnel C, Juin PP, Lasla H, et al. bc-GenExMiner 4.5: new mining module computes breast cancer differential gene expression analyses. *Database.* (2021) 2021:baab007 doi: 10.1093/database/baab007

20. Mizuno H, Kitada K, Nakai K, Sarai A. PrognoScan: a new database for meta-analysis of the prognostic value of genes. *BMC Med Genom.* (2009) 2:18. doi: 10.1186/1755-8794-2-18

21. Szklarczyk D, Gable AL, Lyon D, Junge A, Wyder S, Huerta-Cepas J, et al. STRING v11: protein-protein association networks with increased coverage, supporting functional discovery in genome-wide experimental datasets. *Nucl Acids Res.* (2019) 47:D607–D13. doi: 10.1093/nar/gky1131

22. Yu G, Wang L-G, Han Y, He Q-Y. clusterProfiler: an R package for comparing biological themes among gene clusters. *OMICS.* (2012) 16:284–7. doi: 10.1089/omi.2011.0118

23. Lin A, Qi C, Wei T, Li M, Cheng Q, Liu Z, et al. CAMOIP: a web server for comprehensive analysis on multi-omics of immunotherapy in pan-cancer. *Brief Bioinform.* (2022) 23:bbac129. doi: 10.1093/bib/bbac129

24. Gao J, Aksoy BA, Dogrusoz U, Dresdner G, Gross B, Sumer SO, et al. Integrative analysis of complex cancer genomics and clinical profiles using the cBioPortal. *Sci Signal.* (2013) 6:pl1. doi: 10.1126/scisignal.2004088

25. Cerami E, Gao J, Dogrusoz U, Gross BE, Sumer SO, Aksoy BA, et al. The cBio cancer genomics portal: an open platform for exploring multidimensional cancer genomics data. *Cancer Discov.* (2012) 2:401–4. doi: 10.1158/2159-8290.CD-12-0095

26. Knijnenburg TA, Wang L, Zimmermann MT, Chambwe N, Gao GF, Cherniack AD, et al. Genomic and molecular landscape of DNA Damage repair deficiency across the cancer genome atlas. *Cell Rep.* (2018) 23:239–64. doi: 10.1016/j.celrep.2018.03.076

27. Yuan H, Yan M, Zhang G, Liu W, Deng C, Liao G, et al. CancerSEA: a cancer single-cell state atlas. *Nucl Acids Res.* (2019) 47:D900–D8. doi: 10.1093/nar/gky939

28. Jordan NV, Bardia A, Wittner BS, Benes C, Ligorio M, Zheng Y, et al. HER2 expression identifies dynamic functional states within circulating breast cancer cells. *Nature.* (2016) 537:102–6. doi: 10.1038/nature19328

29. Kaemmerer D, Peter L, Lupp A, Schulz S, Sänger J, Baum RP, et al. Comparing of IRS and Her2 as immunohistochemical scoring schemes in gastroenteropancreatic neuroendocrine tumors. *Int J Clin Exp Pathol.* (2012) 5:187–94. doi: 10.1111/his.12662

30. Min K-W, Chae SW, Kim D-H, Do S-I, Kim K, Lee HJ, et al. Fascin expression predicts an aggressive clinical course in patients with advanced breast cancer. *Oncol Lett.* (2015) 10:121–30. doi: 10.3892/ol.2015.3191

31. Jessurun CAC, Vos JAM, Limpens J, Luiten RM. Biomarkers for response of melanoma patients to immune checkpoint inhibitors: a systematic review. *Front Oncol.* (2017) 7:233. doi: 10.3389/fonc.2017.00233

32. Zhang X, Shi M, Chen T, Zhang B. Characterization of the immune cell infiltration landscape in head and neck squamous cell carcinoma to aid immunotherapy. *Mol Ther Nucl Acids.* (2020) 22:298–309. doi: 10.1016/j.omtn.2020.08.030

33. Ochiai K, Watanabe M, Ueki H, Huang P, Fujii Y, Nasu Y, et al. Tumor suppressor REIC/Dkk-3 interacts with the dynein light chain, Tctex-1. *Biochem Biophys Res Commun.* (2011) 412:391–5. doi: 10.1016/j.bbrc.2011.07.109

34. Mizobuchi Y, Matsuzaki K, Kuwayama K, Kitazato K, Mure H, Kageji T, et al. REIC/Dkk-3 induces cell death in human malignant glioma. *Neuro Oncol.* (2008) 10:244–53. doi: 10.1215/15228517-2008-016

35. Kawasaki K, Watanabe M, Sakaguchi M, Ogasawara Y, Ochiai K, Nasu Y, et al. REIC/Dkk-3 overexpression downregulates P-glycoprotein in multidrug-resistant MCF7/ADR cells and induces apoptosis in breast cancer. *Cancer Gene Ther.* (2009) 16:65–72. doi: 10.1038/cgt.2008.58

36. Gubin MM, Zhang X, Schuster H, Caron E, Ward JP, Noguchi T, et al. Checkpoint blockade cancer immunotherapy targets tumour-specific mutant antigens. *Nature.* (2014) 515:577–81. doi: 10.1038/nature13988

37. Carreno BM, Magrini V, Becker-Hapak M, Kaabinejadian S, Hundal J, Petti AA, et al. Cancer immunotherapy. A dendritic cell vaccine increases the breadth and diversity of melanoma neoantigen-specific T cells. *Science.* (2015) 348:803–8. doi: 10.1126/science.aaa3828

38. Sharma P, Shen Y, Wen S, Yamada S, Jungbluth AA, Gnjatic S, et al. CD8 tumor-infiltrating lymphocytes are predictive of survival in muscle-invasive urothelial carcinoma. *Proc Natl Acad Sci U S A.* (2007) 104:3967–72. doi: 10.1073/pnas.0611618104

39. Ni Y, Soliman A, Joehlin-Price A, Rose PG, Vlad A, Edwards RP, et al. High TGF-β signature predicts immunotherapy resistance in gynecologic cancer patients treated with immune checkpoint inhibition. *NPJ Precis Oncol.* (2021) 5:101. doi: 10.1038/s41698-021-00242-8

frontiers | Frontiers in Medicine

TYPE Original Research
PUBLISHED 18 May 2023
DOI 10.3389/fmed.2023.1194046

OPEN ACCESS

EDITED BY
Zheng Wang,
Shanghai Jiao Tong University, China

REVIEWED BY
Xinyuan Ding,
Suzhou Municipal Hospital, China
Yanfeng Liu,
Shanghai Jiao Tong University, China

*CORRESPONDENCE
Chuan Wang
✉ dr_chuanwang@fjmu.edu.cn
Debo Chen
✉ debochensr@fjmu.edu.cn

RECEIVED 26 March 2023
ACCEPTED 17 April 2023
PUBLISHED 18 May 2023

CITATION
Lian W, Yang P, Li L, Chen D and Wang C (2023) A ceRNA network-mediated over-expression of cuproptosis-related gene SLC31A1 correlates with poor prognosis and positive immune infiltration in breast cancer.
Front. Med. 10:1194046.
doi: 10.3389/fmed.2023.1194046

A ceRNA network-mediated over-expression of cuproptosis-related gene SLC31A1 correlates with poor prognosis and positive immune infiltration in breast cancer

Weibin Lian[1,2], Peidong Yang[1], Liangqiang Li[1], Debo Chen[1]* and Chuan Wang[2]*

[1]Department of Breast Surgery, Quanzhou First Hospital Affiliated to Fujian Medical University, Quanzhou, Fujian, China, [2]Department of Breast Surgery, Fujian Medical University Union Hospital, Fuzhou, Fujian, China

Introduction: Solute carrier family 31 member 1(SLC31A1) has been reported as the copper importer, and was identified to be involved in the process of "cuproptosis". However, the mechanism of SLC31A1 in breast cancer remains unclear.

Methods: We examined the expression of SLC31A1 mRNA in breast cancer tissues and cell lines using Real-time PCR. The data for this study were obtained from The Cancer Genome Atlas (TCGA) database and analyzed via R 3.6.3. TIMER, UALCAN, GEPIA2, STRING, Metascape, Kaplan–Meier Plotter, starBase and miRNet websites were used for a comprehensive analysis of SLC31A1.

Results: Our study suggested that SLC31A1 mRNA was over-expressed in breast tumor tissue and breast cancer cell lines, and which was closely related to poor relapse-free survival (RFS) and distant metastasis-free survival (DMFS). In addition, we constructed a co-expression network of SLC31A1. Functional enrichment analysis indicated that they were mainly involved in copper ion transport. Interestingly, SLC31A1 expression was positively associated with all m6A-related genes, especially with YTHDF3 (r = 0.479). Importantly, the LINC00511/miR-29c-3p/SLC31A1 axis was identified as the most potential pathway promoting breast cancer progress by affecting copper transport. Furthermore, the expression level of SLC31A1 in breast cancer was positively correlated with tumor immune cell infiltration, immune cell biomarkers and cancer-associated fibroblast (CAF).

Conclusion: Up-regulation of SLC31A1 expression and regulation of copper ion transport mediated by LINC00511-miR-29-3p axis is related to poor prognosis and positively correlated with tumor immune infiltration in breast cancer.

KEYWORDS

SLC31A1, breast cancer, ceRNA, prognosis, immune infiltrates, m6A

Background

As the Global Cancer Statistics 2020 reported, breast cancer (BRCA) had become the world's most commonly diagnosed cancer (1). Although there are many comprehensive treatments including surgery, chemotherapy, radiotherapy, and targeted therapy, some people still experience recurrence and death. The development of novel biomarkers and more effective treatments for breast cancer is needed desperately.

Recently, the term "cuproptosis" was first proposed by Peter et al. and is considerably different from other cell death types (2). Solute carrier family 31 member 1 (SLC31A1) has been reported as the copper importer and was identified as a critical gene involved in the process of "cuproptosis" (2, 3). SLC31A1 over-expression induces a distinct form of necrotic cell death in cells, i.e., cuproptosis, which differed from the classical cell death entities known. Caroline et al. have reported that the genetic loss of SLC31A1 decreased the viability and clonogenic survival of human hepatocellular carcinoma cell lines (4). The study of Yu et al. identified SLC31A1 as a regulatory node mediating copper ion transport and revealed a mechanism through which copper promotes pancreatic cancer progression (5). However, as a copper death-related gene, the mechanism of SLC31A1 in breast cancer remains unclear.

Numerous studies have shown that long non-coding RNA (lncRNA) or microRNA (miRNA) promotes breast cancer progression by regulating target genes (6, 7). Competing endogenous RNA (ceRNA) is an acting element capable of competitive binding to RNA. Previous studies indicated that ceRNA networks could link the functions of protein-coding mRNAs with non-coding RNA (ncRNA) functions to promote tumorigenesis (8). In this study, we predicted the regulation of non-coding RNA (ncRNA) related to SLC31A1 in breast cancer and attempted to construct a ceRNA network. In addition, a recent study from Chen et al. showed that mRNA N6-methyladenosine (m6A) could promote lung metastasis of breast cancer by affecting the translation efficiency of KRT7 (9). Therefore, we try to explore the correlation between the SLC31A1 expression and m6A-related genes. At present, programmed death receptor 1 (PD-1) and programmed death ligand 1 (PD-L1) immune checkpoint inhibitors have been approved for the treatment of triple-negative breast cancer. Our study further explores the connection between SLC31A1 and tumor immune infiltration to search for more suitable immunotherapy targets.

Materials and methods

Expression and survival analysis

Solute carrier family 31 member 1 (SLC31A1) mRNA expression data and clinicopathological characteristics in breast cancer were downloaded from the Cancer Genome Atlas (TCGA). The median expression of SLC31A1 was used to separate high/low expression groups. Human breast cancer tissues ($n = 27$) and normal breast tissues adjacent to the tumor ($n = 27$) were obtained from our breast center, Fujian Medical University Union Hospital. We perform prognostic analysis through the Kaplan–Meier Plotter website[1].

Functional enrichment analysis

STRINGS[2] is an online website, which was used for protein–protein interaction (PPI) network analysis on SLC31A1. The result revealed that there were 10 proteins binding with SLC31A1, including ATP7B, MTF1, SLC22A2, ZBED3, CCS, CP, COX17, ATP7A, SLC11A2, and ATOX1. Furthermore, we, respectively, obtained the top 50 significant genes that are positively correlated and negatively correlated with SLC31A1 through the GEPIA2 website[3] and the UALCAN website[4]. We took an intersection of 100 related genes between these two data sets and obtained 65 common genes (Figure 1A). Combined with 10 binding proteins and 65 related genes of SLC31A1, the functional enrichment analysis was performed by the Metascape website[5].

Relationship between the SLC31A1 expression and m6A-related genes

Our study attempted to explore the relationship between the SLC31A1 expression and the expression of m6A-related genes in BRCA, and a correlation heat map was used to demonstrate them. All m6A-related genes analyzed are shown in Figure 2.

Prediction of miRNA

The starBase website[6] is an open-source platform, which was used for decoding miRNA–ceRNA and miRNA–ncRNA interaction networks in our study (10, 11). The website integrates seven databases, containing PITA, RNA22, miRmap, microT, miRanda, PicTar, and TargetScan, and was employed to forecast upstream miRNAs potentially binding to SLC31A1. The CLIP data of the website for this study was set as strict stringency (≥5), and the other basic settings as default. In this study, at least three database-predicted miRNAs were included in the analysis. Then, we established the miRNA-SLC31A1 regulatory network with Cytoscape software. In addition, we used this website for the correlation analysis between target lncRNA and miRNA.

Prediction of lncRNA and ceRNA network construction

The website miRNet[7] is an integrated open-source platform linking miRNAs from several miRNA-linked databases (TarBase, miRTarBase, miRecords, and miRanda). In this study, we predicted potential target lncRNAs of miRNA via this website. Subsequently, lncRNAs predicted by miRNet and starBase database were intersected to obtain the most potential regulatory lncRNAs. A comprehensive analysis of integrative miRNA–mRNA and miRNA–lncRNA was

1 http://kmplot.com/analysis/index.php?p=service

2 https://string-db.org/, version: 11.5.

3 http://gepia2.cancer-pku.cn/#index

4 http://ualcan.path.uab.edu/analysis-prot.html

5 https://metascape.org/gp/index.html#/main/step1

6 www.starbase.sysu.edu.cn

7 https://www.mirnet.ca/

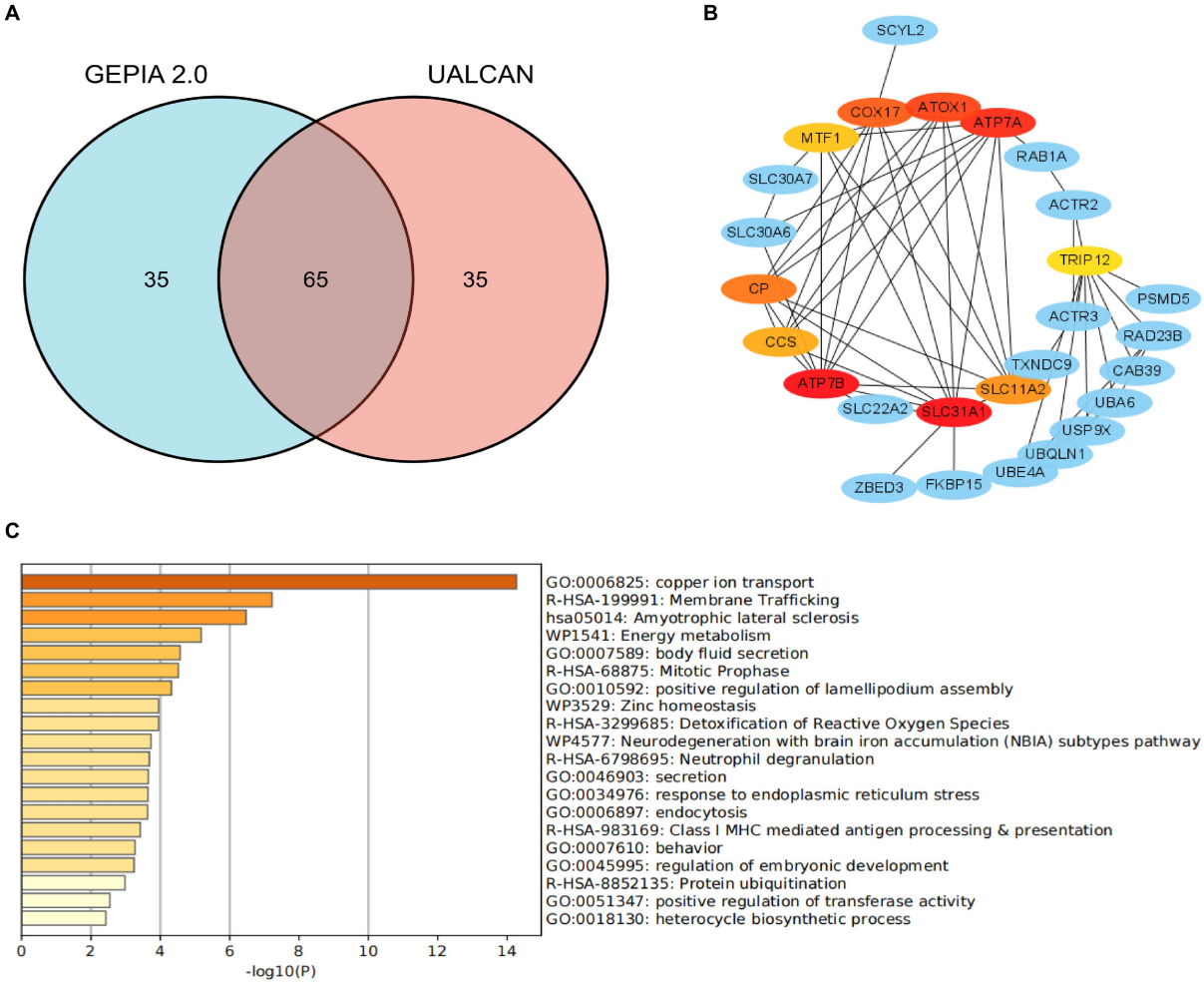

FIGURE 1
Co-expression network of SLC31A1 and functional enrichment analysis. **(A)** Venn diagram of the SLC31A1-related genes of breast cancer from GEPIA2.0 and UALCAN websites. **(B)** SLC31A1-related gene co-expressed network. **(C)** Functional enrichment analysis of co-expressed genes of SLC31A1.

conducted with a negative correlation between expression levels to establish a key lncRNA–miRNA–mRNA (SLC31A1) ceRNA network for BRCA.

Immune infiltration analysis

The Tumor Immune Estimation Resource (TIMER)[8] was used for a comprehensive analysis of tumor-infiltrating immune cells in our study. Several researchers have suggested that tumor-infiltrating lymphocytes(TILs) were evaluated as a prognostic feature in multiple molecular subtypes of BRCA (12–14). Our study attempted to analyze the associations and prognosis between immune infiltrate cells (CD8+ T cells, CD4+ T cells, B cells, dendritic cells, macrophages, and neutrophils) and SLC31A1 expression by the TIMER website. In addition, we analyzed the correlation between the expression level of SLC31A1 in BRCA and the immune marker. A recent study has shown that cancer-associated fibroblast(CAF)plays a vital role in cancer progression and immunity (15). CAF is a stromal component that constitutes the tumor microenvironment (TME). To evaluate the role of SLC31A1 in the tumor microenvironment, we analyzed the correlation between the SLC31A1 expression and CAF in pan-cancer by the TIMER 2.0 website[9].

Cell lines culture

In this study, breast cancer cell lines (MCF-7 and BT-549) and the non-tumorigenic epithelial breast cell line (MCF-10A) were purchased from the Chinese Academy of Sciences (Shanghai, China) and cultured at 37°C with 5% CO_2 in a humidified incubator. The DMEM medium (Gibco) with 10% fetal bovine serum (FBS; Gibco) was used

8 https://cistrome.shinyapps.io/timer/

9 http://timer.cistrome.org/

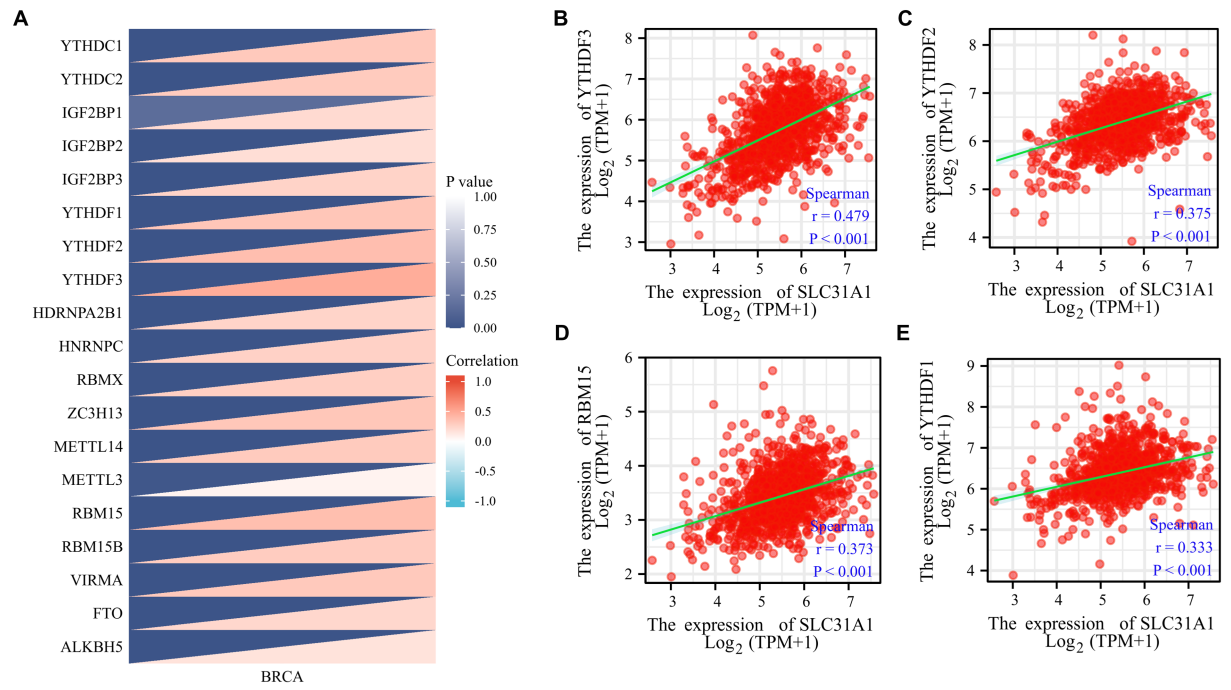

FIGURE 2
Correlations of the SLC31A1 expression with m6A-related genes in breast cancer based on the TCGA database. **(A)** Correlation between the expression level of SLC31A1 and m6A-related genes. **(B–E)** The expression of SLC31A1 was positively associated with YTHDF3 **(B)**, YTHDF2 **(C)**, RBM15 **(D)**, and YTHDF1 **(E)**. Spearman's rank correlation coefficient was applied for correlation analysis.

to culture MCF-7 and BT-549 cell lines. DMEM/Ham's F-12 (1,1; Gibco) with 5% FBS (Gibco) was used to culture MCF-10A.

RNA extraction and quantitative real-time PCR

Total RNA was isolated from cells using Trizol (Takara, Dalian, China) and reverse transcribed by using the PrimeScriptTM RT reagent kit (TaKaRa). Real-time PCR(RT-qPCR)was performed using the SYBR Premix Ex Taq II kit (Takara). GAPDH was used as an internal reference, and the relative expression of SLC31A1 mRNAs was quantified using the $2-\Delta\Delta Ct$ method. Primer sequences were: SLC31A1 forward, 5'-GCTACTTCCTCATGCTCATCTTC-3′; SLC31A1 reverse, 5'-TATCCACTACCACTGCCTTCTT-3′; GAPDH forward, 5'-GTCTCCTCTGACTTCAACAGCG-3′; and. GAPDH reverse, 5'-ACCACCCTGTTGCTGTAGCCAA-3′.

Statistical analysis

In this study, the Xiantao Academic website[10] was used to perform most of the statistical analysis. Furthermore, we also conducted mapping and statistical analysis through GraphPad Prism software (version 7.0). Spearman's rank correlation coefficient was applied for correlation analysis. A value of p of <0.05 was considered statistically significant. The *t*-test was used to compute statistical significance and annotated by the number of stars (*, value of p <0.05; **, value of p <0.01; and ***, value of p <0.001).

Results

SLC31A1 was over-expressed in breast tumor tissues and cell lines

To determine whether SLC31A1 plays a role in human cancers, we first examined the expression level of SLC31A1 in the TCGA database. Our result suggested that the expression of SLC31A1 mRNA was upregulated in 22 tumor types while downregulated in four tumor types compared with the normal tissue (Figure 3A). In a further pairwise comparison, SLC31A1 mRNA expression was also upregulated in BRCA (Figure 3B). Furthermore, we examined the expression of SLC31A1 using real-time PCR in human breast samples, breast tumor cell lines (MCF-7 and BT-549), and human mammary epithelial cells (MCF10A). The result revealed that the mRNA expression level of SLC31A1 was higher in breast cancer tissues than in normal breast tissues (Figure 3C). Similarly, the mRNA expression level of SLC31A1 was also higher in the luminal (MCF-7) cell line and triple-negative breast tumor cell line (BT-549) than in normal breast cell lines (MCF-10A) (Figure 3D). Furthermore, we found that the expression level of SLC31A1 in the tumor tissue of all breast cancer subtypes was higher than that in the normal tissue through the UALCAN website (Figure 3E).

10 https://www.xiantao.love/products/apply/c0b6febb-52dd-4525-970a-61bbe9e263ff/collect

Correlation of SLC31A1 with clinicopathological characteristics and survival analysis

In our study, the correlation between the SLC31A1 expression and clinicopathological characteristics in breast cancer patients based on the TCGA database was analyzed. As shown in Table 1, the differential expression of SLC31A1 was significantly related to race ($p = 0.004$), ER status ($p < 0.001$), HER2 status ($p = 0.026$), and PAM50 ($p < 0.001$). Furthermore, the Kaplan–Meier survival analysis showed that the high expression of SLC31A1 in breast cancer patients was related to the worse relapse-free survival (RFS) (HR = 1.48, $p = 2.7e\text{-}14$) (Figure 4A), distant metastasis-free survival (DMFS) (HR = 1.24, $p = 0.0061$) (Figure 4B), and worse overall survival (OS) trend (HR = 1.19, $p = 0.075$) (Figure 4C).

Co-expression network of SLC31A1 and functional enrichment analysis

As shown in Figure 1B, we constructed a co-expression network with 10 interacting proteins and 65 common co-expressed genes. Functional enrichment analysis indicated that these genes were significantly related to copper ion transport, body fluid secretion, positive regulation of lamellipodium assembly, and so on (Figure 1C). These results suggested that SLC31A1 interaction with these proteins may affect the transfer of copper ions and induce cuproptosis.

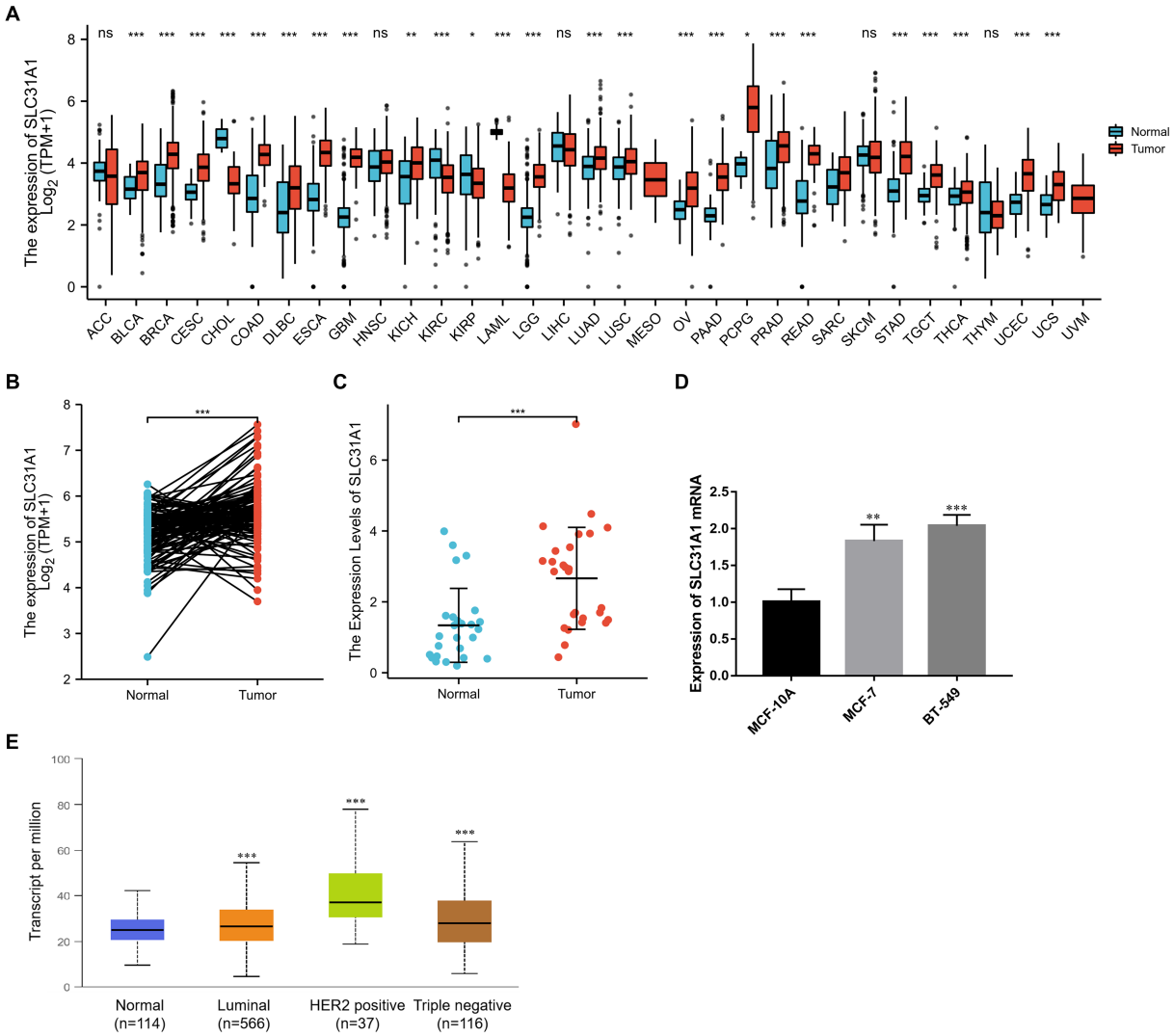

FIGURE 3
Differential expression of SLC31A1 in breast cancer (BRCA). **(A)** SLC31A1 mRNA expression in pan-cancer tissues compared to normal tissues based on the TCGA database. **(B)** SLC31A1 mRNA expression of tumor tissues in BRCA compared to pairwise normal tissues based on TCGA database. **(C)** The mRNA expression level of SLC31A1 is higher in breast cancer tissues (n =27) than in paired normal breast tissues (n =27). **(D)** SLC31A1 mRNA expression in different breast cancer cell lines (MCF-7 and BT-549) and human mammary epithelial cells (MCF-10A). **(E)** SLC31A1 mRNA expression in different breast cancer molecular subtypes. The t-test was used to compare the expression differences between the two groups. *p <0.05, **p <0.01, and ***p <0.001.

TABLE 1 Correlation of SLC31A1 with clinicopathological characteristics in The Cancer Genome Atlas (TCGA) cohort.

Characteristic	Low expression of SLC31A1	High expression of SLC31A1	*p*
N (%)	541	542	
Age			0.739
<=60	297 (27.4%)	304 (28.1%)	
>60	244 (22.5%)	238 (22%)	
Race			0.004
Asian	26 (2.6%)	34 (3.4%)	
Black or African American	112 (11.3%)	69 (6.9%)	
White	370 (37.2%)	383 (38.5%)	
T stage			0.610
T1	140 (13%)	137 (12.7%)	
T2	312 (28.9%)	317 (29.4%)	
T3	73 (6.8%)	66 (6.1%)	
T4	14 (1.3%)	21 (1.9%)	
N stage			0.251
N0	266 (25%)	248 (23.3%)	
N1	179 (16.8%)	179 (16.8%)	
N2	60 (5.6%)	56 (5.3%)	
N3	30 (2.8%)	46 (4.3%)	
M stage			0.616
M0	435 (47.2%)	467 (50.7%)	
M1	8 (0.9%)	12 (1.3%)	
Pathologic stage			0.769
Stage I	97 (9.2%)	84 (7.9%)	
Stage II	308 (29.1%)	311 (29.3%)	
Stage III	124 (11.7%)	118 (11.1%)	
Stage IV	8 (0.8%)	10 (0.9%)	
ER status			< 0.001
Negative	94 (9.1%)	146 (14.1%)	
Indeterminate	1 (0.1%)	1 (0.1%)	
Positive	421 (40.7%)	372 (35.9%)	
PR status			0.062
Negative	155 (15%)	187 (18.1%)	
Indeterminate	3 (0.3%)	1 (0.1%)	
Positive	358 (34.6%)	330 (31.9%)	
HER2 status			0.026
Negative	276 (38%)	282 (38.8%)	
Indeterminate	8 (1.1%)	4 (0.6%)	
Positive	61 (8.4%)	96 (13.2%)	
PAM50			< 0.001
Normal	17 (1.6%)	23 (2.1%)	
LumA	320 (29.5%)	242 (22.3%)	
LumB	94 (8.7%)	110 (10.2%)	
Her2	21 (1.9%)	61 (5.6%)	
Basal	89 (8.2%)	106 (9.8%)	

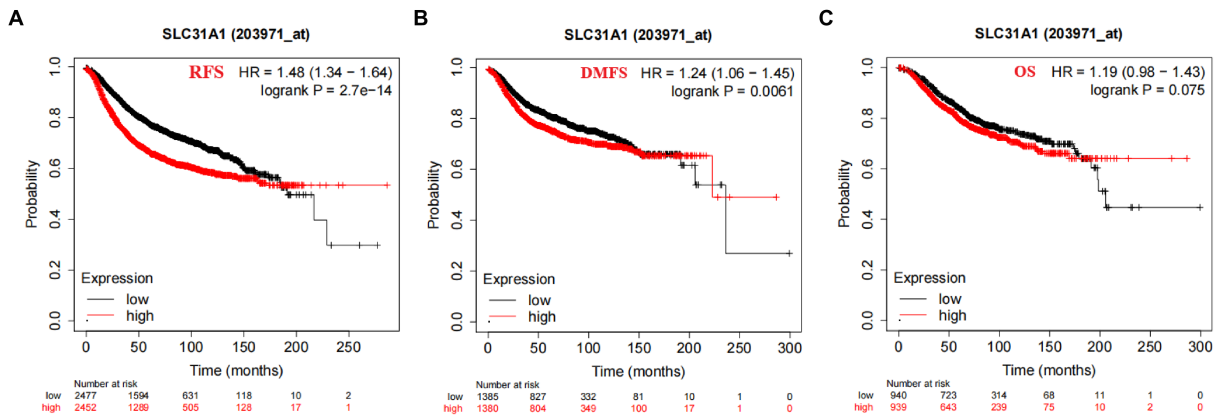

FIGURE 4
Correlation of SLC31A1 mRNA expression and survival in breast cancer from the Kaplan–Meier Plotter website. **(A)** The Kaplan–Meier curve of the relapse-free survival (RFS) probability in 203971_at breast cancer cohort. **(B)** The Kaplan–Meier curve of the distant metastasis-free survival (DMFS) probability in 203971_ at the breast cancer cohort. **(C)** The Kaplan–Meier curve of the overall survival (OS) probability in 203971_ at the breast cancer cohort.

The SLC31A1 expression and m6A RNA methylation-related genes

More recently, m6A modifications are associated with breast cancer progression (16, 17). To further assess whether SLC31A1 is related to m6A modification, we assessed the association between the expression of SLC31A1 and 20 m6A-related genes in breast cancer. Results revealed that the SLC31A1 expression was significantly positively associated with all m6A-related genes in breast cancer (Figure 2A). Importantly, the SLC31A1 expression was strongly positively associated with YTHDF3 ($r = 0.479$, $p < 0.001$), YTHDF2 ($r = 0.375$, $p < 0.001$), RBM15 ($r = 0.373$, $p < 0.001$), and YTHDF1 ($r = 0.333$, $p < 0.001$) (Figures 2B–E).

Predicted upstream potential miRNA of SLC31A1

Many studies have proven that miRNA plays its biological function by participating in the regulation of the translation process of its downstream genes. A recent study showed that an ATPase copper transporter promotes breast cancer cells' cisplatin resistance by being negatively regulated by miR-148a-3p (18). Therefore, our study attempted to predict the upstream regulatory miRNA genes of SLC31A-the copper death-related gene. As shown in Figure 5A, we finally screened out 15 predicted miRNAs that could bind to SLC31A1 through the starBase website. Furthermore, we performed a prognostic analysis of predicted miRNAs and an expression correlation analysis between miRNA and SLC31A1. Hsa-miR-28-5p, hsa-miR-29a-3p, hsa-miR-31-5p, hsa-miR-98-5p, hsa-miR-29b-3p, hsa-miR-124-3p, hsa-miR-29c-3p (Figure 5D), hsa-miR-196b-5p, and hsa-miR-543 were favorable prognostic biomarkers for OS of patients with breast cancer, while hsa-miR-105-5p, hsa-miR-219a-5p, and hsa-miR-193b-5p were unfavorable prognostic biomarkers (Figure 5B). The expression correlation between predicted miRNAs and SLC31A1 in breast cancer using the starBase database is shown in Figure 5C and Supplementary Table S1. As shown in Figure 5E, hsa-miR-29c-3p had the strongest negative correlation with SLC31A1 expression. Combined with these results, hsa-miR-29c-3p was identified to be the most potential miRNA regulating SLC31A1 in breast cancer.

LINC00511-Mir-29c-3p-SLC31A1 axis is a potential pathway promoting breast cancer progress by affecting copper transport

A growing body of evidence has revealed that lncRNA promotes breast cancer progression and functions as ceRNA to target genes by affecting mi-RNA (6, 19, 20). Therefore, we predicted potential lncRNAs that might bind to hsa-miR-29c-3p by starBase and miRNet websites and then took the intersection (Figure 6A). We finally found 52 common predicted lncRNAs, and then the lncRNA-hsa-miR-29c-3p regulatory network was constructed using Cytoscape software (Figure 6B). The TCGA database was used to determine whether these lncRNAs were differentially expressed in breast cancer tissues compared to normal tissues. As shown in Figure 6C, a total of eight lncRNAs were significantly downregulated or upregulated in breast cancer compared to the normal tissues. The prognostic value of these eight lncRNAs in breast cancer was then evaluated. However, all eight lncRNAs show no statistically significant difference in survival(data not shown). Subsequently, the starBase database was used to evaluate the expression correlation between these eight lncRNAs and hsa-miR-29c-3p. The strongest negative expression correlation between LINC00511 and hsa-miR-29c-3p ($R = -0.368$, $p = 4.62e\text{-}36$) is shown in Figure 6D and Supplementary Table S2. Combined with the expression analysis, survival analysis, and correlation analysis, LINC00511 was considered the most significant lncRNA upstream of the hsa-miR-29c-3p/SLC31A1 axis in breast cancer.

Positive correlation between the SLC31A1 expression and tumor immune infiltration

A recent study showed that intratumoral and stromal CD4+ T cell density is an independent predictor of pCR in triple-negative patients

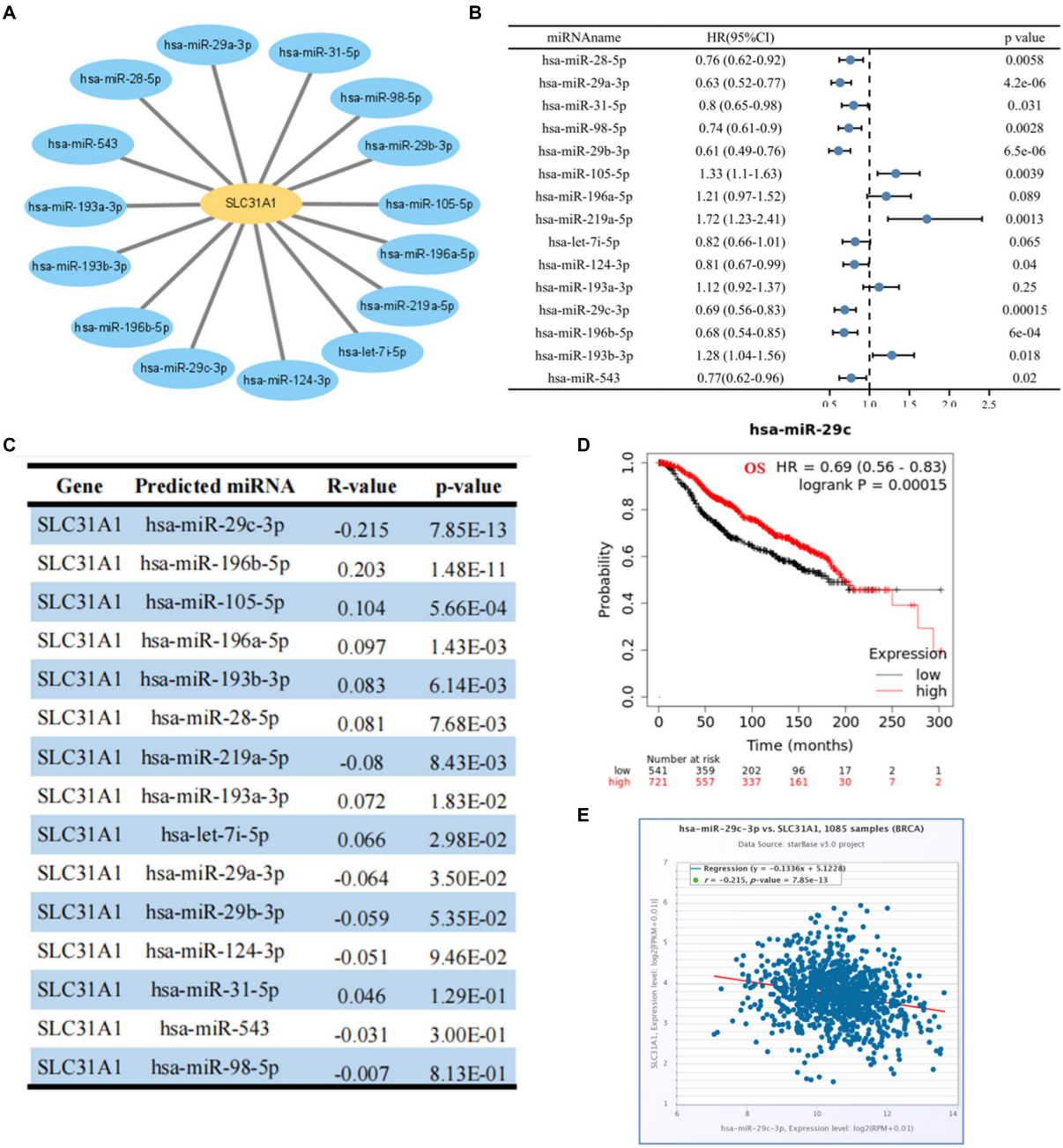

FIGURE 5
Identification of upstream potential miRNA of SLC31A1 in breast cancer. **(A)** miRNA-SLC31A1 network constructed by Cytoscape software. **(B)** Prognostic analysis (overall survival, OS) of potential upstream miRNAs of SLC31A1 in breast cancer using forest plots. **(C)** Expression correlation between predicted miRNAs and SLC31A1 in breast cancer using starBase database. **(D)** Overall survival (OS) analysis for hsa-miR-29c-3p in breast cancer. **(E)** Scatter plot about the correlation between the expression of SLC31A1 and hsa-miR-29c-3p in breast cancer obtained from the starBase database.

(21). Our study attempted to investigate whether the expression of SLC31A1 is related to the level of immune infiltration in breast cancer through the TIMER website. The SLC31A1 expression showed a positive correlation with the levels of B cells (cor = 0.186, p = 4.44e-6), CD8+ T cells (cor = 0.341, p = 5.58e-28), CD4 + T cells (cor = 0.103, p = 1.32e-3), macrophages (cor = 0.24, p = 2.12e-14), neutrophils (cor = 0.291, p = 5.07e-20), and dendritic cells (DC, cor = 0.231, p = 5.84e-13) (Figure 7A). B cells, macrophages, and dendritic cells have been reported to be associated with tumor immune escape. Therefore, SLC31A1 may positively regulate B cells, macrophages, and dendritic cells to promote tumor immune escape. Furthermore, we analyzed the differential expression of 24 immune cells between the high SLC31A1 expression group and the low SLC31A1 expression group in breast cancer. Compared with the low expression group, aDC, DC, iDC, macrophage, neutrophil, T helper cells, Tcm, Tgd, Th1, and Th2 increased in the high expression group of SLC31A1,

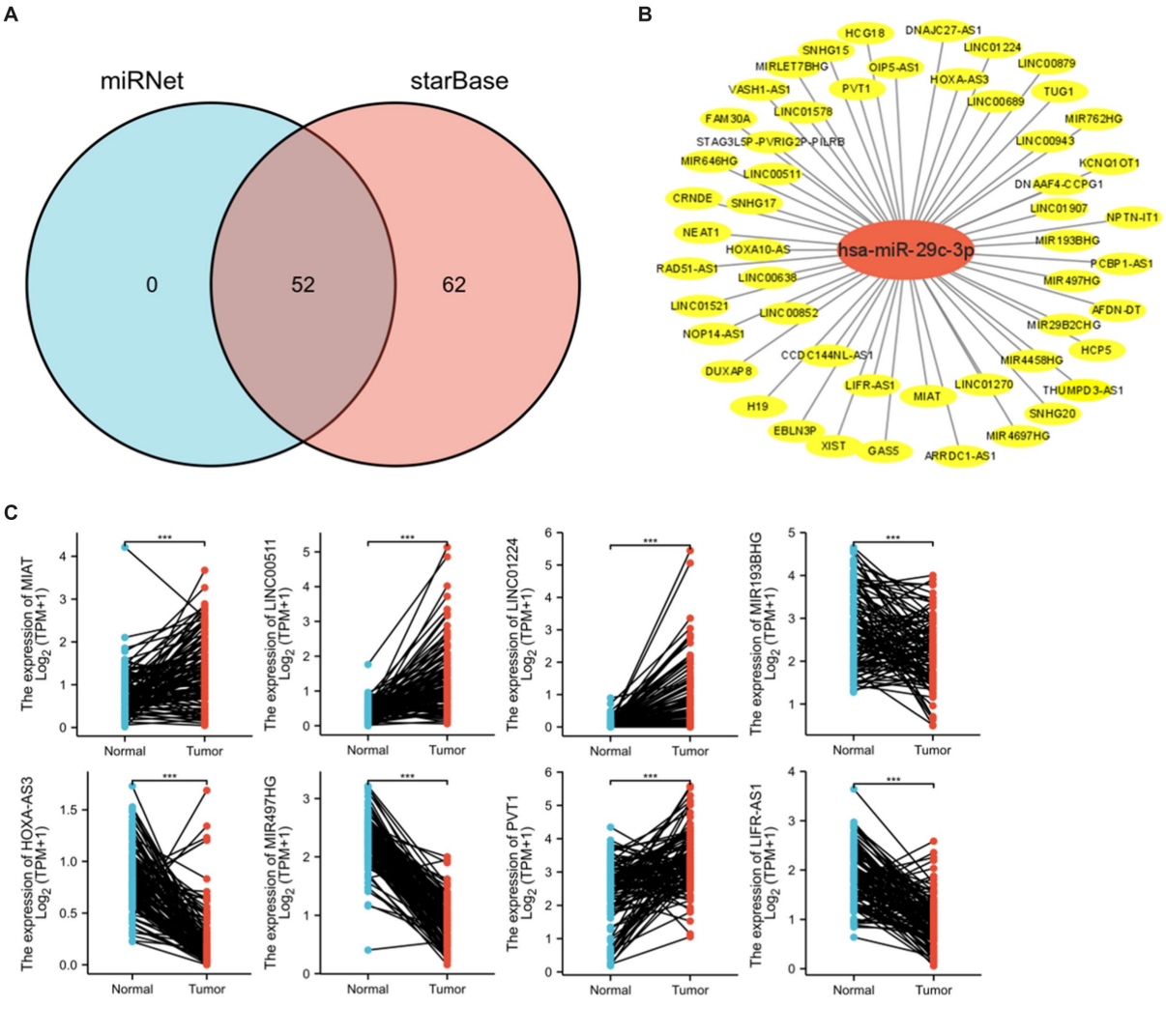

D

miRNA	Predicted lncRNA	R-value	*p*-value
hsa-miR-29C-3P	LINC00511	-0.368	4.62E-36
hsa-miR-29C-3P	LIFR-AS1	0.256	1.13E-17
hsa-miR-29C-3P	MIR497HG	0.247	1.33E-16
hsa-miR-29C-3P	LINC01224	0.123	4.95E-05
hsa-miR-29C-3P	HOXA-AS3	-0.091	2.58E-03
hsa-miR-29C-3P	PVT1	0.087	4.10E-03
hsa-miR-29C-3P	MIAT	0.048	1.13E-01
hsa-miR-29C-3P	MIR193BHG	0.013	6.71E-01

FIGURE 6
Identification of upstream potential lncRNA of hsa-miR-29c-3p in breast cancer. **(A)** Venn diagram of upstream potential lncRNA of hsa-miR-29c-3p from miRNet and starBase websites. **(B)** lncRNA-hsa-miR-29c-3p network constructed by Cytoscape software. **(C)** Eight of the 52 predicted lncRNAs are differentially expressed in breast cancer based on the TCGA database. **(D)** Expression correlation in breast cancer between predicted lncRNAs and hsa-miR-29c-3p using starBase database. The *t*-test was used to compare the expression differences between the two groups. **p* <0.05, ***p* <0.01, ****p* <0.001.

while CD8 + T cell, NK CD56bright cells, and pDC decreased (Figure 7B). In addition, we explored the correlation between SLC31A1 and immune markers of various tumor immune infiltration cells in breast cancer. The results showed that the expression of SLC31A1 was significantly positively correlated with immune markers in breast cancer, especially for STAT3 of Th17 ($r = 0.382$, $p < 0.001$),

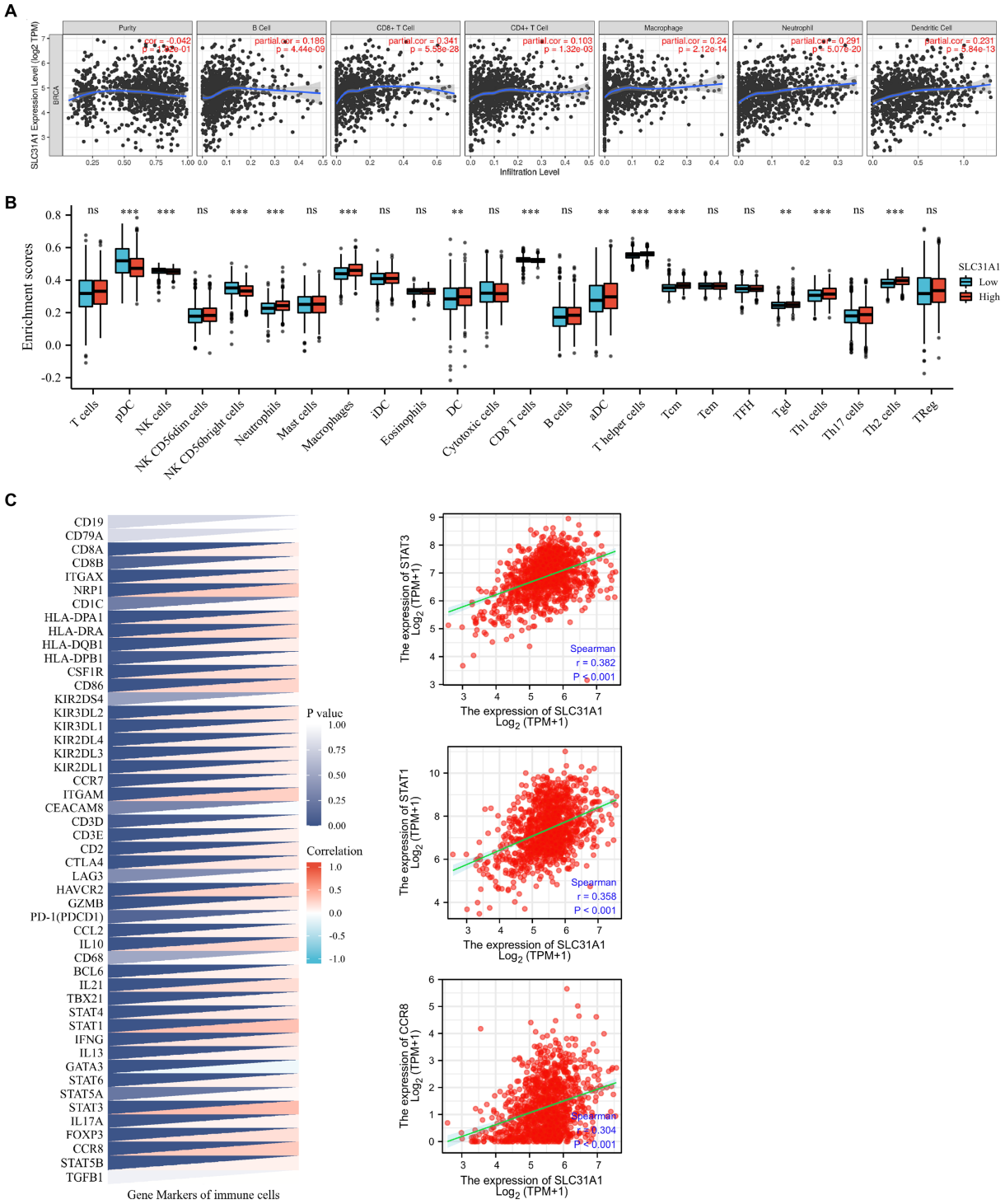

FIGURE 7
Correlations of the SLC31A1 expression with immune cells infiltration and immune markers in breast cancer. **(A)** The expression of SLC31A1 was significantly correlated with infiltrating levels of B cells, CD8+T cells, CD4+T cells, macrophages, neutrophils, and dendritic cells in breast cancer. The SLC31A1 expression levels against tumor purity adjustment are displayed on the left-most panel. **(B)** The difference in enrichment scores of 24 immune cell types between the SLC31A1 high and low expression groups. **(C)** Correlation between SLC31A1 and immune markers of various tumor immune infiltration cells in breast cancer. The *t*-test is used to compare the expression differences between the two groups. **p* <0.05, ***p* <0.01, ****p* <0.001.

STAT1 of Th1 ($r = 0.358$, $p < 0.001$), and CCR8 of Treg ($r = 0.304$, $p < 0.001$) (Figure 7C).

Several studies have shown that CAF plays an essential role in TME and correlates with resistance and tumor progression (22–24). Therefore, we analyzed the correlation between the SLC31A1 expression and CAF by the TIMER 2.0 website. We found that the SLC31A1 expression was positively related to CAF in most tumors (Figure 8A). For BRCA-LumA disease, the SLC31A1 expression was

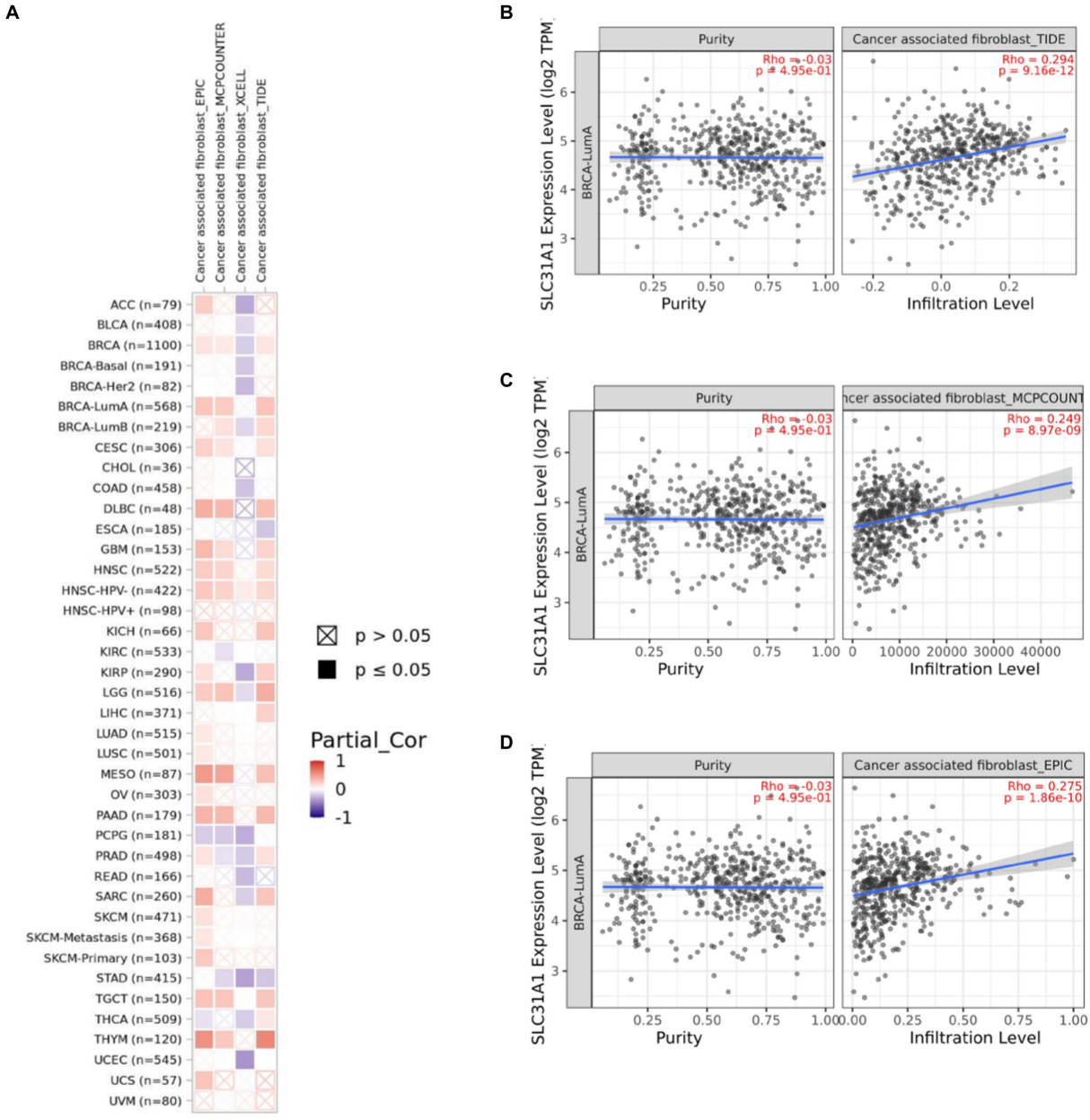

FIGURE 8
Correlation of the SLC31A1 expression and cancer-associated fibroblast(CAF)by TIMER 2.0 website. **(A)** Correlation of the SLC31A1 expression and CAF in pan-cancers. **(B)** The SLC31A1 expression in the BRCA-LumA subtype was positively associated with CAF by the TIDE algorithm. **(C)** The SLC31A1 expression in the BRCA-LumA subtype was positively associated with CAF by the MCPCOUNTER algorithm. **(D)** The SLC31A1 expression in the BRCA-LumA subtype was positively associated with the CAF by EPIC algorithm. *The SLC31A1 expression levels against tumor purity adjustment were displayed on the left panel.

positively associated with CAF by TIDE (Figure 8B), MCPCOUNTER (Figure 8C), and EPIC (Figure 8D) algorithms on the TIMER 2.0 website.

Discussion

Copper is an essential metal nutrient for normal physiology. It has been demonstrated that enhanced copper levels in tumors lead to cancer progression (25). As the copper importer, SLC31A1 was identified as an important regulatory gene in copper death. Research has shown that the SLC31A1 expression level was correlated with the malignant degree of pancreatic cancer. However, the expression level and function of SLC31A1 in breast cancer are still unclear.

This study analyzed the expression and prognostic value of SLC31A1 in breast cancer and constructed a ceRNA regulatory network. We found that the expression of SLC31A1 mRNA was upregulated in breast cancer tissues and breast cancer cell lines. Further subgroup analysis showed that the expression level of SLC31A1 in breast cancer tissues of all subtypes (luminal, HER2

positive, and triple negative) was higher than that in normal breast tissues. In addition, high expression of SLC31A1 was associated with worse RFS and DMFS. The study by Rachel et al. showed that the expression of SLC31A1 is closely related to the efficacy of platinum-based anticancer regimens (26). Furthermore, we constructed a co-expression network of SLC31A1 and performed functional enrichment analysis, which is mainly responsible for the transport of copper ions. As shown in Figure 1B, ATP7A and ATP7B were the most important interacting proteins of SLC31A1. Previous studies have shown that ATPases-ATP7A and ATP7B serve as the major copper exporters and synergize with SLC31A1 maintaining copper homeostasis (27). Yu et al. found that copper deficiency makes pancreatic cancer cells dormant and leads to increased autophagy to resist the death of pancreatic cancer cells (5).

As is known, one of the most abundant posttranscriptional modifications in eukaryotic mRNA is m6A methylation. Yu et al. have reported that m6A "writer" METTL3 can downregulate COL3A1 expression by increasing its m6A methylation to inhibit TNBC cell metastasis (28). Our study suggested that the expression of SLC31A1 is strongly positively associated with YTHDF3, YTHDF2, RBM15, and YTHDF1. Chang et al. found that m6A "reader" YTHDF3 over-expression enhances the translation of m6A-enriched transcripts for ST6GALNAC5, GJA1, and EGFR, promoting brain metastases in breast cancer patients (29). A recent study from Ramesh et al. also showed that YTHDF3/ZEB1 axis plays an important role in the progression and metastasis of TNBC (30). However, there is no relevant study to prove the regulatory relationship between YTHDF3 and SLC31A1. Combined with our correlation analysis, YTHDF3 may upregulate the expression of SLC31A1 by increasing its m6A methylation, promoting the metastasis of breast cancer cells.

MicroRNAs (miRNAs) are a class of evolutionarily highly conserved small non-coding RNAs and primarily affect gene expression levels *via* targeting mRNA (31). Growing research suggested that miRNAs contribute to cancer progression by regulating target genes (32–34). Our study supported that miR-29c-3p is the most potentially binding miRNA of SLC31A1. Correlation analysis suggested a strongly negative relationship between SLC31A1 and hsa-miR-29c-3p. The hsa-miR-29c-3p-SLC31A1 axis was considered as the potential pathway involved in the progression of breast cancer by regulating copper transport. Kong et al. suggested that lncRNA-CDC6 promotes breast cancer progression and functions as ceRNA to target CDC6 by sponging microRNA-215 (20). A recent study from Lou et al. showed that RP11-480I12.5–004 promoted growth and tumorigenesis of breast cancer by competitively binding to miR-29c-3p (35). These studies suggested that lncRNA serves as a ceRNA to regulate the expression of target genes in cancer *via* sponging miRNA. Our study further predicted the upstream potential lncRNAs of hsa-miR-29c-3p. As shown in Figure 6F analysis, LINC00511 was considered the most potential lncRNA upstream of hsa-miR-29c-3p. Through comprehensive analysis of lncRNA, miRNA, and mRNA expression, we constructed a ceRNA network and named it the LINC00511/miR-29c-3p/SLC31A1 axis (Figure 9). The LINC00511/miR-29c-3p/SLC31A1 axis may promote invasion and metastasis in breast cancer through the regulation of copper transport.

A deep analysis based on TCGA and tissue microarrays showed a strong correlation between the expression of SLC31A1 and PD-L1 in many cancers but not in normal tissues. Florida et al. found that adequate copper can increase the expression of PD-1/PD-L1 in cancer cells, while a copper deficiency can be linked to PD-L1-driven cancer immune escape (36). Moreover, the addition of copper-chelating drugs significantly increased the number of CD8 + T and natural killer cells and slowed down the growth of tumors in mice (36). These results suggest that SLC31A1 is closely related to tumor immune infiltration. Our results suggest that SLC31A1 was closely and positively associated with these major immune-infiltrating cells, especially with CD8 + T cells. Furthermore, we found that SLC31A1 was highly expressed in many immune cells in breast cancer, including aDC, DC, iDC, macrophage, neutrophil, T helper cells, Tcm, Tgd, Th1, and Th2. At present, a variety of immunocheckpoint inhibitors targeting PD-1 or PDL-1 have been approved by FDA for the treatment of breast cancer. Therefore, we further analyzed the relationship between SLC31A1 and immune checkpoints. The results revealed that the upregulation of the SLC31A1 expression is significantly correlated with STAT3 and STAT1. A study by Sasidharan et al. showed that dual inhibition of STAT1 and STAT3 activation could downregulate the expression of PD-L1 in human breast cancer cells (37). Florida et al. have reported that copper chelators inhibited the phosphorylation of STAT3 and promoted ubiquitin-mediated degradation of PD-L1 (36). These results suggested that SLC31A1 may affect STAT3 and STAT1 phosphorylation by regulating the concentration of copper ions in cells and then affecting the expression of PDL1.

CAF served as the predominant stromal cell type in the breast tumor microenvironment. Wen et al. have found that CAF-secreted IL32 promotes breast cancer cell invasion and metastasis *via* integrinβ3-p38 MAPK signaling (38). Research from Gao et al. indicated that CD63 + CAF induces tamoxifen resistance in breast cancer *via* exosomal miR-22 (39). These results showed that CAF plays a tumor promotion role in breast cancer. Moreover, we found that the expression of SLC31A1 was positively correlated with CAF in luminal A breast cancer (Figure 8). However, there is no report on SLC31A1 and CAF in breast cancer. Based on our analysis, future studies may focus on the underlining mechanism of SLC31A1 regulating CAF in luminal A breast cancer.

Conclusion

In summary, SLC31A1 mRNA is upregulated in breast cancer and correlated with unfavorable prognosis. The expression level of

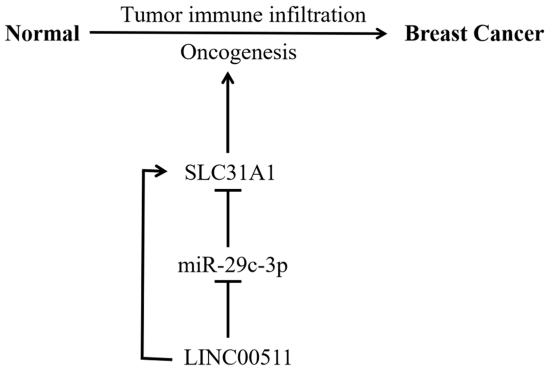

FIGURE 9
Model of LINC00511-miR-29c-3p-SLC31A1 axis in carcinogenesis of breast cancer.

SLC31A1 was positively correlated with tumor immune infiltration. We identified the LINC00511/miR-29c-3p axis as the upstream regulatory mechanism of SLC31A1 in breast cancer.

Data availability statement

The datasets generated and analyzed during the current study are available in the persistent web link presented in the material and methods. All the persistent web links are given at: Kaplan–Meier Plotter (http://kmplot.com/analysis/index.php?p=service), STRINGS (https://string-db.org/, version: 11.5), GEPIA2 (http://gepia2.cancer-pku.cn/#index), UALCAN (http://ualcan.path.uab.edu/analysis-prot.html), Metascape (https://metascape.org/gp/index.html#/main/step1), starBase (www.starbase.sysu.edu.cn), miRNet (https://www.mirnet.ca/), TIMER (https://cistrome.shinyapps.io/timer/), TIMER 2.0 (http://timer.cistrome.org/), and Xiantao (https://www.xiantao.love/products/apply/c0b6febb-52dd-4525-970a-61bbe9e263ff/collect).

Ethics statement

The studies involving human participants were reviewed and approved by the Ethics Committee of Fujian Medical University Union Hospital. The patients/participants provided their written informed consent to participate in this study.

Author contributions

WL, DC, and CW designed the overall study and discussed and edited the manuscript. PY and LL contributed to the data analysis. WL drafted the manuscript and prepared all the figures and tables. All authors read and approved the manuscript.

Funding

This study was supported by the Natural Science Foundation of Fujian Province, China (Grant No. 2020J011275) and the Quanzhou City Science and Technology Programme of China (Grant No. 2020N07319S).

Conflict of interest

The authors declare that the research was conducted in the absence of any commercial or financial relationships that could be construed as a potential conflict of interest.

Publisher's note

All claims expressed in this article are solely those of the authors and do not necessarily represent those of their affiliated organizations, or those of the publisher, the editors and the reviewers. Any product that may be evaluated in this article, or claim that may be made by its manufacturer, is not guaranteed or endorsed by the publisher.

Supplementary material

The Supplementary material for this article can be found online at: https://www.frontiersin.org/articles/10.3389/fmed.2023.1194046/full#supplementary-material

References

1. Sung H, Ferlay J, Siegel RL, Laversanne M, Soerjomataram I, Jemal A, et al. Global Cancer statistics 2020: GLOBOCAN estimates of incidence and mortality worldwide for 36 cancers in 185 countries. *CA Cancer J Clin*. (2021) 71:209–49. doi: 10.3322/caac.21660

2. Tsvetkov P, Coy S, Petrova B, Dreishpoon M, Verma A, Abdusamad M, et al. Copper induces cell death by targeting lipoylated TCA cycle proteins. *Science*. (2022) 375:1254–61. doi: 10.1126/science.abf0529

3. Lutsenko S. Human copper homeostasis: a network of interconnected pathways. *Curr Opin Chem Biol*. (2010) 14:211–7. doi: 10.1016/j.cbpa.2010.01.003

4. Davis CI, Gu X, Kiefer RM, Ralle M, Gade TP, Brady DC. Altered copper homeostasis underlies sensitivity of hepatocellular carcinoma to copper chelation. *Metallomics*. (2020) 12:1995–2008. doi: 10.1039/d0mt00156b

5. Yu Z, Zhou R, Zhao Y, Pan Y, Liang H, Zhang JS, et al. Blockage of SLC31A1-dependent copper absorption increases pancreatic cancer cell autophagy to resist cell death. *Cell Prolif*. (2019) 52:e12568. doi: 10.1111/cpr.12568

6. Liang Y, Song X, Li Y, Chen B, Zhao W, Wang L, et al. LncRNA BCRT1 promotes breast cancer progression by targeting miR-1303/PTBP3 axis. *Mol Cancer*. (2020) 19:85. doi: 10.1186/s12943-020-01206-5

7. McGuire A, Brown JA, Kerin MJ. Metastatic breast cancer: the potential of miRNA for diagnosis and treatment monitoring. *Cancer Metastasis Rev*. (2015) 34:145–55. doi: 10.1007/s10555-015-9551-7

8. Qi X, Zhang DH, Wu N, Xiao JH, Wang X, Ma W. ceRNA in cancer: possible functions and clinical implications. *J Med Genet*. (2015) 52:710–8. doi: 10.1136/jmedgenet-2015-103334

9. Chen F, Chen Z, Guan T, Zhou Y, Ge L, Zhang H, et al. N(6) -Methyladenosine regulates mRNA stability and translation efficiency of KRT7 to promote breast cancer lung metastasis. *Cancer Res*. (2021) 81:2847–60. doi: 10.1158/0008-5472.CAN-20-3779

10. Li JH, Liu S, Zhou H, Qu LH, Yang JH. starBase v2.0: decoding miRNA-ceRNA, miRNA-ncRNA and protein-RNA interaction networks from large-scale CLIP-Seq data. *Nucleic Acids Res*. (2014) 42:D92–7. doi: 10.1093/nar/gkt1248

11. Yang JH, Li JH, Shao P, Zhou H, Chen YQ, Qu LH. StarBase: a database for exploring microRNA-mRNA interaction maps from Argonaute CLIP-Seq and Degradome-Seq data. *Nucleic Acids Res*. (2011) 39:D202–9. doi: 10.1093/nar/gkq1056

12. Criscitiello C, Vingiani A, Maisonneuve P, Viale G, Viale G, Curigliano G. Tumor-infiltrating lymphocytes (TILs) in ER+/HER2- breast cancer. *Breast Cancer Res Treat*. (2020) 183:347–54. doi: 10.1007/s10549-020-05771-7

13. Loi S, Drubay D, Adams S, Pruneri G, Francis PA, Lacroix-Triki M, et al. Tumor-infiltrating lymphocytes and prognosis: a pooled individual patient analysis of early-stage triple-negative breast cancers. *J Clin Oncol*. (2019) 37:559–69. doi: 10.1200/JCO.18.01010

14. Vihervuori H, Autere TA, Repo H, Kurki S, Kallio L, Lintunen MM, et al. Tumor-infiltrating lymphocytes and CD8(+) T cells predict survival of triple-negative breast cancer. *J Cancer Res Clin Oncol*. (2019) 145:3105–14. doi: 10.1007/s00432-019-03036-5

15. Gentric G, Mechta-Grigoriou F. Tumor cells and Cancer-associated fibroblasts: an updated metabolic perspective. *Cancers*. (2021) 13:399. doi: 10.3390/cancers13030399

16. Shi W, Tang Y, Lu J, Zhuang Y, Wang J. MIR210HG promotes breast cancer progression by IGF2BP1 mediated m6A modification. *Cell Biosci*. (2022) 12:38. doi: 10.1186/s13578-022-00772-z

17. Chen H, Yu Y, Yang M, Huang H, Ma S, Hu J, et al. YTHDF1 promotes breast cancer progression by facilitating FOXM1 translation in an m6A-dependent manner. *Cell Biosci*. (2022) 12:19. doi: 10.1186/s13578-022-00759-w

18. Yu Z, Cao W, Ren Y, Zhang Q, Liu J. ATPase copper transporter a, negatively regulated by miR-148a-3p, contributes to cisplatin resistance in breast cancer cells. *Clin Transl Med*. (2020) 10:57–73. doi: 10.1002/ctm2.19

19. Zhao W, Geng D, Li S, Chen Z, Sun M. LncRNA HOTAIR influences cell growth, migration, invasion, and apoptosis via the miR-20a-5p/HMGA2 axis in breast cancer. *Cancer Med*. (2018) 7:842–55. doi: 10.1002/cam4.1353

20. Kong X, Duan Y, Sang Y, Li Y, Zhang H, Liang Y, et al. LncRNA-CDC6 promotes breast cancer progression and function as ceRNA to target CDC6 by sponging microRNA-215. *J Cell Physiol*. (2019) 234:9105–17. doi: 10.1002/jcp.27587

21. Ueno T, Kitano S, Masuda N, Ikarashi D, Yamashita M, Chiba T, et al. Immune microenvironment, homologous recombination deficiency, and therapeutic response to neoadjuvant chemotherapy in triple-negative breast cancer: Japan breast Cancer research group (JBCRG)22 TR. *BMC Med*. (2022) 20:136. doi: 10.1186/s12916-022-02332-1

22. Zheng S, Zou Y, Tang Y, Yang A, Liang JY, Wu L, et al. Landscape of cancer-associated fibroblasts identifies the secreted biglycan as a protumor and immunosuppressive factor in triple-negative breast cancer. *Onco Targets Ther*. (2022) 11:2020984. doi: 10.1080/2162402X.2021.2020984

23. Scognamiglio I, Cocca L, Puoti I, Palma F, Ingenito F, Quintavalle C, et al. Exosomal microRNAs synergistically trigger stromal fibroblasts in breast cancer. *Mol Ther Nucleic Acids*. (2022) 28:17–31. doi: 10.1016/j.omtn.2022.02.013

24. Luque M, Sanz-Alvarez M, Santamaria A, Zazo S, Cristobal I, de la Fuente L, et al. Targeted therapy modulates the secretome of cancer-associated fibroblasts to induce resistance in HER2-positive breast cancer. *Int J Mol Sci*. (2021) 22:13297. doi: 10.3390/ijms222413297

25. Park KC, Fouani L, Jansson PJ, Wooi D, Sahni S, Lane DJ, et al. Copper and conquer: copper complexes of di-2-pyridylketone thiosemicarbazones as novel anti-cancer therapeutics. *Metallomics*. (2016) 8:874–86. doi: 10.1039/c6mt00105j

26. Curnock R, Cullen PJ. Mammalian copper homeostasis requires retromer-dependent recycling of the high-affinity copper transporter 1. *J Cell Sci*. (2020) 133:jcs249201. doi: 10.1242/jcs.249201

27. Lutsenko S. Dynamic and cell-specific transport networks for intracellular copper ions. *J Cell Sci*. (2021) 134:jcs240523. doi: 10.1242/jcs.240523

28. Shi Y, Zheng C, Jin Y, Bao B, Wang D, Hou K, et al. Reduced expression of METTL3 promotes metastasis of triple-negative breast Cancer by m6A methylation-mediated COL3A1 up-regulation. *Front Oncol*. (2020) 10:1126. doi: 10.3389/fonc.2020.01126

29. Chang G, Shi L, Ye Y, Shi H, Zeng L, Tiwary S, et al. YTHDF3 induces the translation of m(6)A-enriched gene transcripts to promote breast Cancer brain metastasis. *Cancer Cell*. (2020) 38:857–871.e7. doi: 10.1016/j.ccell.2020.10.004

30. Lin Y, Jin X, Nie Q, Chen M, Guo W, Chen L, et al. YTHDF3 facilitates triple-negative breast cancer progression and metastasis by stabilizing ZEB1 mRNA in an m(6)A-dependent manner. *Ann Transl Med*. (2022) 10:83. doi: 10.21037/atm-21-6857

31. Macfarlane LA, Murphy PR. MicroRNA: biogenesis, function and role in cancer. *Curr Genomics*. (2010) 11:537–61. doi: 10.2174/138920210793175895

32. Ren W, Hu J, Li H, Chen J, Ding J, Zu X, et al. miR-616-5p promotes invasion and migration of bladder cancer via downregulating NR2C2 expression. *Front Oncol*. (2021) 11:762946. doi: 10.3389/fonc.2021.762946

33. Chen J, Jiang Q, Jiang XQ, Li DQ, Jiang XC, Wu XB, et al. miR-146a promoted breast cancer proliferation and invasion by regulating NM23-H1. *J Biochem*. (2020) 167:41–8. doi: 10.1093/jb/mvz079

34. Wang B, Mao JH, Wang BY, Wang LX, Wen HY, Xu LJ, et al. Exosomal miR-1910-3p promotes proliferation, metastasis, and autophagy of breast cancer cells by targeting MTMR3 and activating the NF-kappaB signaling pathway. *Cancer Lett*. (2020) 489:87–99. doi: 10.1016/j.canlet.2020.05.038

35. Normann LS, Aure MR, Leivonen SK, Haugen MH, Hongisto V, Kristensen VN, et al. MicroRNA in combination with HER2-targeting drugs reduces breast cancer cell viability in vitro. *Sci Rep*. (2021) 11:10893. doi: 10.1038/s41598-021-90385-2

36. Voli F, Valli E, Lerra L, Kimpton K, Saletta F, Giorgi FM, et al. Intratumoral copper modulates PD-L1 expression and influences tumor immune evasion. *Cancer Res*. (2020) 80:4129–44. doi: 10.1158/0008-5472.CAN-20-0471

37. Sasidharan NV, Toor SM, Ali BR, Elkord E. Dual inhibition of STAT1 and STAT3 activation downregulates expression of PD-L1 in human breast cancer cells. *Expert Opin Ther Targets*. (2018) 22:547–57. doi: 10.1080/14728222.2018.1471137

38. Wen S, Hou Y, Fu L, Xi L, Yang D, Zhao M, et al. Cancer-associated fibroblast (CAF)-derived IL32 promotes breast cancer cell invasion and metastasis via integrin beta3-p38 MAPK signalling. *Cancer Lett*. (2019) 442:320–32. doi: 10.1016/j.canlet.2018.10.015

39. Gao Y, Li X, Zeng C, Liu C, Hao Q, Li W, et al. CD63(+) Cancer-associated fibroblasts confer tamoxifen resistance to breast Cancer cells through Exosomal miR-22. *Adv Sci*. (2020) 7:2002518. doi: 10.1002/advs.202002518

frontiers | Frontiers in Medicine

TYPE Original Research
PUBLISHED 24 May 2023
DOI 10.3389/fmed.2023.1195678

OPEN ACCESS

EDITED BY
Zheng Wang,
Shanghai Jiao Tong University, China

REVIEWED BY
Yasha Wang,
Peking University, China
Chao Chen,
Chongqing University, China

*CORRESPONDENCE
Zhi Guo Mao
✉ maozhiguo518@126.com
Lin Li
✉ lilin_616@163.com

†These authors have contributed equally to this work

RECEIVED 28 March 2023
ACCEPTED 03 May 2023
PUBLISHED 24 May 2023

CITATION
Wang L, Peng F, Li ZH, Deng YF, Ruan MN, Mao ZG and Li L (2023) Identification of AKI signatures and classification patterns in ccRCC based on machine learning.
Front. Med. 10:1195678.
doi: 10.3389/fmed.2023.1195678

Identification of AKI signatures and classification patterns in ccRCC based on machine learning

Li Wang[1†], Fei Peng[2†], Zhen Hua Li[3], Yu Fei Deng[1], Meng Na Ruan[1], Zhi Guo Mao[1*] and Lin Li[1*]

[1]Department of Nephrology, Changzheng Hospital, Naval Medical University, Shanghai, China, [2]Department of Cardiology, Jinshan Hospital of Fudan University, Shanghai, China, [3]Department of Cardiology, Changzheng Hospital, Naval Medical University, Shanghai, China

Background: Acute kidney injury can be mitigated if detected early. There are limited biomarkers for predicting acute kidney injury (AKI). In this study, we used public databases with machine learning algorithms to identify novel biomarkers to predict AKI. In addition, the interaction between AKI and clear cell renal cell carcinoma (ccRCC) remain elusive.

Methods: Four public AKI datasets (GSE126805, GSE139061, GSE30718, and GSE90861) treated as discovery datasets and one (GSE43974) treated as a validation dataset were downloaded from the Gene Expression Omnibus (GEO) database. Differentially expressed genes (DEGs) between AKI and normal kidney tissues were identified using the R package limma. Four machine learning algorithms were used to identify the novel AKI biomarkers. The correlations between the seven biomarkers and immune cells or their components were calculated using the R package ggcor. Furthermore, two distinct ccRCC subtypes with different prognoses and immune characteristics were identified and verified using seven novel biomarkers.

Results: Seven robust AKI signatures were identified using the four machine learning methods. The immune infiltration analysis revealed that the numbers of activated CD4 T cells, CD56^{dim} natural killer cells, eosinophils, mast cells, memory B cells, natural killer T cells, neutrophils, T follicular helper cells, and type 1T helper cells were significantly higher in the AKI cluster. The nomogram for prediction of AKI risk demonstrated satisfactory discrimination with an Area Under the Curve (AUC) of 0.919 in the training set and 0.945 in the testing set. In addition, the calibration plot demonstrated few errors between the predicted and actual values. In a separate analysis, the immune components and cellular differences between the two ccRCC subtypes based on their AKI signatures were compared. Patients in the CS1 had better overall survival, progression-free survival, drug sensitivity, and survival probability.

Conclusion: Our study identified seven distinct AKI-related biomarkers based on four machine learning methods and proposed a nomogram for stratified AKI risk prediction. We also confirmed that AKI signatures were valuable for predicting ccRCC prognosis. The current work not only sheds light on the early prediction of AKI, but also provides new insights into the correlation between AKI and ccRCC.

KEYWORDS

acute kidney injury, machine learning, molecular subtypes, immunity, clear cell renal cell carcinoma

1. Introduction

Acute kidney injury (AKI) is a complex clinical disorder that manifests as a rapid decrease in glomerular filtration rate within three months and an increase in serum creatinine levels (1). Several stimuli may contribute to the development of AKI. Ischemia–reperfusion injury is one of the major clinical challenges faced by clinicians, especially during the perioperative period of renal transplantation. In AKI patients, persistent renal dysfunction and irreversible nephron loss can lead to chronic kidney failure. In addition, the risk of cardiovascular problems and other complications increases over time in renal failure patients (2), and critically ill patients have even worse prognoses (3). Therefore, the prevention and early detection of AKI are of paramount importance, and it is essential to identify specific signatures in patients with AKI. However, although biomarkers for the detection of AKI such as cystatin C, liver-type fatty acid-binding protein, interleukin-18, and neutrophil gelatinase-associated lipocalin have begun to emerge, these have some limitations (4). A useful tool related to this type of research is machine learning, a field of artificial intelligence that uses computer systems to process data using complex mathematical algorithms. With its powerful algorithms, machine learning has recently been applied in the field of medicine (5, 6). However, few studies have used machine learning to identify novel AKI biomarkers.

Several lines of evidence suggest that AKI induces or promotes the occurrence and progression of renal cancer. For instance, kidney injury may trigger DNA damage and promote mutated cell clonal proliferation in different kidney compartments (7). In one study, Peired et al. demonstrated a correlation between AKI and the subsequent development of renal cancer by analyzing patients with AKI from multiple independent cohorts (8). In addition, previous studies have shown that renal cancer progression is based on the increased systemic production of various chemokines, cytokines, and inflammatory immune cells (9–11). In another study, Zhou et al. demonstrated that AKI induces a systemic inflammatory response through modulation by inhibitors of the CXCL1/CXCR2 axis, thus increasing the risk of clear cell renal cell carcinoma (ccRCC) formation (12). Moreover, several studies have suggested that renal carcinoma occurs after an AKI episode or after years of chronic kidney disease, as kidney injury is an initial factor in renal cancer (8, 13). Indeed, ccRCCs account for approximately 75% of renal carcinoma cases (14). However, there is no satisfactory AKI-based prognostic model for accurate risk stratification in these patients. Therefore, it is essential to identify specific classifications for ccRCC prognostic prediction at the AKI level.

In this study, public datasets on AKI and ccRCC were downloaded and analyzed. We identified AKI-related biomarkers using functional pathway analysis, immune analysis, and AKI risk prediction. In addition, we carried out an AKI-related signature study by classifying ccRCC patients and integrating biological function enrichment, immune infiltration, chemical drug sensitivity data, and prognostic analyses. Furthermore, reliable signature subtyping was performed to predict the prognosis of patients with ccRCC based on the crucial roles of novel AKI biomarkers. Notably, this is the first study to elucidate novel AKI-related biomarkers with prognostic predictive value in ccRCC.

2. Materials and methods

2.1. Data collection and processing

Five public AKI datasets from the Gene Expression Omnibus (GEO) were downloaded and processed: GSE126805 (n = 83; normal tissues = 41, AKI tissues = 42), GSE139061 (n = 48; normal tissues = 9, AKI tissues = 39), GSE30718 (n = 47; normal tissues = 19, AKI tissues = 28), GSE90861 (n = 46; normal tissues = 23, AKI tissues = 23), and GSE43974 (n = 391; normal tissues = 188, AKI tissues = 203). The former four datasets were integrated and the batch was removed to construct a training cohort, whereas GSE43974 was treated as an independent test cohort. GSE126805, GSE139061, GSE30718, and GSE90861 were used to test whether these biomarkers could distinguish AKI tissues from normal tissues. Approval and informed consent from the institutional review board were not required for the AKI cohorts from the public databases. To reveal the connection between AKI and ccRCC, ccRCC multi-omics information was retrieved from the GDC TCGA portal.

2.2. Batch effect removal

To remove batch effects derived from the study design, sequence platform, and technological replication, we filtered only normal and AKI tissue expression matrices and clinical characteristics from four cohorts: GSE126805, GSE139061, GSE30718, and GSE90861. The batch effect was removed using the default function in the sva package. A principal component analysis (PCA) was used to visualize the efficacy of the batch removal.

2.3. Differential expression and enrichment analysis

We used the limma package to identify differentially expressed genes (DEGs) between normal and AKI tissues in the merged expression matrix. DEGs were identified using a significance threshold of $p < 0.05$ and an absolute log-fold change >1.5. An enrichment analysis of the DEGs was performed using the clusterProfiler and ggpplot2 packages, and these were visualized using an enrichment plot. Additionally, Gene Ontology (GO), Kyoto Encyclopedia of Genes and Genomes (KEGG), and gene set enrichment analyses (GSEA) were performed to better understand the biological roles of these DEGs. The significantly differentially expressed terms or pathways were identified by a threshold value of p <0.05 and q-value <0.05.

2.4. Identification and verification of AKI-related biomarkers

After identifying the DEGs from the combined expression profile of the combined expression matrix, we sought to identify the most relevant AKI-related biomarkers. We adopted four machine-learning algorithms, including Least Absolute Shrinkage and Selection Operator (LASSO) logistic regression, Random Forest (RF), eXtreme Gradient Boosting (XGBoost), and support vector machine (SVM), to select reliable biomarkers to distinguish AKI from normal tissues. The detailed

parameters adopted for these were as recommended in each of the R packages. The detailed parameters of LASSO logistics were as follow: alpha = 1, maximum number of iterations = 8,000, tol = 1e-4). The detailed parameters of Random Forest were as follow: n_estimators = 80, criterion = gini, min_samples_split = 2, min_samples_leaf = 1. And for XGBoost, the detailed hyperparameters were as follow: n_estimators = 500, max_depth = 6, reg_alpha = 0, colsample_bytree = 1. Finally, the detailed parameters of SVM were as follow: tol = 1e-3, max_iter = −1. Furthermore, the receiver operating characteristic (ROC) curve was adopted to further evaluate the accuracy of the filtered biomarkers in the training and testing cohorts using the R package pROC. The GSE90861 dataset was used as a validation cohort to verify the specificity and sensitivity of the biomarkers retrieved from the test cohort.

2.5. Immune components and cell differences between AKI and normal tissues

Single-sample gene set enrichment analysis (ssGSEA) and bulk sequence-based deconvolution algorithms from the GSVA and ESTIMATE packages were used to detect different immune cells and components between normal and AKI tissues. The gene sets used for ssGSEA consisted of 28 types of immune cells, including activated B cells, activated CD4 T cells, activated CD8 T cells, activated dendritic cells, $CD56^{bright}$ natural killer cells, $CD56^{dim}$ natural killer cells, central memory CD4 T cells, central memory CD8 T cells, effector memory CD4 T cells, effector memory CD8 T cells, eosinophils, gamma delta T cells, immature B cells, immature dendritic cells, macrophages, mast cells, MDSCs, memory B cells, monocytes, natural killer cells, natural killer T cells, neutrophils, plasmacytoid dendritic cells, regulatory T cells, T follicular helper cells, type 1 T helper cells, type 17 T helper cells, and type 2 T helper cells. The estimated algorithms contained three scores: ESTIMATE, immune, and stromal scores. The correlations between the seven biomarkers and immune cells or their components were calculated using the R package ggcor.

2.6. Identification of different subtypes of AKI and ccRCC

To further reveal the heterogeneity of AKI and the potential relationship between AKI and ccRCC, we performed an unsupervised cluster analysis based on seven novel biomarkers (*CCNL1*, *NFKBIZ*, *HBB*, *TRIB1*, *SOCS3*, *HSPA6*, and *EGR1*) using the Consensus Cluster Plus package. The optimal cluster number was identified based on the PCA algorithm and cumulative distribution function curve. Differences in estimates, immune scores, and immune components were also qualified and compared between the ccRCC subtypes. A detailed description of the parameters employed are described in previous studies (15, 16).

3. Results

3.1. Batch effects removal and data integration

Figure 1A shows a flowchart of our study. Figure 1B shows the raw PCA results for the four microarray databases (GSE126805, GSE139061, GSE30718, and GSE90861). The four different colors represent different datasets. Every dataset was discrete without any intersection. Figure 1C shows the combat PCA results following batch removal.

3.2. Functional pathway enrichment analysis

A volcano map (Figure 2A) was created to visually display the expression changes of the DEGs between normal and AKI tissues. A total of 108 genes were identified as DEGs according to adjusted *p*-values <0.05 and logFC cutoffs >1.5; among these, 101 genes were upregulated and 7 genes were downregulated. Next, we performed GO and KEGG enrichment analyses. As depicted in Figures 2B–D, in terms of biological processes (BP), the DEGs were mostly associated with lipopolysaccharides and molecules of bacterial origin. Regarding cellular components (CC), these were mainly involved in the RNA polymerase II transcription regulator complex and transcription regulator complex. In terms of molecular functions (MF), the DEGs were largely associated with tyrosine proteins, threonine phosphatase activity, and MAP kinases. The 20 most significant KEGG pathway terms are shown in Figure 2E. These genes were primarily associated with the TNF signaling pathway, the IL-17 signaling pathway, lipid and atherosclerosis pathways, the AGE – RAGE signaling pathway in those with diabetic complications, and the MAPK signaling pathway.

3.3. GSEA analysis of the AKI and normal groups

GSEA was performed to determine which KEGG pathways were differentially enriched between the AKI and normal groups according to the NES and value of p ($p < 0.01$) criteria. As presented in Figures 2F–K, the top three significantly upregulated KEGG pathways enriched in the AKI group were pathways related to cytokine-cytokine receptor interactions, IL-17 signaling, and TNF signaling. In addition, oxidative phosphorylation, fatty acid degradation, and peroxisomes were significantly downregulated in the AKI tissues. These data reveal that numerous pathways may be directly or indirectly involved in the regulation of AKI.

3.4. AKI signature identification and validation

Four machine learning algorithms were applied to identify feature genes: LASSO regression (Figures 3A,B), SVM (Figure 3C), and Random Forest (Figures 3D,E). These were combined with a feature selection analysis to determine the top 30 genes with relative importance, and an XGBoost analysis was then performed using these 30 relatively important genes (Figure 3F). A Venn diagram was used to display the overlapping signatures of the four methods (Figure 4G). After applying the four machine learning algorithms, eight signatures were selected, as shown in Figures 3A–G: tribbles homolog 1 (*TRIB1*), *ST6GALNAC3*, suppressors of cytokine signaling 3 (*SOCS3*), NF-κB inhibitor ζ (*NFKBIZ*), heat shock protein family A 6 (*HSPA6*), hemoglobin subunit beta (*HBB*), early growth response 1 (*EGR1*), and cyclin L1 (*CCNL1*).

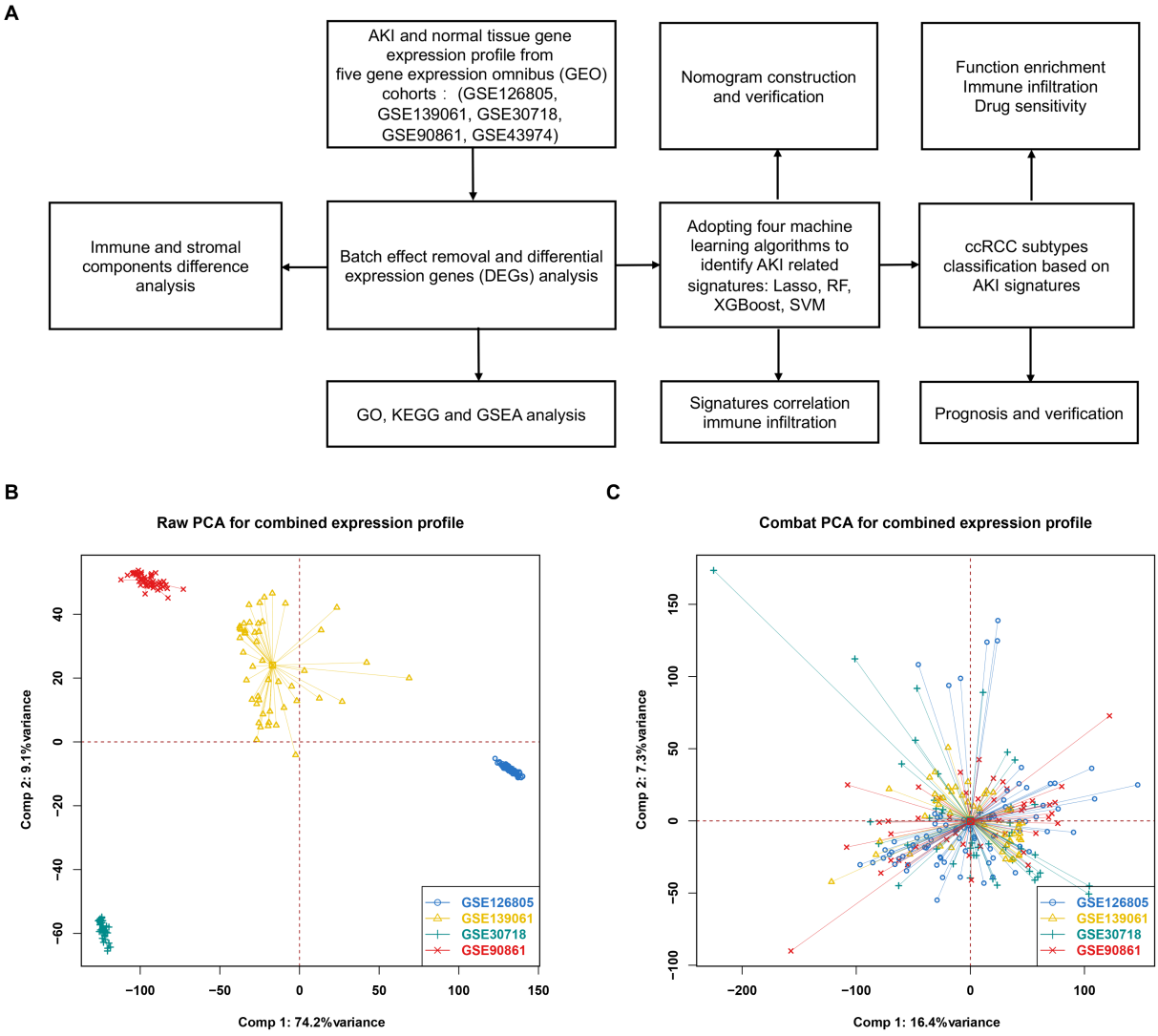

FIGURE 1
Differentially expressed genes between AKI and normal tissues. **(A)** Workflow of our study. **(B)** PCA plot before batch effect removal. **(C)** PCA after batch effect removal. PCA, principal component analysis.

As shown in Figures 3H,I, to further test the diagnostic efficacy of the above genes, ROC analysis was performed to evaluate the accuracy of each gene. The ROC curve showed that the seven biomarkers identified based on the logistic regression were reliable, with the following AUCs in the training set: *CCNL1*, 0.972; *NFKBIZ*, 0.937; *HBB*, 0.726; *TRIB1*, 0.908; *SOCS3*, 0.928; *HSPA6*, 0.905; and *EGR1*, 0.981. In the validation set, the AUCs were as follows: *CCNL1*, 0.825; *NFKBIZ*, 0.868; *HBB*, 0.821; *TRIB1*, 0.817; *SOCS3*, 0.826; *HSPA6*, 0.781; and *EGR1*, 0.814. *ST6GALNAC3* (AUC = 0.517 in the test set) was not analyzed further in the next workflow.

3.5. AKI marker genes and immune cell infiltration

We analyzed the heterogeneous compositions of the tumor microenvironments (TMEs) in the AKI and normal groups. As depicted in Figures 4A–C, all estimated scores, including the immune, stromal, and estimated scores, were lower in the AKI group compared to the normal group. We then examined the specific correlations between the estimated scores and each of the signatures using Spearman's correlation analyses, which revealed that *TRIB1*, *EGR1*, and *CCNL1* were related to the estimate and stromal scores (Figure 4D). As shown in Figure 4E, almost all of these genes were positively or negatively correlated with immune cell infiltration. Of these, *EGR1* and eosinophil, *HSPA6* and mast cells were significantly and positively relevant. In contrast, *TRIB1* and activated B cells, *CCNL1* and central memory CD8 T cells were negatively correlated ($p < 0.01$).

As shown in Figure 4F, the hub gene correlation analysis revealed that the expression levels of *CCNL1* and *NFKBIZ* were mostly positively correlated, and *CCNL1* was linked to every other gene. Figure 4G shows that 28 immune cells were differentially concentrated between the AKI and control groups. Among these, activated CD4 T cells, $CD56^{dim}$ natural killer cells, eosinophils, mast cells, memory B cells, natural killer T cells, neutrophils, T follicular helper cells, and type 1 T helper cells were more enriched in the AKI cluster.

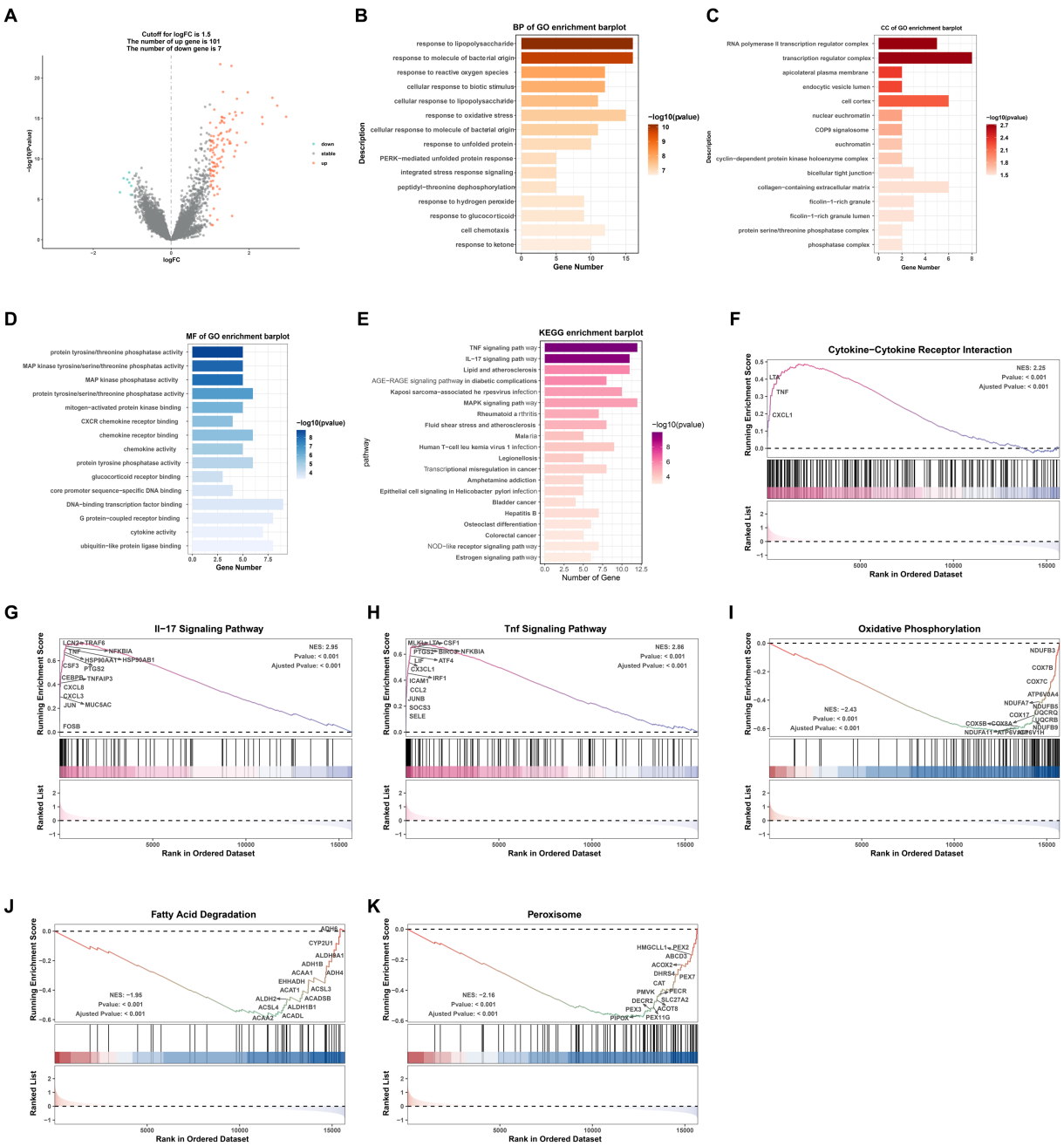

FIGURE 2
GO/KEGG/GSEA analysis of common differentially expressed genes (DEGs). **(A)** Volcano plot of the DEGs. **(B)** BP identified through GO analysis of the DEGs. **(C)** CC identified through GO analysis of the DEGs. **(D)** MF identified through GO analysis of the DEGs. **(E)** KEGG analysis of the differentially expressed signatures. **(F–K)** GSEA plot showing the most enriched gene sets based on KEGG analysis of all detected genes. BP, biological process; CC, cellular component; MF, molecular function; GO, Gene Ontology; KEGG, Kyoto Encyclopedia of Genes and Genomes; GSEA, gene set enrichment analysis; FC, fold change.

3.6. Construction of the nomogram model

In order to accurately predict AKI risk using these signatures, a nomogram was constructed. As shown in Figure 5A, in the nomogram, each biomarker gene had a parallel score within the range of 0–100 points in terms of its association with the risk of AKI. As shown in Figures 5B–E, the AUC value was 0.919 in the training set and 0.945 in the testing set. In both the training and validation sets, the calibration plot demonstrated a good fit of the constructed nomogram, indicating satisfactory model accuracy.

3.7. ccRCC subtypes with the AKI-related gene classification

We investigated the expression patterns of AKI-related signatures in ccRCC to comprehensively explore the association

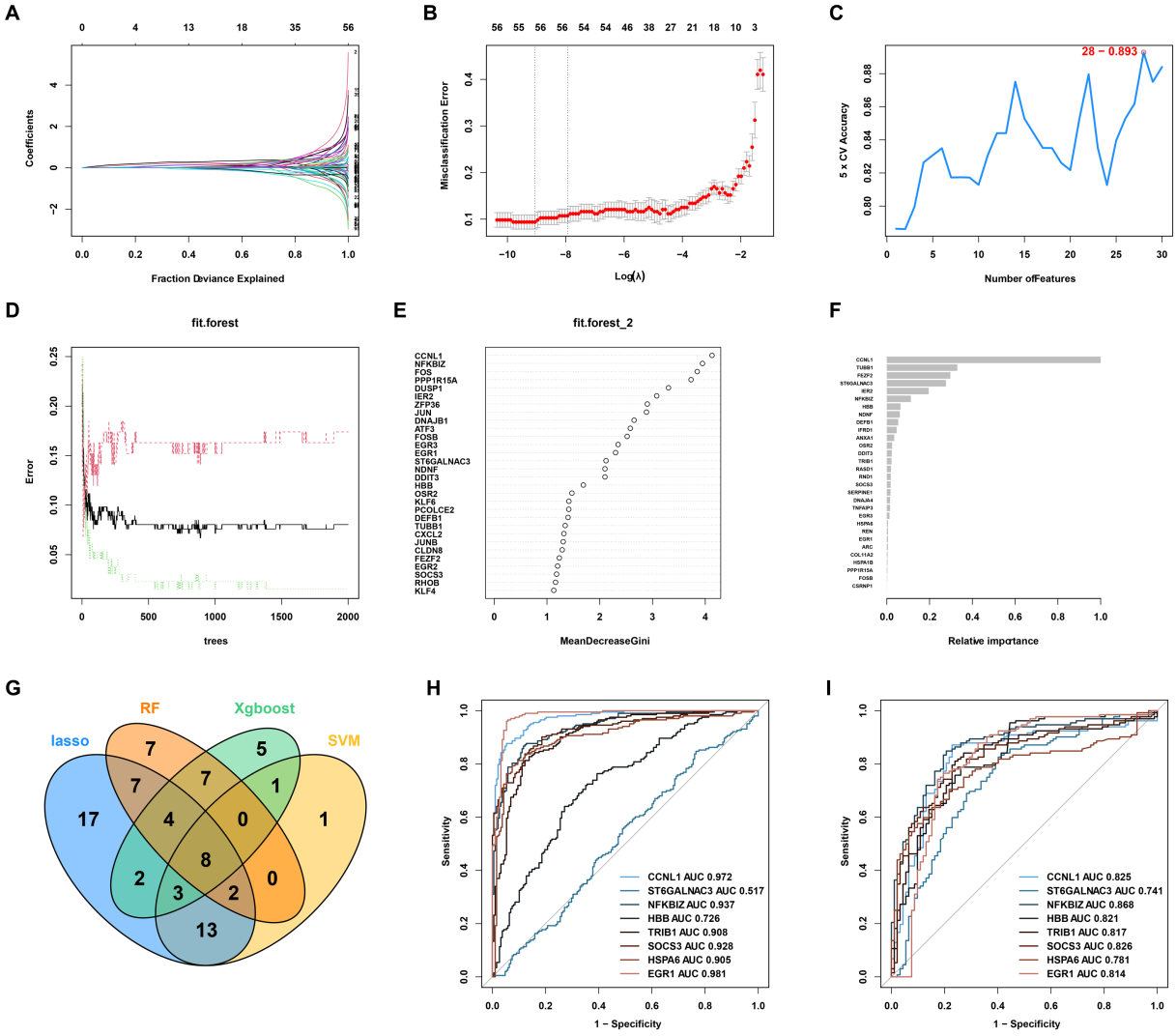

FIGURE 3
AKI signature identification and verification. **(A,B)** LASSO. **(C)** SVM. **(D,E)** RF 2. **(F)** XGBoost. **(G)** Venn diagram for the four machine learning algorithms. **(H)** ROC curves for the eight genes in the training cohorts. **(I)** Testing cohorts. LASSO, Least Absolute Shrinkage and Selection Operator; SVM, support vector machine; RF, Random Forest; XGBoost, Xtreme Gradient Boosting; ROC, receiver operating characteristic.

between AKI and cancer. TCGA-ccRCC samples were classified into different molecular subtypes according to AKI signature expression levels. For this, we divided the optimal cluster numbers using an unsupervised clustering method. As depicted in Figures 6A–C, considering the relative change in area under cumulative distribution function curve and consensus index, we chose k = 2 as the optimal cluster number. The TCGA ccRCC dataset was classified into two optimal clusters: CS1 and CS2. Compared to CS2 patients, CS1 patients had better overall survival (OS) ($p = 0.0026$, log-rank test) and progression-free survival (PFS) ($p = 0.00033$, log-rank test) (Figures 6D,E). In addition, we analyzed the expression levels of AKI genes in normal tissues and in the two ccRCC subtypes using a heatmap. *CCNL1*, *NFKBIZ*, *SOCS3*, and *HSPA6* were significantly upregulated in the ccRCC subtype compared to normal tissues, whereas *TRIB1* and *EGR1* were significantly upregulated in the ccRCC subtypes ($p < 0.05$; Figure 6F).

3.8. Gene expression profiles of the ccRCC subtypes and results of the function enrichment analysis

Considering the varying characteristics of each cluster, we identified the gene expression profiles of CS1 and CS2. Supplementary Figure S1A presents an enhanced volcano map that displays the differential gene expression between CS1 and CS2, with 19,168 total differentially expressed genes. In addition, the GO analysis demonstrated that DEGs between ccRCC subtypes were annotated in receptor antagonist, receptor inhibitor, peptidase inhibitor, peptidase regulator, and enzyme inhibitor activity in biological process (Supplementary Figure S1B).

Supplementary Figure S1C shows the results of the GSVA algorithm analysis, which demonstrates that G2M-checkpoint, TGFβ signaling, and E2F oncogenes were more enriched in CS2 than in CS1. In addition, regulon analysis was used to detect transcriptome

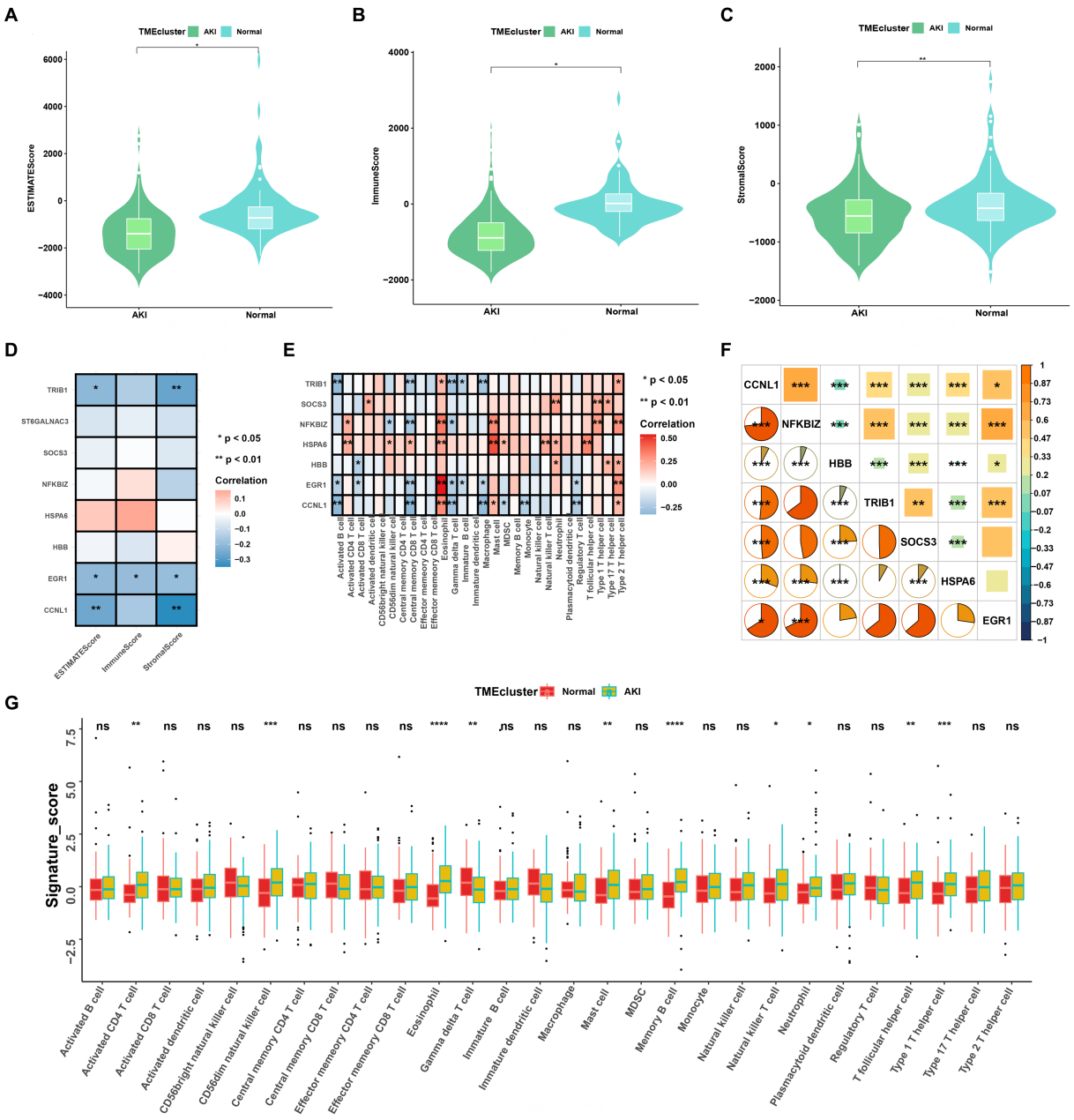

FIGURE 4
Immune cell infiltration rates and the correlations among these and the signatures. **(A–C)** ESTIMATE, immune, and stromal score differences between the ccRCC subtypes. **(D)** Correlations between ESTIMATE scores and significant genes. **(E)** Enriched signatures in the immune cells. **(F)** Correlations among the seven signatures according to Pearson and Spearman analyses. **(G)** Boxplot of immune cell infiltration between the normal and AKI clusters. ns>0.05, *p<0.05, **p<0.01, ***p<0.001, ns, not significant.

differences, which demonstrated that *HNF1A*, *EPAS1*, *ZEB2*, *TFE3*, and *TP53* were downregulated in CS2, whereas *FOXE1* and *TBX18* were upregulated in CS1 (Supplementary Figure S1D).

3.9. Comparison of immune infiltration between the two ccRCC subtypes

To further elucidate the molecular distinctions between the two ccRCC subtypes, we conducted a comprehensive analysis of the immune-related signatures, signaling pathways, anticancer responses, and other relevant factors in both subtypes. We found that the dysfunction scores and Tumor Immune Dysfunction and Exclusion (TIDE) scores in CS1 were significantly lower than those in CS2 (Figures 7A,B), which indicated lower tumor immune evasion and resistance to checkpoint blockage in this cluster. In addition, the expression levels of nine immune checkpoint inhibitor genes were compared between the CS1 and CS2 cells; among them, *CD274* was significantly upregulated in CS1 cells, whereas *LAG3* and *PDCD1* were significantly downregulated in CS2 cells (Figure 7C).

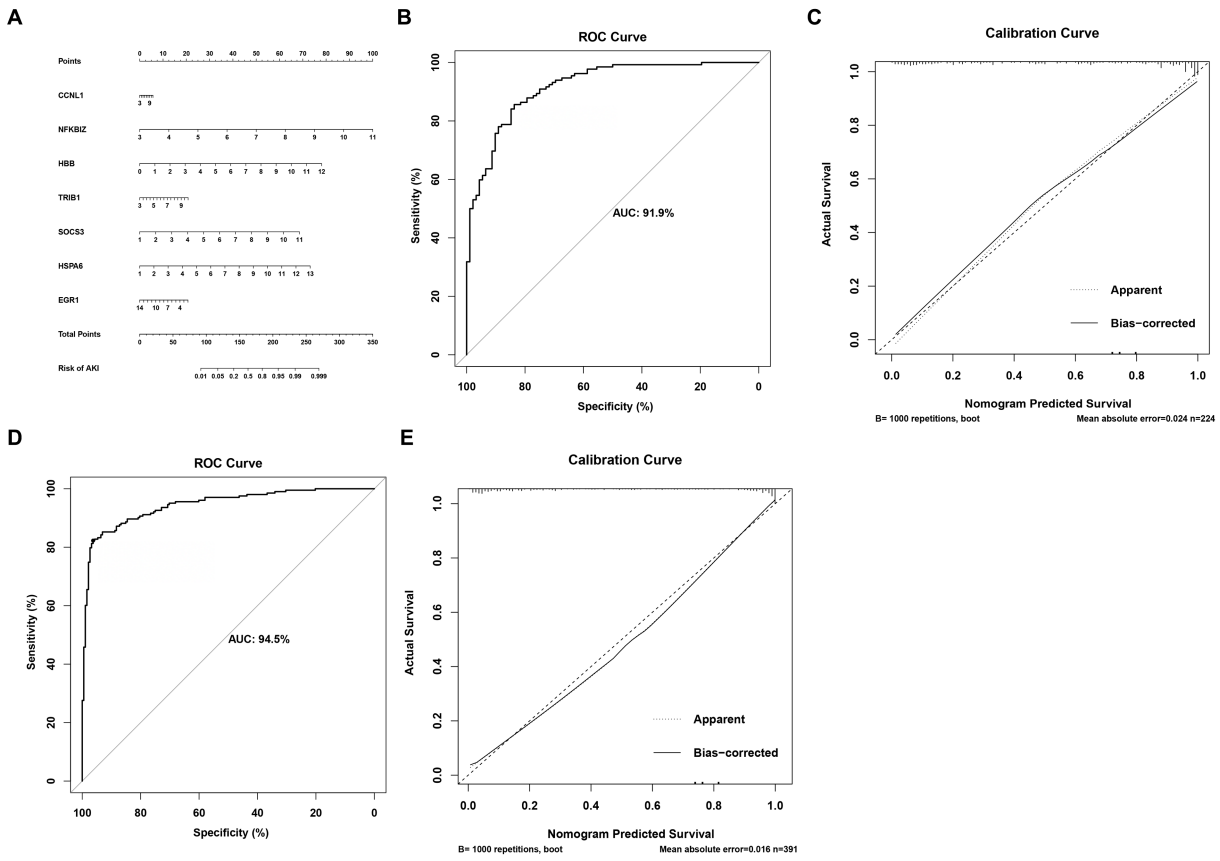

FIGURE 5
Nomogram for predicting the risk of AKI. **(A)** Nomogram. **(B,C)** ROC curves for the sensitivity of the nomogram and the calibration curves in the training set. **(D,E)** ROC curves and calibration curves in the validation set.

Among the different immune-related signatures expressed between the two ccRCC subtypes in the heatmap (Supplementary Figure S2A), chemokines, chemokine receptors, major histocompatibility complexes, and immunoinhibitory and immunostimulatory signatures were significantly differentially expressed. The CS1 subtype showed lower expression of *CXCL11*, *CCR4*, *HLA-DOA*, *CD244*, and *IL2RA*. Moreover, CS1 showed higher immune cell infiltration than CS2 in the TME infiltration cell-type heatmap (Supplementary Figure S2B). Mismatch repair, nucleotide excision repair, and base excision repair signatures were significantly higher in CS1, whereas EMT1, EMT2, signatures were significantly lower this cluster (Figure 7D).

As the anticancer immune response can be interpreted as a series of immune cell combat processes, we evaluated the tumor immunophenotypes in the two clusters. As shown in Figure 7E, the CS2 cluster demonstrated higher activity associated with priming and activation (step3), T cell recruiting (step4), dendritic cell recruiting (step4), macrophage recruiting (step4), B cell recruiting (step4), Th2 cell recruiting (step4) and recognition of cancer cells by T cell (step6). In contrast, CS1 demonstrated higher activity associated with the release of cancer antigen (step1) and cancer antigen presentation activity (step2) ($p < 0.05$).

3.10. Drug sensitivity and genomic mutation analysis of the two subtypes

To evaluate the drug responses of the ccRCC subtypes, the estimated IC50 data for each drug were collected from the GDSC database to explore the potential chemotherapy sensitivity of ccRCC. We found that the CS1 subtype was more sensitive to sunitinib, pazopanib, crizotinib, erlotinib, temsirolimus, and axitinib, whereas the CS2 subtype was more sensitive to lisitinib and gefitinib (Figure 8A). A significant difference was also observed in other omics. For instance, the tumor mutation burden was higher in CS2 (Figure 8B), which may have led to poor prognoses in CS2. In addition, Figure 8C shows that CS2 had higher amounts of copy number alterations, copy number losses, and copy number-gained genomes compared to CS1 ($p < 0.001$).

3.11. Subtype classification verification using an external dataset

To further confirm the credibility of the ccRCC subtypes, the nearest template prediction algorithms were applied to reconstruct the subtypes in the TCGA–KIRC cohort and divide this cohort into two

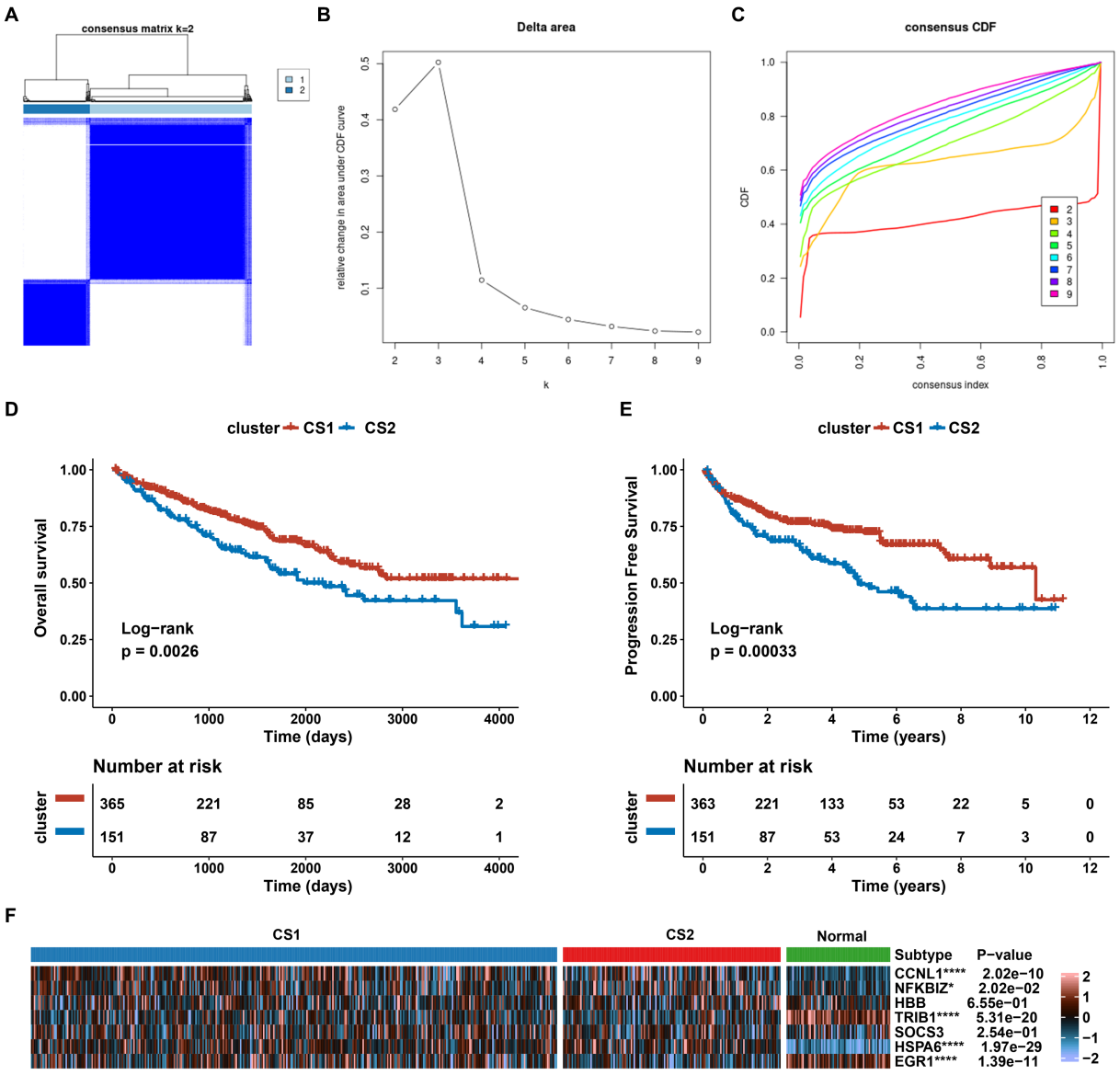

FIGURE 6
Establishment of two clusters based on AKI signatures in ccRCC. **(A)** Consensus cluster matrix of TCGA-ccRCC samples when k=2. **(B)** Relative change of delta area under different cluster number. **(C)** Cumulative distribution function curves, k=2 to 9. **(D,E)** Survival analysis for overall survival (OS) and progression-free survival (PFS) among the two subtypes in the TCGA-ccRCC dataset. **(F)** Expression profiles of AKI biomarker genes among the two subtypes and normal tissues. ns>0.05, *p<0.05, **p<0.01, ***p<0.001, ****p<0.0001. ns, not significant.

different subgroups. As shown in Figures 9A–D, the four Kaplan–Meier curves created using the data from different databases revealed that CS1 had a significantly better survival probability than CS2. In the Cancer Cell database, the value of p was 0.012; in the GSE22541 database, the value of p was 0.038; in the CheckMate OS database, the value of p was 0.015; and in the E-MTAB-3267 database, the value of p was 0.046. The stability and reliability of the subtypes were verified based on these results.

4. Discussion

AKI is a global concern and challenge associated with high mortality and healthcare costs worldwide (17). It can be classified into pre-renal, intrinsically renal, or post-renal types. Meanwhile, ischemia-reperfusion, a pre-renal injury, is an inevitable event in kidney transplantation surgery (18). In addition, various components of the innate and adaptive immune systems are involved in AKI pathogenesis and repair. After ischemia and reperfusion, free radical-mediated injury releases pro-inflammatory cytokines and induces innate immunity (18, 19). Following this, immune cells traverse the postischemic kidney and demonstrate changes in the associated signaling pathways, and ischemic kidney injury is also established over time (20).

Kidney function biomarkers have emerged as new tools for risk assessment and clinical therapy guidance. These biomarkers are of particular interest because several microarray studies have demonstrated differential expression of single molecules or hub genes,

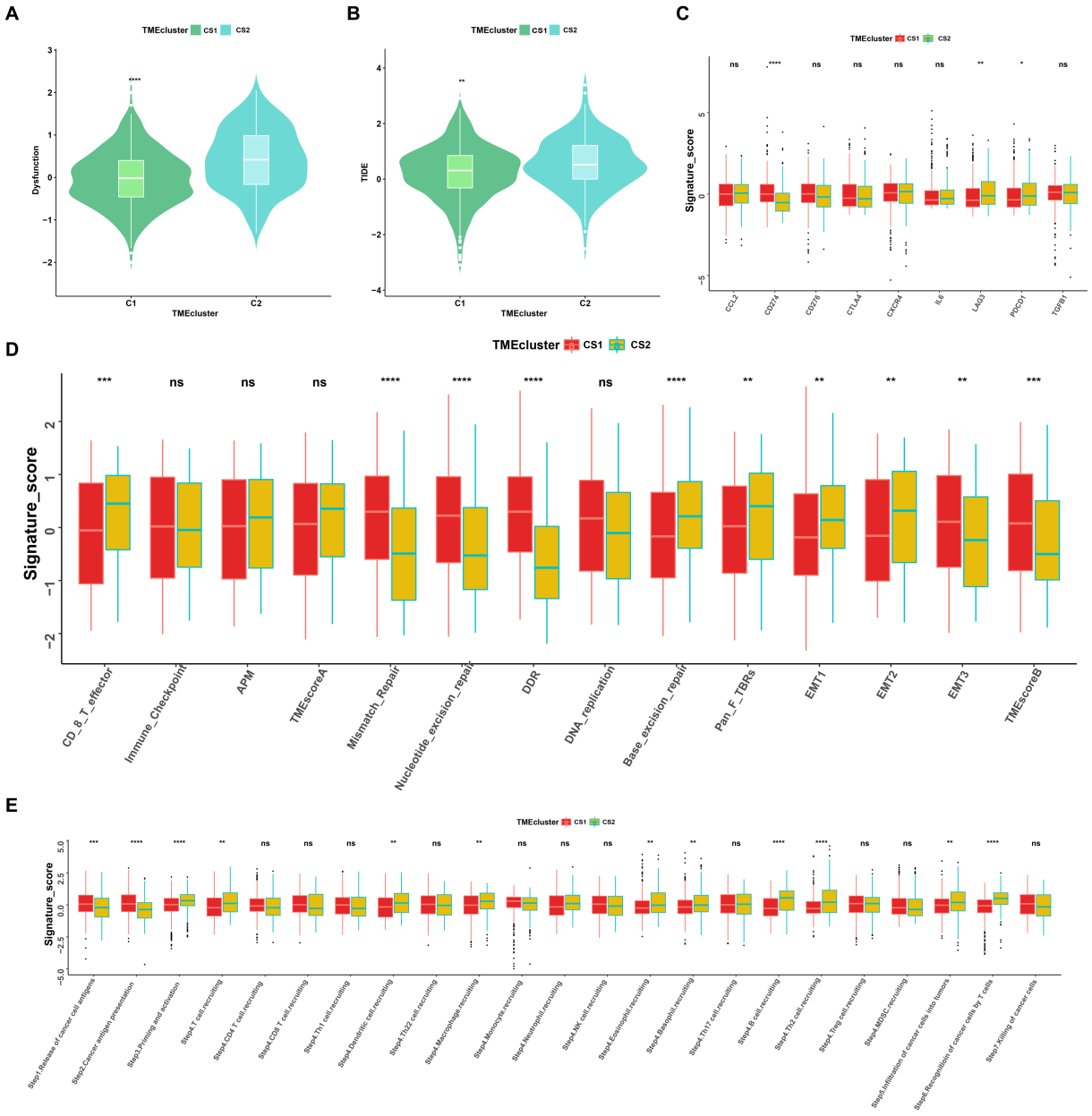

FIGURE 7
Landscapes of specific immune function scores and immune components. **(A,B)** Immune function scores (Dysfunction and TIDE) among the two ccRCC subtypes. **(C–E)** Immune antigens, immune pathways, and anti-cancer steps among the two subtypes. ns>0.05, *p<0.05, **p<0.01, ***p<0.001, ****p<0.0001. ns, not significant.

which are believed to play a role in the development of certain incentive-induced AKI models (21–25). In this study, we screened early-stage AKI profiles derived from renal transplant and ordinary kidney biopsy tissues from the GEO database, conducted comprehensive analyses of four GEO datasets, and obtained seven genes from four machine learning models for ischemia–reperfusion injury AKI prediction. Moreover, we integrated the identified DEGs to identify potential biomarkers and pathways involved in AKI pathogenesis. In the GO database, protein tyrosine/threonine phosphatase activity, MAP kinase tyrosine/serine/threonine phosphatase activity, and MAP kinase phosphatase activity were significant associated with AKI. Moreover, the GSEA revealed that the cytokine-cytokine receptor interaction, IL-17, and TNF signaling pathways were positively upregulated in AKI.

Numerous studies have shown that tyrosine phosphatase and MAP kinase activities have essential physiological and pathological functions in kidney diseases (26, 27). Previous studies have also suggested that IL-17 mediates renal fibrosis and neutrophil infiltration in ischemia reperfusion (28, 29). In addition, the TNF pathway was reported to participate in renal glomerular endothelial injury (30). To clarify the differential enrichment of immune cells and elucidate their possible mechanisms of action in AKI, we analyzed marker genes associated with renal immunity. Our analysis revealed significant differences in immune, stromal, and estimated scores between the AKI and normal clusters. Additionally, immune cells, including activated CD4 T cells, $CD56^{dim}$ natural killer cells, eosinophils, mast cells, memory B cells, natural killer T cells, neutrophils, T follicular helper cells, and type 1 T helper cells were significantly upregulated in

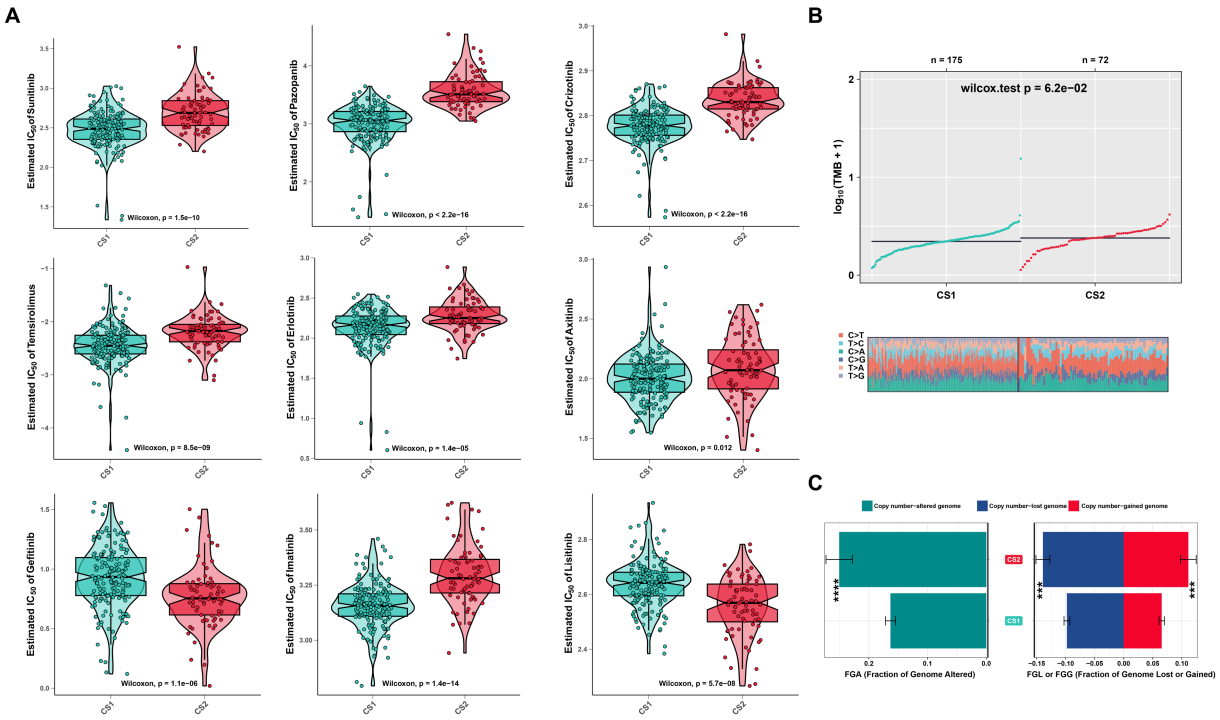

FIGURE 8
Drug sensitivity analysis and other omics of the two ccRCC subtypes. **(A)** Estimated IC50 of the indicated molecular-targeted drugs among the two ccRCC subtypes. **(B)** Tumor mutation burden between the two subtypes. **(C)** Bar plot of the genomic fractions that were altered between the two subtypes. ns>0.05, *p<0.05, **p<0.01, ***p<0.001, ****p<0.0001. ns, not significant.

the AKI group. Consistent with previous studies, T cells are known to release proinflammatory cytokines and chemokines to promote acute renal injury, whereas natural killer T cells can induce renal inflammation and injury or protect against it, depending on the context of their activation (31, 32). Furthermore, to determine the exact AKI risk-prediction efficiency, a highly accurate predictive nomogram was constructed by integrating a seven-gene risk score. Satisfactory agreement was observed in the calibration plot of the nomogram, suggesting that our seven-gene-based risk nomogram may contribute to predicting the risk of AKI and provide early treatment guidance beyond single conventional clinical parameters.

Facilitated by bioinformatics and sequencing technology, seven genes (*EGR1*, *SOCS3*, *TRIB1*, *CCNL1*, *HBB*, *HSPA6*, and *NFKBIZ*) were identified as precise indicators of AKI. Notably, earlier studies have confirmed that these genes participate in the renal physiology and pathology of AKI. Early growth response 1 (EGR1) is an early transcription factor that is induced by many cellular factors, including growth factors and hypoxia (33). Previous studies have validated that EGR1 is associated with mediating renal epithelial cell regeneration and is significantly upregulated in AKI kidney samples (34, 35). EGR1 also regulates inflammation and fibrosis in kidney tissues (36). And upregulation of SOCS3 in stressed proximal tubules also plays an important role in AKI by modulating the macrophage phenotype and inhibiting reparative proliferation (37). TRIB1 (38) might be a therapeutic target for renal injury through the regulation of renal tubular cell proliferation. Gunther et al. reported an increase in blood-derived CCNL1 expression in kidney transplant recipients with acute rejection compared to recipients with no rejection (39). Other studies have indicated that *HBB*, *HSPA6*, and *NFKBIZ* may play essential roles in kidney disease (40–42). The roles of these genes in ccRCC also have been reported. For instance, EGR1 serves as an independent prognostic factor in ccRCC patients by inhibiting the proliferation, invasion, and metastasis of ccRCC (43). In addition, Tomita et al. found that SOCS3 might be a potential target in IFN-α-resistant RCC treatment (44). Furthermore, studies have reported that NFKBIZ and HSPA6 are associated with ccRCC (42, 45).

Inflammatory microenvironments often develop prior to malignant changes and tumorigenesis (46). A previous study indicated that AKI induces malignant renal cell carcinoma *via* CXCR2 in the proximal tubular kidney epithelial cells of mice (12). These findings highlight the potential of using these seven genes (*CCNL1*, *NFKBIZ*, *HBB*, *TRIB1*, *SOCS3*, *HSPA6*, *EGR1*) in guiding clinical decision-making and the early prevention of AKI. In order to determine if certain AKI signatures have predictive value for ccRCC, we divided the ccRCC patient data into two clusters based on the key AKI genes. We found that CS1 had better prognostic value compared to CS2 in terms of OS and PFS. In addition, the expression profile of *EGR1* was more enriched in normal tissues than in CS1 and CS2. This suggests that *EGR1* may inhibit the proliferation, invasion, and metastasis of ccRCC, which is consistent with previous results (43). *CCNL1*, *SOCS3*, and *HSPA6*, which are highly expressed in patients with ccRCC, may promote tumor generation. Immune-related signatures were highly expressed in CS2 cells, whereas immune-related inhibitors were dysregulated. Another observation was that oncogenes related to G2M-checkpoint, TGFβ signaling, and E2F targets were more enriched in CS2. The higher tumor mutation burden and fraction of genome alerts may also explain the poor prognosis of CS2. Furthermore, the CS1 subtype was more sensitive to drug therapy.

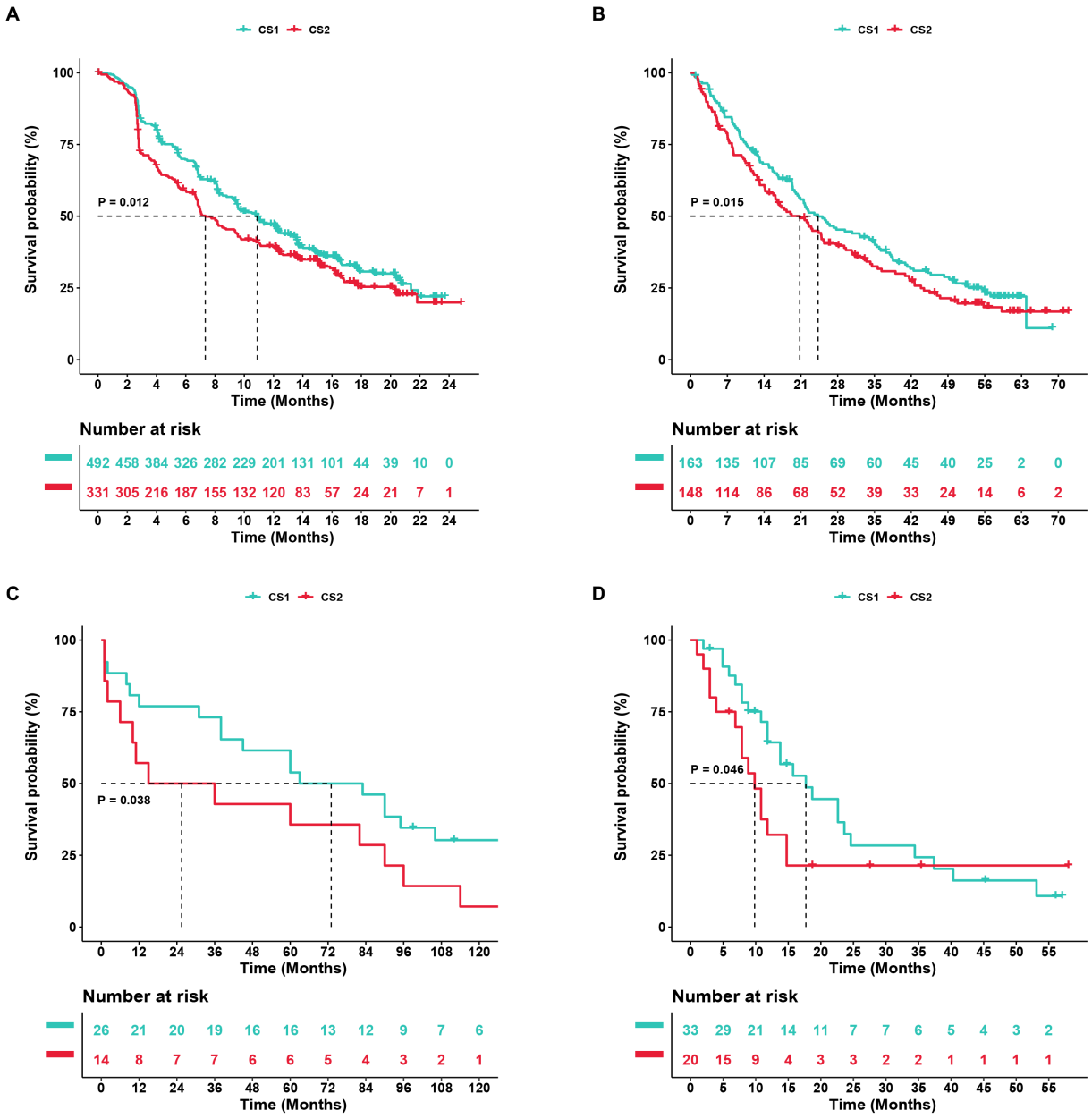

FIGURE 9
Subtype classification verification using an external dataset. **(A–D)** Kaplan–Meier curve of the NTP (nearest template prediction) by the Cancer Cell, Checkmate OS, GSE22541, and E-MTAB-3267 databases.

Thus, this subtype classification will contribute to ccRCC prognostic analysis, the early prevention of carcinogenesis, and guidelines for clinical immunotherapy.

Machine learning, which benefits from artificial intelligence and computer science, is widely used in nephrology research (47). Chen et al. used a XGBoost model to predict progression at 5 years in patients with biopsy-proven IgA nephropathy (48). For other applications, several studies have utilized machine learning to predict the development of acute kidney injury following surgery and volume responsiveness in patients with oliguric acute kidney injury (49–51). Recently, shared gene signatures and molecular mechanisms have been demonstrated between these two diseases (52, 53). This is relevant because shared genes are important for disease prevention and early treatment. In contrast to other studies, we obtained AKI signatures using machine learning and elaborated on the value of these biomarkers for predicting AKI risk and ccRCC prognosis. However, our study does have some limitations, as most of our results were based on bioinformatics analyses. Therefore, follow-up experiments should be conducted in AKI and ccRCC, and the specific roles of these seven signatures require further investigation in future molecular experiments.

5. Conclusion

In conclusion, a comprehensive bioinformatics analysis of AKI was conducted, and seven genes (*CCNL1*, *NFKBIZ*, *HBB*, *TRIB1*,

SOCS3, *HSPA6*, and *EGR1*) that may be involved in the biological processes of AKI were identified. We also explored the immune correlations associated with these seven signatures and evaluated their risk associations. Our analysis showed that CS1, along with the AKI signature cluster, may lead to better outcomes and treatment sensitivity for ccRCC. These findings provide potential targets for risk prediction and offer a new perspective on the relationship between kidney injury and kidney cancer.

Data availability statement

The datasets presented in this study can be found in online repositories. The names of the repository/repositories and accession number(s) can be found in the article/Supplementary material.

Author contributions

LW designed and wrote this manuscript. FP analyzed the data. ZL, MR, and YD collected the data. ZM and LL supervised the manuscript. All authors contributed to the study and approved the submitted version.

Funding

This study was supported by the Youth Scientific Research Project of Shanghai Municipal Health Commission [grant number: 20214Y0367] and the Youth Startup Fund of Jinshan Hospital of Fudan University [grant number: JYQN-LC-202007].

Acknowledgments

The authors would like to thank the five GEO dataset contributors for generously sharing their precious data.

Conflict of interest

The authors declare that the research was conducted in the absence of any commercial or financial relationships that could be construed as a potential conflict of interest.

Publisher's note

Supplementary material

The Supplementary material for this article can be found online at: https://www.frontiersin.org/articles/10.3389/fmed.2023.1195678/full#supplementary-material

SUPPLEMENTARY FIGURE S1

Function enrichment analysis between the CS1 and CS2 subgroups. **(A)** Enhanced volcano map of the differentially expressed genes in the two clusters. **(B)** GO enrichment analysis. **(C)** GSVA analysis of the differential pathways between the two ccRCC subtypes. **(D)** Regulon scores of different transcriptional factors. Yellow represents active expression of the transcription factors. Blue represents repressed expression of the transcription factors.

SUPPLEMENTARY FIGURE S2

Immune landscapes of the two ccRCC subtypes. **(A)** Heatmap of the immune signatures between CS1 and CS2, including chemokine, chemokine receptor, MHC, immunoinhibitory, and immunostimulatory signatures. **(B)** Heatmap of tumor-infiltrating immune cells between CS1 and CS2 based on the TIMER, CIBERSORT, CIBERSORT-ABS, quanTIseq, MCP-counter, xCell, and EPIC algorithms. MHC, major histocompatibility complex.

References

1. Levey AS, James MT. Acute kidney injury. *Ann Intern Med*. (2017) 167:ITC66-ITC80. doi: 10.7326/AITC201711070

2. Coca SG, Singanamala S, Parikh CR. Chronic kidney disease after acute kidney injury: a systematic review and Meta-analysis. *Kidney Int*. (2012) 81:442–8. doi: 10.1038/ki.2011.379

3. Hoste EA, Clermont G, Kersten A, Venkataraman R, Angus DC, De Bacquer D, et al. Rifle criteria for acute kidney injury are associated with hospital mortality in critically ill patients: a cohort analysis. *Crit Care*. (2006) 10:R73. doi: 10.1186/cc4915

4. Oh DJ. A long journey for acute kidney injury biomarkers. *Ren Fail*. (2020) 42:154–65. doi: 10.1080/0886022X.2020.1721300

5. Bejnordi BE, Veta M, Van Diest PJ, Van Ginneken B, Karssemeijer N, Litjens G, et al. Diagnostic assessment of deep learning algorithms for detection of lymph node metastases in women with breast Cancer. *JAMA*. (2017) 318:2199–10. doi: 10.1001/jama.2017.14585

6. Lee CK, Hofer I, Gabel E, Baldi P, Cannesson M. Development and validation of a deep neural network model for prediction of postoperative in-hospital mortality. *Anesthesiology*. (2018) 129:649–2. doi: 10.1097/ALN.0000000000002186

7. Peired AJ, Lazzeri E, Guzzi F, Anders HJ, Romagnani P. From kidney injury to kidney Cancer. *Kidney Int*. (2021) 100:55–66. doi: 10.1016/j.kint.2021.03.011

8. Peired AJ, Antonelli G, Angelotti ML, Allinovi M, Guzzi F, Sisti A, et al. Acute kidney injury promotes development of papillary renal cell adenoma and carcinoma from renal progenitor cells. *Sci Transl Med*. (2020) 12:eaaw6003. doi: 10.1126/scitranslmed.aaw6003

9. Gahan JC, Gosalbez M, Yates T, Young EE, Escudero DO, Chi A, et al. Chemokine and chemokine receptor expression in kidney tumors: molecular profiling of histological subtypes and association with metastasis. *J Urol*. (2012) 187:827–3. doi: 10.1016/j.juro.2011.10.150

10. Eruslanov E, Stoffs T, Kim WJ, Daurkin I, Gilbert SM, Su LM, et al. Expansion of Ccr8(+) inflammatory myeloid cells in Cancer patients with Urothelial and renal carcinomas. *Clin Cancer Res*. (2013) 19:1670–80. doi: 10.1158/1078-0432.CCR-12-2091

11. de Vivar Chevez AR, Finke J, Bukowski R. The role of inflammation in kidney Cancer. *Adv Exp Med Biol*. (2014) 816:197–4. doi: 10.1007/978-3-0348-0837-8_9

12. Zhou X, Xiao F, Sugimoto H, Li B, McAndrews KM, Kalluri R. Acute kidney injury instigates malignant renal cell carcinoma via Cxcr2 in mice with inactivated Trp53 and Pten in proximal tubular kidney epithelial cells. *Cancer Res*. (2021) 81:2690–02. doi: 10.1158/0008-5472.CAN-20-2930

13. Lowrance WT, Ordoñez J, Udaltsova N, Russo P, Go AS. Ckd and the risk of incident Cancer. *J Am Soc Nephrol*. (2014) 25:2327–34. doi: 10.1681/ASN.2013060604

14. Hsieh JJ, Purdue MP, Signoretti S, Swanton C, Albiges L, Schmidinger M, et al. Renal Cell Carcinoma. *Nat Rev Dis Primers*. (2017) 3:1–19. doi: 10.1038/nrdp.2017.9

15. Jiang A, Pang Q, Gan X, Wang A, Wu Z, Liu B, et al. Definition and verification of novel metastasis and recurrence related signatures of Ccrcc: a multicohort study. *Cancer Innovation*. (2022) 1:146–7. doi: 10.1002/cai2.25

16. Jiang A, Wu X, Wang D, Wang A, Dong K, Liu B, et al. A new thinking: deciphering the aberrance and clinical implication of Igf Axis regulation pattern in clear cell renal cell carcinoma. *Front Immunol*. (2022) 13:935595. doi: 10.3389/fimmu.2022.935595

17. Lameire NH, Bagga A, Cruz D, De Maeseneer J, Endre Z, Kellum JA, et al. Acute kidney injury: An increasing global concern. *Lancet*. (2013) 382:170–9. doi: 10.1016/S0140-6736(13)60647-9

18. Kosieradzki M, Rowinski W. Ischemia/reperfusion injury in kidney transplantation: mechanisms and prevention. *Transplant Proc*. (2008) 40:3279–88. doi: 10.1016/j.transproceed.2008.10.004

19. Jang HR, Rabb H. The innate immune response in ischemic acute kidney injury. *Clin Immunol*. (2009) 130:41–50. doi: 10.1016/j.clim.2008.08.016

20. Zheng L, Gao W, Hu C, Yang C, Rong R. Immune cells in ischemic acute kidney injury. *Curr Protein Pept Sci*. (2019) 20:770–6. doi: 10.2174/1389203720666190507102529

21. Yang JJ, Wu BB, Han F, Chen JH, Yang Y. Gene expression profiling of Sepsis-associated acute kidney injury. *Exp Ther Med*. (2020) 20:34. doi: 10.3892/etm.2020.9161

22. Tang Y, Yang X, Shu H, Yu Y, Pan S, Xu J, et al. Bioinformatic analysis identifies potential biomarkers and therapeutic targets of septic-shock-associated acute kidney injury. *Hereditas*. (2021) 158:13. doi: 10.1186/s41065-021-00176-y

23. Lin X, Li J, Tan R, Zhong X, Yang J, Wang L. Identification of hub genes associated with the development of acute kidney injury by weighted gene co-expression network analysis. *Kidney Blood Press Res*. (2021) 46:63–73. doi: 10.1159/000511661

24. Wei J, Zhang J, Wei J, Hu M, Chen X, Qin X, et al. Identification of Agxt2, Shmt1, and Aco2 as important biomarkers of acute kidney injury by Wgcna. *PLoS One*. (2023) 18:e0281439. doi: 10.1371/journal.pone.0281439

25. Kagawa T, Zarybnicky T, Omi T, Shirai Y, Toyokuni S, Oda S, et al. A scrutiny of circulating Microrna biomarkers for drug-induced tubular and glomerular injury in rats. *Toxicology*. (2019) 415:26–36. doi: 10.1016/j.tox.2019.01.011

26. Jung YJ, Park W, Kang KP, Kim WJNDT. Sirt2 is involved in Cisplatin-induced acute kidney injury through regulation of mitogen-activated protein kinase Phosphatase-1. *Nephrol Dialysis Transpl*. (2020) 35:1145–56. doi: 10.1093/ndt/gfaa042

27. Li H, Xiong J, Du Y, Huang Y, Zhao J. Dual-specificity phosphatases and kidney diseases. *Kidney Dis (Basel)*. (2022) 8:13–25. doi: 10.1159/000520142

28. Li L, Huang L, Vergis AL, Ye H, Bajwa A, Narayan V, et al. Il-17 produced by neutrophils regulates Ifn-gamma-mediated neutrophil migration in mouse kidney ischemia-reperfusion injury. *J Clin Invest*. (2010) 120:331–2. doi: 10.1172/JCI38702

29. Mehrotra P, Collett JA, McKinney SD, Stevens J, Ivancic CM, Basile DP. Il-17 mediates neutrophil infiltration and renal fibrosis following recovery from ischemia reperfusion: compensatory role of natural killer cells in Athymic rats. *Am J Physiol Renal Physiol*. (2017) 312:F385–97. doi: 10.1152/ajprenal.00462.2016

30. Xu C, Chang A, Hack BK, Eadon MT, Alper SL, Cunningham PN. Tnf-mediated damage to glomerular endothelium is an important determinant of acute kidney injury in Sepsis. *Kidney Int*. (2014) 85:72–81. doi: 10.1038/ki.2013.286

31. Kinsey GR, Okusa MD. Expanding role of T cells in acute kidney injury. *Curr Opin Nephrol Hypertens*. (2014) 23:9–16. doi: 10.1097/01.mnh.0000436695.29173.de

32. Jang HR, Rabb H. Immune cells in experimental acute kidney injury. *Nat Rev Nephrol*. (2015) 11:88–1. doi: 10.1038/nrneph.2014.180

33. Huh J-E, Nam D-W, Baek Y-H, Kang JW, Park D-S, Choi D-Y, et al. Formononetin accelerates wound repair by the regulation of early growth response Factor-1 transcription factor through the phosphorylation of the Erk and P38 Mapk pathways. *Int Immunopharmacol*. (2011) 11:46–54. doi: 10.1016/j.intimp.2010.10.003

34. Chen J, Chen Y, Olivero A, Chen XJ. Identification and validation of potential biomarkers and their functions in acute kidney injury. *Front Genet*. (2020) 11:1. doi: 10.3389/fgene.2020.00411

35. Chen JW, Huang MJ, Chen XN, Wu LL, Li QG, Hong Q, et al. Transient Upregulation of Egr1 signaling enhances kidney repair by activating Sox9(+) renal tubular cells. *Theranostics*. (2022) 12:5434–50. doi: 10.7150/thno.73426

36. Ho LC, Sung JM, Shen YT, Jheng HF, Chen SH, Tsai PJ, et al. Egr-1 deficiency protects from renal inflammation and fibrosis. *J Mol Med (Berl)*. (2016) 94:933–2. doi: 10.1007/s00109-016-1403-6

37. Susnik N, Sorensen-Zender I, Rong S, von Vietinghoff S, Lu X, Rubera I, et al. Ablation of proximal tubular suppressor of cytokine signaling 3 enhances tubular cell cycling and modifies macrophage phenotype during acute kidney injury. *Kidney Int*. (2014) 85:1357–68. doi: 10.1038/ki.2013.525

38. Xie X, Yang X, Wu J, Ma J, Wei W, Fei X, et al. Trib1 contributes to recovery from ischemia/reperfusion-induced acute kidney injury by regulating the polarization of renal macrophages. *Front Immunol*. (2020) 11:473. doi: 10.3389/fimmu.2020.00473

39. Gunther OP, Shin H, Ng RT, McMaster WR, McManus BM, Keown PA, et al. Novel multivariate methods for integration of genomics and proteomics data: applications in a kidney transplant rejection study. *OMICS*. (2014) 18:682–5. doi: 10.1089/omi.2014.0062

40. Liu Z, Tang C, He L, Yang D, Cai J, Zhu J, et al. The negative feedback loop of Nf-Kappab/Mir-376b/Nfkbiz in septic acute kidney injury. JCI. *Insight*. (2020) 5:1–17. doi: 10.1172/jci.insight.142272

41. Naik RP, Derebail VK, Grams ME, Franceschini N, Auer PL, Peloso GM, et al. Association of Sickle Cell Trait with chronic kidney disease and albuminuria in African Americans. *JAMA*. (2014) 312:2115–25. doi: 10.1001/jama.2014.15063

42. Yang ES, Nassar AH, Adib E, Jegede OA, Alaiwi SA, Manna DLD, et al. Gene expression signature correlates with outcomes in metastatic renal cell carcinoma patients treated with Everolimus alone or with a vascular disrupting Agentgene signature correlates with outcomes for metastatic Rcc. *Mol Cancer Ther*. (2021) 20:1454–61. doi: 10.1158/1535-7163.MCT-20-1091

43. Zhang ZY, Zhang SL, Chen HL, Mao YQ, Kong CY, Li ZM, et al. Low Egr1 expression predicts poor prognosis in clear cell renal cell carcinoma. *Pathol Res Pract*. (2021) 228:153666. doi: 10.1016/j.prp.2021.153666

44. Tomita S, Ishibashi K, Hashimoto K, Sugino T, Yanagida T, Kushida N, et al. Suppression of Socs3 increases susceptibility of renal cell carcinoma to interferon-alpha. *Cancer Sci*. (2011) 102:57–63. doi: 10.1111/j.1349-7006.2010.01751.x

45. Hao J, Cao Y, Yu H, Zong L, An R, Xue Y. Effect of Map3k8 on prognosis and tumor-related inflammation in renal clear cell carcinoma. *Front Genet*. (2021) 12:674613. doi: 10.3389/fgene.2021.674613

46. Mantovani A, Allavena P, Sica A, Balkwill F. Cancer-related inflammation. *Nature*. (2008) 454:436–4. doi: 10.1038/nature07205

47. Jordan MI, Mitchell TM. Machine learning: trends, perspectives, and prospects. *Science*. (2015) 349:255–0. doi: 10.1126/science.aaa8415

48. Chen T, Li X, Li Y, Xia E, Qin Y, Liang S, et al. Prediction and risk stratification of kidney outcomes in Iga nephropathy. *Am J Kidney Dis*. (2019) 74:300–9. doi: 10.1053/j.ajkd.2019.02.016

49. Tseng PY, Chen YT, Wang CH, Chiu KM, Peng YS, Hsu SP, et al. Prediction of the development of acute kidney injury following cardiac surgery by machine learning. *Crit Care*. (2020) 24:478. doi: 10.1186/s13054-020-03179-9

50. Zhang Z, Ho KM, Hong Y. Machine learning for the prediction of volume responsiveness in patients with Oliguric acute kidney injury in critical care. *Crit Care*. (2019) 23:112. doi: 10.1186/s13054-019-2411-z

51. Mohamadlou H, Lynn-Palevsky A, Barton C, Chettipally U, Shieh L, Calvert J, et al. Prediction of acute kidney injury with a machine learning algorithm using electronic health record data. *Can J Kidney Health Dis*. (2018) 5:776326. doi: 10.1177/2054358118776326

52. Liang Z, Hu X, Lin R, Tang Z, Ye Z, Mao R, et al. Identification of shared gene signatures and molecular mechanisms between chronic kidney disease and ulcerative colitis. *Front Immunol*. (2023) 14:1078310. doi: 10.3389/fimmu.2023.1078310

53. Yao M, Zhang C, Gao C, Wang Q, Dai M, Yue R, et al. Exploration of the shared gene signatures and molecular mechanisms between systemic lupus Erythematosus and pulmonary arterial hypertension: evidence from Transcriptome data. *Front Immunol*. (2021) 12:658341. doi: 10.3389/fimmu.2021.658341

frontiers | Frontiers in Oncology

TYPE Original Research
PUBLISHED 06 June 2023
DOI 10.3389/fonc.2023.1172670

OPEN ACCESS

EDITED BY
Zheng Wang,
Shanghai Jiao Tong University, China

REVIEWED BY
Sonia Tewani Orcutt,
University of Arkansas for Medical Sciences, United States
Belgin Sever,
Anadolu University, Türkiye

*CORRESPONDENCE
Juan Ren
869491533@qq.com

RECEIVED 23 March 2023
ACCEPTED 10 May 2023
PUBLISHED 06 June 2023

CITATION
Bai S, Chen L, Zhu G, Xuan W, Hu F, Liu W, Li W, Lan N, Chen M, Yan Y, Li R, Yang Y and Ren J (2023) Prognostic value of extrahepatic metastasis on colon cancer with liver metastasis: a retrospective cohort study. *Front. Oncol.* 13:1172670. doi: 10.3389/fonc.2023.1172670

Prognostic value of extrahepatic metastasis on colon cancer with liver metastasis: a retrospective cohort study

Shuheng Bai[1], Ling Chen[2], Guixian Zhu[3], Wang Xuan[1], Fengyuan Hu[1], Wanyi Liu[1], Wenyang Li[1], Ning Lan[1], Min Chen[1], Yanli Yan[1], Rong Li[1], Yiping Yang[4] and Juan Ren[1]*

[1]Department of Radiotherapy, The First Affiliated Hospital of Xi'an Jiaotong University, Xi'an, China, [2]Department of Chemotherapy, The First Affiliated Hospital of Xi'an Jiaotong University, Xi'an, China, [3]Department of Oncology, The Second Affiliated Hospital of Xi'an Jiaotong University, Xi'an, China, [4]Department of Radiotherapy, Radiotherapy Clinical Medical Research Center of Shaanxi Province, Xi'an, China

Introduction: The occurrence of metastasis is a threat to patients with colon cancer (CC), and the liver is the most common metastasis organ. However, the role of the extrahepatic organs in patients with liver metastasis (LM) has not been distinctly demonstrated. Therefore, this research aimed to explore the prognostic value of extrahepatic metastases (EHMs).

Methods: In this retrospective study, a total of 13,662 colon patients with LM between 2010 and 2015 were selected from the Surveillance, Epidemiology, and End Results database (SEER). Fine and Gray's analysis and K–M survival analysis were utilized to explore the impacts of the number of sites of EHMs and different sites of EHMs on prognosis. Finally, a prognostic nomogram model based on the number of sites of EHMs was constructed, and a string of validation methods was conducted, including concordance index (C-index), receiver operating characteristic curves (ROC), and decision curve analysis (DCA).

Results: Patients without EHMs had better prognoses in cancer-specific survival (CSS) and overall survival (OS) than patients with EHMs ($p < 0.001$). Varied EHM sites of patients had different characteristics of primary location site, grade, and histology. Cumulative incidence rates for CSS surpassed that for other causes in patients with 0, 1, 2, ≥ 3 EHMs, and the patients with more numbers of sites of EHMs revealed worse prognosis in CSS ($p < 0.001$). However, patients with different EHM sites had a minor difference in cumulative incidence rates for CSS ($p = 0.106$). Finally, a nomogram was constructed to predict the survival probability of patients with EHMs, which is based on the number of sites of EHMs and has been proven an excellent predictive ability.

Conclusion: The number of sites of EHMs was a significant prognostic factor of CC patients with LM. However, the sites of EHMs showed limited impact on survival. Furthermore, a nomogram based on the number of sites of EHMs was constructed to predict the OS of patients with EHMs accurately.

KEYWORDS

colorectal cancer, competing risk analysis, extrahepatic metastasis, prognostic model, SEER, risk factor

Introduction

Colorectal cancer (CRC) leads to a vast health program in the world, with an incidence of 10.2% and a mortality of 9.2% all over the world in 2018, which is the third most common cancer and the second leading cause of cancer-related mortality (1). Moreover, the incidence and deaths are increasing for both males and females in most countries, especially in developing countries (2). CRC can be divided into colon cancer (CC), and rectum cancer. CC, the most common of these subtypes, was responsible for 59.46% of new cases and 61.68% of fatalities globally in 2020. Additionally, among all malignancies, CC alone ranks seventh in terms of new cases and fatalities (2, 3).

The occurrence of metastasis is a threat for CRC patients and may be fatal (4). At the time of first diagnosis, 20% of CRC patients had metastases, and this percentage has remained constant over the past two decades (5). The prognosis for CRC patients with distant metastases is substantially worse, and the 5-year survival rates for CRC patients with or without localized tumors are 91 and 14%, respectively (6). The liver is the most common organ for distant metastasis of CRC with a relatively poor prognosis (7). Population-based research reported that 24.7% of patients with CRC developed liver metastasis (LM) during the disease. About 71% of patients with LM were found at first diagnosis (8). The 5-year survival rate is lower than 5% for these patients with only palliative intent (9). However, in patients who have received successful radical resection of LM, a 5-year survival rate can achieve to 30–57% (10–12).

Great effort has been made to predict how CRC patients with LM would do. AJCC stage system is a reliable criterion for evaluating patients' prognoses. However, it is unsuitable for patients with distant metastasis (Stage IV), especially patients with more than one metastasis organ. Some population-based research constructed a prognostic model for CRC with distant metastasis (13, 14). Nevertheless, the number of sites of extrahepatic metastases (EHMs) was not involved in these prognostic analyses, which may be an efficient indicator for the survival of patients with LM. To our best research, the role of the number of extrahepatic organs in LM has not been clearly demonstrated. Additionally, a certain extrahepatic organ metastasis may result in a particular prognosis. It may be efficient to improve the prognostic value of these models when considering the information on the number of sites of EHMs and metastatic sites.

Thus, in this research, we mainly investigated the prognostic values of the number of sites of EHMs and explored the prognostic features among different EHM sites. Moreover, in order to estimate survival time, we also created a unique risk framework, and the nomogram was validated in a validation cohort.

Methods

Data acquisition and eligibility criteria

This was a retrospective research employing information from the Surveillance, Epidemiology, and End Results (SEER) database (https://seer.cancer.gov/data/), which is a public cancer statistic database founded by the National Cancer Institute (NCI), providing a string of clinical and pathological data including treatment, metastasis, and survival time of many tumors. In this present study, data from patients were extracted by utilizing SEER*Stat (version 8.4.0). The requirement of the Declaration of Helsinki was honored in this research.

In this study, individuals with LM of the colon who were diagnosed between 2010 and 2015 were included after meeting certain inclusion and exclusion criteria. The inclusion criteria were as follows: (a) malignancies that originated in colon without rectum, (b) patients with confirmed pathological diagnosis (biopsy or surgical samples), and (c) patients with confirmed LM from CC. Exclusion criteria were as follows: (a) patients with unknown metastasis information, (b) evidence of other coexisting malignancies, and (c) patients without complete records for American Joint Committee on Cancer (AJCC)-TNM staging, treatment, overall survival (OS), and cancer-specific survival (CSS).

Variable extraction and cohort identification

Clinical variables were extracted from this dataset, including demographic features, location site of the primary lesion, grade, T stage, N stage, M stage, detailed information about metastasis, histology, anticancer treatment (surgery, radiotherapy, and chemotherapy), survival status, and survival time (CSS and OS). The location of the primary lesion was further divided into the right-sided colon and left-sided colon. The histology was classified into four subtypes: adenocarcinoma, mucinous adenocarcinoma, signet ring cell carcinoma, and other. Furthermore, T stage fell into two categories: "T1-2" and "T3-4." In this research, all eligible patients were randomly divided into a training cohort and a validation cohort according to a ratio of 7:3 before constructing our nomogram.

Statistical analysis

All categorical variables were summarized as count and percentage, and Chi-square test and Fisher's exact test were utilized for categorized data. The clinical and demographic features of eligible patients with involvement of 0, 1, 2, or 3 extrahepatic organs were compiled using descriptive statistics. Kaplan–Meier analysis was performed by utilizing the "survival" and "survmine" packages in R software, and a Log-Rank test was used to assess how the curves differed from one another. By using the R software's "Survival" package, univariate and multivariate regression analyses were used to pinpoint OS and CSS prognostic risk variables. Using the "cmprsk" package in R, the Fine and Gray's model was adjusted to forecast the cumulative incidence function (CIF) of mortality from CSS and other causes. The "rms" R program was used to create the nomogram for our model. Moreover, a string of validation measurements, including concordance index (Cindex), receiver operating characteristic curves (ROC), and calibration

curves, were conducted to evaluate the discrimination ability and calibration ability of our nomogram by utilizing "riskRegression," "timeROC," "pec," "cmprsk," and "survival" R packages. In this study, R software (version 4.1.2) was adopted for all statistical analyses. *P* value < 0.05 was considered statistically significant, and all statistical tests were two-sided.

Results

Clinical characteristics of eligible patients

A total of 13,662 CC patients with LM were enrolled in our research, among whom 6,262 were women and 7,400 were men. For the distribution of the number of EHM in our overall cohort, 10,131 (74%) patients had zero involved extrahepatic organs; 2,766 (20%) patients had one involved extrahepatic organ; 673 (4.9%) patients had two involved extrahepatic organs, and 92 (0.7%) patients had three or more than three involved extrahepatic organs. Detailed information about other clinical features of the overall cohort was summarized in Table 1.

In our research, we also divided all patients into train-cohort and test-cohort randomly according to a ratio of 7:3 for our prognostic model's construction and validation subsequently. Moreover, we found no significant statistical difference among clinicopathological characteristics between these two cohorts *via* the Chi-square test (Table 1).

The correlation between clinicopathological characteristics and the number of extrahepatic metastasis sites

As shown in Table 2, CC patients with different numbers of EHMs presented a significant difference in some clinicopathological features, including age, grade, T stage, N stage, CEA, radiotherapy, and surgery (all $p < 0.05$). However, other characteristics did not present an obvious association with the number of EHM. It is worth noting that patients with a larger number of EHMs were more likely to have a higher rate of N1 stage (the percentages of patients with N1 stage in patients with none EHM site *vs.* patients with 1 EHM site *vs.* patients with 2 EHM sites *vs.* patients with ≥3 EHM sites: 37% *vs.* 39% *vs.* 44% *vs.* 45%, $p < 0.001$), nevertheless, a lower rate of N0 stage (the percentages of patients with N0 stage in patients with none EHM site *vs.* patients with 1 EHM site *vs.* patients with 2 EHM sites *vs.* patients with ≥ 3 EHM sites: 27% *vs.* 27% *vs.* 26% *vs.* 21%, $p < 0.001$).

TABLE 1 Clinicopathological characteristics between training cohort and validation cohort.

Variable	*N*	Overall, *N* = 13,662	Train cohort, *N* = 9,628	Test cohort, *N* = 4,034	*p*-value
Sex	13,662				> 0.9
Female		6,262 (46%)	4,412 (46%)	1,850 (46%)	
Male		7,400 (54%)	5,216 (54%)	2,184 (54%)	
Age	13,662				0.2
1–49		1,893 (14%)	1,338 (14%)	555 (14%)	
50–59		2,973 (22%)	2,104 (22%)	869 (22%)	
60–69		3,651 (27%)	2,583 (27%)	1,068 (26%)	
70–79		2,868 (21%)	1,971 (20%)	897 (22%)	
80+		2,277 (17%)	1,632 (17%)	645 (16%)	
Race	13,662				0.3
White		10,236 (75%)	7,204 (75%)	3,032 (75%)	
Black		2,318 (17%)	1,658 (17%)	660 (16%)	
Other		1,108 (8.1%)	766 (8.0%)	342 (8.5%)	
Marital.status	13,662				0.4
Married		7,099 (52%)	5,030 (52%)	2,069 (51%)	
Unmarried		5,948 (44%)	4,158 (43%)	1,790 (44%)	
Unknown		615 (4.5%)	440 (4.6%)	175 (4.3%)	
primary.location	13,662				0.7
Left		6,050 (44%)	4,253 (44%)	1,797 (45%)	
Right		7,612 (56%)	5,375 (56%)	2,237 (55%)	

(Continued)

TABLE 1 Continued

Variable	*N*	Overall, *N* = 13,662	Train cohort, *N* = 9,628	Test cohort, *N* = 4,034	*p*-value
Histology	13,662				> 0.9
Adenocarcinoma		11,808 (86%)	8,326 (86%)	3,482 (86%)	
Mucinous adenocarcinoma		867 (6.3%)	613 (6.4%)	254 (6.3%)	
Signet ring cell carcinoma		80 (0.6%)	54 (0.6%)	26 (0.6%)	
Other		907 (6.6%)	635 (6.6%)	272 (6.7%)	
Grade	13,662				0.6
Grade I		552 (4.0%)	391 (4.1%)	161 (4.0%)	
Grade II		7,793 (57%)	5,516 (57%)	2,277 (56%)	
Grade III		2,827 (21%)	1,957 (20%)	870 (22%)	
Grade IV		662 (4.8%)	463 (4.8%)	199 (4.9%)	
Unknown		1,828 (13%)	1,301 (14%)	527 (13%)	
pT	13,662				0.9
T1		1,822 (13%)	1,287 (13%)	535 (13%)	
T2		378 (2.8%)	260 (2.7%)	118 (2.9%)	
T3		6,437 (47%)	4,550 (47%)	1,887 (47%)	
T4		5,025 (37%)	3,531 (37%)	1,494 (37%)	
pN	13,662				0.4
N0		3,721 (27%)	2,602 (27%)	1,119 (28%)	
N1		5,133 (38%)	3,652 (38%)	1,481 (37%)	
N2		4,808 (35%)	3,374 (35%)	1,434 (36%)	
Radiotherapy	13,662				0.8
None		13,171 (96%)	9,279 (96%)	3,892 (96%)	
Performed		491 (3.6%)	349 (3.6%)	142 (3.5%)	
Cheomtherapy	13,662				0.12
None		4,698 (34%)	3,271 (34%)	1,427 (35%)	
Performed		8,964 (66%)	6,357 (66%)	2,607 (65%)	
Surgery	13,662				>0.9
None		3,168 (23%)	2,231 (23%)	937 (23%)	
Performed		10,494 (77%)	7,397 (77%)	3,097 (77%)	
CEA	13,662				0.3
Negative		1,485 (11%)	1,061 (11%)	424 (11%)	
Positive		7,972 (58%)	5,637 (59%)	2,335 (58%)	
Unknown		4,205 (31%)	2,930 (30%)	1,275 (32%)	
extrehepatic.metastates.number	13,662				0.7
0		10,131 (74%)	7,136 (74%)	2,995 (74%)	
1		2,766 (20%)	1,945 (20%)	821 (20%)	
2		673 (4.9%)	485 (5.0%)	188 (4.7%)	
≥3		92 (0.7%)	62 (0.6%)	30 (0.7%)	

[1]n (%).
[2] Pearson's Chi-squared test.

TABLE 2 Characteristics of CC patients with liver metastasis.

		The number of involved extrahepatic organs				
Variable	Overall, *N* = 13,662	0, *N* = 10,131	1, *N* = 2,766	2, *N* = 673	>= 3, *N* = 92	*p*-value
Sex						0.1
Female	6,262 (46%)	4,670 (46%)	1,272 (46%)	277 (41%)	43 (47%)	
Male	7,400 (54%)	5,461 (54%)	1,494 (54%)	396 (59%)	49 (53%)	
Age						0.001
1–49	1,893 (14%)	1,386 (14%)	398 (14%)	96 (14%)	13 (14%)	
50–59	2,973 (22%)	2,161 (21%)	624 (23%)	158 (23%)	30 (33%)	
60–69	3,651 (27%)	2,670 (26%)	762 (28%)	193 (29%)	26 (28%)	
70–79	2,868 (21%)	2,138 (21%)	575 (21%)	139 (21%)	16 (17%)	
80+	2,277 (17%)	1,776 (18%)	407 (15%)	87 (13%)	7 (7.6%)	
Race						0.054
White	10,236 (75%)	7,652 (76%)	2,021 (73%)	491 (73%)	72 (78%)	
Black	2,318 (17%)	1,687 (17%)	503 (18%)	113 (17%)	15 (16%)	
Other	1,108 (8.1%)	792 (7.8%)	242 (8.7%)	69 (10%)	5 (5.4%)	
Marital status						0.19
Married	7,099 (52%)	5,275 (52%)	1,423 (51%)	343 (51%)	58 (63%)	
Unmarried	5,948 (44%)	4,391 (43%)	1,232 (45%)	293 (44%)	32 (35%)	
Unknown	615 (4.5%)	465 (4.6%)	111 (4.0%)	37 (5.5%)	2 (2.2%)	
Primary location						0.7
Left	6,050 (44%)	4,461 (44%)	1,242 (45%)	308 (46%)	39 (42%)	
Right	7,612 (56%)	5,670 (56%)	1,524 (55%)	365 (54%)	53 (58%)	
Histology						0.18
Adenocarcinoma	11,808 (86%)	8,767 (87%)	2,376 (86%)	588 (87%)	77 (84%)	
Mucinous adenocarcinoma	867 (6.3%)	658 (6.5%)	170 (6.1%)	31 (4.6%)	8 (8.7%)	
Signet ring cell carcinoma	80 (0.6%)	55 (0.5%)	17 (0.6%)	7 (1.0%)	1 (1.1%)	
Other	907 (6.6%)	651 (6.4%)	203 (7.3%)	47 (7.0%)	6 (6.5%)	
Grade						< 0.001
Grade I	552 (4.0%)	428 (4.2%)	102 (3.7%)	18 (2.7%)	4 (4.3%)	
Grade II	7,793 (57%)	5,983 (59%)	1,449 (52%)	329 (49%)	32 (35%)	
Grade III	2,827 (21%)	2,093 (21%)	565 (20%)	148 (22%)	21 (23%)	
Grade IV	662 (4.8%)	500 (4.9%)	137 (5.0%)	20 (3.0%)	5 (5.4%)	
Unknown	1,828 (13%)	1,127 (11%)	513 (19%)	158 (23%)	30 (33%)	
pT						< 0.001
T1-2	2,200 (16%)	1,431 (14%)	562 (20%)	185 (27%)	22 (24%)	
T3-4	11,462 (84%)	8,700 (86%)	2,204 (80%)	488 (73%)	70 (76%)	
pN						0.003
N0	3,721 (27%)	2,777 (27%)	749 (27%)	176 (26%)	19 (21%)	
N1	5,133 (38%)	3,725 (37%)	1,073 (39%)	294 (44%)	41 (45%)	

(Continued)

TABLE 2 Continued

Variable	Overall, N = 13,662	The number of involved extrahepatic organs				p-value
		0, N = 10,131	1, N = 2,766	2, N = 673	>= 3, N = 92	
N2	4,808 (35%)	3,629 (36%)	944 (34%)	203 (30%)	32 (35%)	
Radiotherapy						< 0.001
None	13,171 (96%)	9,880 (98%)	2,633 (95%)	599 (89%)	59 (64%)	
Performed	491 (3.6%)	251 (2.5%)	133 (4.8%)	74 (11%)	33 (36%)	
Chemotherapy						0.3
None	4,698 (34%)	3,521 (35%)	913 (33%)	235 (35%)	29 (32%)	
Performed	8,964 (66%)	6,610 (65%)	1,853 (67%)	438 (65%)	63 (68%)	
Surgery						< 0.001
None	3,168 (23%)	1,787 (18%)	977 (35%)	349 (52%)	55 (60%)	
Performed	10,494 (77%)	8,344 (82%)	1,789 (65%)	324 (48%)	37 (40%)	
CEA						< 0.001
Negative	1,485 (11%)	1,201 (12%)	236 (8.5%)	46 (6.8%)	2 (2.2%)	
Positive	7,972 (58%)	5,703 (56%)	1,749 (63%)	454 (67%)	66 (72%)	
Unknown	4,205 (31%)	3,227 (32%)	781 (28%)	173 (26%)	24 (26%)	

[1]n (%).
[2]Pearson's Chi-squared test; Fisher's exact test.

Meanwhile, we also found an interesting phenomenon that patients with a more significant number of EHM sites were more likely to present a positive result of CEA (the percentages of patients with positive CEA in patients with none EHM site *vs.* patients with 1 EHM site *vs.* patients with 2 EHM sites *vs.* patients with ≥ 3 EHM sites: 56% *vs.* 63% *vs.* 67% *vs.* 72%, $p < 0.001$); however, the opposite result was presented in CEA negative (12% *vs.* 8.5% *vs.* 6.8% *vs.* 2.2%, $p < 0.001$). For the therapy aspect, patients with a smaller number of EHMs were more likely to accept surgery and radiotherapy. Nevertheless, there were no differences in the amount of ECM across chemotherapy patients.

Extrahepatic metastasis sites

In our cohort, the most and least frequent EHM sites were the lung (57.54%) and brain (2.31%), respectively. Moreover, the frequent EHM sites of distant lymph nodes (dLNs) and bone were 11.6 and 35.46%, respectively. Then, we selected patients with only one EHM site to explore whether different EHM sites presented various patterns of some clinical features, including sex, primary location site, grade, and histology. As Figure 1 shown, patients with various EHM sites presented different distributed characteristics significantly for primary location site, grade, and histology. We easily found that the primary location on the right accounted for the highest rate (88%) of brain metastasis, and the rate was higher than other metastasis sites. Patients with lung metastasis had the highest rate of adenocarcinoma (90%). Nevertheless, patients with bone metastasis had the lowest (75%).

Moreover, it is notable that patients of Grade II accounted for the most prominent rate in all different metastases sites, rather than patients of Grade IV or III. Meanwhile, patients with lung metastasis had different frequencies for grade compared with patients with others metastasis. Grade III+IV accounted for only 23% of patients with lung metastasis. However, the rates of grade III +IV were 47, 43, and 42% in patients with metastases of bone, brain, and dLNs, respectively.

The prognostics value of the number of sites of extrahepatic metastases

We first explored whether the presence of EHMs had an impact on prognosis. As shown in Figures 2A, B, patients without EHMs had better prognosis both in CSS and OS than patients with others who had EHMs [median CSS: 20 months (without EHMs) *vs.* 11 months (with EHMs), $p < 0.001$; median OS: 18 months (without EHMs) *vs.* 11 months (with EHMs), $p < 0.001$].

The cumulative incidence rates for CSS outnumbered those for other causes in patients with 0, 1, 2, or ≥ 3 EHMs, and cumulative incidence rates for CSS were increased gradually with time since initial (Figure 2C). In addition, the patients with a larger number of EHMs revealed worse prognosis in CSS ($p < 0.001$); however, it is not different in other causes ($p = 0.83$). Moreover, we found that the CSS and OS were correlated with the number of sites of EHMs significantly [median CSS: 20 months *vs.* 12 months *vs.* 8 months *vs.* 5 months (EHMs number: 0 *vs.* 1 *vs.* 2 *vs.* ≥3), $p < 0.001$; median CSS: 18 months *vs.* 11 months *vs.* 8 months *vs.* 5 months (EHMs

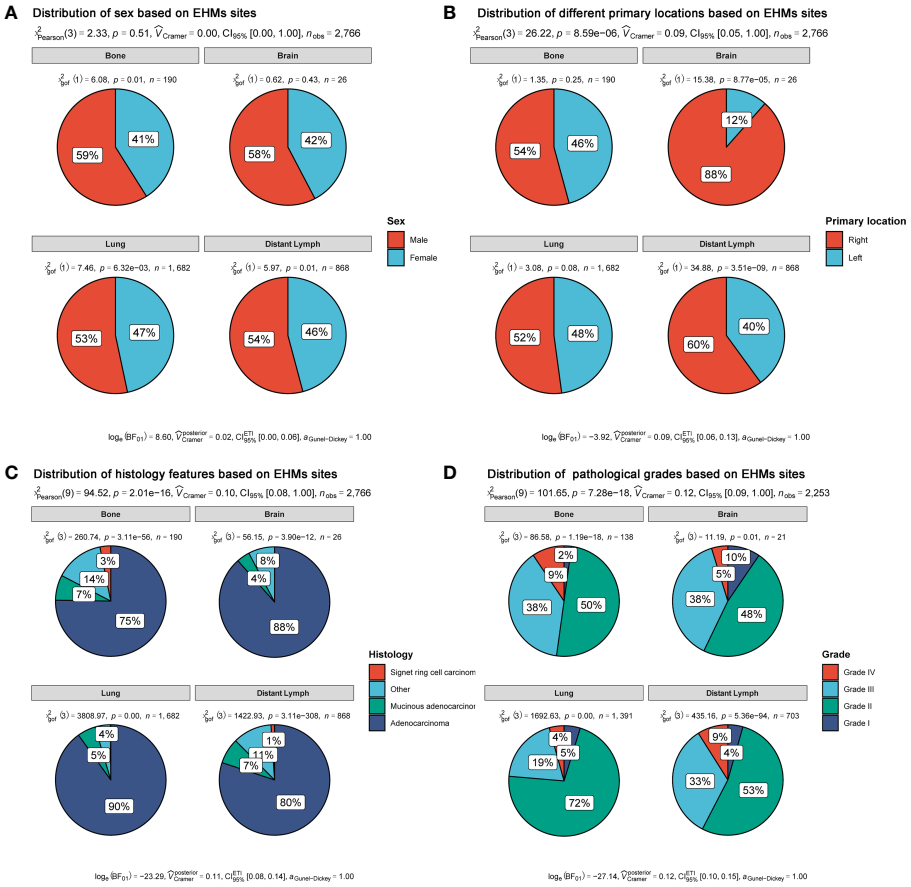

FIGURE 1
Distribution of clinical features based on EHM sites. **(A)** Sex feature. **(B)** Primary location. **(C)** Histology feature. **(D)** Pathological grades.

number: 0 *vs.* 1 *vs.* 2 *vs.* ≥3)] by utilizing K-M analysis for survival rates (Figures 3A, B). Univariate cox regression analysis was also conducted to explore the prognostic value of the number EHMs. As shown in Figures 4A, B, patients with a larger number of EHMs presented a higher hazard ratio (HR) for CSS and OS [CSS-HR: 1.6 (1 *vs.* 0), 2.1(2 *vs.* 0), 2.8 (≥3 *vs.* 0); OS-HR: 1.5(1 *vs.* 0), 2.0(2 *vs.* 0), 2.6 (≥ 3 *vs.* 0), all $p < 0.001$]. In addition, multivariate cox regression analysis showed a consistent result after adjustment for age, race, gender, histology, marital status, grade, CEA, and stage N and T, and treatment [CSS-HR: 1.44(1 *vs.* 0), 1.61(2 *vs.* 0), 2.12 (≥ 3 *vs.* 0); OS-HR: 1.41(1 *vs.* 0), 1.57(2 *vs.* 0), 2.03 (≥3 *vs.* 0), all $p < 0.001$] (Table 3).

The prognostic difference among variant extrahepatic metastasis sites

To further understand whether different EHM sites impacted survival time, we also compared CSS and OS in patients with bong, lung, dLNs, and brain as the only EHMs organ. As Figure 2B shown, patients with different EHM sites had a more negligible difference in cumulative incidence rates for CSS ($p = 0.106$). However, patients with brain metastasis presented the highest cumulative incidence rate for other causes ($p = 0.015$). In addition, as shown in Figures 3C, D, we found that brain metastasis and bone metastasis brought worse prognosis than lung metastasis and dLNs [CSS: 6 months *vs.* 13 months *vs.* 12 months (bone *vs.* brain *vs.* lung *vs.* dLNs), $p > 0.05$(bone *vs.* brain; lung *vs.* dLNs) other $p < 0.05$; OS: 5.5 months *vs.* 4 *vs.* 12 months *vs.* 12 months (bone *vs.* brain *vs.* lung *vs.* dLNs), $p > 0.05$(Bone *vs.* brain; lung *vs.* dLNs) other $p < 0.05$]. Moreover, Univariate cox regression analysis showed that EHMs presented a higher hazard ratio (HR) for CSS and OS (Figures 4C, D), and HRs of bone and brain were more severe that lung and dLNs ($p < 0.001$), which was consisted with our other results above.

Construction and validation of nomogram for patients with extrahepatic metastases

Finally, we constructed a nomogram to predict the survival probability of patients with EHMs (Figure 5A). EHMs number, age, primary location, histology, grade, CEA, stage N, and treatments were involved in this nomogram, which were employed to predict the total point of each patient, thus predicting the 6-, 12-, 18-, 24-, and 36-month OS probability of these patients. In addition, we calculated the C-index of this nomogram to estimate its predictive power, suggesting the model had excellent performance in

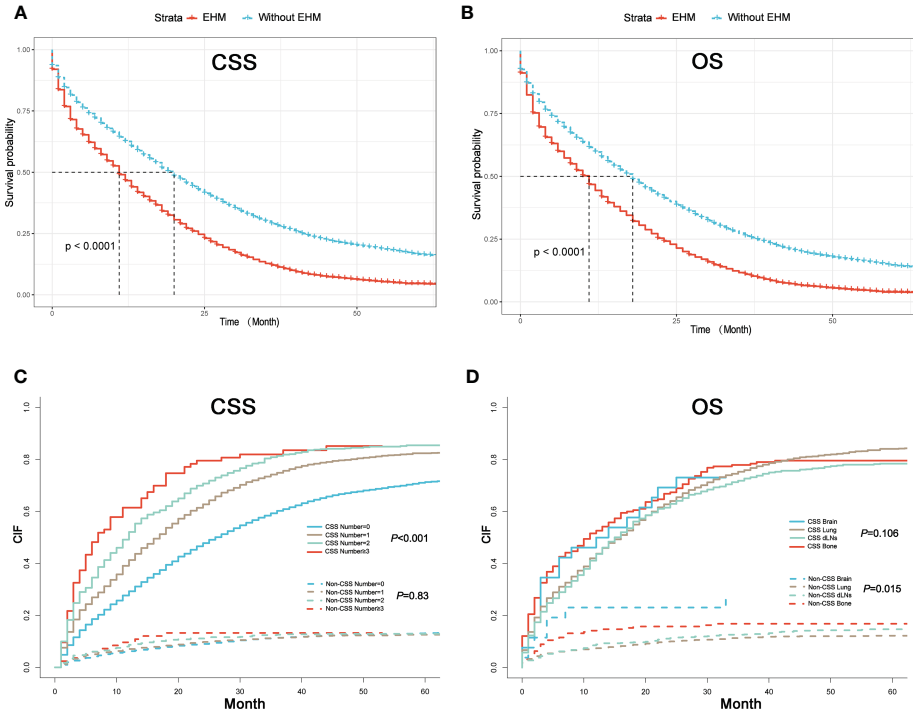

FIGURE 2
(A) K–M curves of CSS for patients with or without extrahepatic metastases (EHMs). **(B)** K–M curves of OS for patients with or without EHMs. **(C)** Cumulative incidence function curves of CSS and non-CSS cause according to the number of sites of EHMs. **(D)** Cumulative incidence function curves of CSS and non-CSS cause according to different sites of EHMs.

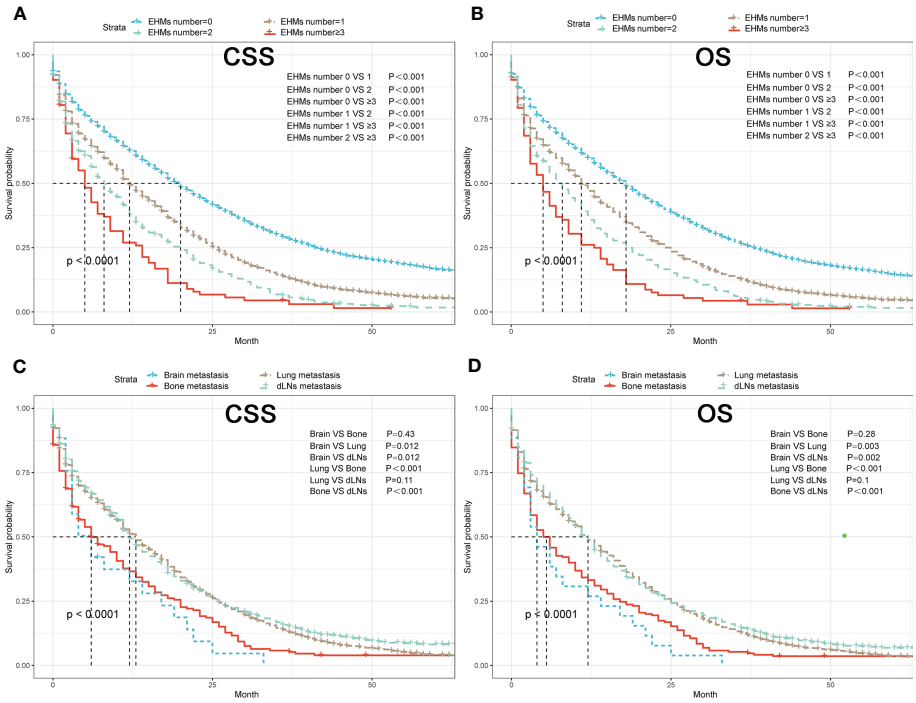

FIGURE 3
(A) K–M curves of CSS for patients with different numbers of extrahepatic metastases (EHMs). **(B)** K–M curves of OS for patients with different numbers of EHMs. **(C)** K–M curves of CSS for patients with different sites of EHMs. **(D)** K–M curves of OS for patients with different sites of EHMs.

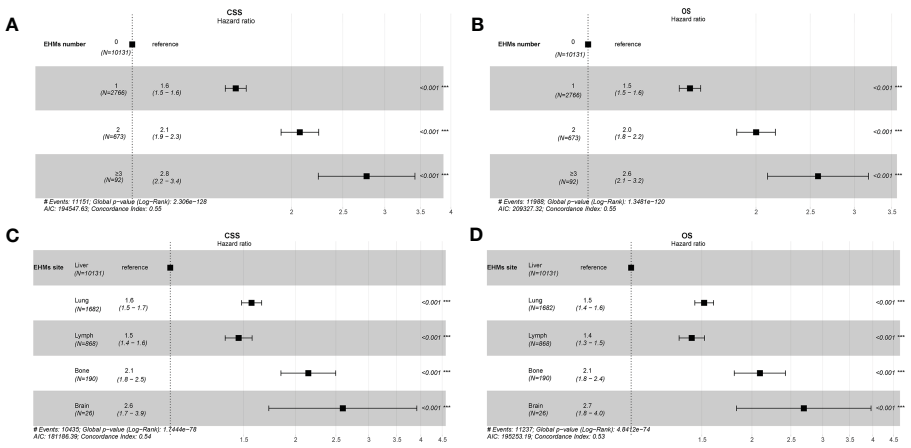

FIGURE 4
(A) Univariate cox regression analysis of CSS for different numbers of extrahepatic metastases (EHMs). **(B)** Univariate cox regression analysis of overall survival (OS) for different numbers of EHMs. **(C)** Univariate cox regression analysis of CSS for different sites of EHMs. **(D)** Univariate cox regression analysis of OS for different sites of EHMs.

TABLE 3 Multivariate cox regression analysis on clinical variables including EHMs.

	CSS			OS		
Characteristic	HR[1]	95% CI[1]	*p*-value	HR[1]	95% CI[1]	*p*-value
EHMs number						
0	—	—		—	—	
1	1.44	1.37, 1.51	< 0.001	1.41	1.34, 1.47	< 0.001
2	1.61	1.48, 1.75	< 0.001	1.57	1.45, 1.71	< 0.001
≥ 3	2.12	1.71, 2.63	< 0.001	2.03	1.64, 2.51	< 0.001
Sex						
Female	—	—		—	—	
Male	1.09	1.04, 1.13	< 0.001	1.1	1.06, 1.14	< 0.001
Age						
1–49	—	—		—	—	
50–59	1.04	0.98, 1.11	0.2	1.06	0.99, 1.13	0.093
60–69	1.1	1.03, 1.17	0.003	1.13	1.07, 1.20	< 0.001
70–79	1.36	1.28, 1.46	< 0.001	1.43	1.34, 1.53	< 0.001
80+	1.78	1.66, 1.91	< 0.001	1.88	1.75, 2.01	< 0.001
Race						
Black	—	—		—	—	
Other	0.83	0.77, 0.90	< 0.001	0.83	0.76, 0.89	< 0.001
White	0.88	0.84, 0.93	< 0.001	0.87	0.83, 0.91	< 0.001
Marital status						
Married	—	—		—	—	
Unknown	0.99	0.90, 1.08	0.8	1.02	0.93, 1.11	0.7
Unmarried	1.11	1.07, 1.16	< 0.001	1.12	1.08, 1.16	< 0.001

(Continued)

10.3389/fonc.2023.1172670

TABLE 3 Continued

	CSS			OS		
Characteristic	HR[1]	95% CI[1]	*p*-value	HR[1]	95% CI[1]	*p*-value
Primary location						
Left	—	—		—	—	
Right	1.17	1.13, 1.22	< 0.001	1.16	1.12, 1.21	< 0.001
Histology						
Adenocarcinoma	—	—		—	—	
Mucinous adenocarcinoma	1.14	1.06, 1.23	< 0.001	1.13	1.05, 1.22	0.001
Other	1.19	1.09, 1.29	< 0.001	1.23	1.14, 1.33	< 0.001
Signet ring cell carcinoma	1.42	1.12, 1.80	0.004	1.46	1.16, 1.84	0.001
Grade						
Grade I	—	—		—	—	
Grade II	1.38	1.24, 1.53	< 0.001	1.39	1.26, 1.53	< 0.001
Grade III	2.09	1.88, 2.33	< 0.001	2.07	1.87, 2.30	< 0.001
Grade IV	2.4	2.11, 2.73	< 0.001	2.37	2.09, 2.68	< 0.001
Unknown	1.7	1.52, 1.91	< 0.001	1.73	1.55, 1.93	< 0.001
pT						
T1-2	—	—		—	—	
T3-4	1.07	1.01, 1.14	0.027	1.06	1.00, 1.13	0.036
pN						
N0	—	—		—	—	
N1	1.15	1.10, 1.21	< 0.001	1.15	1.09, 1.20	< 0.001
N2	1.64	1.55, 1.74	< 0.001	1.59	1.51, 1.68	< 0.001
Radiotherapy						
None	—	—		—	—	
Performed	1.03	0.93, 1.14	0.6	1.02	0.92, 1.12	0.7
Cheomtherapy						
None	—	—		—	—	
Performed	0.37	0.36, 0.39	< 0.001	0.36	0.35, 0.38	< 0.001
Surgery						
None	—	—		—	—	
Performed	0.39	0.36, 0.41	< 0.001	0.4	0.38, 0.42	< 0.001
CEA						
Negative	—	—		—	—	
Positive	1.52	1.42, 1.62	< 0.001	1.52	1.42, 1.62	< 0.001
Unknown	1.4	1.31, 1.50	< 0.001	1.42	1.33, 1.52	< 0.001

[1]HR, hazard ratio; CI, confidence interval; —, Reference.

predicting the OS of CC patients with EHMs (training cohort: 0.738; validation cohort: 0.739). Moreover, ROC curves and calibration curves were generated of our nomogram. As shown in Figure 5B, the area under the curve (AUC) of our nomogram were 0.863, 0.833, 0.815, 0.8, and 0.784 in predicting 6-, 12-, 18-, 24-, and 36- month OS, respectively, of patients in training cohort. Moreover, the AUCs of validation cohort were 0.862, 0.833, 0.817, 0.807, and 0.792, respectively (Figure 5C). Additionally, we displayed the calibration curves, which showed excellent concordance between the actual and projected OS in the training cohort and validation cohort (Figures 5D, E). All of these findings showed how well our nomogram predicted the likelihood that patients with EHMs would survive.

Discussion

The liver is the most common distant metastatic organ in patients with CC and threaten patients' survival time (15–17). Our results also revelated that CC patients with LM presented high cancer mortality. Some clinicopathological features affect patients' prognosis, including TNM stage, age, TP53, KRAS, MSI, and so on (18–21). However, the way of EHMs impacts the prognosis of CC is still unclearly.

We found that the number of sites of EHMs was a significant prognostic factor for CC patients with LM. In our research, the patient with no EHMs had a better prognosis, while a patient with 1, 2, ≥ 3 EHMs presented a worse survival. It might result from that patient with EHMs would not receive liver resection. A study of 1,600 patients demonstrated that 5-year survival rates of patients who received liver resection could achieve above 50%, compared with only 5% for patients treated with palliative (10). Moreover, the survival time decreased as the number of EHMs increased, which may be attributed to the limited effectiveness of systemic treatment for patients with multiple metastases. A similar result was obtained by other research. Wang et al. found that more numbers of sites of EHMs were associated with poor prognosis in NSCLC patients with brain metastasis (22). Meanwhile, the results of cox regression analysis also implied that the number of sites of EHMs caused different hazard ratios significantly, which implied that it might be a suitable prognostic indicator for patients with EHMs.

Moreover, we also explored the impact of sites of EHMs on survival. In our research, patients with different EHM sites had a smaller difference in cumulative incidence rates for CSS, which indicted that the site of EHMs could not be a suitable index for prediction of survival time. Also, patient with brain metastasis and bone metastasis tended to present a worse prognosis than with lung metastasis and dLNs, which was consistent with other research. Tokore had reported that the median survival time of CC patient with brain metastasis was only 2.8 months (23). Moreover, the median survival time of bone metastasis was similar to brain metastasis, which was 5–7 months (24). Compared with the worse prognosis of brain and bone metastasis, the median survival time of lung and dLNs were 10 months and 8 months,

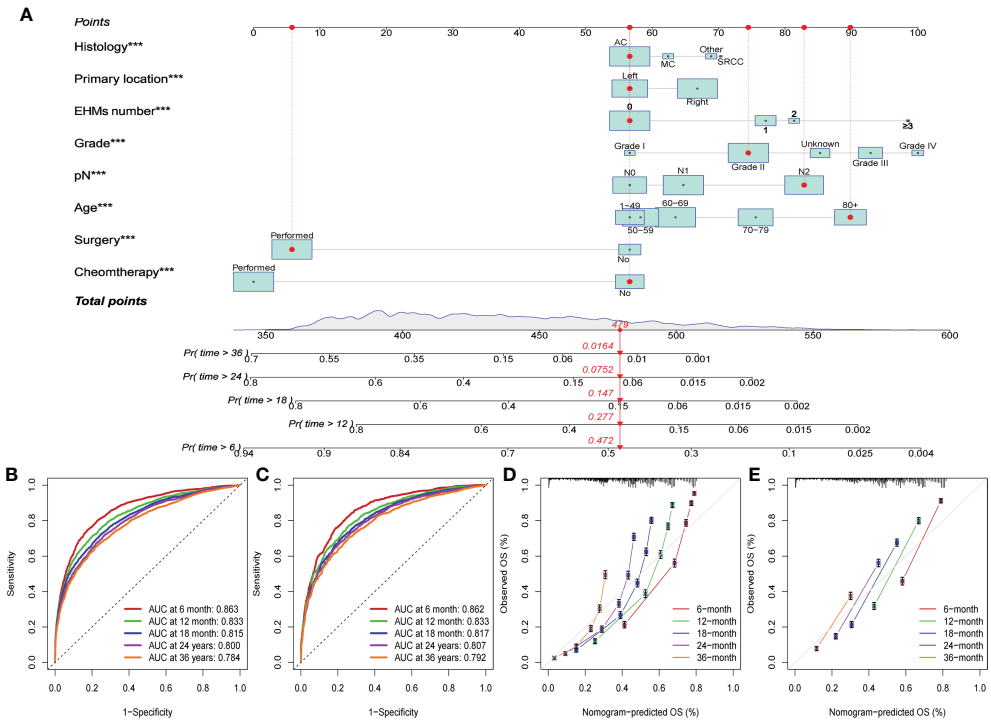

FIGURE 5
(A) The constructed nomogram for predicting 6-, 12-, 18-, 24-, and 36-month overall survival (OS) of patients with EHMs. ***: p≤0.001. **(B)** The ROC curves for predicting 6-, 12-, 18-, 24-, and 36-month OS in the training cohort. **(C)** The ROC curves for predicting 6-, 12-, 18-, 24-, and 36-month OS in the validation cohort. **(D)** The calibration curves for predicting 6-, 12-, 18-, 24-, and 36-month OS in the training cohort. **(E)** The calibration curves for predicting 6-, 12-, 18-, 24-, and 36-month OS in the validation cohort.

respectively (4, 25). However, there were no difference in survival time between brain metastasis and bone metastasis, which was revelated again that EHM site was not a suitable prognostic indicator for patients with EHMs.

In this present research, the lung was the most common EHM site, and the brain was the least common site, which implied that it is essential to consider lung metastasis when patients with CC have LM. We also found an interesting result that the primary location of the right tended to have EHMs than of the left, and it accounted for the highest rate (88%) of brain metastasis, which was higher than other metastasis sites. The difference might be induced by the different features between right-sided CC and left-side CC, including molecular, embryological, biological, and anatomical characteristics (26). Research also demonstrated that the sidedness of CC not only has an essential role in the metastatic setting but also is a predictive marker of response to anti-EGFR drugs (26, 27). Previous studies also found that right-sided CC has a more advanced stage at diagnosis (7, 28). In addition, Price et al. speculated that it was induced by the delay in diagnosis for right-sided cancer, which could lead to more metastasis, resulting in worse survival in patients with right-sided cancer (29). Moreover, it is notable that patients with lung metastasis had different frequencies for grade compared with patients with others metastasis. Grade III+IV accounted for only 23% of patients with lung metastasis. However, the rates of grade III+IV were 47, 43, and 42% in patients with metastases of bone, brain, and dLNs, respectively. This result indicated that the occurrence of lung metastasis for patients with LM might not be associated with the level of pathological grade. Li et al. also found that CC patients with lung metastasis were mainly presented as a well-differentiated grade rather than poorly differentiated grade, which is in line with our result (30). However, the detailed mechanism is not revealed, and a string of research is still being urged for this issue.

Based on our results, we concluded that the number of sites of EHMs was a significant predictive factor for CC patients with LM, while the sites of EHMs showed limited impact on survival. Therefore, we constructed a nomogram to predict the survival probability of patients with EHMs. Some clinical features, especially the EHMs number, were involved in this nomogram. Additionally, our nomogram demonstrated strong predictive capacity for the clinical outcome of patients with EHMs in both the training group and the validation cohort. To our best research, it was the first study that aimed to construct a nomogram based on EHMs number. In addition, compared with other research which constructed a prognostic model for CC patients with stage IV, our model also had an obvious advantage. Deng et al. constructed a nomogram model to predict survival time in patients with CRC hepato-pulmonary metastasis. The AUC values of 1 and 3 years were 0.802, 0.759 in the training cohort; 0.814, 0.769 in the validation cohort (31). Han et al. also constructed a model, and the AUC for 1 year was 0.705, for 2 years was 0.675, and for 3 year was 0.648 (32). All these were not excellent as our model, based on that AUC were 0.863, 0.833, 0.815, 0.8, and 0.784 in predicting 6-, 12-, 18-, 24-, and 36- month OS in the training cohort, and 0.862, 0.833, 0.817, 0.807, and 0.792 in a validation cohort.

Conclusion

In conclusion, the number of sites of EHMs was a significant prognostic factor of CC patients with LM. Patients with zero or one involved extrahepatic organ exhibited better survival compared with patients with two or more EHM sites. Patients with a more significant number of ECMs presented a higher cumulative incidence rate of CSS. Moreover, patients with various EHM sites had different impacts on survival and presented variant distribution features of primary location site, grade, and histology. Finally, a nomogram based on the number of sites of EHMs was constructed that can accurately predict the OS of patients with EHMs.

Data availability statement

The original contributions presented in the study are included in the article/supplementary material. Further inquiries can be directed to the corresponding author.

Author contributions

JR supervised the study; SB conceived the study. JR, SB, LC, GZ, YLY, WX, WaL, WeL, FH, NL, MC, and YPY analyzed data; SB wrote the manuscript; JR and SB made manuscript revisions. All authors have read and approved the final version of this submission.

Funding

This manuscript is supported by the Scientific and Technological Research Foundation of Shaan'xi Province, Key Research and Development Project, General project (JR, 2023-YBSF-666); supported by the Shaanxi Provincial Key Research and Development Plan Project(Key support projects Category A) (JR, 2021A011); supported by the Basic and Clinical Integration Innovation Project of Xi'an Jiao tong University, (JR,YXJLRH2022006).

Conflict of interest

The authors declare that the research was conducted in the absence of any commercial or financial relationships that could be construed as a potential conflict of interest.

Publisher's note

References

1. Bray F, Ferlay J, Soerjomataram I, Siegel RL, Torre LA, Jemal A. Global cancer statistics 2018: GLOBOCAN estimates of incidence and mortality worldwide for 36 cancers in 185 countries. *CA Cancer J Clin* (2018) 68:394–424. doi: 10.3322/caac.21492

2. Hossain MS, Karuniawati H, Jairoun AA, Urbi Z, Ooi J, John A, et al. Colorectal cancer: a review of carcinogenesis, global epidemiology, current challenges, risk factors, preventive and treatment strategies. *Cancers (Basel)* (2022) 14. doi: 10.3390/cancers14071732

3. Sung H, Ferlay J, Siegel RL, Laversanne M, Soerjomataram I, Jemal A, et al. Global cancer statistics 2020: GLOBOCAN estimates of incidence and mortality worldwide for 36 cancers in 185 countries. *CA Cancer J Clin* (2021) 71:209–49. doi: 10.3322/caac.21660

4. Riihimaki M, Hemminki A, Sundquist J, Hemminki K. Patterns of metastasis in colon and rectal cancer. *Sci Rep* (2016) 6:29765. doi: 10.1038/srep29765

5. van der Geest LG, Lam-Boer J, Koopman M, Verhoef C, Elferink MA, de Wilt JH. Nationwide trends in incidence, treatment and survival of colorectal cancer patients with synchronous metastases. *Clin Exp Metastasis* (2015) 32:457–65. doi: 10.1007/s10585-015-9719-0

6. Siegel RL, Miller KD, Fedewa SA, Ahnen DJ, Meester RGS, Barzi A, et al. Colorectal cancer statistics. *CA Cancer J Clin* (2017) 67:177–93. doi: 10.3322/caac.21395

7. Engstrand J, Nilsson H, Stromberg C, Jonas E, Freedman J. Colorectal cancer liver metastases - a population-based study on incidence, management and survival. *BMC Cancer* (2018) 18:78. doi: 10.1186/s12885-017-3925-x

8. Hackl C, Neumann P, Gerken M, Loss M, Klinkhammer-Schalke M, Schlitt HJ. Treatment of colorectal liver metastases in Germany: a ten-year population-based analysis of 5772 cases of primary colorectal adenocarcinoma. *BMC Cancer* (2014) 14:810. doi: 10.1186/1471-2407-14-810

9. Noren A, Eriksson HG, Olsson LI. Selection for surgery and survival of synchronous colorectal liver metastases; a nationwide study. *Eur J Cancer* (2016) 53:105–14. doi: 10.1016/j.ejca.2015.10.055

10. House MG, Ito H, Gonen M, Fong Y, Allen PJ, DeMatteo RP, et al. Survival after hepatic resection for metastatic colorectal cancer: trends in outcomes for 1,600 patients during two decades at a single institution. *J Am Coll Surg* (2010) 210:744–52. doi: 10.1016/j.jamcollsurg.2009.12.040

11. Noren A, Sandstrom P, Gunnarsdottir K, Ardnor B, Isaksson B, Lindell G, et al. Identification of inequalities in the selection of liver surgery for colorectal liver metastases in Sweden. *Scand J Surg* (2018) 107:294–301. doi: 10.1177/1457496918766706

12. Ren L, Zhu D, Benson AB, Nordlinger B, Koehne CH, Delaney CP, et al. Shanghai international consensus on diagnosis and comprehensive treatment of colorectal liver metastases (version 2019). *Eur J Surg Oncol* (2020) 46:955–66. doi: 10.1016/j.ejso.2020.02.019

13. Liu Z, Xu Y, Xu G, Baklaushev VP, Chekhonin VP, Peltzer K, et al. Nomogram for predicting overall survival in colorectal cancer with distant metastasis. *BMC Gastroenterol* (2021) 21:103. doi: 10.1186/s12876-021-01692-x

14. Tang M, Wang H, Cao Y, Zeng Z, Shan X, Wang L. Nomogram for predicting occurrence and prognosis of liver metastasis in colorectal cancer: a population-based study. *Int J Colorectal Dis* (2021) 36:271–82. doi: 10.1007/s00384-020-03722-8

15. Bhullar DS, Barriuso J, Mullamitha S, Saunders MP, O'Dwyer ST, Aziz O. Biomarker concordance between primary colorectal cancer and its metastases. *EBioMedicine* (2019) 40:363–74. doi: 10.1016/j.ebiom.2019.01.050

16. Czauderna C, Luley K, von Bubnoff N, Marquardt JU. Tailored systemic therapy for colorectal cancer liver metastases. *Int J Mol Sci* (2021) 22. doi: 10.3390/ijms222111780

17. Saad AM, Abdel-Rahman O. Initial systemic chemotherapeutic and targeted therapy strategies for the treatment of colorectal cancer patients with liver metastases. *Expert Opin Pharmacother* (2019) 20:1767–75. doi: 10.1080/14656566.2019.1642324

18. Lee JH, Jung S, Park WS, Choe EK, Kim E, Shin R, et al. Prognostic nomogram of hypoxia-related genes predicting overall survival of colorectal cancer-analysis of TCGA database. *Sci Rep* (2019) 9:1803. doi: 10.1038/s41598-018-38116-y

19. Pietrantonio F, Di Nicolantonio F, Schrock AB, Lee J, Tejpar S, Sartore-Bianchi A, et al. ALK, ROS1, and NTRK rearrangements in metastatic colorectal cancer. *J Natl Cancer Inst* (2017) 109. doi: 10.1093/jnci/djx089

20. Torshizi Esfahani A, Seyedna SY, Nazemalhosseini Mojarad E, Majd A, Asadzadeh Aghdaei H. MSI-L/EMAST is a predictive biomarker for metastasis in colorectal cancer patients. *J Cell Physiol* (2019) 234:13128–36. doi: 10.1002/jcp.27983

21. Tsilimigras DI, Ntanasis-Stathopoulos I, Bagante F, Moris D, Cloyd J, Spartalis E, et al. Clinical significance and prognostic relevance of KRAS, BRAF, PI3K and TP53 genetic mutation analysis for resectable and unresectable colorectal liver metastases: a systematic review of the current evidence. *Surg Oncol* (2018) 27:280–8. doi: 10.1016/j.suronc.2018.05.012

22. Wang M, Wu Q, Zhang J, Qin G, Yang T, Liu Y, et al. Prognostic impacts of extracranial metastasis on non-small cell lung cancer with brain metastasis: a retrospective study based on surveillance, epidemiology, and end results database. *Cancer Med* (2021) 10:471–82. doi: 10.1002/cam4.3562

23. Tokoro T, Okuno K, Hida JC, Ueda K, Yoshifuji T, Daito K, et al. Prognostic factors for patients with advanced colorectal cancer and symptomatic brain metastases. *Clin Colorectal Cancer* (2014) 13:226–31. doi: 10.1016/j.clcc.2014.09.008

24. Khattak MA, Martin HL, Beeke C, Price T, Carruthers S, Kim S, et al. Survival differences in patients with metastatic colorectal cancer and with single site metastatic disease at initial presentation: results from south Australian clinical registry for advanced colorectal cancer. *Clin Colorectal Cancer* (2012) 11:247–54. doi: 10.1016/j.clcc.2012.06.004

25. Ge Y, Lei S, Cai B, Gao X, Wang G, Wang L, et al. Incidence and prognosis of pulmonary metastasis in colorectal cancer: a population-based study. *Int J Colorectal Dis* (2020) 35:223–32. doi: 10.1007/s00384-019-03434-8

26. Dekker E, Tanis PJ, Vleugels JLA, Kasi PM, Wallace MB. Colorectal cancer. *Lancet* (2019) 394:1467–80. doi: 10.1016/S0140-6736(19)32319-0

27. Loree JM, Pereira AAL, Lam M, Willauer AN, Raghav K, Dasari A, et al. Classifying colorectal cancer by tumor location rather than sidedness highlights a continuum in mutation profiles and consensus molecular subtypes. *Clin Cancer Res* (2018) 24:1062–72. doi: 10.1158/1078-0432.CCR-17-2484

28. Meguid RA, Slidell MB, Wolfgang CL, Chang DC, Ahuja N. Is there a difference in survival between right- versus left-sided colon cancers? *Ann Surg Oncol* (2008) 15:2388–94. doi: 10.1245/s10434-008-0015-y

29. Price TJ, Beeke C, Ullah S, Padbury R, Maddern G, Roder D, et al. Does the primary site of colorectal cancer impact outcomes for patients with metastatic disease? *Cancer* (2015) 121:830–5. doi: 10.1002/cncr.29129

30. Li X, Hu W, Sun H, Gou H. Survival outcome and prognostic factors for colorectal cancer with synchronous bone metastasis: a population-based study. *Clin Exp Metastasis* (2021) 38:89–95. doi: 10.1007/s10585-020-10069-5

31. Deng S, Jiang Z, Cao Y, Gu J, Mao F, Xue Y, et al. Development and validation of a prognostic scoring system for patients with colorectal cancer hepato-pulmonary metastasis: a retrospective study. *BMC Cancer* (2022) 22:643. doi: 10.1186/s12885-022-09738-3

32. Han L, Dai W, Mo S, Xiang W, Li Q, Xu Y, et al. Nomogram of conditional survival probability of long-term survival for metastatic colorectal cancer: a real-world data retrospective cohort study from SEER database. *Int J Surg* (2021) 92:106013. doi: 10.1016/j.ijsu.2021.106013

frontiers | Frontiers in Medicine

TYPE Original Research
PUBLISHED 06 July 2023
DOI 10.3389/fmed.2023.1218369

OPEN ACCESS

EDITED BY
Hangcheng Fu,
University of Louisville, United States

REVIEWED BY
Lifan Liang,
Jacobi Medical Center, United States
Xiangyi Kong,
Chinese Academy of Medical Sciences and Peking Union Medical College, China

*CORRESPONDENCE
Nan Zhang
✉ zn21076@rjh.com.cn

†These authors have contributed equally to this work and share first authorship

RECEIVED 07 May 2023
ACCEPTED 21 June 2023
PUBLISHED 06 July 2023

CITATION
Gan L, Miao Y-M, Dong X-J, Zhang Q-R, Ren Q and Zhang N (2023) Investigation on sexual function in young breast cancer patients during endocrine therapy: a latent class analysis.
Front. Med. 10:1218369.
doi: 10.3389/fmed.2023.1218369

Investigation on sexual function in young breast cancer patients during endocrine therapy: a latent class analysis

Lu Gan[1,2†], Yi-Ming Miao[1†], Xiao-Jing Dong[1], Qi-Rong Zhang[1], Qing Ren[1] and Nan Zhang[1*]

[1]Comprehensive Breast Health Center, Ruijin Hospital, Shanghai Jiao Tong University School of Medicine, Shanghai, China, [2]School of Medicine, Shanghai Jiao Tong University, Shanghai, China

Backgrounds: The aim of this study was to investigate the sexual function status of young breast cancer patients during endocrine therapy, identify potential categories of sexual function status, and analyze the factors affecting the potential categories of sexual function status during endocrine therapy.

Methods: A cross-sectional survey was conducted on 189 young breast cancer patients who underwent postoperative adjuvant endocrine therapy in Shanghai Ruijin Hospital. The latent class analysis was used to identify potential categories of patient sexual function characteristics with respect to the FSFI sex health measures. Logistic regression analysis was used to analyze the influencing factors for the high risk latent class groups. A nomogram prognostic model were then established to identify high risk patients for female sexual dysfunction (FSD), and C-index was used to determine the prognostic accuracy.

Results: Patients were divided into a "high dysfunction-low satisfaction" group and a "low dysfunction-high satisfaction" group depending on the latent class analysis, accounting for 69.3% and 30.7%, respectively. Patients who received aromatase inhibitors (AI) combined with ovarian function suppression (OFS) treatment (p=0.027), had poor body-image after surgery (p=0.007), beared heavy medical economy burden(p<0.001), and had a delayed recovery of sexual function after surgery (p=0.001) were more likely to be classified into the "high dysfunction-low satisfaction" group, and then conducted into the nomogram. The *C*-index value of the nomogram for predicting FSD was 0.782.

Conclusion: The study revealed the heterogeneity of sexual function status among young breast cancer patients during endocrine therapy, which may help identify high-risk patients and provide early intervention.

KEYWORDS

breast cancer, postoperative, endocrine therapy, female sexual dysfunction, latent class analysis

Introduction

Breast cancer (BC) is currently the most common malignant tumor among women worldwide (1). The incidence of breast cancer in China is on a rapid upward trend, with a tendency toward younger patients (2). About 60% of patients are premenopausal at the time of diagnosis, while between 50% and 60% of premenopausal women with early-stage breast cancer

are diagnosed as estrogen receptor-positive in China (3). Adjuvant endocrine therapy plays a vital role in reducing the risk of recurrence for these patients. However, endocrine therapy for breast cancer can lead to a decrease in hormone levels, which can cause sexual dysfunction, including sexual desire and arousal disorders, vaginal dryness, decreased tissue elasticity, and increased tissue fragility in the vulva and vagina, resulting in discomfort or pain during intercourse (4), thus triggering female sexual dysfunction.

Breast cancer patients may experience a range of physical changes resulting from comprehensive treatments, such as surgery, chemotherapy, radiotherapy, and targeted therapy. These changes include alterations in body image, hormonal fluctuations, and ovarian dysfunction, which may contribute to sexual dysfunction. Adjuvant endocrine therapy can cause or exacerbate menopausal symptoms in patients (5). Adding ovarian suppressants to classic endocrine therapy can bring therapeutic benefits, but can also increase toxic side effects, mainly manifested as menopausal symptoms, decreased sexual activity, and decreased quality of life (6). In addition to treatment factors, other factors such as age, mental health status, overall physical health, and marital relationships can also have a significant impact on sexual health and may be associated with sexual dysfunction (7).

Sexual quality is an important component of the quality of life of young cancer patients and an essential part of overall cancer management (8). Sexual activity is an important way for couples to express emotions and convey love. Sexual activity is a crucial means for couples to express emotions and convey affection, serving as both a lubricant for enhancing conjugal harmony and a vital way of maintaining a healthy marriage. During sexual intercourse, the body releases beta-endorphins, a natural sedative and analgesic that creates a relaxed and carefree internal environment in the nervous system, stabilizes emotions and behavior, and relieves symptoms such as anxiety and depression (9). High levels of sexual satisfaction can make people happy and improve their physical and mental well-being, stabilize their marital relationships, and enhance their immune function, which is conducive to disease recovery.

As endocrine therapy lasts for 5 years or even longer, it is meaningful to pay attention to the sexual function of breast cancer patients during adjuvant endocrine therapy. Younger patients are more concerned about their quality of life, especially their sexual quality of life, compared to middle-aged and older patients. In the cultural context of China, young patients often bear heavier social responsibilities and family burdens, and may face more difficulties. Currently, there is limited research focused on the sexual function of young breast cancer patients during endocrine therapy, so it is necessary to investigate and analyze the current status of sexual function and its related factors in young breast cancer patients during endocrine therapy in China's unique cultural and medical environment.

Abbreviations: OFS, Ovarian Function Suppression; FSD, Female Sexual Dysfunction; SERM, Selective Estrogen Receptor Modulator; TAM, Tamoxifen; AIs, Aromatase inhibitors; FSFI, Female Sexual Function Index; BIS, Body Image Scale for Breast Cancer Patients; HADS, Hospital Anxiety and Depression Scale-Depression Subscale; SSRS, Social Science Research Solutions; RDAS, The Revised Dyadic Adjustment Scale; LCA , Latent Class Analysis; AIC, Akaike Information Criterion; BIC, Bayesian Information Criterion; LMR, Lo–Mendell–Rubin; BLRT, Bootstrap Likelihood Ratio Test.

Materials and methods

Study design and patient selection

A convenience sampling method was employed to survey patients who underwent postoperative adjuvant endocrine therapy for breast cancer at Shanghai Ruijin Hospital between January 2021 and July 2021, and who met the inclusion and exclusion criteria. The inclusion criteria were: diagnosed with breast cancer at or before 40 years of age and having a long-term fixed partner; pathologically confirmed primary breast cancer with stage I to IIIA; estrogen receptor and/or progesterone receptor positive; completed comprehensive treatment for breast cancer other than endocrine therapy and took endocrine drugs for at least 6 months; no cognitive impairment, aware of their own condition, and willing to participate in the study. The exclusion criteria were as follows: discontinued endocrine therapy for more than 1 month cognitive impairment or a history of psychiatric illness (meets diagnostic criteria for symptoms of diseases listed in the DSM or ICD; system psychiatric history was determined mainly by referring to medical records); severe disabilities, or mobility impairments [we used Barthel index (10) as an assessment tool for functional independence, and respondents in this survey who scored less than 60 were excluded]. This study was approved by the Ethics Committee of Ruijin Hospital affiliated to Shanghai Jiao Tong University School of Medicine (No. 2019115).

Data collection

Data collection was conducted during patients' outpatient medication dispensing, treatment, and follow-up visits. After obtaining informed consent from the patients, eligible participants were invited to complete the survey using either a paper or electronic questionnaire. A total of 220 questionnaires were distributed, and 189 valid questionnaires were returned, resulting in an effective response rate of 85.91%.

This study investigated the potential factors that may influence the sexual function of young breast cancer patients during endocrine therapy, based on Ganz's breast cancer health concept model (7). The research team identified the relevant measurement variables for this investigation which are listed in Table 1.

TABLE 1 Measuring variables and measurement for patients with breast cancer undergoing endocrine therapy.

Elements	Factors	Measurements
Basic characteristics	Demographic and disease characteristics	Patient information survey
Sexual function	Sexual function and sexual satisfaction	Female sexual function index
Physiologic factor	Treatment-related symptoms	Modified Kupperman scale
Psychologic factor	Body image	Body image scale for breast cancer patients
	Anxiety and depression	Hospital anxiety and depression scale
Family and social support	Social support	Social science research solutions
	Conjugal relation	Revised dyadic adjustment scale

Patient information survey

The data collection form was designed by the researchers and included two parts: (1) demographic information, education level, marital status, work status, reproductive status, and medical payment method; (2) disease and sexual health-related information, which includes the time of disease diagnosis, disease staging, surgical methods, postoperative adjuvant therapy, information on endocrine therapy, preoperative sexual satisfaction, and the start time of the first sexual activity after surgery.

Female sexual function index

The Chinese version of the female sexual function index (FSFI) (11) was used to evaluate the sexual function of patients. The FSFI consists of six dimensions: sexual desire, sexual arousal, vaginal lubrication, orgasm, sexual satisfaction, and sexual pain. Higher scores indicate better sexual function. The critical value standard based on the study of Song et al. (12) was used in this study.

Modified Kupperman scale

The modified Kupperman scale (13) was used to evaluate the occurrence and severity of menopausal symptoms in patients within the last month.

Body image scale for breast cancer patients

The body image scale for breast cancer patients (BIS) was used to assess the self-image in female breast cancer patients (14).

Hospital anxiety and depression scale

The hospital anxiety and depression scale-depression subscale (HADS) was used for the evaluation of anxiety and depression symptoms (15).

Social science research solutions

The social science research solutions (SSRS) compiled by Xiao (16), is used to measure the degree of social support of individuals, which has been widely used in the Chinese population and has good reliability and validity (17). In this study, a score of 37 was used as the threshold, dividing social support into low level (<37 points) and high level (≥37 points).

Revised dyadic adjustment scale

The revised dyadic adjustment scale (RDAS) is used to evaluate the marital relationship (18). The higher the score, the more harmonious the marital adjustment relationship (19).

Statistical analyses

Latent class analysis (LCA) was used to construct a latent class model of sexual function characteristics of young breast cancer patients during endocrine therapy. The LCA was conducted using Mplus 8.2. The result of the latent class analysis was used for the identification of FSD high risk patients. Chi-squared test or Fisher's exact test were performed for the comparison between two groups. Logistic regression was used to analyze the influencing factors of different sexual function characteristics classification in young breast cancer patients during endocrine therapy. SPSS 19.0 for Windows was used for the descriptive statistics and logistic regression analysis. R 3.6.3[1] and rms package (20) was used for the establishment of nomogram and the analysis of *C*-index and calibration curve. All statistical tests were two-tailed, and a p-value of <0.05 was considered statistically significant.

Results

Sample description

This study included a total of 189 patients, aged 23 to 40 years, with a median age of 36 years. Of these, 157 patients (83.1%) had completed college education or higher, 180 patients (95.2%) were married, and 162 patients (85.7%) had a history of childbirth. All patients had undergone breast cancer surgery, including 81 cases (42.9%) of mastectomy without breast reconstruction, 84 cases (44.4%) of breast-conserving surgery for breast cancer, and 24 cases (12.7%) of breast reconstruction surgery. 66.1% of patients had received chemotherapy before endocrine therapy, 66.1% had received radiotherapy, and 11.6% had received targeted therapy. The duration of endocrine therapy ranged from 6 months to 10 years, with a median time of 2 years. Among them, 138 patients (73.0%) received ovarian function suppression therapy while receiving endocrine therapy.

In this study of 189 young breast cancer patients, 71 (37.6%) resumed sexual activity for the first time within 6 months after surgery, 61 (32.3%) resumed sexual activity between 6 months and 1 year after surgery, and 57 (30.2%) resumed sexual activity more than 1 year after surgery. 170 patients (89.9%) were satisfied with their sexual life before surgery. Only 54 patients (28.6%) had discussed sexual issues with healthcare providers. 125 patients (66.1%) believed that they did not need sexual health guidance from healthcare providers for their illness. The total incidence of female sexual dysfunction (FSD) in this study was 81.0%, with the following FSFI dimension disorders: low sexual desire (83.1%), sexual arousal disorder (69.3%), orgasmic disorder (68.8%), vaginal lubrication difficulties (57.1%), decreased sexual satisfaction (54.5%), and dyspareunia (54.0%) (Table 2).

Latent class analysis

In this study, latent class analysis was performed to explore the sexual function status of 189 young breast cancer patients during

1 http://www.r-project.org/

TABLE 2 Demographic characteristics, medical information and Sexual health related information of the sample (n =189).

Characteristics	*N* (%)
Age of diagnosis	
≤30	30 (15.9)
>30, ≤35	62 (32.8)
>35, ≤40	97 (51.3)
Educational level	
Junior high school	16 (8.5)
High school	16 (8.5)
College degree	133 (70.4)
Postgraduate or above	24 (12.7)
Marital status	
Married	180 (95.2)
Single	6 (3.2)
Divorced	3 (1.6)
Family structure	
Live alone	4 (2.1)
Living with spouse	23 (12.2)
Living with spouse and children	123 (65.1)
Live with many members	39 (20.6)
Fertility circumstance	
Childless	27 (14.3)
One child	124 (65.5)
Two children or more	38 (20.1)
Work status	
Employed	147 (77.8)
Unemployed	42 (22.2)
Monthly household income *per capita*, CNY	
≤2,500	10 (5.3)
>2, 500, ≤5,000	25 (13.2)
>5,000, ≤10,000	58 (30.7)
>10,000	96 (50.8)
Payment manner of the medical expenses	
Medical insurance	178 (94.2)
Self-paying	11 (5.8)
Medical economy burden	
No	112 (59.3)
Yes	77 (40.7)
Surgical approach	
Mastectomy	81 (42.9)
Breast conserving surgery	84 (44.4)
Mastectomy with breast reconstruction	24 (12.7)
Endocrine therapy	
AIs	91 (48.1)
SERM	98 (51.9)
Radiotherapy	
No	64 (33.9)
Yes	125 (66.1)
Targeted therapy	
No	167 (88.4)
Yes	22 (11.6)
Ovarian function suppression	
No	51 (27.0)
Yes	138 (73.0)
Adjuvant chemotherapy	
No	64 (33.9)
Yes	125 (66.1)
Interval from surgery to first sexual activity	
≤6 months	71 (37.6)
>6 months	118 (62.5)
Satisfaction with sexual activity before breast cancer diagnosis	
No	19 (10.1)
Yes	170 (89.9)
Communication with health care providers about sexual issues	
No	135 (71.4)
Yes	54 (28.6)
The need of medical staff to provide sexual health guidance	
No	125 (66.1)
Yes	64 (33.9)

endocrine therapy. To obtain the optimal model, the occurrence of dysfunction in 6 domains of sexual health (desire, arousal, lubrication, orgasm, satisfaction, and pain) based on FSFI were used as indicators (scored as 0/1; 0 indicating no dysfunction, 1 indicating dysfunction) and one to five latent classes were fitted sequentially, with the fit indices for each model assessed (Table 3) using AIC, BIC, Entropy, LMR, and BLRT. The model with one class was analyzed firstly (M1), and as the number of classes increased, the AIC and aBIC values decreased while the entropy values remained stable. The two-class model (M2) had the smallest BIC value. However, considering the unreliable representation of the class that accounted for less than 1% of the total sample (21), the optimal model was determined based on a comprehensive evaluation of the fit indices and clinical significance, which indicated that the two-class model (M2) was the optimal model.

When the model included two classes (M2), the average probability of membership for each class was above 90%, with C1 at 98.8% and C2 at 97.6%, indicating a high level of fit quality and model reliability for M2.

In the two identified latent classes, C1 had higher rates of sexual dysfunction across all dimensions compared to C2, hence it was labeled as the "high dysfunction-low satisfaction" group with 131 patients (69.3%) falling into this category. Conversely, C2 was labeled as the "low dysfunction-high satisfaction" group relative to C1, with

TABLE 3 Fitting results of the latent category model of sexual function status in young breast cancer patients during endocrine therapy.

Model	Loglikelihood	AIC	BIC	aBIC	Entropy	LMR	BLRT	Class probability
M1	432.155	1431.087	1450.537	1431.532	–	–	–	1
M2	87.869	1100.801	1142.943	1101.766	0.934	<0.0001	<0.0001	0.693/0.307
M3	53.710	1080.642	1145.477	1082.127	0.901	0.0002	<0.0001	0.212/0.127/0.661
M4	35.787	1076.719	1164.247	1078.723	0.798	0.0363	<0.0001	0.212/0.312/0.360/0.116
M5	18.686	1073.618	1183.837	1076.141	0.942	0.0016	<0.0001	0.021/0.212/0.249/0.127/0.391

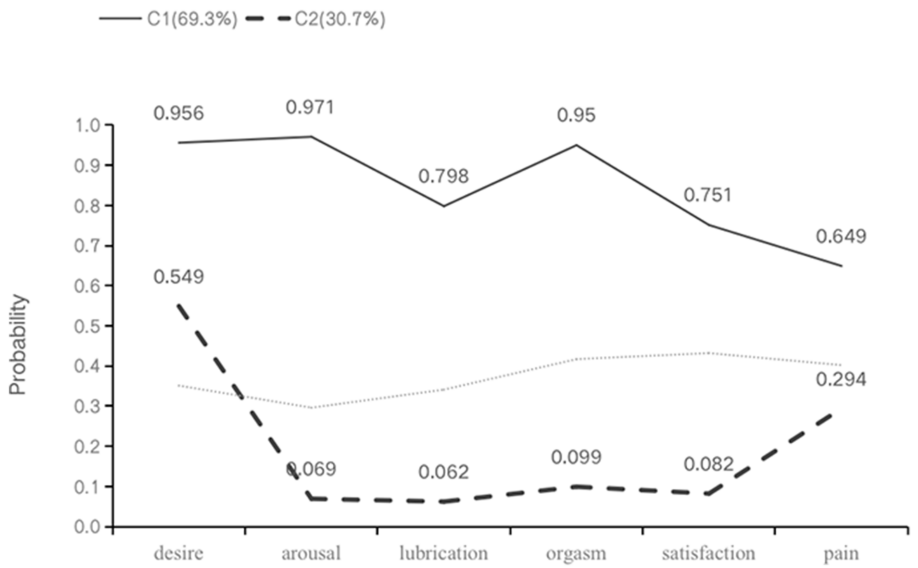

FIGURE 1
Profiles for two-class LCA model of sexual health. Class 1: C1, high dysfunction-low satisfaction group; class 2: C2, low dysfunction-high satisfaction group.

58 patients (30.7%) belonging to this category (Figure 1). The result of the latent class analysis was used for the identification of FSD high risk patients.

The logistic regression analysis

In this study, the potential categories of patient sexual function status (C1: low dysfunction-high satisfaction, C2: high dysfunction-low satisfaction) were used as the dependent variable. The variables with $p < 0.1$ in the univariate analysis (marital status, family structure, economic burden, surgical approach, chemotherapy, endocrine therapy, interval from surgery to first sexual activity, satisfaction with sexual activity before breast cancer diagnosis, menopausal symptoms, pre-operative body image, postoperative body image anxiety, depression, social support) and clinically relevant variables (age) were selected as independent variables for binary logistic regression analysis (Table 4). The forward stepwise regression method was used to screen for independent variables. The results showed that the endocrine therapy regimen (AIs/SERM, OR = 2.311, 95% CI 1.101–4.854), postoperative body image (high/low, OR = 2.774, 95% CI 1.329–5.793), medical economic burden (yes/no, OR = 4.385, 95% CI 1.982–9.699), and time of first sexual activity after surgery (late/early，OR = 3.561, 95% CI 1.703–7.444) were the features associated with potential differences in sexual function status among young breast cancer patients during endocrine therapy ($p < 0.05$). However, there were no significant differences in marital status, family structure, surgical approach, satisfaction with sexual activity before breast cancer diagnosis, body image, anxiety, depression, and social support among the potential categories (see Table 5).

Prognostic nomogram for female sexual dysfunction

The four independent prognostic factors: Patients received AI combined with OFS treatment ($p = 0.027$), had poor body-image after surgery ($p = 0.007$), beared heavy medical economy burden ($p < 0.001$), and had a delayed recovery of sexual function after surgery ($p = 0.001$) were included in the process of establishment of the nomogram. Patients in class I according to the latent class analysis were identified as patients with female sexual dysfunction.

Prognostic nomograms that integrated the significant independent factors for FSD are established and shown in Figure 2. The *C*-index values of the nomogram in predicting FSD was 0.782.

The calibration plot for the probability of FSD showed an optimal agreement between the prediction by the nomogram and actual observations (Figure 3).

TABLE 4 Analysis of different characteristics of young breast cancer patients during endocrine therapy in two identified latent classes (*n*, %).

Factors	"High dysfunction-low satisfaction" group (C1)	"Low dysfunction-high satisfaction" group (C2)	*p*
Age of diagnosis			0.226
≤30	17 (13.0%)	13 (22.4%)	
>30, ≤35	46 (35.1%)	16 (27.6%)	
>35, ≤40	68 (51.9%)	29 (50.0%)	
Educational level			
Junior high school	9 (6.9%)	7 (12.1%)	0.317
High school	12 (9.2%)	4 (6.9%)	
College degree	96 (73.3%)	37 (63.8%)	
Postgraduate or above	14 (10.7%)	10 (17.2%)	
Marital status			
Married	127 (96.9%)	53 (91.4%)	0.011
Single	1 (0.8%)	5 (8.6%)	
Divorced	3 (2.3%)	0 (0.0%)	
Family structure			
Live alone	0 (0.0%)	4 (6.9%)	0.028
Living with spouse	18 (13.7%)	5 (8.6%)	
Living with spouse and children	85 (64.9%)	38 (65.5%)	
Live with many members	28 (21.4%)	11 (19.0%)	
Fertility circumstance			
Childless	17 (13.0%)	10 (17.2%)	0.672
One child	86 (65.6%)	38 (65.5%)	
Two children or more	28 (21.4%)	10 (17.2%)	
Work status			
Employed	98 (74.8%)	49 (84.5%)	0.140
Unemployed	33 (25.2%)	9 (15.5%)	
Monthly household income *per capita*, RMB			
≤2,500	10 (7.6%)	0 (0.0%)	0.190
>2,500, ≤5,000	17 (13.0%)	8 (13.8%)	
>5,000, ≤10,000	40 (30.5%)	18 (31.0%)	
>10,000	64 (48.9%)	32 (55.2%)	
Payment manner of the medical expenses			
Medical insurance	124 (94.7%)	54 (93.1%)	0.739
Self-paying	7 (5.3%)	4 (6.9%)	
Medical economy burden			
No	66 (50.4%)	46 (79.3%)	<0.001
Yes	65 (49.6%)	12 (20.7%)	
Surgical approach			
Mastectomy	53 (40.5%)	28 (48.3%)	0.057
Breast conserving surgery	65 (49.6%)	19 (32.8%)	
Mastectomy with breast reconstruction	13 (9.9%)	11 (19.0%)	
Ovarian function suppression			
No	32 (24.4%)	19 (32.8%)	0.234
Yes	99 (75.6%)	39 (67.2%)	
Chemotherapy			
No	39 (29.8%)	25 (43.1%)	0.074
Yes	92 (70.2%)	33 (56.9%)	
Radiotherapy			
No	41 (31.3%)	23 (39.7%)	0.263
Yes	90 (68.7%)	35 (60.3%)	
Targeted therapy			
No	114 (87.0%)	53 (91.4%)	0.389
Yes	17 (13.0%)	5 (8.6%)	
Endocrine therapy			
AIs	69 (52.7%)	22 (37.9%)	0.061
SERM	62 (47.3%)	36 (62.1%)	
Interval from surgery to first sexual activity			
≤6 months	36 (27.5%)	35 (60.3%)	<0.001
>6 months	95 (72.5%)	23 (39.7%)	
Satisfaction with sexual activity before breast cancer diagnosis			
No	19 (14.5%)	0 (0.0%)	0.002
Yes	112 (85.5%)	58 (100.0%)	
Post-operative body image			
Poor	90 (68.7%)	24 (41.1%)	<0.001
Well	41 (31.3%)	34 (58.6%)	
Communication with health care providers about sexual issues			
No	97 (74.0%)	38 (65.5%)	0.231
Yes	34 (26.0%)	20 (34.5%)	
The need of medical staff to provide sexual health guidance			
No	44 (33.6%)	20 (34.5%)	0.905
Yes	87 (66.4%)	38 (65.5%)	

Discussion

In this study, the incidence of female sexual dysfunction (FSD) among young breast cancer patients during endocrine therapy was found to be 81.0% based on the FSFI score. The incidence of each dimension of sexual dysfunction ranged from 54.0% to 83.1%. To better evaluate FSD, latent class analysis was performed. Compared with previous studies on sexual function in breast cancer patients (22), the incidence of FSD in young patients in this study was higher. Lee et al. (23) found that 32% of young breast cancer patients who were sexually active before diagnosis had sexual dysfunction. Zhang's study

of 80 young (≤50 years old) breast cancer patients who received comprehensive treatment found that 70.15% of the patients had sexual dysfunction after treatment (24). The high incidence of FSD in this study may be related to regional and cultural differences in the study population, as well as to the fact that the patients in this study were receiving endocrine therapy. Endocrine therapy can lead to a decrease in estrogen levels, causing sexual desire and arousal disorders, as well as vaginal dryness, decreased elasticity and increased fragility of the vulva and vaginal tissues, resulting in discomfort or pain during sexual intercourse. Other studies have reported that endocrine therapy is a risk factor for sexual desire disorders, vaginal lubrication difficulties and sexual pain in breast cancer patients (25, 26). Domestic studies have also found that patients' sexual function significantly decreased after 6 months of endocrine therapy, especially in the areas of sexual desire, vaginal lubrication, sexual satisfaction and sexual pain (27).

Moreover, our study found that 71.4% of patients had not discussed their sexual issues with medical staff, and 66.1% of patients believed that they did not need sexual guidance from medical staff. This may be related to the cultural background and social customs in China, where both patients and medical staff often consider sex a private matter. It also reflects that some medical staff do not fully recognize the importance of sexual rehabilitation. Overall, the study findings indicated considerable variability in sexual function among young breast cancer patients undergoing endocrine therapy. The assessment of sexual function using latent class analysis was supported by several statistical fitting indices, and the clinical significance of the identified sexual dysfunction was also demonstrated. Overall, this study highlights the complexity and diversity of sexual function in this patient population and emphasizes the importance of addressing sexual health concerns in the context of breast cancer care. The patients were ultimately divided into a "high disorder-low satisfaction" group and a "low disorder-high satisfaction" group. In both groups, the incidence of decreased sexual desire was higher than the norm, which may be related to the decrease in estrogen levels caused by endocrine therapy.

Currently, there is limited research on the heterogeneity of female sexual dysfunction both domestically and internationally. One study conducted by Yuan et al. (19) on the sexual health characteristics of breast cancer patients had conducted research on it. The latent categories of sexual dysfunction in young breast cancer patients during endocrine therapy identified in this study share some similarities and differences with the research of Yuan et al. (19). Their study classified breast cancer patients based on their sexual activity and analyzed the heterogeneity of their sexual health, identifying five subgroups with different sexual health characteristics. The difference in the classification results may be due to differences in the study population. The subjects included in this study were young patients diagnosed before the age of 40, a population with a strong sexual demand and physiological function, and high sexual activity. In contrast, the study of Yuan et al. (19) included patients with an age range of 25 to 70 years and a median age of 46 years. The results of her heterogeneity analysis of sexually active individuals are consistent with this study, with sexual function and sexual satisfaction being significant classification features of sexual health.

Multivariate analysis showed that the type of endocrine therapy, postoperative body image, medical economic burden, and timing of

TABLE 5 Logistic regression analysis of for breast cancer patients undergoing endocrine therapy in different latent class.

Factors	OR	95% CI	*p*
Endocrine therapy, AIs vs. SERM	2.311	1.101–4.854	0.027
Post-operative body image poor vs. well[a]	2.774	1.329–5.793	0.007
Medical economic burden yes vs. no	4.385	1.982–9.699	<0.001
Interval from surgery to first sexual activity late vs. early[a]	3.561	1.703–7.444	0.001

[a]The postoperative body image score of 5 was taken as the cut-off value; and the delayed first postoperative sex time was defined half a year after breast cancer surgery.

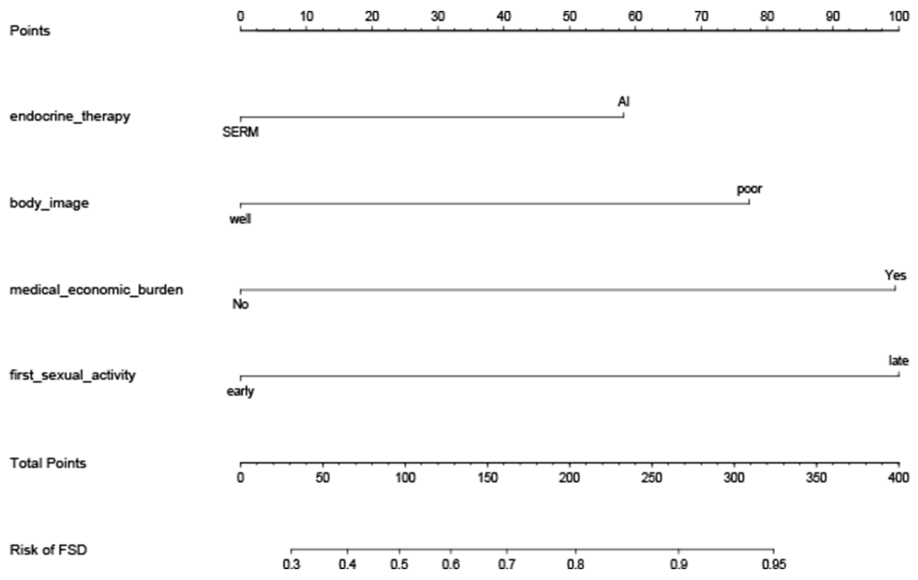

FIGURE 2
Nomogram for the prediction of FSD. Nomogram for the prediction of FSD in young breast cancer patients during endocrine therapy, with a *C*-index of 0.782.

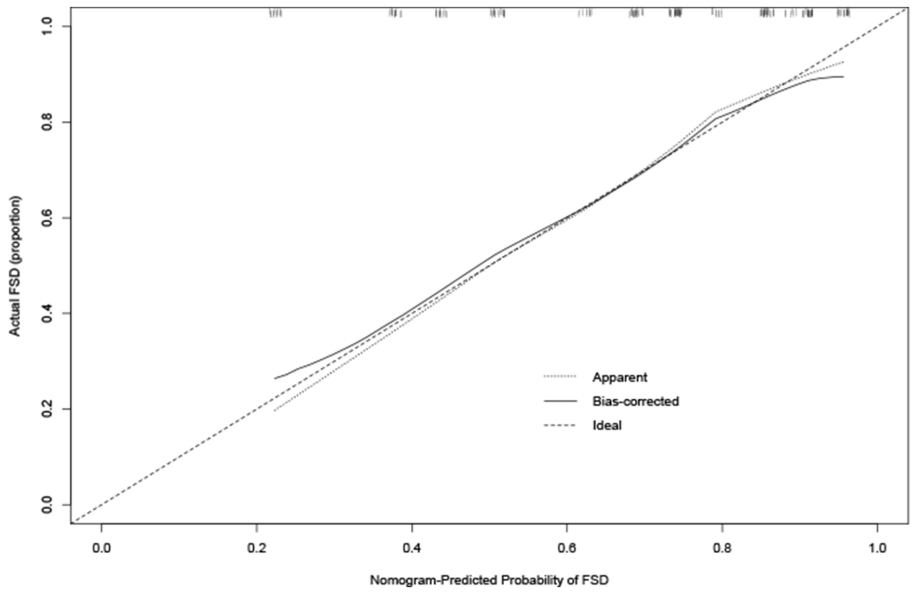

FIGURE 3
Calibration curve for predicting FSD. Calibration curve for predicting FSD in young breast cancer patients during endocrine therapy. Nomogram-predicted probability of FSD is plotted on the *x*-axis, while actual rate of FSD is plotted on the *y*-axis.

first sexual activity after surgery were the characteristics associated with latent categories of sexual dysfunction in young breast cancer patients during endocrine therapy.

This study reveals that young breast cancer patients who take AIs are more likely to be classified as "high dysfunction-low satisfaction" group. While endocrine therapy brings therapeutic benefits, it also leads to a series of treatment-related adverse reactions, such as sleep disorders, bone and joint pain, hot flashes, and effects on sexual function. In the ATAC trial comparing the efficacy and safety of AIs and TAM endocrine therapy, researchers evaluated the sexual quality of life of the subjects and found that anastrozole had a greater impact on reduced libido and painful intercourse in patients than TAM (28). In the IES 031 trial, the sexual assessment index showed a lower incidence of vaginal dryness in the TAM group (29). The results of this study are consistent with previous research.

As the use of AIs in young breast cancer patients requires the combination of OFS, the addition of OFS can cause certain toxic side effects, mainly focused on the occurrence of menopausal symptoms, reduced sexual activity, and decreased quality of life. These symptoms are not age-restricted in premenopausal women (30). According to existing literature on the 5 years SOFT and TEXT studies (31), adverse reactions were observed, including significant changes in sexual symptoms from baseline. Patients receiving exemestane + OFS had more severe vaginal dryness symptoms than patients receiving tamoxifen + OFS, and the difference persisted. In terms of libido, patients receiving exemestane + OFS were more likely to experience a decrease in libido than patients receiving tamoxifen + OFS, and the difference increased with the duration of treatment. For sexually active patients at baseline, the risk of sexual arousal difficulties in the exemestane + OFS group was higher than that in the tamoxifen + OFS group. Furthermore, the study results of patients under 35 years old in both trials (32) showed that the use of OFS increased the risk of decreased libido and sexual arousal difficulties, and the risk difference persisted with the increase in treatment time. The AI+OFS group had a higher incidence of vaginal dryness, decreased libido, and sexual arousal difficulties compared to the TAM + OFS group, which may be related to the different mechanisms of action of the drugs. Since there are abundant estrogen receptors in brain tissue, the decrease in estrogen levels and the prevention of estrogen from binding to its receptors may affect the emotional function of the human body (29). Further research is needed to determine whether drug-induced changes in emotional function affect patient sexual function. Therefore, this study suggests that interventions for sexual dysfunction in young breast cancer patients during endocrine therapy should focus on those who use AI in combination with OFS.

The results of this study indicate that patients with poor postoperative body image are more likely to be in the "high dysfunction-low satisfaction" group. Body image reflects the objective perception and subjective evaluation and feelings of patients towards their own body, and is related to characteristics such as emotional expression, appearance recognition, and social interaction. These constituent factors interact in a multidimensional manner in the context of breast cancer (33). The disease itself and its treatment can cause varying degrees of damage to the patient's body image, which in turn reduces sexual response between spouses. Poor quality of sexual life can also have a negative impact on a patient's self-image (34). Previous research results have also shown that low self-image scores are significant predictors of low sexual satisfaction, and "feeling unattractive" is the most common reason for not engaging in sexual activity with a partner (35). At the same time, breast cancer patients after surgery are troubled by body image issues for a long time, and the longer the postoperative time, the worse their self-image perception becomes (36). These findings suggest that effective measures to improve body image should be provided to patients as early as possible to improve their sexual function.

The financial burden of medical treatment is often an overlooked factor in studies of this kind. The results of this study show that patients with a heavy economic burden are more likely to be classified in the "high dysfunction-low satisfaction" group. Although more than 90% (94.2%) of the patients in this study were covered by medical insurance, about 40% of them still had varying degrees of economic burden. Some researchers have found that the total medical expenses in the whole society have continued to rise over the past decade, and the average out-of-pocket expenses for patients are also increasing rapidly (37). This phenomenon can provide some explanation for the results of this study. Breast cancer patients undergoing endocrine therapy require regular medication and follow-up, which may result in various indirect economic burdens due to missed work and frequent hospital visits. Economic factors play a significant role in the dynamic changes in patients' physical and psychological aspects and may be one of the causes of sexual dysfunction in patients.

The research findings indicate that patients with a longer recovery time for sexual activity after surgery are more likely to be classified as belonging to the "high dysfunction-low satisfaction" group. In this study, the proportion of breast cancer patients who resumed sexual activity within 1 month after surgery was 6.9%, which was higher than the reported rate in Anhui province (6.0%) (38), but lower than that in Xi'an (12.64%). Compared to western countries (39), the time for breast cancer patients to resume sexual activity in China is generally later. The appropriate time for sexual activity to resume after surgery should be based on the patient's recovery status. If there are no complications after surgery, sexual activity can be resumed once the surgical wound has healed. Engaging in sexual activity after breast cancer surgery does not increase the risk of cancer recurrence. On the contrary, sexual activity has been found to enhance emotional intimacy between partners, promote physical and emotional well-being, and potentially contribute to disease recovery. According to the research by Jankowska (40), the first sexual activity after surgery is a turning point for spousal sexual adaptation and adjustment. Communication with spouses, sharing feelings related to breast cancer, and understanding each other's sexual needs and expectations can promote better sexual satisfaction for both spouses. A follow-up study on young breast cancer patients (41) found that the higher the quality of the first sexual intercourse after surgery, the less emotional distress related to subsequent sexual activity. Researchers have pointed out that breast cancer patients and their spouses will experience a period of sexual recovery after surgery (40). During this period, medical staff should proactively provide relevant guidance on sexual issues to patients, promote effective communication and emotional exchange between spouses, and help patients better cope with sexual problems.

This study has several limitations that need to be addressed. Firstly, its prospective nature and single-center design at Ruijin Hospital affiliated with Shanghai Jiao Tong University School of Medicine may limit the generalizability of the study findings. Although the patient sample included individuals from various regions of the country, the treatment environment was still relatively limited. Therefore, future studies with larger sample sizes and recruitment from multiple centers are needed to validate and enhance the external validity of the findings. Secondly, some patients declined participation in the study due to the sensitive nature of the research topic, which may cause bias. Furthermore, this study focuses on female sexual dysfunction, which is influenced by various factors such as social, physiological, and psychological factors from spouses. However, there is still some missing information about the factors associated with spouses, which may have an impact on the study results. The establishment and validation of the nomogram was based on the data in a single center. Further studies with larger sample sizes are needed to verify the accuracy of the nomogram. Further investigation is needed to explore and clarify the factors that affect sexual function in young breast cancer patients during the endocrine therapy period.

Conclusion

This study has revealed that among young breast cancer patients undergoing endocrine therapy, the incidence of FSD was high, and FSD was found to be heterogenous. It suggests that healthcare providers should strengthen the evaluation of sexual function status among young breast cancer patients during endocrine therapy, especially those who use AIs, have poor postoperative body image, experience medical economic burden, and delay the recovery of their first sexual intercourse after surgery. Timely targeted support should be provided based on their different characteristics to help breast cancer patients cope with the negative impact of sexual dysfunction and improve their quality of life. The proposed nomogram performed well in predicting FSD for young breast cancer patients undergoing endocrine therapy.

Data availability statement

The raw data supporting the conclusions of this article will be made available by the authors, without undue reservation.

Ethics statement

This study was approved by the Ethics Committee of Ruijin Hospital affiliated to Shanghai Jiao Tong University School of Medicine (No. 2019115). Written informed consent from the patient was not required to participate in this study in accordance with the national legislation and the institutional requirements.

Author contributions

LG and Y-MM contributed equally to this study. LG and NZ designed the research. LG, X-JD, Q-RZ, and QR collected the data. LG and Y-MM analyzed the data and prepared the manuscript. All authors contributed to the article and approved the submitted version.

Funding

The study was also funded by Nursing Research Fund of Ruijin Hospital Affiliated to Shanghai Jiaotong University School of Medicine (RJ KH-2023-9).

Conflict of interest

The authors declare that the research was conducted in the absence of any commercial or financial relationships that could be construed as a potential conflict of interest.

Publisher's note

References

1. IARC. Latest global cancer data: cancer burden rises to 19.3 million new cases and 10.0 million cancer deaths in 2020 questions and answers (Q & A) [EB/OL]. Available at: https://www.iarc.who.int/faq/latest-global-cancer-data-2020-qa/2022.8

2. Liu LY, Wang YJ, Wang F, Yu LX, Xiang YJ, Zhou F, et al. Factors associated with insufficient awareness of breast cancer among women in northern and eastern China: a case-control study. *BMJ Open*. (2018) 8:e018523. doi: 10.1136/bmjopen-2017-018523

3. Fan L, Strasser-Weippl K, Li JJ, St Louis J, Finkelstein DM, Yu KD, et al. Breast cancer in China. *Lancet Oncol*. (2014) 15:e279–89. doi: 10.1016/S1470-2045(13)70567-9

4. Hungr C, Sanchez-Varela V. Self-image and sexuality issues among young women with breast cancer: practical recommendations. *Rev Investig Clin*. (2017) 69:114–22. doi: 10.24875/RIC.17002200

5. Bradford A. Sexual outcomes of aromatase inhibitor therapy in women with breast cancel time for intervention. *Menopause*. (2013) 20:128–9. doi: 10.1097/GME.0b013e31828094b0

6. Tevaarwerk AJ, Wang M, Zhao F, Fetting JH, Cella D, Wagner LI, et al. Phase III comparison of tamoxifen versus tamoxifen plus ovarian function suppression in premenopausal women with node-negative, hormone receptor-positive breast cancer (E-3193, INT-0142): a trial of the Eastern Cooperative Oncology Group. *J Clin Oncol*. (2014) 32:3948–58. doi: 10.1200/JCO.2014.55.6993

7. Ganz PA, Desmond KA, Belin TR, Meyerowitz BE, Rowland JH. Predictors of sexual health in women after a breast cancer diagnosis. *J Clin Oncol*. (1999) 17:2371–80. doi: 10.1200/JCO.1999.17.8.2371

8. Kedde H, van de Wiel HBM, Weijmar Schultz WCM, Wijsen C. Sexual dysfunction in young women with breast cancer. *Support Care Cancer*. (2013) 21:271–80. doi: 10.1007/s00520-012-1521-9

9. Veening JG, Barendregt HP. The effects of beta-endorphin: state change modification. *Fluids Barriers CNS*. (2015) 12:3. doi: 10.1186/2045-8118-12-3

10. dos Santos Barros V, Bassi-Dibai D, Guedes CLR, Morais DN, Coutinho SM, de Oliveira Simões G, et al. Barthel index is a valid and reliable tool to measure the functional independence of cancer patients in palliative care. *BMC Palliat Care*. (2022) 21:124. doi: 10.1186/s12904-022-01017-z

11. Wang Q, Geng H, Lu C, Jin Z, Xu C, Tang D. Association between the international index of erectile function-15 and female sexual function index in Chinese infertile couples. *Andrologia*. (2022) 54:e14360. doi: 10.1111/and.14360

12. Song SH, Jeon H, Kim SW, Paick JS, Son H. The prevalence and risk factors of female sexual dysfunction in young Korean women: an internet-based survey. *J Sex Med*. (2008) 5:1694–701. doi: 10.1111/j.1743-6109.2008.00840.x

13. Tao M, Shao H, Li C, Teng Y. Correlation between the modified Kupperman index and the menopause rating scale in Chinese women. *Patient Prefer Adherence*. (2013) 7:223–9. doi: 10.2147/PPA.S42852

14. Tounkel I, Nalubola S, Schulz A, Lakhi N. Sexual health screening for gynecologic and breast cancer survivors: a review and critical analysis of validated screening tools. *Sex Med*. (2022) 10:100498. doi: 10.1016/j.esxm.2022.100498

15. Mykletun A, Stordal E, Dahl AA. Hospital anxiety and depression (HAD) scale: factor structure, item analyses and internal consistency in a large population. *Br J Psychiatry*. (2001) 179:540–4. doi: 10.1192/bjp.179.6.540

16. Xiao S. The theoretical basis and application of social support rating scale. *J Clin Psychiatry*. (1994) 4:98–100. doi: CNKI:SUN:LCJS.0.1994-02-019

17. Liu JW, Li WY. Reliability and validity of social support rating scale. *J Xinjiang Med Univ*. (2008) 1:4–6. doi: 10.3389/fpubh.2022.987526

18. Maroufizadeh S, Omani-Samani R, Hosseini M, Almasi-Hashiani A, Sepidarkish M, Amini P. The Persian version of the revised dyadic adjustment scale (RDAS): a validation study in infertile patients. *BMC Psychol*. (2020) 8:6. doi: 10.1186/s40359-020-0375-z

19. Yuan X, Wang J, Bender CM, Zhang N, Yuan C. Patterns of sexual health in patients with breast cancer in China: a latent class analysis. *Support Care Cancer*. (2020) 28:5147–56. doi: 10.1007/s00520-020-05332-0

20. Harrell Frank E Jr. (2023) RMS: regression modeling strategies. R Package version 3.4-0. Available at: http://CRAN.R-project.org/packagerms

21. Ferguson SLG, Moore EW, Hull DM. Finding latent groups in observed data: a primer on latent profile analysis in Mplus for applied researchers. *Int J Behav Dev*. (2020) 44:458–68. doi: 10.1177/0165025419881721

22. Jing L, Zhang C, Li W, Jin F, Wang A. Incidence and severity of sexual dysfunction among women with breast cancer: a meta-analysis based on female sexual function index. *Support Care Cancer*. (2019) 27:1171–80. doi: 10.1007/s00520-019-04667-7

23. Lee M, Kim YH, Jeon MJ. Risk factors for negative impacts on sexual activity and function in younger breast cancer survivors. *Psychooncology*. (2015) 24:1097–103. doi: 10.1002/pon.3772

24. Zhang C, Pan L, Bao J, and Hu G. A cross sectional surveyon sexual dysfunctions of young female breast cancer patients in Shanghai. *Chin J Hum Sexual*. (2018) 27:141–7. doi: 10.3969/j.issn.1672-1993.2018.10.042

25. Hummel SB, Hahn DEE, van Lankveld JJDM, Oldenburg HSA, Broomans E, Aaronson NK. Factors associated with specific diagnostic and statistical manual of mental disorders, fourth edition sexual dysfunctions in breast cancer survivors: a study of patients and their partners. *J Sex Med*. (2017) 14:1248–59. doi: 10.1016/j.jsxm.2017.08.004

26. Gambardella A, Esposito D, Accardo G, Taddeo M, Letizia A, Tagliafierro R, et al. Sexual function and sex hormones in breast cancer patients. *Endocrine*. (2018) 60:510–5. doi: 10.1007/s12020-017-1470-7

27. Wang H. Investigation on the effect of adjuvant endocrine therapy on sexual function of postmenopausal breast cancer patients. *Tianjin J Nurs*. (2016) 24:411–2. doi: 10.3969/j.issn.1006-9143.2016.05.018

28. Francis PA, Pagani O, Fleming GF, Walley BA, Colleoni M, Láng I, et al. Tailoring adjuvant endocrine therapy for premenopausal breast Cancer. *N Engl J Med*. (2018) 379:122–37. doi: 10.1056/NEJMoa1803164

29. Baum M, Budzar AU, Cuzick J, Forbes J, Houghton JH, Klijn JG, et al. Anastrozole alone or in combination with tamoxifen versus tamoxifen alone for adjuvant treatment of postmenopausal women with early breast cancer: first results of the ATAC randomised trial. *Lancet*. (2002) 359:2131–9. doi: 10.1016/S0140-6736(02)09088-8

30. Boccardo F, Rubagotti A, Perrotta A, Amoroso D, Balestrero M, de Matteis A, et al. Ovarian ablation versus goserelin with or without tamoxifen in perimenopausal patients with advanced breast cancer: results of a multicentric Italian study. *Ann Oncol*. (1994) 5:337–42. doi: 10.1093/oxfordjournals.annonc.a058837

31. Bernhard J, Luo W, Ribi K, Colleoni M, Burstein HJ, Tondini C, et al. Patient-reported outcomes with adjuvant exemestane versus tamoxifen in premenopausal women with early breast cancer undergoing ovarian suppression (TEXT and SOFT): a combined analysis of two phase 3 randomised trials. *Lancet Oncol*. (2015) 16:848–58. doi: 10.1016/S1470-2045(15)00049-2

32. Saha P, Regan MM, Pagani O, Francis PA, Walley BA, Ribi K, et al. Treatment efficacy, adherence, and quality of life among women younger than 35 years in the international Breast Cancer Study Group TEXT and SOFT adjuvant endocrine therapy trials. *J Clin Oncol*. (2017) 35:3113–22. doi: 10.1200/JCO.2016.72.0946

33. Schilder P. *The image and appearance of the human body: studies in the constructive energies of the psyche* London, Routledge (1999). 170 p.

34. Pelusi J. Sexuality and body image. Research on breast cancer survivors documents altered body image and sexuality. *Am J Nurs*. (2006) 106:32–8. doi: 10.1097/00000446-200603003-00013

35. Ljungman L, Ahlgren J, Petersson LM, Flynn KE, Weinfurt K, Gorman JR, et al. Sexual dysfunction and reproductive concerns in young women with breast cancer: type, prevalence, and predictors of problems. *Psychooncology*. (2018) 27:2770–7. doi: 10.1002/pon.4886

36. Paterson CL, Lengacher CA, Donovan KA, Kip KE, Tofthagen CS. Body image in younger breast cancer survivors: a systematic review. *Cancer Nurs*. (2016) 39:E39–58. doi: 10.1097/NCC.0000000000000251

37. Gan X, You M, Hu K. Reimbursement gap, patient behavior and medical expenses-a three-stage dynamic game analyses. *Syst Eng-Theor Pract*. (2014) 34:2974–83. doi: 10.12011/1000-6788(2014)11-2974

38. Du H, Chen C, Yuan F, Hu A, Han J. Correlation analysis of body image level and female sexual dysfunction in young patients with postoperative breast cancer. *J Cancer Res Ther*. (2022) 18:1360–71. doi: 10.4103/jcrt.jcrt_629_21

39. Rottmann N, Larsen PV, Johansen C, Hagedoorn M, Dalton SO, Hansen DG. Sexual activity in couples dealing with breast Cancer: a cohort study of associations with patient, partner and relationship-related factors. *Front Psychol*. (2022) 13:828422. doi: 10.3389/fpsyg.2022.828422

40. Jankowska M. Sexual functioning in young women in the context of breast cancer treatment. *Rep Pract Oncol Radiother*. (2013) 18:193–200. doi: 10.1016/j.rpor.2013.04.032

41. Baucom DH, Porter LS, Kirby JS, Gremore TM, Keefe FJ. Psychosocial issues confronting young women with breast cancer. *Breast Dis*. (2005) 23:103–13. doi: 10.3233/bd-2006-23114

frontiers | Frontiers in Medicine

TYPE Original Research
PUBLISHED 12 July 2023
DOI 10.3389/fmed.2023.1232814

OPEN ACCESS

EDITED BY
Hangcheng Fu,
University of Louisville, United States

REVIEWED BY
Raquel Alarcon Rodriguez,
University of Almeria, Spain
Jinwei Li,
Sichuan University, China
Chen Li,
Free University of Berlin, Germany

*CORRESPONDENCE
Zheng Lu
✉ luzhengdr@bbmc.edu.cn
Wanliang Sun
✉ 527897470@qq.com

RECEIVED 01 June 2023
ACCEPTED 27 June 2023
PUBLISHED 12 July 2023

CITATION
Zhang D, Liu S, Wu Q, Ma Y, Zhou S, Liu Z, Sun W and Lu Z (2023) Prognostic model for hepatocellular carcinoma based on anoikis-related genes: immune landscape analysis and prediction of drug sensitivity.
Front. Med. 10:1232814.
doi: 10.3389/fmed.2023.1232814

Prognostic model for hepatocellular carcinoma based on anoikis-related genes: immune landscape analysis and prediction of drug sensitivity

Dengyong Zhang[1,2], Sihua Liu[2], Qiong Wu[2], Yang Ma[2], Shuo Zhou[2], Zhong Liu[2], Wanliang Sun[2]* and Zheng Lu[1,2]*

[1]Graduate School, Anhui Medical University, Hefei, China, [2]Department of General Surgery, The First Affiliated Hospital of Bengbu Medical College, Bengbu, China

Background: Hepatocellular carcinoma (HCC) represents a complex ailment characterized by an unfavorable prognosis in advanced stages. The involvement of immune cells in HCC progression is of significant importance. Moreover, metastasis poses a substantial impediment to enhanced prognostication for HCC patients, with anoikis playing an indispensable role in facilitating the distant metastasis of tumor cells. Nevertheless, limited investigations have been conducted regarding the utilization of anoikis factors for predicting HCC prognosis and assessing immune infiltration. This present study aims to identify hepatocellular carcinoma-associated anoikis-related genes (ANRGs), establish a robust prognostic model for HCC, and delineate distinct immune characteristics based on the anoikis signature. Cell migration and cytotoxicity experiments were performed to validate the accuracy of the ANRGs model.

Methods: Consensus clustering based on ANRGs was employed in this investigation to categorize HCC samples obtained from both TCGA and Gene Expression Omnibus (GEO) cohorts. To assess the differentially expressed genes, Cox regression analysis was conducted, and subsequently, prognostic gene signatures were constructed using LASSO-Cox methodology. External validation was performed at the International Cancer Genome Conference. The tumor microenvironment (TME) was characterized utilizing ESTIMATE and CIBERSORT algorithms, while machine learning techniques facilitated the identification of potential target drugs. The wound healing assay and CCK-8 assay were employed to evaluate the migratory capacity and drug sensitivity of HCC cell lines, respectively.

Results: Utilizing the TCGA-LIHC dataset, we devised a nomogram integrating a ten-gene signature with diverse clinicopathological features. Furthermore, the discriminative potential and clinical utility of the ten-gene signature and nomogram were substantiated through ROC analysis and DCA. Subsequently, we devised a prognostic framework leveraging gene expression data from distinct risk cohorts to predict the drug responsiveness of HCC subtypes.

Conclusion: In this study, we have established a promising HCC prognostic ANRGs model, which can serve as a valuable tool for clinicians in selecting targeted therapeutic drugs, thereby improving overall patient survival rates. Additionally, this model has also revealed a strong connection between anoikis and immune cells, providing a potential avenue for elucidating the mechanisms underlying immune cell infiltration regulated by anoikis.

KEYWORDS
HCC, anoikis, metastasis, immune, prognosis, signature

1. Introduction

Hepatocellular carcinoma (HCC) accounts for 90% of primary liver malignancies, rendering it the sixth most prevalent neoplasm on a global scale and the fourth leading cause of cancer-related mortality (1, 2). Aflatoxin exposure, hepatitis virus infection, excessive alcohol consumption, type 2 diabetes, and obesity are firmly established as risk factors associated with HCC (3, 4). The distinctive heterogeneity and aggressive behavior exhibited by HCC, coupled with its elevated recurrence rate, contribute to unfavorable prognoses and overall survival (OS) outcomes among patients (5–7). The emergence of metastatic lesions signifies a pivotal event in cancer advancement and continues to pose a substantial hindrance to achieving improved long-term survival (8, 9). While multiple genes have been linked to the metastasis of HCC, their association with the prognosis of liver cancer remains uncertain.

The dissemination of cancer requires the dissociation of cells from the primary neoplasm, their viability during transit, extravasation, and establishment of secondary tumors at remote locations (10). The extracellular matrix (ECM) functions as a scaffold for cellular adhesion, instigates signal transduction, and governs essential cellular processes such as proliferation, migration, differentiation, and viability (11, 12). The acquisition of resistance against anoikis is considered a critical event in initiating and perpetuating metastasis (10, 13), which is also an obligatory prerequisite for both intrahepatic and extrahepatic dissemination of HCC. Upon detachment from the ECM, adherent cells undergo apoptosis, a process referred to as anokis (14). Malignant and highly invasive tumor cells employ diverse mechanisms to surmount anoikis and evade the primary site to establish distant metastases (15–17). While certain crucial functions of apoptosis in tumor advancement and metastasis have been elucidated (18–20), limited research has been conducted to explore the prognostic significance of genes associated with anoikis in HCC. Pseudouridine (Ψ) represents the initial post-transcriptional alteration identified and constitutes a prevalent RNA modification (21). Two distinct modes of pseudouridylation are observed, namely RNA-independent and RNA-dependent. The RNA substrate engages in the formation of complementary base pairs, enabling ncRNA recognition, while catalytic activity is conferred by DKC1 (22, 23). Pseudouridine synthases (PUS) represent a singular enzyme class responsible for catalyzing RNA-independent pseudouridylation, thereby obviating the necessity of RNA template strands (24). Certain instances involve RNA synthases, such as tRNA, exhibiting relatively restricted substrate specificities.

In this investigation, we integrated the GSE14520 and TCGA-LIHC datasets comprising HCC tissues to explore the putative roles of ANRGs. Our aim was to construct an authenticated nomogram capable of prognostic prediction and clinical guidance, accomplished through the development of a scoring, namely "riskScore," and the categorization of HCC patients according to ANRGs expression patterns. By categorizing patients with HCC based on cellular ANRGs expression, we successfully discerned distinct subgroups that exhibit associations with prognosis and immune infiltration. Employing the LASSO-Cox method, we developed a predictive model for determining the riskScore related to anoikis. Furthermore, through the integration of clinicopathological characteristics, we devised a nomogram for comprehensive risk assessment. Furthermore, we investigated the associations between RNA modifications (Ψ) and the occurrence of anoikis, a programmed cell death process, in relation to the risk of HCC. The predictive accuracy of the nomogram was validated using time-dependent receiver operating characteristic (ROC) and decision curve analysis. Our results indicated a plausible correlation among anoikis, the immune microenvironment, and the prognostic outlook for individuals with HCC.

2. Materials and methods

2.1. Data and cell lines acquisition

On the TCGA data portal,[1] which contains 374 LIHC and 50 normal tissue samples, we found gene expression profiles and clinical information for our research, including TNM classification, age, gender, and overall survival. Additionally, we obtained the ICGC dataset from https://icgc.org/, which comprised 240 HCC samples, and the GSE14520 dataset from the GEO database, which contained 221 HCC samples. For analysis, only data that had all available clinical information were used (25, 26). To obtain a comprehensive set of genes associated with anoikis, we use the keywords "anoikis" to search ANRGs in Genecards website. Eventually, a total of 63 ANRGs were retrieved.[2] HCC cell lines were all obtained from kmcellbank (No. KCB200507YJ; KCB200970YJ).

2.2. Consensus clustering with ANRGs

In order to identify distinctive expression patterns associated with regulators of anoikis, we conducted consensus clustering employing the K-means algorithm. The determination of cluster number and stability was accomplished using the "ConsensuClusterPlus" package (27–29). To validate the clustering outcomes, the UMAP algorithm in conjunction with the "ggplot2" R package was employed (30, 31).

2.3. GSVA analysis

The Gene Set Variation Analysis (GSVA) analysis was conducted employing the "GSVA" R package (32, 33) using the "c2.cp.kegg.v7.4.symbols.gmt" dataset sourced from the MSigDB

1 https://portal.gdc.cancer.gov/
2 https://www.genecards.org/

database. The determination of statistical significance among subgroups was accomplished through the utilization of the adjusted $p < 0.05$, as provided by the "limma" package (34–36). Subsequent to this, a functional enrichment analysis was performed with the purpose of investigating the functional annotation and enrichment pathways pertaining to differentially expressed genes in hepatocellular carcinoma in relation to ANRGs. T The ClusterProfiler software was employed for the examination of Gene Ontology (GO) and Kyoto Encyclopedia of Genes and Genomes (KEGG) pathways (37). A statistical significance threshold of 0.05 was applied to determine the significance of the results.

2.4. LASSO regression analysis

Survival-associated genes were identified through univariate Cox regression analysis. To further refine the selection, LASSO regression analysis was conducted using the "glmnet" package in R, employing cross-validation to determine the optimal penalty regularization parameter (λ) (38). Subsequently, multivariate Cox regression modeling was applied to identify pivotal genes and estimate their corresponding coefficients. The ANRGs risk score was computed f for each patient was calculated using the formula: riskScore = e^(0.149*FZD7 + 0.395*ADAMTS5 + 0.108*VNN2 + 0.268*MRPL9– 0.233*PPARGC1A + 0.111*EPO + 0.127*TSPAN13+ ANP32B*0.561– 0.524*TRAC +0.208*RAB328). The predictive performance of the model was assessed through the utilization of Kaplan–Meier curves as well as ROC curves.

2.5. Risk score and immune cell infiltration

The composition of infiltrating immune cells was assessed through the utilization of CIBERSORT and ssGSEA (39). The contrasting immune cell types between low-risk and high-risk HCC patients were examined via CIBERSORT.

2.6. Chemotherapy response

Protein-drug interactions were investigated through the utilization of Quartata Web (40). To assess the median inhibitory concentration (IC50) values of individual small molecule drugs, the "pRRophetic" R package was employed (41). Briefly, according to the expression levels of 10 ANRGs, HCC patients were divided into high-risk and low-risk groups. Based on the expression patterns of these two groups, drug sensitivity differences between the high-risk and low-risk groups in HCC were evaluated using the drug sensitivity data from "pRRophetic."

2.7. Nomogram

A nomogram was developed employing clinicopathological characteristics. Internal validation encompassed the use of calibration plots to evaluate the precision of the nomogram. In order to assess the predictive efficacy of the nomogram, the Time-C index was employed. Furthermore, DCA method was conducted to ascertain the clinical utility of the intervention (42).

2.8. Migration ability test

The ANRGs prognostic model was validated using Huh7 and HepG2 cell lines as experimental models. To evaluate the prognostic accuracy, wound healing assays were performed separately on Huh7 cells exhibiting high-risk scores and HepG2 cells displaying low-risk scores. The migration rates were subsequently compared to determine the relative migration capabilities of these two HCC cell lines.

2.9. CCK-8 experiment

In order to validate the accuracy of ANRGs' drug sensitivity predictions, we selected Erlotinib, which exhibited the most significant differences, for cell viability experiments. HepG2 and Huh7 cells were treated with various concentrations of Erlotinib for 36 h. Subsequently, 10 μL of CCK-8 reagent was added, and the optical density (OD) at 450 nm was measured using a spectrophotometer after a 2-h incubation period, representing the cell viability.

2.10. Statistical analysis

R software 4.1.3 was used to conduct the statistical analysis. Graphpad and Image J (version 9.4.0, 1.8.0) were used to analyze the experimental data. T-test was used to assess the difference between the two groups in the cell experiment. $p < 0.05$ were used to determine statistical significance.

3. Results

3.1. Genetic aberrations in HCC and differential expression of ANRGs

Among the 364 TCGA-LIHC samples analyzed, regulatory mutations associated with anoikis were identified in 231 samples, accounting for approximately 63.46% of the examined samples. Noteworthy, the highest mutation rates were observed in TP53 and CTNNB1 (Figure 1A). Moreover, we detected CNVs in 16 out of the 63 ANRGs within TCGA-LIHC. Predominantly, these alterations manifested as copy number amplifications (Figure 1B), with modifications observed in 16 regulators across different chromosomes (Figure 1C). The expression profiles of the 63 identified regulators were subjected to analysis aimed at discriminating between normal and tumor samples obtained from patients diagnosed with HCC (Figure 1D). Among these regulators, 55 ANRGs exhibited statistically significant alterations. Notably, 49 of them exhibited elevated expression levels in HCC samples. To gain deeper insights into the association between these regulators and patient survival, a new cohort named "LIHC-GSE14520" was generated by integrating clinical data and gene expression data from the GEO and TCGA HCC datasets. Following the data analysis, we proceeded to construct a comprehensive network diagram utilizing the 51 identified regulatory factors (Figures 1E,F).

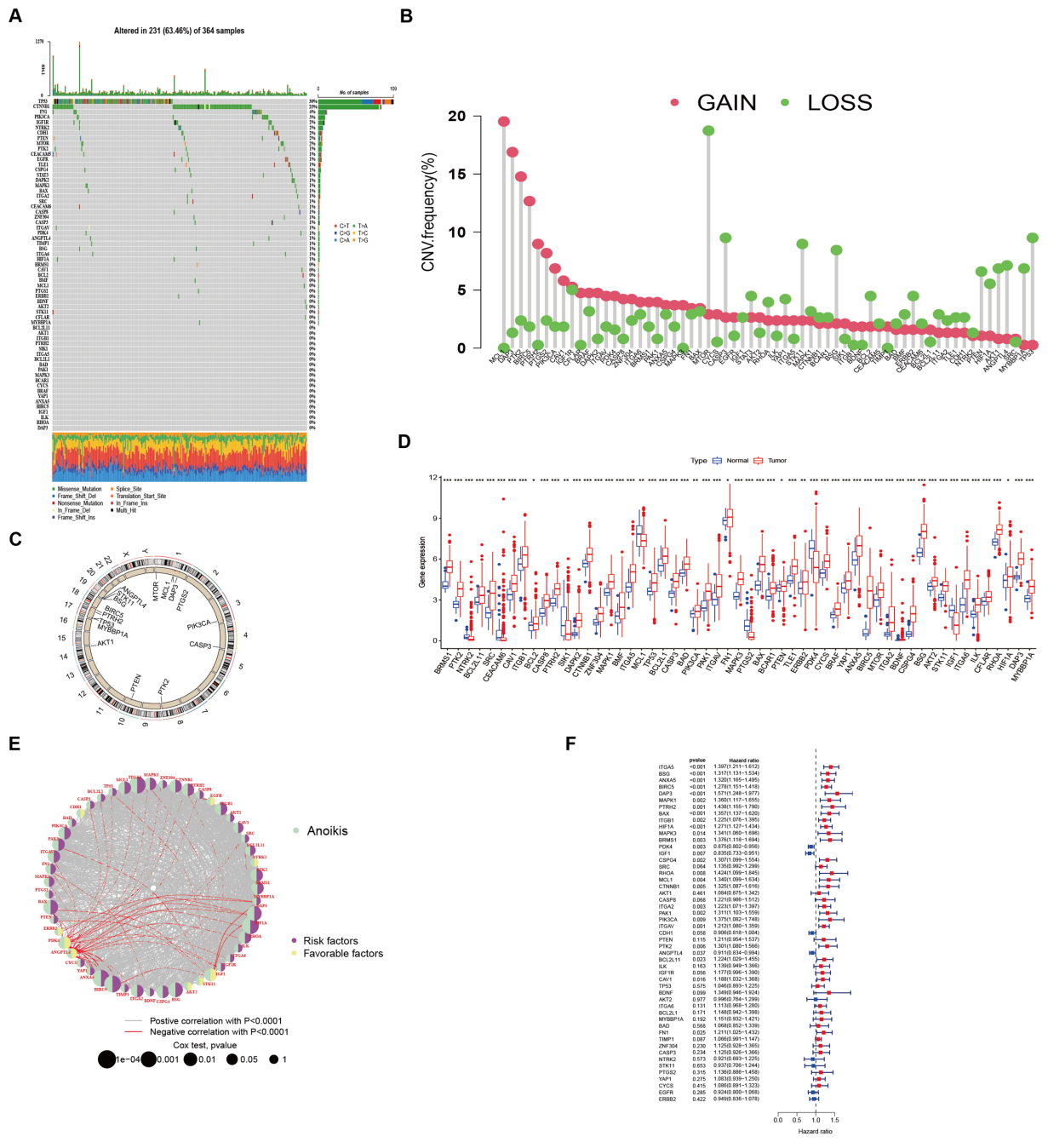

FIGURE 1
Characteristics and differences of anoikis-related regulators in HCC. **(A)** Mutation profiles of 364 hepatocellular carcinoma samples from the TCGA-LIHC cohort. Each waterfall plot represented mutational information for each anoikis-associated regulator. Corresponding colors were annotated at the bottom to indicate the different mutation types. The top bar graph showed the mutation burden. The numbers on the right side represented mutation frequencies, respectively. **(B,C)** Copy number variations (CNVs) in 16 of the 63 ANRGs in TCGA-LIHC. **(D)** The expressions of anoikis-related regulators between normal tissues (n=50) and HCC tissues (n=364) in TCGA-LIHC cohort (Wilcox test, *p<0.05; **p<0.01; ***p<0.001). **(E)** Network diagram showed the correlations between the 51 regulatory significantly associated with OS. **(F)** Forrest plot of the univariate association of the significantly different genes with OS.

3.2. Identification of HCC patterns through analysis of ANRGs

Two distinct regulatory patterns were identified through unsupervised clustering using ANRG expression levels. Cluster A comprised 220 cases, while cluster B comprised 371 cases (Figure 2A). UMAP dimensional reduction analysis validated the effective separation of the two clusters based on gene expression levels (Figure 2B). Remarkably, cluster B exhibited a superior survival advantage in comparison to cluster A (Figure 2C). It was also looked at how the cluster related to the clinicopathological traits. When compared to patients in cluster B, patients in cluster A had greater TNM stages (Figure 2D). 53 ANRG genes were found to be substantially different between the two clusters after

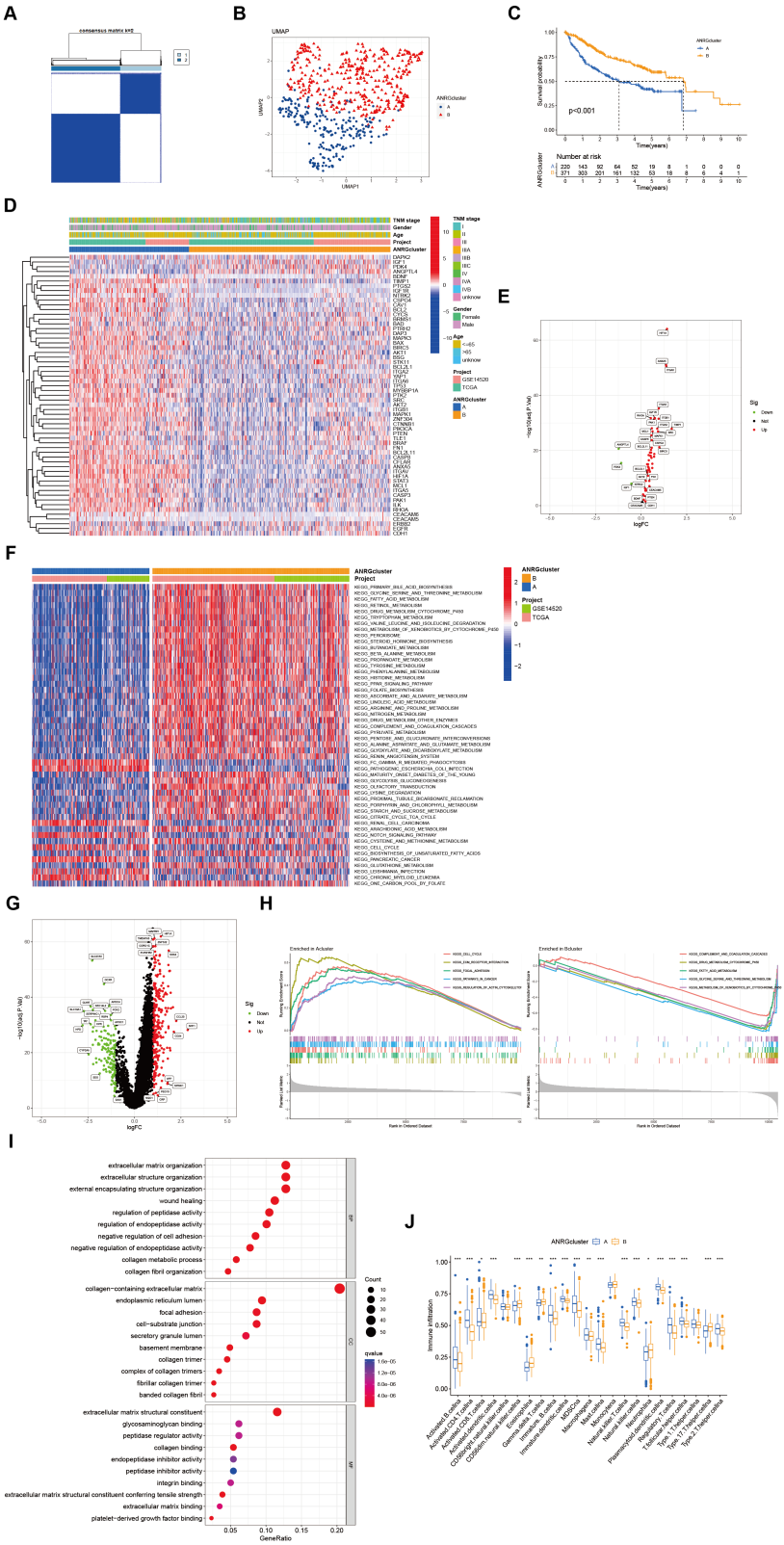

FIGURE 2
Subgroups of liver cancer related by anoikis-related genes. **(A)** Consensus matrix for k=2 was obtained by applying consensus clustering. **(B)** UMAP distinguished cluster A from cluster B based on the expression of ANRGs. **(C)** Overall survival of cluster A and cluster B (p<0.001). **(D)** Heat map of clinicopathological features of the two subtypes using GSVA enrichment analysis. **(E)** Volcanic diagram of differentially expressed ANRGs. **(F)** Heat map of KEGG pathways of the two subtypes. **(G)** Volcanic diagram of differentially expressed genes (DEG) between cluster A and cluster B. **(H)** GSEA analysis of the most significantly enriched pathways in each of the two clusters, showing the top 5 enriched pathways in cluster A (left) and cluster B (right), individually. **(I)** GO analysis of cluster A vs. cluster B based on 266 upregulated genes obtained from panel **(G)**. **(J)** Box plot showing the abundance of TME infiltrating cells between cluster A and cluster B (Wilcox test, *p<0.05, **p<0.01, ***p<0.001).

further gene expression analysis (Figure 2E). The top 50 differential KEGG pathways were shown to be substantially different across the two HCC clusters, according to our GSVA enrichment analysis (Figure 2F). 408 genes were found to be differentially expressed after the DEG analysis of the A-B cluster (Figure 2G). The most significantly enriched pathways were found in both clusters A and B by GSEA enrichment analysis (Figure 2H).

In a total of 266 genes exhibiting upregulation in cluster A were identified in comparison to cluster B, exhibiting a logFC >1 and p value <0.05. Subsequently, these genes were subjected to GO enrichment analysis (Figure 2I). The interplay between tumor occurrence and development is substantially influenced by the immune microenvironment. Analysis of the relative abundance of 23 distinct subsets of immune cells within two subpopulations unveils conspicuous infiltration of MDSCs and Tregs in group A, which exhibits diminished rates of survival (Figure 2J).

3.3. Development and validation of ANRGs model

To streamline the clinical management of hepatocellular carcinoma (HCC), our objective was to construct a subtype-specific scoring system based on patient characteristics. To accomplish this, we performed univariate Cox regression analysis to identify a set of 312 genes associated with survival. Subsequently, we subjected these prognosis-related genes to consensus clustering analysis, resulting in the discovery of three distinct regulatory patterns (Figures 3A,B). Notably, principal component analysis (PCA) unveiled substantial expression discrepancies of the aforementioned genes among these three HCC subtypes (Figure 3C). Moreover, each subtype exhibited unique overall survival outcomes (Figure 3D), affirming the prognostic reliability of the identified genes. Additionally, a comparative examination of clinical parameters between clusters A and C revealed significant differences (Figure 3E). Importantly, among the 59 genes analyzed, a striking 53 ANRGs displayed significant variations across the three regulatory patterns (Figure 3F). To establish a measurable framework applicable to individual patients, a LASSO-Cox regression analysis was subsequently executed on the set of differentially expressed genes, leveraging the training cohort. Consequently, a total of 10 risk-associated genes were identified (Figure 4A). Utilizing these 10 genes, a risk scoring system was devised for each HCC sample. Through Kaplan–Meier analysis, a noteworthy survival advantage was observed in the low-risk group compared to the high-risk group, as validated in both the training and test cohorts (Figures 4B,C). Furthermore, the derived risk score exhibited significant predictive value for 1-year, 3-year, and 5-year survival rates in HCC patients (Figures 4E,F). Ultimately, the ANRGs model was subjected to validation using an independent ICGC cohort (Figures 4D,G).

3.4. Immune infiltration

Through its function in immune evasion, TME, and particularly the immune system, is crucial to the development of malignancies. Notably, there were notable variations between clusters B and C in the riskScores of three clusters (Figures 4H,I). We next looked into the immunological infiltration between these groups, and the results revealed that cluster C had the highest levels of Tregs and macrophages M0 (Figure 4J). Additionally, we determined each patient's relative number of various immune cells and rated HCC patients according to their riskScore values (Figure 4K). As expected, the high-risk group had much greater levels of macrophages M0 and M2 (Figure 4L). To explore variations in immune cell populations among different risk groups, we applied a screening criterion given the continuous nature of riskScore in our cohort. This screening approach enabled us to identify noteworthy changes specifically within macrophages and CD8 T cells (Figure 4M). Furthermore, employing t-SNE analysis on the dataset comprising differential expression profiles of immune cells, we observed a discernible segregation of samples into three distinct subgroups (Figure 4N). Furthermore, Moreover, the TME encompasses the extracellular matrix (ECM), a critical constituent that substantially influences the migratory capability, adhesion propensity, and angiogenic processes of neoplastic cells. In order to ascertain the tumor purity for individual specimens, we employed the "Estimate" R package to evaluate the stromal and immune cell scores. Remarkably, HCC patients classified as high-risk exhibited diminished immune cell quantities and elevated tumor purity levels compared to their low-risk counterparts (Figures 5A,B).

Tumor mutational burden (TMB) serves as a biomarker for immunotherapy in diverse solid malignancies. We performed an analysis of TMB variations within distinct risk groups and clusters (Figure 5C). TMB exhibits predictive value for immune checkpoint inhibitor (ICI) efficacy, suggesting heightened responsiveness of high-risk patients to ICI treatment. Additionally, cluster C may potentially derive greater benefits from ICI therapy compared to cluster B (Figures 5D,E). Moreover, cancer stem cells (CSCs) possess the capacity for self-renewal, differentiation, and contribute to HCC development and treatment resistance. A significant upregulation of mRNA-based stemness index (SI) was observed in the high-risk group (Figure 5F). Furthermore, a positive association between risk score and SI was noted, with cluster C displaying a more pronounced correlation relative to cluster B (Figure 5G). To identify potential therapeutic agents for the high-risk group, QuartataWeb Server was employed, considering the unfavorable prognosis linked to this subgroup (Figure 5H).

3.5. Prediction of drug response

A predictive model was developed to estimate the response of HCC patients to chemotherapeutic treatment, leveraging the notable variances in gene expression profiles observed across distinct risk categories. The pRRophetic software was used in our method to foresee variations in the susceptibility of tumors to anticancer drugs using gene expression data collected from various risk categories. The results of our investigation revealed a significantly elevated probability of response to axitinib in the high-risk group, whereas the low-risk group exhibited a greater propensity for responding to epothilone B (Figure 6).

3.6. Association between ANRGs and Pseudouridine (Ψ)

Upregulation of RNA modifiers is linked to the prognosis of tumor illnesses. rRNA, snoRNA, and snRNA are all modified during

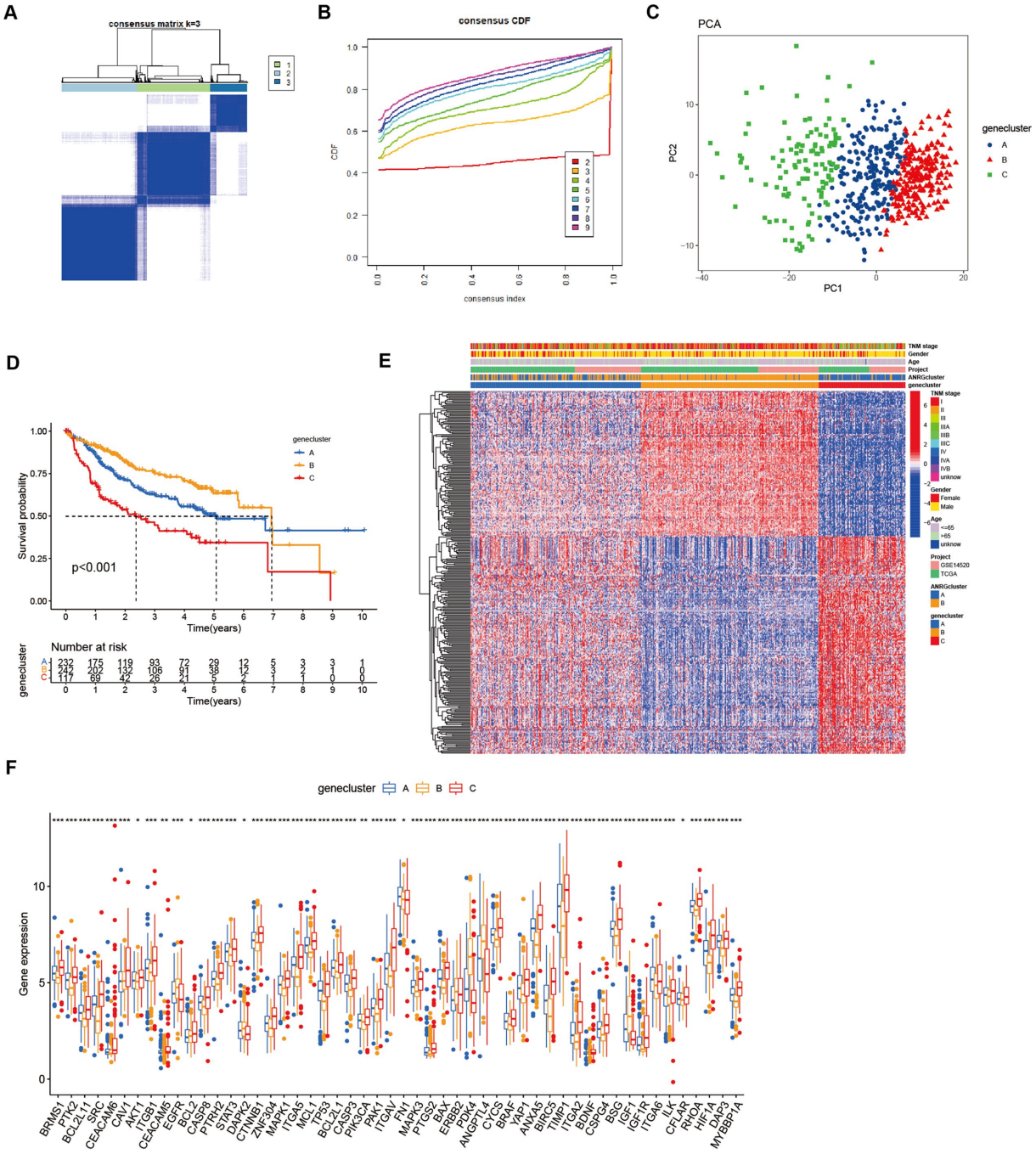

FIGURE 3
Subgroups of liver cancer related by new gene signature based on two anoikis-related clusters. **(A,B)** Consensus matrix for k=3 was obtained by applying consensus clustering, according to CDF curve. **(C)** Principal component analysis (PCA) for the expression of DEGs to distinguish the three clusters in LIHC-GSE14520 cohort. **(D)** OS in the three clusters in LIHC-GSE14520 cohort. **(E)** Heat map of clinicopathological features of the three subtypes based on DEG. **(F)** ANRGs expression level between cluster A–C (Wilcox test, *p<0.05, **p<0.01, ***p<0.001).

the RNA pseudouridylation process. Through the investigation of the correlation between risk scores and the expression patterns of pseudouridylation genes (Figure 7A), as well as the comparative analysis of gene expression levels between high-risk and low-risk cohorts (Figure 7B), we have elucidated the possible involvement of in anoikis resistance in HCC patients. Our results reveal a robust association between genes involved in pseudouridylation and aberrantly expressed ANRGs, thereby implying a notable involvement of pseudouridylation in the prognostic implications for HCC patients' survival outcomes (Figure 7C).

3.7. Establishing the HCC nomogram

We devised a nomogram to forecast the overall survival rate with the aim of exploring the therapeutic applications of riskScore in

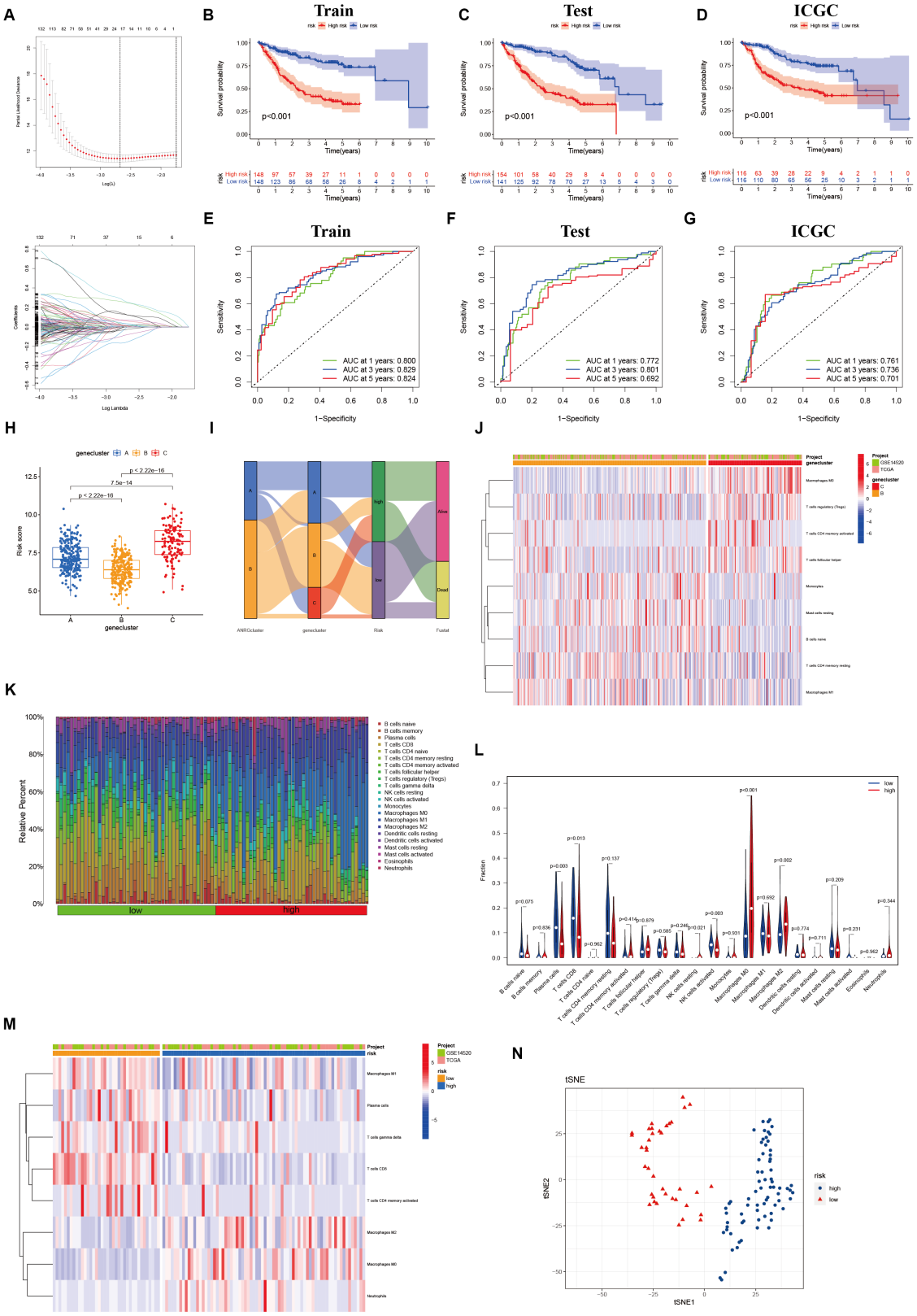

FIGURE 4
Lasso analysis and Kaplan–Meier curve for the patients in the LIHC-GSE14520 and ICGC cohorts. **(A)** LASSO coefficient profiles of the 312 DEGs based on anoikis-related genes, and the super parameter (λ) was obtained based on the minimum standard with 10-fold cross-validation. **(B–D)** Kaplan–Meier plot of high-risk and low-risk in LIHC-GSE14520 cohort and ICGC cohort, which represented training group **(B)**, test group **(C)** from LIHC-GSE14520 cohort and ICGC validation group **(D)**, individually. **(E–G)** AUC time-dependent ROC curves for OS in training, test and validation cohort. **(H)** The level of "riskScore" in different clusters. **(I)** The Sankey diagram of the relationship between different clusters and living risk. **(J)** Immune infiltration between cluster B and cluster C. **(K–M)** Immune cell infiltration in different risk groups based on DEGs in the two ANRGs clusters. **(N)** The tSNE analysis demonstrated the differentiation between high and low risk groups.

determining the prognosis of individuals afflicted with HCC (Figure 8A). The nomogram encompasses four autonomous prognostic factors, wherein riskScore and TNM classification play principal roles (Figure 8C). Verification of the model's accuracy and the nomogram's reliability was achieved through the application of the Schoenfeld Residuals Test and calibration curve analysis (Figures 8B,D). The predictive capacity of the integrated nomogram was found to be significantly superior, as evidenced by the time-dependent ROC curve analysis. The time-C index surpassed 0.7, affirming its robustness in forecasting (Figure 8E). Furthermore, decision curve analysis (DCA) corroborated that the nomogram represents the most precise approach to prognosticate HCC patients' survival (Figure 8F). The cumulative hazard curve demonstrated a gradual escalation in the jeopardy of overall survival among patients exhibiting elevated scores in the nomogram (Figure 8G), thereby underscoring the significance of employing the nomogram in conjunction with risk scores derived from ANRGs as a potent approach to prognosticate patient outcomes in the realm of clinical application.

3.8. Migration ability between HCC cell lines in different risk scores

The predictive performance of the ANRGs prognostic model was assessed using Huh7 and HepG2 cell lines. To evaluate their migratory abilities, wound healing experiments were conducted on Huh7 cells exhibiting high-risk scores and HepG2 cells exhibiting low-risk scores. A comparative analysis of the migration rates between these two HCC cell lines was conducted. Our findings demonstrated a significantly diminished migration rate in HepG2 cells with low-risk scores in contrast to Huh7 cells with high-risk scores ($p < 0.01$; Figures 9A–C). These results suggest that a high-risk score is indicative of heightened metastatic potential in tumors, which may contribute, in part, to the unfavorable prognosis observed in HCC patients. These findings are consistent with the outcomes derived from our ANRGs prognostic model.

3.9. Validation of drug sensitivity in HCC cell lines

To evaluate drug sensitivity, the CCK-8 assay was employed. Higher absorbance values indicate stronger cellular viability, thus reflecting decreased sensitivity to the tested drug. We observed differential sensitivity of HepG2 and Huh7 cells to Erlotinib at various concentrations (Figures 9D,E). Huh7 cells with higher risk scores exhibited greater sensitivity to Erlotinib, as evidenced by lower OD values, compared to HepG2 cells with lower risk scores. These findings align with our drug prediction outcomes, thereby affirming the reliability of the predictive model.

4. Discussion

Globally, HCC continues to be a particularly deadly kind of cancer (43). Given the intricate molecular pathways implicated, enhancing the prognosis of HCC patients through singular targeted pathways or drug interventions proves arduous. The major contributors to diminished survival rates among these patients are metastasis and postoperative recurrence. Although several genetic markers with predictive potential for HCC have been discovered (44–46), their count remains inadequate. Hence, there exists a pressing requirement to identify supplementary biomarkers exhibiting robust predictive efficacy to expand the pool of potential candidates.

Anoikis is a form of regulated cellular apoptosis triggered by the detachment of cells from the appropriate extracellular matrix, thereby disrupting integrin-mediated adhesion. This process serves as a vital mechanism in safeguarding tissue homeostasis and development by inhibiting the growth and attachment of dysplastic cells to unsuitable substrates (47). Dysregulation of anoikis, characterized by resistance to anchorage-dependent growth and epithelial-mesenchymal transition, has garnered considerable scientific interest owing to its implication in tumor progression and the metastatic dissemination of malignant cells. In HCC, multiple signaling cascades possess the capability to disrupt the phenomenon of anoikis resistance, consequently leading to the attenuation of tumor metastasis. Consequently, therapeutic intervention strategies targeting genes associated with anoikis have surfaced as a promising avenue for surmounting the advancement and metastatic potential of HCC. Employing a polygenic profiling approach, encompassing multiple genes, affords a comprehensive assessment of the intricate interplay among diverse factors governing tumor pathology and the acquisition of anoikis resistance. This innovative approach holds substantial promise in providing crucial insights into tumor biology, thereby furnishing indispensable support for clinical decision-making in the epoch of precision medicine within the domain of oncology (48).

In this investigation, the expression patterns of genes associated with HCC in relation to anoikis were initially ascertained (Figure 1D). Subsequently, a comprehensive screening was conducted to identify ANRGs that exhibit associations with the prognosis of HCC (Figures 1E,F). By employing KEGG and ssGSEA for further analysis, differential enrichment of pathways was discovered, indicating a potential influence of these anoikis-associated genes on the survival outcomes of HCC patients by modulating these pathways (Figures 2C,F,H). Leveraging the Lasso technique, we successfully identified ten ANRGs as crucial genes for the prognostic model, enabling the categorization of HCC patients into high-risk and low-risk groups (Figure 4A). Immunotherapy and the advancement of cancer treatment rely heavily on the immune system (49). Moreover, the modulation of cytokine equilibrium significantly influences the progression of the disease (50). Ongoing investigations are currently focused on exploring the potential of exosome-based immunotherapy (51). In addition, the development of deep learning models is underway to predict the efficacy of immunotherapy (52). Within the TME, a diverse repertoire of chemokines and cytokines is generated by both immune and cancer cells, playing pivotal roles in regulating tumor progression and expansion. By utilizing the Cibersort software, we conducted an additional investigation into the immune infiltration patterns within the high-risk and low-risk cohorts (Figures 4K–M). This analysis revealed that the immunosuppressive phenotype characterizes this particular subgroup.We have identified a cohort of ten genes displaying robust associations with the risk of cancer (Figures 4B–D).

In the course of our investigation, a collection of eight genes displaying strong associations with cancer risk has been identified.

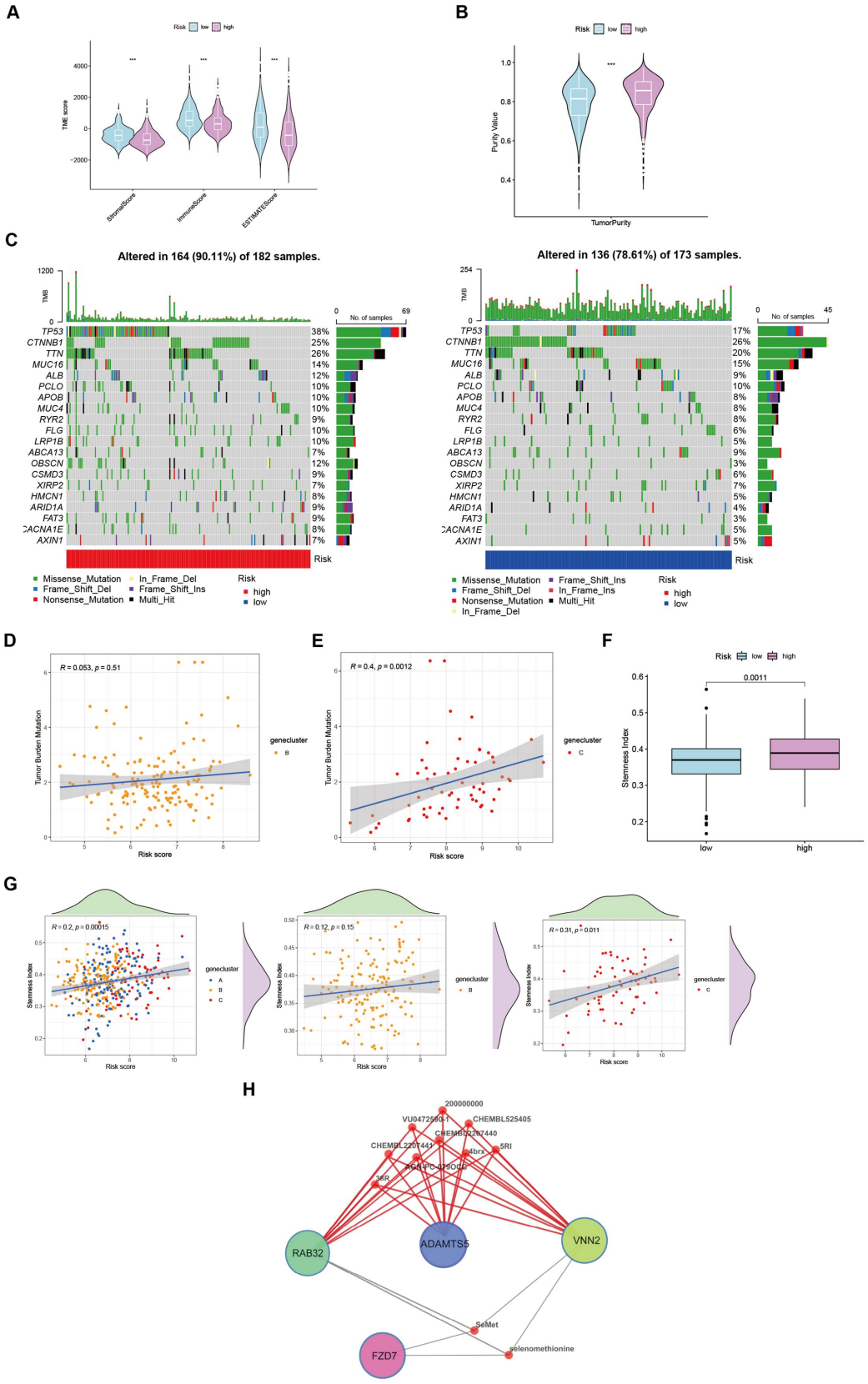

FIGURE 5
Characteristics and differences between different risk-groups in HCC. **(A)** The score of components in tumor microenvironment (Wilcox test, ***p<0.001). **(B)** Influence of tumor purity to risk score (Wilcox test, ***p<0.001). **(C–E)** Mutation profiles of TCGA-LIHC cohort with different risk statue as well as cluster B and cluster C (Spearman test, p=0.51; p=0.0012). **(F)** Stemness Index in different risk groups (Wilcox test, p=0.0011). **(G)** The relationship between stemness index and risk score in LIHC-GSE14520 cohort (Spearman test). **(H)** Potential targeting drugs prediction via QuartataWeb Server.

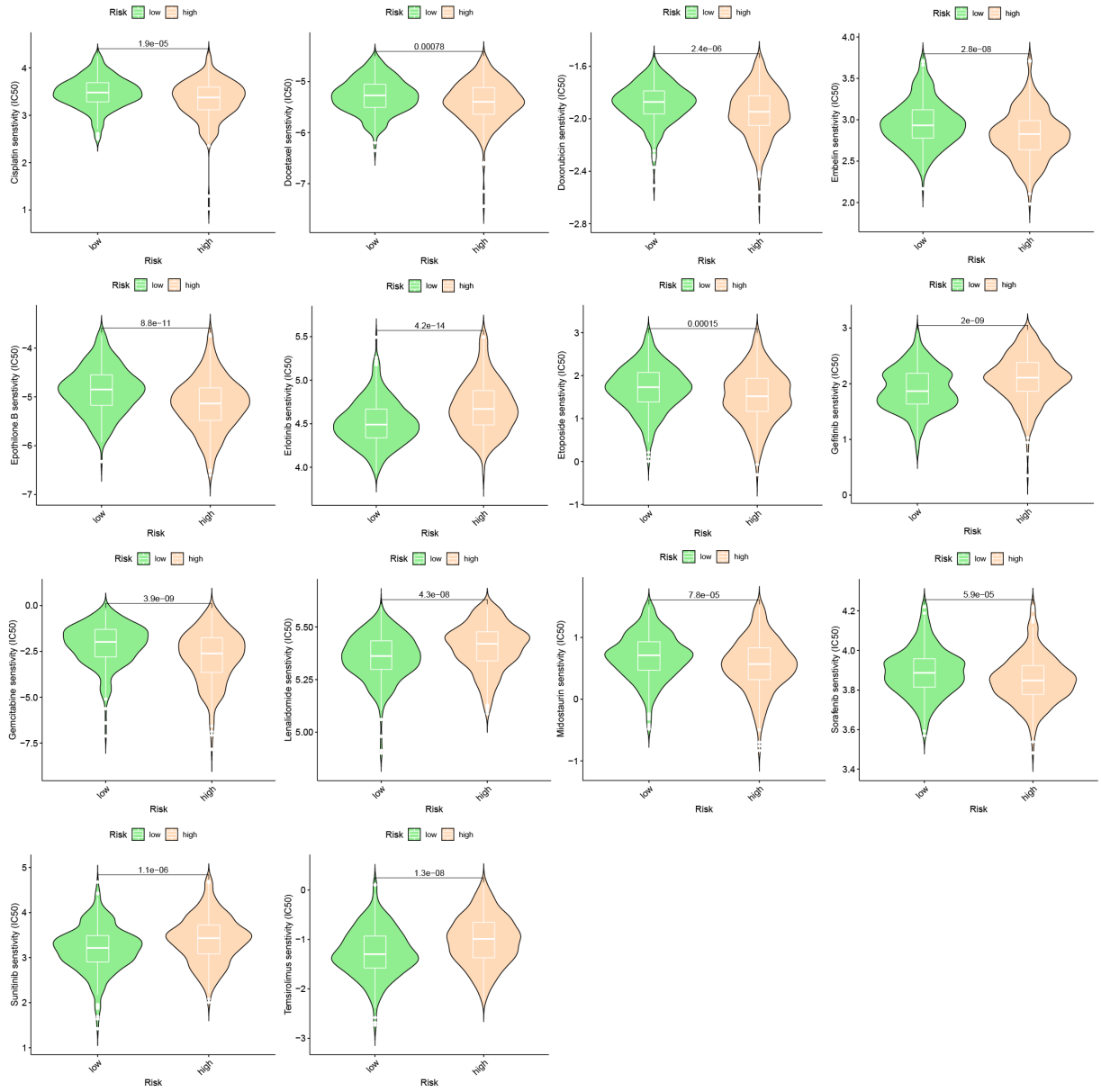

FIGURE 6
Drug sensitivity between high-risk group and low-risk group.

Previous studies have established multiple connections between these genes and the growth and advancement of tumors. Notably, Arechederra M and co-authors have provided evidence showcasing the pivotal role of ADAMTSL5, a protein synthesized by liver cancer cells, in the formation of tumors. Targeting this gene effectively has demonstrated reductions in both *in vitro* and *in vivo* tumor growth (53). Furthermore, in the context of colorectal cancer, heightened expression of ADAMTS5 has emerged as a significant indicator of lymphatic infiltration and metastasis (54). According to research conducted on HCC cell lines, FZD7, which is overexpressed in gastric, esophageal, and HCC (55), directly interacts with Wnt signaling to activate the traditional Wnt/−linked protein pathway (56). Epithelial mesenchymal transition (EMT), which is triggered by this activation, encourages HCC to migrate and invade more widely (57). The FZD7/Wnt axis may be blocked to drastically reduce the production of tumor-related proteins and to slow the HCC development (58). Furthermore, FZD7 exhibits anti-apoptotic actions in HCC (59). Despite having received less attention in oncology research, MRPL9 has been discovered to have an oncogenic characteristic in breast cancer (60). The VNN2 protein is essential for cell transendothelial migration and is linked to non-adhesive proliferation, which raises the possibility that it contributes to tumor anoikis resistance (61). VNN2 was discovered to be up-regulated in a human metastasizing esophageal cancer cell line (T.Tn-AT1) in comparison to the parental non-metastasizing cell line (T.Tn), emphasizing its significance in metastasis (62). Rab32, on the other hand, is connected to mTORC1 signaling and the stimulation of -catenin/TCF signaling and expressed in a variety of secretory epithelial cells (63). The proliferation, migration, and metastasis of esophageal squamous cell carcinoma (ESCC) cells have been demonstrated to be inhibited by suppression of

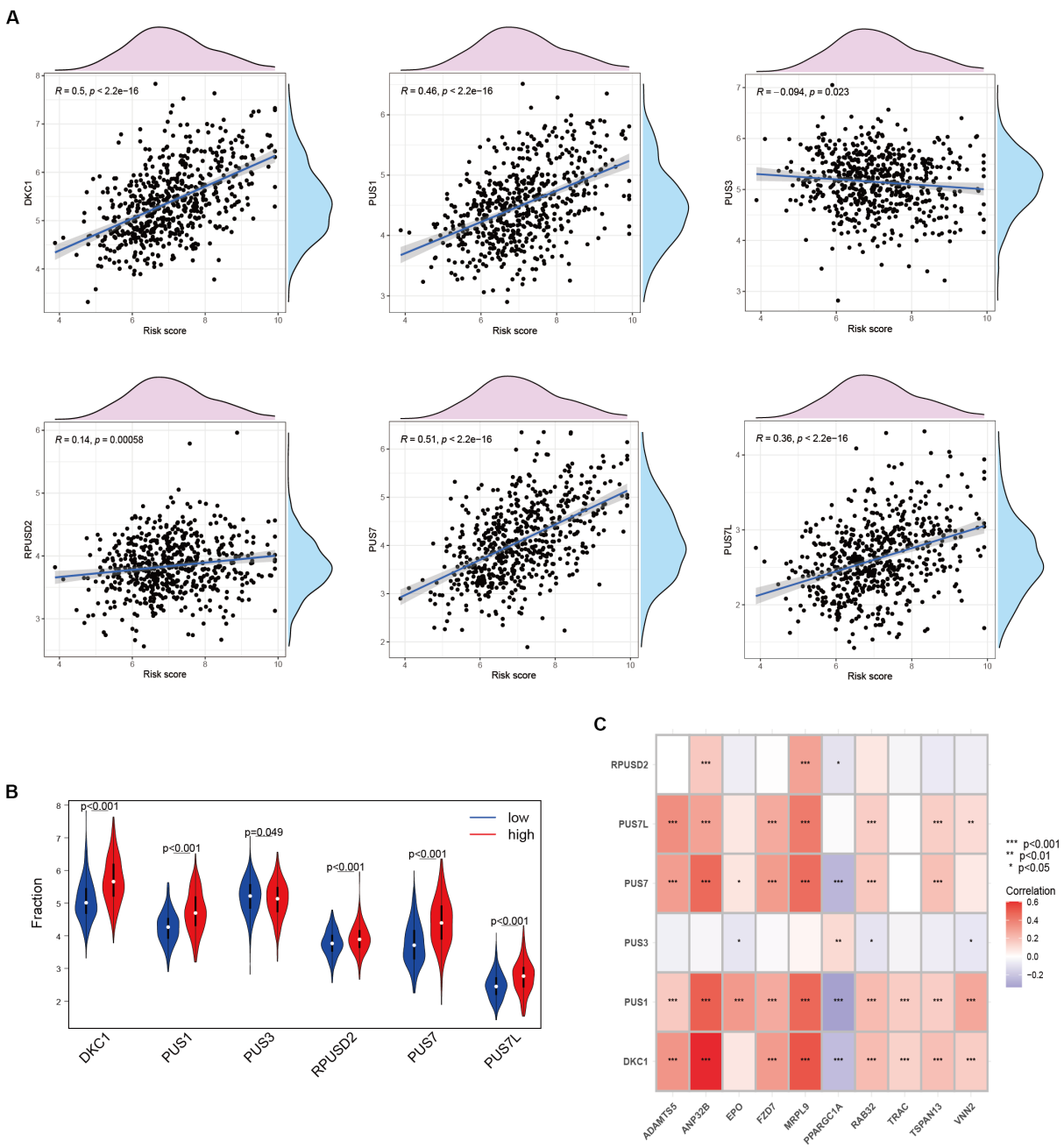

FIGURE 7
Relationship between Anoikis and Pseudouridine (Ψ) in HCC. **(A)** The relationship between Ψ regulator and risk score in LIHC-GSE14520 cohort. **(B)** The expressions of Ψ regulators with different risk status (Wilcox test). **(C)** Correlation of ANRGs and Ψ regulators (Wilcox test, *p<0.05; **p<0.01; ***p<0.001).

RAB23 expression but promoted by overexpression of RAB23 (64). Tetraubiquitin superfamily member TSPAN13, commonly known as NET-6, has been linked to a number of biological activities, including motility and metastasis (65). TSPAN13 expression has been demonstrated to be suppressed by certain miRNAs (66–68), which results in mesenchymal–epithelial transition (MET) and less tumor invasion and growth (69) The pleiotropic growth factor erythropoietin (EPO), on the other hand, has been shown to encourage the development of soft agar colonies in human hepatoma cells, indicating that it may play a part in conferring anoikis-resistance (70). Contrarily, PPARGC1A expression has been found to be downregulated in HCC, and *in vitro* and *in vivo* tests have demonstrated that upregulation of PPARGC1A can successfully prevent HCC cell invasion and migration by blocking the Wnt/−catenin/PDK1 axis and thereby inhibiting aerobic glycolysis (71).

Pseudouridine (Ψ) stands out as a prominent RNA modification and represents the inaugural post-transcriptional alteration to have been identified. Unlike methylation, Ψ exhibits irreversibility within mammalian systems (72). DKC1 assumes an indispensable role as a constituent of the telomerase complex, with

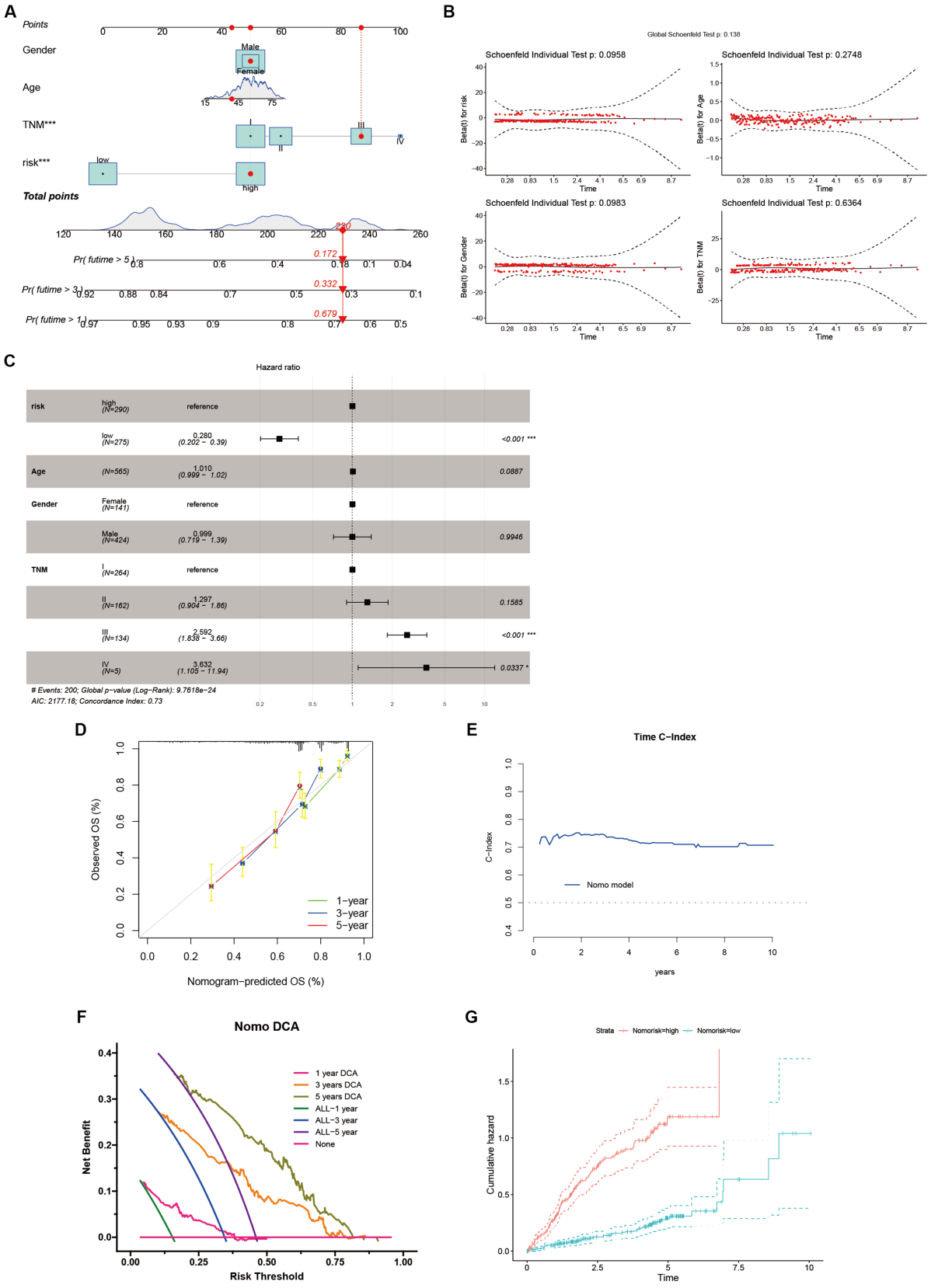

FIGURE 8
Identification and Verification of Nomograms. **(A)** A nomogram prediction ability at 1, 3, and 5years. **(B,D,E)** Schoenfeld Residuals Test was performed to verify the validity of nomogram, and calibration plot for internal validation of the nomogram. Time C-index evaluated the predictive performance of nomogram at different times. **(C)** Forest plot summary of multivariable Cox regression analyses of the clinical features as well as risk score in the LIHC-GSE14520 cohort. **(F)** DCA curves of the nomogram for 1-, 3- and 5- year OS in LIHC-GSE14520 cohort indicated the clinical decision-making benefits of this model. **(G)** Cumulative hazard curve represented the probability of survival over time progression.

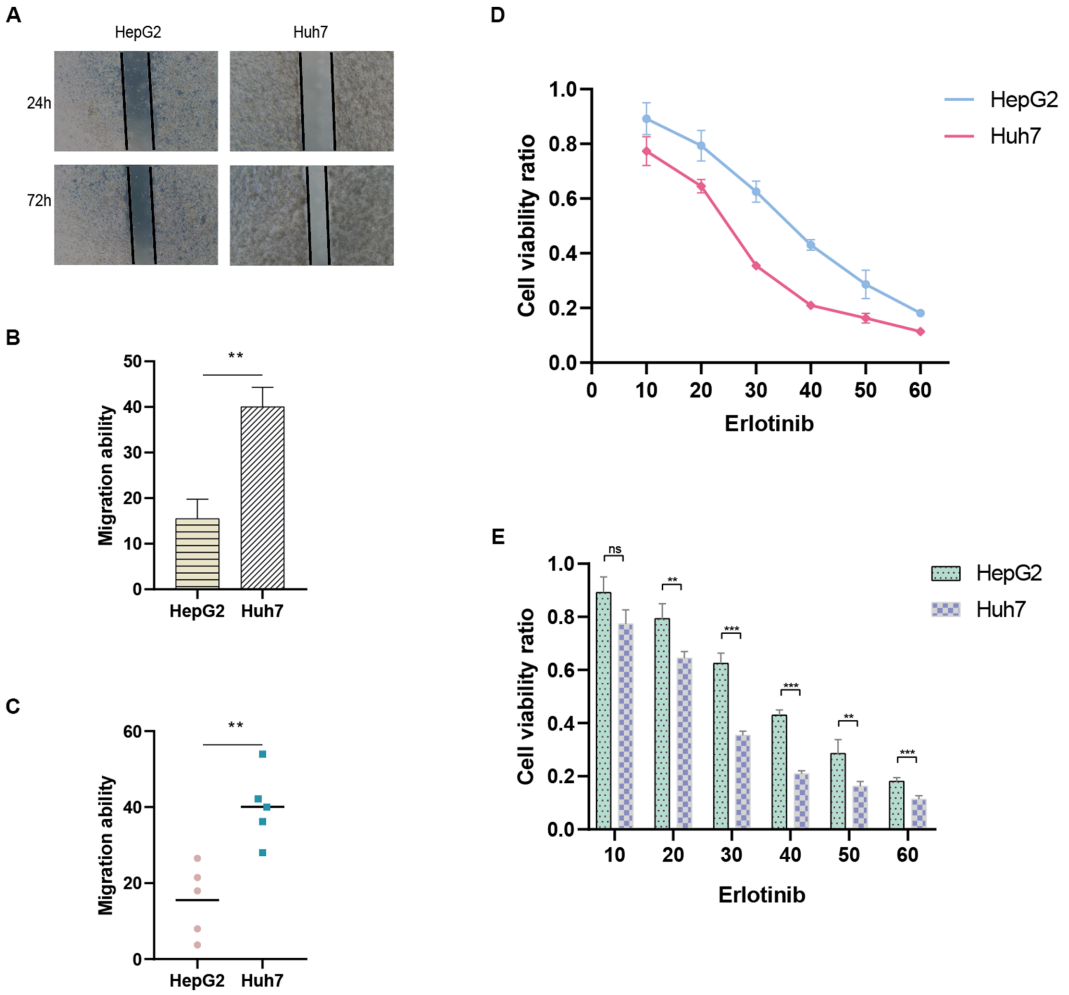

FIGURE 9
Wound healing assay. **(A)** Migration ability detected via wound healing assay. **(B,C)** Results of migration ability between HepG2 and Huh7 cell lines. **(D,E)** Drug sensitivity to Erlotinib in HCC cell lines.

its participation being crucial in the post-transcriptional processing of precursor rRNA, thereby exerting a pivotal influence on the progression of tumor cells (73). During our investigation, we assessed the expression levels of DKC1, PUS1, and PUS7 among patients diagnosed with HCC, revealing a robust and significant correlation between pseudouridine and anoikis (Figure 7A). Significantly elevated expression of these genes was observed in the high-risk cohort (Figure 7B), implying a vital contribution of Ψ in the advancement of HCC and its metastatic dissemination. Furthermore, our correlation analysis has provided preliminary evidence suggesting a plausible association between Ψ and anoikis in the context of HCC (Figure 7C).

Sample classification using established gene expression characteristics is a widely employed methodology (74, 75). In our study, we utilized a comparable strategy to classify HCC patients by analyzing the expression profiles of cellular regulators associated with anoikis, in conjunction with clinicopathological indicators (Figure 8A). Our results revealed substantial differential expression of these regulators among distinct subgroups, and their expression patterns were associated with diverse prognoses, substantiating the effectiveness of our ten-gene signature in discerning patient outcomes. This signature holds the potential to aid clinicians in formulating personalized therapeutic approaches. Furthermore, the decision curve analysis indicates that the nomogram constructed using the ten-gene signature could yield long-term advantages for hepatocellular carcinoma patients (Figure 8F).

Finally, to validate the reliability of the ANRGs model, we conducted wound healing assay and CCK-8 assay to examine the migration ability and drug sensitivity of different risk-scored HCC cell lines, HepG2 and Huh7. We observed that the migration ability of the high-risk Huh7 cells was significantly higher than that of the low-risk-scored HepG2 cells (Figures 9A–C), which partly explains the poor prognosis of high-risk HCC patients. Furthermore, Huh7 cells exhibited a significantly higher response to Erlotinib compared to HepG2 cells (Figures 9D,E), confirming the accuracy of our drug prediction (Figure 6).

Although our riskScore model and the corresponding nomogram demonstrate enhanced predictive efficacy, the cellular heterogeneity implies that investigating the influence of ANRGs on hepatocellular carcinoma advancement and prognosis at the individual cell level could provide heightened precision.

Furthermore, the utilization of a restricted dataset in this investigation necessitates the inclusion of a more extensive sample size to adequately calibrate the predictive model.

5. Conclusion

Our investigation has devised a signature composed of ten genes and accompanying nomograms, which hold potential utility for clinicians in the individualized selection of chemotherapy regimens for patients with HCC. The ten-gene signature, intricately linked to anoikis, exhibits remarkable efficacy in prognosticating the survival outcomes of HCC patients. Additionally, the nomogram derived from this predictive model holds promise as a valuable tool for healthcare professionals in formulating personalized treatment strategies within clinical contexts. Future explorations into the molecular underpinnings of resistance to anoikis hold significant clinical implications, with the potential to provide a novel precision medicine approach for HCC.

Data availability statement

The datasets utilized in the present investigation can be accessed from the TCGA database (http://cancergenome.nih.gov/), GEO (https://www.ncbi.nlm.nih.gov/geo/), and the ICGC (https://icgc.org/). All raw data are available at https://www.jianguoyun.com/p/DexQH4oQovD_ChjWlvwEIAA.

Author contributions

ZLu, WS, and DZ conceived the study. DZ drafted the manuscript. DZ, SL, QW, and YM analyzed and visualized the data. SZ, ZLiu, and WS performed the literature search and collected the data. ZLu and WS helped with the final revision of this manuscript. All authors reviewed and approved the final manuscript.

Funding

This study was supported by Anhui University Natural Science Research Project (KJ2021A0731), the sixth batch of "special support plan" leading talent projects in Anhui Province, the Natural Science Foundation of Bengbu Medical College (2020byzd106), and the Overseas visiting and training program for outstanding colleges teachers in Anhui (gxgwfx2022024).

Acknowledgments

The authors acknowledge the contributions from the TCGA, GEO, and ICGC project.

Conflict of interest

The authors declare that the research was conducted in the absence of any commercial or financial relationships that could be construed as a potential conflict of interest.

Publisher's note

References

1. Sung H, Ferlay J, Siegel RL, Laversanne M, Soerjomataram I, Jemal A, et al. Global cancer statistics 2020: GLOBOCAN estimates of incidence and mortality worldwide for 36 cancers in 185 countries. *CA Cancer J Clin*. (2021) 71:209–49. doi: 10.3322/caac.21660

2. Devarbhavi H, Asrani SK, Arab JP, Nartey YA, Pose E, Kamath PS. Global burden of liver disease: 2023 update. *J Hepatol*. (2023). doi: 10.1016/j.jhep.2023.03.017

3. Llovet JM, Willoughby CE, Singal AG, Greten TF, Heikenwalder M, El-Serag HB, et al. Nonalcoholic steatohepatitis-related hepatocellular carcinoma: pathogenesis and treatment. *Nat Rev Gastroenterol Hepatol*. (2023). doi: 10.1038/s41575-023-00754-7

4. Yang TH, Chan C, Yang PJ, Huang YH, Lee MH. Genetic susceptibility to hepatocellular carcinoma in patients with chronic hepatitis virus infection. *Viruses*. (2023):15. doi: 10.3390/v15020559

5. Missiaen R, Anderson NM, Kim LC, Nance B, Burrows M, Skuli N, et al. GCN2 inhibition sensitizes arginine-deprived hepatocellular carcinoma cells to senolytic treatment. *Cell Metab*. (2022) 34:e1157. doi: 10.1016/j.cmet.2022.06.010

6. Husain A, Chiu YT, Sze KM, Ho DW, Tsui YM, Suarez EMS, et al. Ephrin-A3/EphA2 axis regulates cellular metabolic plasticity to enhance cancer stemness in hypoxic hepatocellular carcinoma. *J Hepatol*. (2022) 77:383–96. doi: 10.1016/j.jhep.2022.02.018

7. Lee TK, Guan XY, Ma S. Cancer stem cells in hepatocellular carcinoma - from origin to clinical implications. *Nat Rev Gastroenterol Hepatol*. (2022) 19:26–44. doi: 10.1038/s41575-021-00508-3

8. Tang ZY, Ye SL, Liu YK, Qin LX, Sun HC, Ye QH, et al. A decade's studies on metastasis of hepatocellular carcinoma. *J Cancer Res Clin Oncol*. (2004) 130:187–96. doi: 10.1007/s00432-003-0511-1

9. Su K, Shen Q, Tong J, Gu T, Xu K, Li H, et al. Construction and validation of a nomogram for HBV-related hepatocellular carcinoma: a large, multicenter study. *Ann Hepatol*. (2023) 28:101109. doi: 10.1016/j.aohep.2023.101109

10. Sattari Fard F, Jalilzadeh N, Mehdizadeh A, Sajjadian F, Velaei K. Understanding and targeting anoikis in metastasis for cancer therapies. *Cell Biol Int*. (2023) 47:683–98. doi: 10.1002/cbin.11970

11. Zhou S, Lu J, Liu S, Shao J, Liu Z, Li J, et al. Role of the tumor microenvironment in malignant melanoma organoids during the development and metastasis of tumors. *Front Cell Dev Biol*. (2023) 11:1166916. doi: 10.3389/fcell.2023.1166916

12. Collins NL, Reginato MJ, Paulus JK, Sgroi DC, Labaer J, Brugge JS. G1/S cell cycle arrest provides anoikis resistance through Erk-mediated Bim suppression. *Mol Cell Biol*. (2005) 25:5282–91. doi: 10.1128/MCB.25.12.5282-5291.2005

13. Taddei ML, Giannoni E, Fiaschi T, Chiarugi P. Anoikis: an emerging hallmark in health and diseases. *J Pathol*. (2012) 226:380–93. doi: 10.1002/path.3000

14. Bose M, Sanders A, De C, Zhou R, Lala P, Shwartz S, et al. Targeting tumor-associated MUC1 overcomes anoikis-resistance in pancreatic cancer. *Transl Res*. (2023) 253:41–56. doi: 10.1016/j.trsl.2022.08.010

15. Zhang T, Wang B, Su F, Gu B, Xiang L, Gao L, et al. TCF7L2 promotes anoikis resistance and metastasis of gastric cancer by transcriptionally activating PLAUR. *Int J Biol Sci*. (2022) 18:4560–77. doi: 10.7150/ijbs.69933

16. Ray U, Jung DB, Jin L, Xiao Y, Dasari S, Sarkar Bhattacharya S, et al. Targeting LRRC15 inhibits metastatic dissemination of ovarian cancer. *Cancer Res*. (2022) 82:1038–54. doi: 10.1158/0008-5472.CAN-21-0622

17. Kim K, Huang H, Parida PK, He L, Marquez-Palencia M, Reese TC, et al. Cell competition shapes metastatic latency and relapse. *Cancer Discov*. (2023) 13:85–97. doi: 10.1158/2159-8290.CD-22-0236

18. Zhu HD, Liu L, Deng H, Li ZB, Sheng JQ, He XX, et al. Astrocyte elevated gene 1 (AEG-1) promotes anoikis resistance and metastasis by inducing autophagy in hepatocellular carcinoma. *J Cell Physiol*. (2020) 235:5084–95. doi: 10.1002/jcp.29377

19. Wang W, Shen XB, Huang DB, Jia W, Liu WB, He YF. Peroxiredoxin 4 suppresses anoikis and augments growth and metastasis of hepatocellular carcinoma cells through the beta-catenin/ID2 pathway. *Cell Oncol (Dordr)*. (2019) 42:769–81. doi: 10.1007/s13402-019-00460-0

20. Wang S, Lv Y, Zhou Y, Ling J, Wang H, Gu D, et al. Acidic extracellular pH induces autophagy to promote anoikis resistance of hepatocellular carcinoma cells via downregulation of miR-3663-3p. *J Cancer*. (2021) 12:3418–26. doi: 10.7150/jca.51849

21. Adachi H, Pan Y, He X, Chen JL, Klein B, Platenburg G, et al. Targeted pseudouridylation: an approach for suppressing nonsense mutations in disease genes. *Mol Cell*. (2023) 83:e639. doi: 10.1016/j.molcel.2023.01.009

22. Jin Z, Song M, Wang J, Zhu W, Sun D, Liu H, et al. Integrative multiomics evaluation reveals the importance of pseudouridine synthases in hepatocellular carcinoma. *Front Genet*. (2022) 13:944681. doi: 10.3389/fgene.2022.944681

23. Zhao Y, Rai J, Yu H, Li H. CryoEM structures of pseudouridine-free ribosome suggest impacts of chemical modifications on ribosome conformations. *Structure*. (2022) 30:e985. doi: 10.1016/j.str.2022.04.002

24. Purchal MK, Eyler DE, Tardu M, Franco MK, Korn MM, Khan T, et al. Pseudouridine synthase 7 is an opportunistic enzyme that binds and modifies substrates with diverse sequences and structures. *Proc Natl Acad Sci U S A*. (2022) 119:4. doi: 10.1073/pnas.2109708119

25. Cerami E, Gao J, Dogrusoz U, Gross BE, Sumer SO, Aksoy BA, et al. The cBio cancer genomics portal: an open platform for exploring multidimensional cancer genomics data. *Cancer Discov*. (2012) 2:401–4. doi: 10.1158/2159-8290.CD-12-0095

26. Roessler S, Jia HL, Budhu A, Forgues M, Ye QH, Lee JS, et al. A unique metastasis gene signature enables prediction of tumor relapse in early-stage hepatocellular carcinoma patients. *Cancer Res*. (2010) 70:10202–12. doi: 10.1158/0008-5472.CAN-10-2607

27. Hartigan JA, Wong MA. Algorithm AS 136: A k-means clustering algorithm. *J R Stat Soc C*. (1979) 28:100–8.

28. Zhang X, Zhuge J, Liu J, Xia Z, Wang H, Gao Q, et al. Prognostic signatures of sphingolipids: understanding the immune landscape and predictive role in immunotherapy response and outcomes of hepatocellular carcinoma. *Front Immunol*. (2023) 14:1153423. doi: 10.3389/fimmu.2023.1153423

29. Zhao S, Zhang X, Gao F, Chi H, Zhang J, Xia Z, et al. Identification of copper metabolism-related subtypes and establishment of the prognostic model in ovarian cancer. *Front Endocrinol (Lausanne)*. (2023) 14:1145797. doi: 10.3389/fendo.2023.1145797

30. Liu J, Zhang P, Yang F, Jiang K, Sun S, Xia Z, et al. Integrating single-cell analysis and machine learning to create glycosylation-based gene signature for prognostic prediction of uveal melanoma. *Front Endocrinol (Lausanne)*. (2023) 14:1163046. doi: 10.3389/fendo.2023.1145797

31. Chi H, Jiang P, Xu K, Zhao Y, Song B, Peng G, et al. A novel anoikis-related gene signature predicts prognosis in patients with head and neck squamous cell carcinoma and reveals immune infiltration. *Front Genet*. (2022) 13:984273. doi: 10.3389/fgene.2022.984273

32. Hanzelmann S, Castelo R, Guinney J. GSVA: gene set variation analysis for microarray and RNA-seq data. *BMC Bioinformatics*. (2013) 14:7. doi: 10.1186/1471-2105-14-7

33. Chi H, Xie X, Yan Y, Peng G, Strohmer DF, Lai G, et al. Natural killer cell-related prognosis signature characterizes immune landscape and predicts prognosis of HNSCC. *Front Immunol*. (2022) 13:1018685. doi: 10.3389/fimmu.2022.1018685

34. Ritchie ME, Phipson B, Wu D, Hu Y, Law CW, Shi W, et al. Limma powers differential expression analyses for RNA-sequencing and microarray studies. *Nucleic Acids Res*. (2015) 43:e47. doi: 10.1093/nar/gkv007

35. Wang X, Zhao Y, Strohmer DF, Yang W, Xia Z, Yu C. The prognostic value of MicroRNAs associated with fatty acid metabolism in head and neck squamous cell carcinoma. *Front Genet*. (2022) 13:983672. doi: 10.3389/fgene.2022.1076156

36. Zhao S, Chi H, Yang Q, Chen S, Wu C, Lai G, et al. Identification and validation of neurotrophic factor-related gene signatures in glioblastoma and Parkinson's disease. *Front Immunol*. (2023) 14:1090040. doi: 10.3389/fimmu.2023.1090040

37. Yu G, Wang LG, Han Y, He QY. clusterProfiler: an R package for comparing biological themes among gene clusters. *OMICS*. (2012) 16:284–7. doi: 10.1089/omi.2011.0118

38. Chi H, Zhao S, Yang J, Gao X, Peng G, Zhang J, et al. T-cell exhaustion signatures characterize the immune landscape and predict HCC prognosis via integrating single-cell RNA-seq and bulk RNA-sequencing. *Front Immunol*. (2023) 14:1137025. doi: 10.3389/fimmu.2023.1137025

39. Newman AM, Liu CL, Green MR, Gentles AJ, Feng W, Xu Y, et al. Robust enumeration of cell subsets from tissue expression profiles. *Nat Methods*. (2015) 12:453–7. doi: 10.1038/nmeth.3337

40. Li H, Pei F, Taylor DL, Bahar I. QuartataWeb: integrated chemical-protein-pathway mapping for polypharmacology and chemogenomics. *Bioinformatics*. (2020) 36:3935–7. doi: 10.1093/bioinformatics/btaa210

41. Chi H, Yang J, Peng G, Zhang J, Song G, Xie X, et al. Circadian rhythm-related genes index: a predictor for HNSCC prognosis, immunotherapy efficacy, and chemosensitivity. *Front Immunol*. (2023) 14:1091218. doi: 10.3389/fimmu.2023.1091218

42. Vickers AJ, Cronin AM, Elkin EB, Gonen M. Extensions to decision curve analysis, a novel method for evaluating diagnostic tests, prediction models and molecular markers. *BMC Med Inform Decis Mak*. (2008) 8:53. doi: 10.1186/1472-6947-8-53

43. Ono M, Fujita K, Kobayashi K, Masaki T. Influence of diabetes mellitus and effectiveness of metformin on hepatocellular carcinoma. *Hepatol Res*. (2023) 53:579–594. doi: 10.1111/hepr.13912

44. Li W, Lu J, Ma Z, Zhao J, Liu J. An integrated model based on a six-gene signature predicts overall survival in patients with hepatocellular carcinoma. *Front Genet*. (2019) 10:1323. doi: 10.3389/fgene.2019.01323

45. Huang J, Kang W, Pan S, Yu C, Jie Z, Chen C. NOL12 as an oncogenic biomarker promotes hepatocellular carcinoma growth and metastasis. *Oxidative Med Cell Longev*. (2022) 2022:6891155. doi: 10.1155/2022/6891155

46. Wu ZH, Li C, Zhang YJ, Lin R. Bioinformatics study revealed significance of exosome transcriptome in hepatocellular carcinoma diagnosis. *Front Cell Dev Biol*. (2022) 10:813701. doi: 10.3389/fcell.2022.1068887

47. Chaffer CL, San Juan BP, Lim E, Weinberg RA. EMT, cell plasticity and metastasis. *Cancer Metastasis Rev*. (2016) 35:645–54. doi: 10.1007/s10555-016-9648-7

48. Zhang Z, Zhu Z, Fu J, Liu X, Mi Z, Tao H, et al. Anoikis patterns exhibit distinct prognostic and immune landscapes in Osteosarcoma. *Int Immunopharmacol*. (2023) 115:109684. doi: 10.1016/j.intimp.2023.109684

49. Zhao Y, Wei K, Chi H, Xia Z, Li X. IL-7: a promising adjuvant ensuring effective T cell responses and memory in combination with cancer vaccines? *Front Immunol*. (2022) 13:1022808. doi: 10.3389/fimmu.2022.1022808

50. Xiao J, Huang K, Lin H, Xia Z, Zhang J, Li D, et al. Mogroside II(E) inhibits digestive enzymes via suppression of interleukin 9/interleukin 9 receptor signalling in acute pancreatitis. *Front Pharmacol*. (2020) 11:859. doi: 10.3389/fphar.2020.00859

51. Gong X, Chi H, Strohmer DF, Teichmann AT, Xia Z, Wang Q. Exosomes: a potential tool for immunotherapy of ovarian cancer. *Front Immunol*. (2022) 13:1089410. doi: 10.3389/fimmu.2022.1089410

52. Jin W, Yang Q, Chi H, Wei K, Zhang P, Zhao G, et al. Ensemble deep learning enhanced with self-attention for predicting immunotherapeutic responses to cancers. *Front Immunol*. (2022) 13:1025330. doi: 10.3389/fimmu.2022.1025330

53. Arechederra M, Bazai SK, Abdouni A, Sequera C, Mead TJ, Richelme S, et al. ADAMTSL5 is an epigenetically activated gene underlying tumorigenesis and drug resistance in hepatocellular carcinoma. *J Hepatol*. (2021) 74:893–906. doi: 10.1016/j.jhep.2020.11.008

54. Haraguchi N, Ohara N, Koseki J, Takahashi H, Nishimura J, Hata T, et al. High expression of ADAMTS5 is a potent marker for lymphatic invasion and lymph node metastasis in colorectal cancer. *Mol Clin Oncol*. (2017) 6:130–4. doi: 10.3892/mco.2016.1088

55. Katoh M, Katoh M. Comparative genomics on Fzd7 orthologs. *Int J Mol Med*. (2005) 15:1051–5. doi: 10.3892/ijmm.15.6.1051

56. Nambotin SB, Tomimaru Y, Merle P, Wands JR, Kim M. Functional consequences of WNT3/Frizzled7-mediated signaling in non-transformed hepatic cells. *Oncogenesis*. (2012) 1:e31. doi: 10.1038/oncsis.2012.31

57. Kim M, Lee HC, Tsedensodnom O, Hartley R, Lim YS, Yu E, et al. Functional interaction between Wnt3 and Frizzled-7 leads to activation of the Wnt/beta-catenin signaling pathway in hepatocellular carcinoma cells. *J Hepatol*. (2008) 48:780–91. doi: 10.1016/j.jhep.2007.12.020

58. Nambotin SB, Lefrancois L, Sainsily X, Berthillon P, Kim M, Wands JR, et al. Pharmacological inhibition of Frizzled-7 displays anti-tumor properties in hepatocellular carcinoma. *J Hepatol*. (2011) 54:288–99. doi: 10.1016/j.jhep.2010.06.033

59. Ohno Y, Koizumi M, Nakayama H, Watanabe T, Hirooka M, Tokumoto Y, et al. Downregulation of ANP32B exerts anti-apoptotic effects in hepatocellular carcinoma. *PLoS One*. (2017) 12:e0177343. doi: 10.1371/journal.pone.0177343

60. Morais-Rodrigues F, Silv Erio-Machado R, Kato RB, Rodrigues DLN, Valdez-Baez J, Fonseca V, et al. Analysis of the microarray gene expression for breast cancer progression after the application modified logistic regression. *Gene*. (2020) 726:144168. doi: 10.1016/j.gene.2019.144168

61. Takeda Y, Kurota Y, Kato T, Ito H, Araki A, Nara H, et al. GPI-80 augments NF-kappaB activation in tumor cells. *Int J Mol Sci*. (2021) 22:12027. doi: 10.3390/ijms222112027

62. Kawamata H, Furihata T, Omotehara F, Sakai T, Horiuchi H, Shinagawa Y, et al. Identification of genes differentially expressed in a newly isolated human metastasizing esophageal cancer cell line, T.Tn-AT1, by cDNA microarray. *Cancer Sci*. (2003) 94:699–706. doi: 10.1111/j.1349-7006.2003.tb01505.x

63. Drizyte-Miller K, Chen J, Cao H, Schott MB, McNiven MA. The small GTPase Rab32 resides on lysosomes to regulate mTORC1 signaling. *J Cell Sci*. (2020) 133:11. doi: 10.1242/jcs.236661

64. Cheng L, Yang F, Zhou B, Yang H, Yuan Y, Li X, et al. RAB23, regulated by miR-92b, promotes the progression of esophageal squamous cell carcinoma. *Gene*. (2016) 595:31–8. doi: 10.1016/j.gene.2016.09.028

65. Berditchevski F. Complexes of tetraspanins with integrins: more than meets the eye. *J Cell Sci*. (2001) 114:4143–51. doi: 10.1242/jcs.114.23.4143

66. Wang YW, Zhao S, Yuan XY, Liu Y, Zhang K, Wang J, et al. miR-4732-5p promotes breast cancer progression by targeting TSPAN13. *J Cell Mol Med*. (2019) 23:2549–57. doi: 10.1111/jcmm.14145

67. Li P, Dong M, Wang Z. Downregulation of TSPAN13 by miR-369-3p inhibits cell proliferation in papillary thyroid cancer (PTC). *Bosn J Basic Med Sci*. (2019) 19:146–54. doi: 10.17305/bjbms.2018.2865

68. Tang X, Liu S, Cui Y, Zhao Y. MicroRNA-4732 is downregulated in non-small cell lung cancer and inhibits tumor cell proliferation, migration, and invasion. *Respir Med Res*. (2021) 80:100865. doi: 10.1016/j.resmer.2021.100865

69. Jaiswal RK, Kumar P, Kumar M, Yadava PK. hTERT promotes tumor progression by enhancing TSPAN13 expression in osteosarcoma cells. *Mol Carcinog*. (2018) 57:1038–54. doi: 10.1002/mc.22824

70. Li Z, Kwon SM, Li D, Li L, Peng X, Zhang J, et al. Human constitutive androstane receptor represses liver cancer development and hepatoma cell proliferation by inhibiting erythropoietin signaling. *J Biol Chem*. (2022) 298:101885. doi: 10.1016/j.jbc.2022.101885

71. Zuo Q, He J, Zhang S, Wang H, Jin G, Jin H, et al. PPARgamma coactivator-1alpha suppresses metastasis of hepatocellular carcinoma by inhibiting warburg effect by PPARgamma-dependent WNT/beta-catenin/pyruvate dehydrogenase kinase isozyme 1 axis. *Hepatology*. (2021) 73:644–60. doi: 10.1002/hep.31280

72. Rasmuson T, Bjork GR. Urinary excretion of pseudouridine and prognosis of patients with malignant lymphoma. *Acta Oncol*. (1995) 34:61–7.

73. Martinez NM, Su A, Burns MC, Nussbacher JK, Schaening C, Sathe S, et al. Pseudouridine synthases modify human pre-mRNA co-transcriptionally and affect pre-mRNA processing. *Mol Cell*. (2022) 82:e649. doi: 10.1016/j.molcel.2021.12.023

74. Wang J, Yuan Y, Tang L, Zhai H, Zhang D, Duan L, et al. Long non-coding RNA-TMPO-AS1 as ceRNA binding to let-7c-5p upregulates STRIP2 expression and predicts poor prognosis in lung adenocarcinoma. *Front Oncol*. (2022) 12:921200. doi: 10.3389/fonc.2022.1109637

75. Chen X, Jiang X, Wang H, Wang C, Wang C, Pan C, et al. DNA methylation-regulated SNX20 overexpression correlates with poor prognosis, immune cell infiltration, and low-grade glioma progression. *Aging*. (2022) 14:5211–22. doi: 10.18632/aging.204144

frontiers | Frontiers in Medicine

TYPE Systematic Review
PUBLISHED 31 July 2023
DOI 10.3389/fmed.2023.1198950

OPEN ACCESS

EDITED BY
Zheng Wang,
Shanghai Jiao Tong University, China

REVIEWED BY
Renhong Huang,
Shanghai Jiao Tong University, China
Ming Yi,
Zhejiang University, China

*CORRESPONDENCE
Jianqing Zheng
✉ 18060108268@189.cn
Xiaohui Chen
✉ josephcxh@fjmu.edu.cn

†These authors have contributed equally to this work and share first authorship

RECEIVED 02 April 2023
ACCEPTED 10 July 2023
PUBLISHED 31 July 2023

CITATION
Zheng J, Deng Y, Huang B and Chen X (2023) Efficacy and safety of immune checkpoint inhibitors combined with chemotherapy as first-line treatment for extensive-stage small cell lung cancer: a meta-analysis based on mixed-effect models. *Front. Med.* 10:1198950. doi: 10.3389/fmed.2023.1198950

Efficacy and safety of immune checkpoint inhibitors combined with chemotherapy as first-line treatment for extensive-stage small cell lung cancer: a meta-analysis based on mixed-effect models

Jianqing Zheng[1*†], Yujie Deng[2†], Bifen Huang[3] and Xiaohui Chen[4,5,6*]

[1]Department of Radiation Oncology, The Second Affiliated Hospital of Fujian Medical University, Quanzhou, Fujian, China, [2]Department of Medical Oncology, The First Affiliated Hospital of Fujian Medical University, Fuzhou, Fujian, China, [3]Department of Obstetrics and Gynecology, Quanzhou Medical College People's Hospital Affiliated, Quanzhou, Fujian, China, [4]Department of Thoracic Surgery, Fujian Cancer Hospital, Clinical Oncology School of Fujian Medical University, Fuzhou, Fujian, China, [5]The Graduate School of Fujian Medical University, Fuzhou, China, [6]Fujian Key Laboratory of Advanced Technology for Cancer Screening and Early Diagnosis, Fuzhou, China

Background: Extensive-stage small cell lung cancer (ES-SCLC) is a highly invasive and fatal disease with limited therapeutic options and poor prognosis. Our study aims to systematically evaluate the efficacy and safety of immune checkpoint inhibitors combined with chemotherapy (ICIs+ChT) vs. chemotherapy alone (ChT) in the first-line treatment of ES-SCLC.

Methods: A literature search was performed for randomized controlled trials (RCTs) related to "ICIs+ChT" vs. "ChT" in the first-line treatment of ES-SCLC in PubMed, Cochrane Library, Embase, CNKI, and other databases. RevMan 5.4 software was used to perform meta-analyses with hazard ratio (HR) and relative risk (RR). SAS 9.4 software was applied to conduct a mixed-effect model meta-analysis of the survival outcomes and draw survival curves.

Results: A total of 2,638 patients with ES-SCLC from 6 RCTs were included, of which 1,341 patients received "ICIs+ChT" and 1,297 received ChT. Based on the meta-analysis results provided by the mixed-effect model, patients receiving the "ICIs+ChT" regimen had a significantly longer overall survival (OS, HR = 0.800, 95% CI = 0.731–0.876, $P < 0.001$) and progression-free survival (PFS, HR = 0.815, 95% CI = 0.757–0.878, $P < 0.001$) in comparison to those receiving ChT only. Compared with ChT, "ICIs+ChT" did neither improve the objective response rate (ORR, RR = 1.06, 95% CI = 1.00–1.12, $P = 0.06$) nor did it improve the disease control rate (DCR, RR = 0.97, 95% CI = 0.92–1.03, $P = 0.35$). Although the incidence of grade 3 to 5 treatment-related adverse events (trAEs) in the "ICIs+ChT" subgroup did not increase (RR = 1.16, 95% CI = 0.97–1.39, $P = 0.11$), the incidence of grade 3 to 5 immune-related adverse events (irAEs) increased significantly (RR = 4.29, 95% CI = 1.73–10.61, $P < 0.00001$).

Conclusion: ICIs+ChT regimen could significantly prolong OS and PFS in patients with ES-SCLC compared with ChT alone. Although the incidence of irAEs in "ICIs+ChT" is higher than that in the "ChT" subgroup, the incidence of

trAEs is similar within the two subgroups. ICIs combined with chemotherapy demonstrated a good choice as first-line treatment for ES-SCLC.

Systematic review registration: PROSPERO, identifier: CRD42022348496.

KEYWORDS

extensive-stage small cell lung cancer, immune checkpoint inhibitors, chemotherapy, programmed death-ligand 1, first-line treatment

1. Introduction

Small cell lung cancer (SCLC) is a neuroendocrine tumor (NET) originating from argyrophilic cells of bronchial mucosal epithelium or glandular epithelium, which is a highly malignant form and accounts for approximately 15–20% of all lung cancers (1). SCLC has completely different molecular markers and biological behaviors from non-small cell lung cancer (NSCLC) (2). Clinically, SCLC is subdivided into extensive-stage (ES-SCLC) and limited-stage (LS-SCLC) diseases, accounting for 60–70% and 30–40% of diagnosed SCLC, respectively (1). The cisplatin-based doublet chemotherapy (ChT), i.e., etoposide/irinotecan plus cisplatin/carboplatin (EP/IP regimen), has been used as standard initial (first-line) treatment of ES-SCLC for decades, with an objective response rate (ORR) of <60% (3). Although SCLC has a unique sensitivity to chemoradiotherapy, the 5-year overall survival (OS) rate is still <5% in ES-SCLC patients receiving standard first-line treatment (4). ES-SCLC patients suffering from recurrence or progression during or shortly after initial treatment are usually embarrassed with limited therapeutic options and poor prognosis (5). With the continuous in-depth study of immune checkpoint inhibitors (ICIs) and immunotherapy, a couple of randomized phase III trials demonstrated that a combination of atezolizumab (IMpower133) (6) or durvalumab (CASPIAN) (7, 8) with EP could improve OS in ES-SCLC patients. Therefore, the combined regimen had been approved as the first-line treatment for ES-SCLC patients, establishing a milestone in the management of SCLC (9). However, not all ICIs exhibited better anti-tumor activity in the first-line treatment of ES-SCLC. The CA184-156 study confirmed that adding ipilimumab to EP would not improve the OS of ES-SCLC patients (10). Nivolumab and pembrolizumab were first approved by the FDA as third-line treatments for ES-SCLC, but recent studies had indicated that the combination of EP with either nivolumab or pembrolizumab as the first-line treatment can significantly improve the OS and PFS of ES-SCLC.

In this study, we conducted a systematic review of the randomized controlled trials published recently to evaluate the "ICIs+ChT" regimen as the first-line treatment of ES-SCLC, aiming to evaluate the abovementioned evidence objectively based on the principles and methods of evidence-based medicine (EBM) and the GRADE criteria developed by the Grading of Recommendations Assessment, Development and Evaluation Working Group. The future development direction of this field was also discussed, with a view to providing evidence that is more in line with the requirements of EBM for the first-line treatment of ICIs for ES-SCLC.

2. Materials and methods

2.1. Study protocol

The current study was conducted according to the Preferred Reporting Items for Systematic Reviews and Meta-analyses (PRISMA) (11), and the quality control and quality assurance (QC and QA) of the manuscript were instructed by the corresponding authors (Jianqing Zheng and Xiaohui Chen). The review was prospectively registered on PROSPERO (CRD42022348496).

2.2. Literature inclusion criteria

2.2.1. Study design

Randomized controlled trials (RCTs) of "ICIs+ChT" vs. "ChT" in the first-line treatment of ES-SCLC were recruited, regardless of whether the blind method is used, and the language is not limited.

2.2.2. Study participants

The study participants are those (1) who had SCLC diagnosed and confirmed by pathology; (2) who were diagnosed as extensive stage according to SCLC staging criteria proposed by the Veterans Administration Lung Study Group (VALG), and some recurrent SCLC are not restricted; and (3) patients who have not received any other first-line treatments in the past, including chemotherapy and targeted therapy.

2.2.3. Interventions

Interventions include (1) conventional chemotherapy in the control group. However, the chemotherapy regimen and chemotherapy cycle were not limited; and (2) ICIs alone or in combination with chemotherapy in the experimental group, and other clinical treatments were the same as those in the control group.

2.2.4. Outcomes

(1) The primary outcomes are OS and PFS. To achieve a meta-analysis based on the linear mixed-effect models, the survival proportions of OS and PFS were also extracted from the survival curves. (2) The secondary outcomes were ORR

and DCR. (3) The incidence of grade 3 to 5 adverse events: According to 1988 WHO anti-cancer drug side effects standard or common adverse event evaluation standard CTCEA version 4.0, adverse events were further subdivided into treatment-related adverse events (trAEs) and immune-related adverse events (irAEs).

2.3. Literature exclusion criteria

The exclusion criteria included (1) studies involving non-clinical trials or non-RCTs; (2) research with incomplete data or the relevant data could not be extracted; (3) repeated publications or serial publications with the latest literature; (4) studies involving patients that received any other first-line treatments in the past, such as chemotherapy combined with irradiation and molecular targeted therapy.

2.4. Search strategies

2.4.1. Database

A comprehensive literature search on the PubMed, Cochrane Library databases Embase, and CNKI was performed, covering all publications in these databases up to 1 February 2021.

2.4.2. Search terms

(1) Search terms related to disease were Small Cell Lung Cancer, Small Cell Cancer of The Lung, Oat Cell Lung Cancer, Small Cell Lung Tumor, Small Cell Lung Neoplasm, Carcinoma, Small Cell Lung, etc. (2) Search terms related to drugs or immunotherapy were Ipilimumab, Pembrolizumab, Nivolumab, Atezolizumab, Durvalumab, and other ICIs. The trade name of the drug includes Yervoy, Keytruda, Opdivo, Tecentriq, Imfinzi, etc. (3) Other search terms included anti-CTLA-4 mAb, anti-PD-L1, anti-PD-1, PD-1 Receptor, Programmed Cell Death 1 Protein, PD-1, PD-L1, etc.

2.4.3. Retrieval strategies

Combined with the RCTs filter of the database, the subject terms with free words were applied to conduct a preliminary retrieval of the literature and the reviews, case reports, meta-analysis, and other types of literature were filtered out. Independent searches were conducted by two investigators (first co-authors) in accordance with the abovementioned search principles. When there was a disagreement, the third investigator (corresponding author) will be consulted. Further manual and electronic database searches were carried out using the reference lists attached to the eligible articles. At the same time, search engines, such as Google Scholar, were used to find relevant literature on the Internet and to trace the references that had been included in the literature, in order to expand the scope of retrieval.

2.5. Literature extraction and quality assessment

2.5.1. Literature extraction

Two independent researchers reviewed and evaluated the title and abstract of each RCT according to the determined search strategies, and the potentially eligible articles that meet the selection criteria would be recruited. After discussion in accordance with the inclusion criteria, literature extraction was performed, a consensus was reached, and a decision was made to finally include or exclude the eligible articles. If a consensus could not be met, the corresponding author of this article was responsible for the final ruling.

2.5.2. Quality assessment

Two independent researchers evaluated the included RCTs according to the bias risk assessment method recommended by the Cochrane Assistance Network. The evaluation methodological criteria and items were as follows: (1) generation of random allocation sequence; (2) the method of allocation concealment; (3) the method of blinding the patients; (4) the method of blinding the doctors or the therapists; (5) the method of blinding the data collectors and analysis personnel; (6) incomplete data reported; (7) selective reporting bias; and (8) other potential bias affecting authenticity.

We evaluated the risk of bias for each RCT according to the following criteria: “Yes” indicates a low risk of bias; “No” indicates a high risk of bias; and “Unclear” indicates that the literature does not provide sufficient information for bias assessment. The two researchers discussed according to the abovementioned standards and methods and reached a consensus according to the opinions of the third researcher.

2.5.3. Assessment of the grade of recommendation and the level of evidence

Overall quality and level of recommendation of evidence were evaluated based on the results of the systematic review. The GRADE system was used to evaluate the quality of evidence (12). Quality of evidence is graded as follows: (1) high quality: further research is unlikely to change our confidence in the estimate of effect; (2) moderate quality: further research is likely to have an important impact on our confidence in the estimate of effect and may change the estimate; (3) low quality: further research is very likely to have an important impact on our confidence in the estimate of effect and is likely to change the estimate; (4) very low quality: we have very little confidence in the effect estimate: the true effect is likely to be substantially different from the estimate of effect. Although the evidence based on RCT was initially rated as high quality, our confidence in this type of evidence may be reduced due to the following five factors: (1) limitations of the research; (2) inconsistent results; (3) indirect evidence; (4) inaccurate results; and (5) biased results. Finally, the GRADEpro software was used to edit, analyze, and map the evidence grade.

2.6. Data extraction

After reading the full text, two researchers extracted and cross-checked the data, including (1) basic information, such as the title of the trial, author's name, year of publication, and source of literature; (2) methodological information about the trial: the sample size of the study included the basic information of the study population, including the entry time, the number of participants, disease stages, the randomization method of the trial, the evaluation method of important outcome indicators, median follow-up duration, death, and withdrawal; (3) detailed information on following intervention measures: ICI medication and medication in the control group; (4) outcome indicators: survival proportions information in the survival curve, HR for OS and PFS with corresponding 95% CIs, ORR and DCR information, and the incidence of related adverse events. Disagreements were resolved by consensus.

2.7. Statistical analysis

For time-survival variables (such as OS and PFS), HR and its corresponding 95% CIs were applied as the effect size. If HR and its 95% CI could not be obtained from the trials directly, they were extracted according to the method introduced by Parmar et al. (13). For binary variables (such as ORR, DCR, and AEs), the relative ratio (RR) and its 95% CI were used as the effect size. RevMan 5.4 software was used to conduct quantitative and comprehensive analyses. The chi-square test (χ^2 test) was applied to determine whether there was heterogeneity within studies, and the index I^2 (range, 0–100%) was selected to measure the degree of heterogeneity within studies. The index $I^2 \geq 50\%$ or *P*-value of χ^2 test <0.1 indicated significant heterogeneity within studies. If there was no statistical heterogeneity, the fixed effects model would be used; if not, the random effects model was used to perform the meta-analysis. If the source of heterogeneity cannot be judged or the data provided by the trials cannot be used for meta-analysis, descriptive analysis would be used.

For survival variables, an additional method based on the mixed-effect model, which was described by Arends et al. (14), was applied to perform a meta-analysis on the survival rate in the survival curves, and some interesting summary survival curves were drawn in this study. Statistical analysis was performed using SAS 9.4 software.

The quality evaluation based on the GRADE system was graded and mapped via GRADE pro 3.6 software. Two independent reviewers rated the evidence based on the quality of the evidence and the subject of the study. If there was a dispute, a third reviewer would be asked to meet a consensus by means of panel discussion.

3. Results

3.1. Literature search results

In total, 459 related literature were initially detected, among which 93 were identified as duplicates and then removed. From the remaining 366, 329 articles were found to be published repeatedly and obviously did not meet our inclusion criteria. After intensively reviewing the titles and abstracts, we identified 37 controlled clinical studies. After further searching and reviewing the full text, we eventually enrolled six RCTs after excluding clinical trials that were inconsistent with our inclusion and exclusion criteria. Those six RCTs were as follows: NCT00527735 (15), NCT01450761 (CA184-156) (10), NCT02763579 (IMpower133) (6), NCT03043872 (CASPIAN) (7, 8), NCT03066778 (KEYNOTE-604) (16), and NCT03382561 (ECOG-ACRIN EA5161) (17). A total of seven articles reported the above six clinical trials, of which ECOG-ACRIN EA5161 was reported at ASCO in 2020. The literature screening process is shown in Figure 1.

3.2. General information of the included studies

A total of 2,638 SCLC patients were included, of which 1,297 patients received chemotherapy alone and 1,341 received "ICIs+ChT" (immunotherapy group). Two studies involved ipilimumab (10, 15), and other studies involved atezolizumab, durvalumab, pembrolizumab, and nivolumab. Six studies were conducted with "ICIs+ChT" vs. "ChT" alone, of which one was a three-arm trial (15) and two were phase II RCTs (15, 17). The basic characteristics of included studies are shown in Table 1.

3.3. Risk of bias assessment of included studies

According to the Cochrane Collaboration tool for assessing the risk of bias of RCTs, five of the six studies had explicitly mentioned the random allocation method, while one study did not specify it (15). All the studies did not mention the detailed method of allocation concealment. Outcome-rater blinding was applied and described in detail in three studies (6, 10, 16), was unspecified in two studies (15, 17), and was not applied in one study (7). One study lacked information on DCR and was considered incomplete outcome data (17). All studies were judged free from selection reporting bias and were judged free from other biases. The risk of bias for each study is shown in Figure 2A, and the risk of bias for the overall study is shown in Figure 2B, with yellow for low risk of bias, green for unclear risk of bias, and blue for high risk of bias. Therefore, the six studies included in this article were all of high quality.

3.4. Classification of quality of evidence and strength of recommendation sistema grade

There were six primary outcomes in this study, namely OS, PFS, ORR, DCR, and the incidence of trAEs and irAEs as well. OS, PFS, and the incidence of irAEs were set as "key outcomes" and others as "important outcomes". The classification of the quality of evidence and the strength of recommendation *via* the GRADE system are shown in Figure 3 with detailed reasons for upgrading or downgrading the quality of evidence for each outcome.

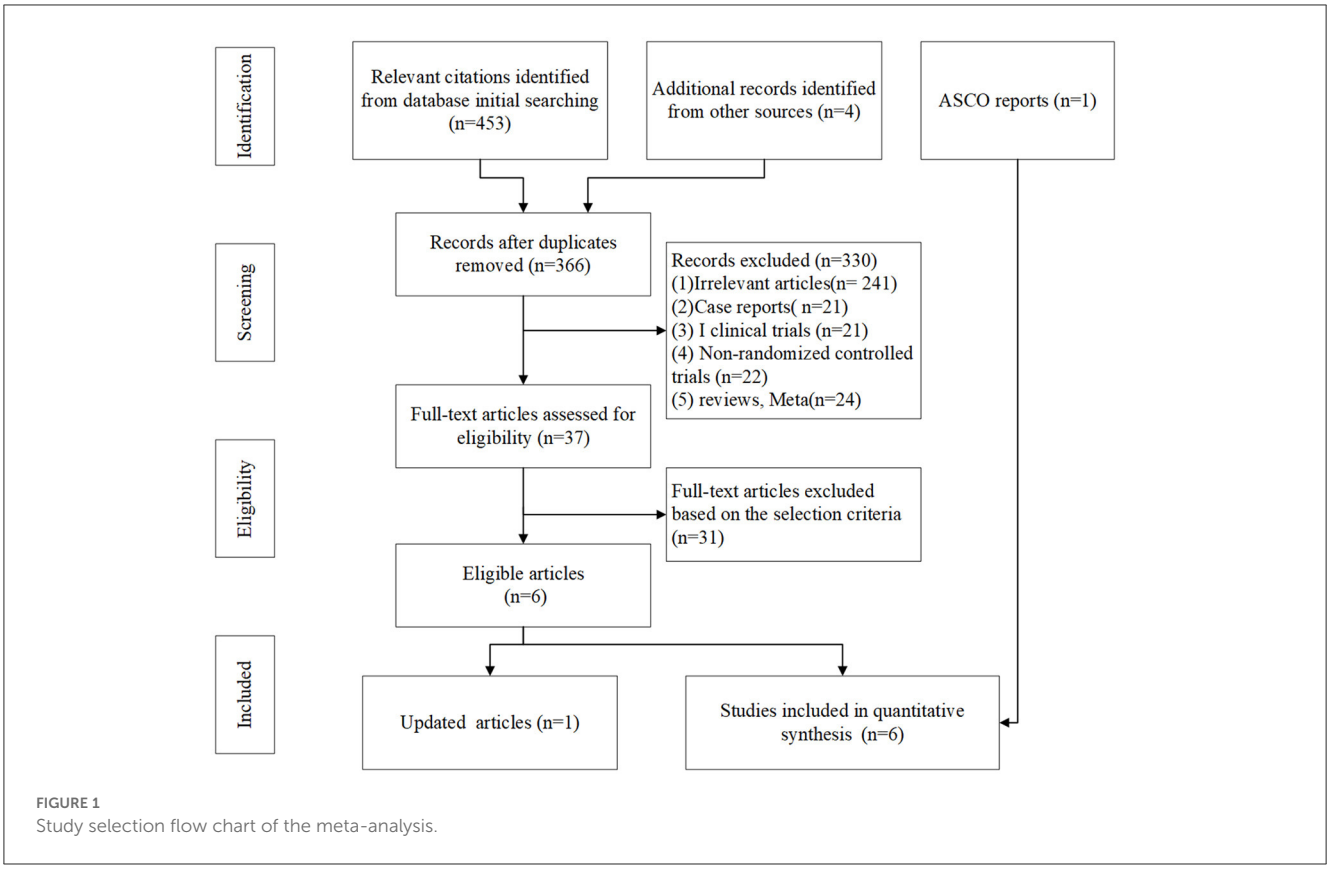

FIGURE 1
Study selection flow chart of the meta-analysis.

TABLE 1 Characteristics of the analyzed trials.

References	Trial name	Phase	Treatment	Sample	Gender/male	Median age	ECOG score/0
Reck et al. (15)	NCT00527735	II	C/IC/IC	45/43/43	33/33/32	58/57/59	12/8/11
Reck et al. (10)	CA184-156	III	C/IC	476/478	326/317	63/62	147/137
Horn et al. (6)	Impower133	III	C/AC	202/201	132/129	64/64	67/73
Paz-Ares et al. (8); Goldman et al. (7)	CASPIAN	III	C/DC	269/268	184/190	63/62	90/99
Rudin et al. (16)	KEYNOTE-604	III	C/PC	225/228	142/152	65/64	56/60
Leal et al. (17)	ECOG-ACRIN EA5161	II	C/NC	80/80	44/45	65/65	24/23

C, chemotherapy; I, ipilimumab; A, atezolizumab; D, durvalumab; N, nivolumab; P, pembrolizumab.

3.5. Meta-analysis of overall survival

Survival curves had been provided in all studies, and the survival proportions at each time point were successfully extracted in all included studies. The detailed distribution of OS proportions is shown in Figure 4A. Reconstructed survival curves based on the extracted survival proportions are shown in Figure 4B and are paneled by different treatments (trts).

Figure 4C shows the meta-analysis results of OS based on the extracted survival proportions *via* the mixed-effect model. The statistical effect value of the difference in survival between the two groups was HR = 0.800, 95% CI = 0.731–0.876, and $P < 0.001$. The summary survival proportions at each time point are shown in Table 2. For the convenience of comparison, the meta-analysis results based on the traditional hazard ratio model are shown in Figure 5. Meta-analysis effect size of OS was HR = 0.82, 95% CI = 0.75–0.90, and $P < 0.00001$.

3.6. Meta-analysis of progression-free survival

The detailed distribution of PFS proportions is shown in Figure 6A. Reconstructed PFS curves based on the extracted survival proportions are shown in Figure 6B and are paneled by different treatments (trts).

Figure 6C shows the meta-analysis results of PFS based on the extracted survival proportions *via* the mixed-effect model. The statistical effect values of the difference in survival between the two

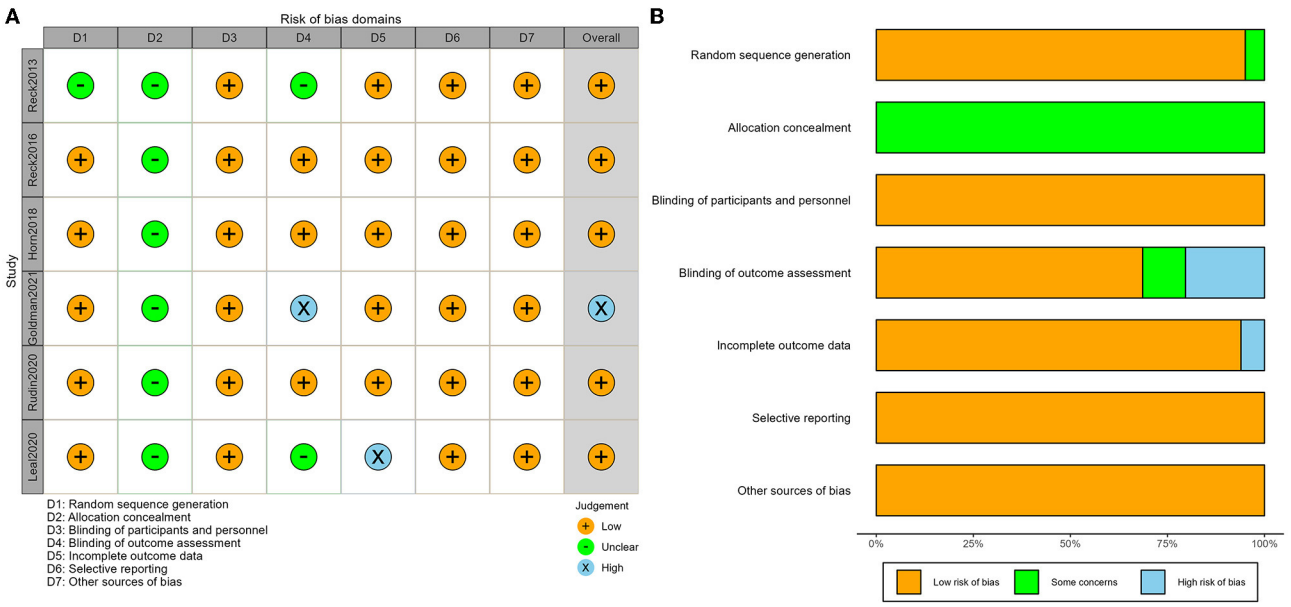

FIGURE 2
Risk of bias assessment of included studies: **(A)** graph of risk of bias and **(B)** summary of risk bias.

groups were HR = 0.815, 95% CI = 0.757–0.878, and $P<0.001$. The summary survival proportions at each time point are shown in Table 2. The meta-analysis results based on the traditional hazard ratio model are shown in Figure 7. The meta-analysis effect size of PFS was HR = 0.80, 95% CI = 0.74–0.87, and $P < 0.00001$.

3.7. Meta-analysis of ORR and DCR

Of the six included studies, five had reported the ORR of "ICIs + ChT" (6, 7, 10, 15, 16). The heterogeneity test showed that $I^2 = 43\%$ and $P = 0.12$, indicating that the included studies were of good homogeneity, and the fixed-effect model should be used. Meta-analysis effect size of ORR was RR = 1.06, 95% CI = 1.00–1.12, and $P = 0.06$, indicating a trend of ascending ORR in "ICIs + ChT" compared with that in the chemotherapy alone, but the difference failed to be statistically significant (Figure 8).

DCR data on "ICIs + ChT" for SCLC were available in five of the six included studies (6, 7, 10, 15, 16). The heterogeneity test showed that $I^2 = 62\%$ and $P = 0.03$, demonstrating that the results of each study were highly heterogeneous, and a random-effect model should be used. The meta-analysis effect size of DCR was RR = 0.97, 95% CI = 0.92–1.03, and $P = 0.35$, indicating that compared with chemotherapy alone, "ICIs + ChT" did not significantly increase the DCR (Figure 9).

3.8. Meta-analysis of adverse events

Of the six included studies, five had reported the incidence of trAEs (6, 7, 10, 15, and 16). The heterogeneity test indicated that $P = 0.0007$ and $I^2 = 79\%$, and the random-effect model should be used for combined analysis. The meta-analysis effect size of trAEs was RR = 1.16, 95% CI = 0.97–1.39, and $P = 0.11$, indicating that the incidence of trAEs of "ICIs + ChT" was similar to that in chemotherapy alone (Figure 10).

Of the six included studies, five had compared the incidence of irAEs with "ICIs+ChT" and "ChT". The heterogeneity test indicated that $P < 0.00001$ and $I^2 = 88\%$, and the random effects model should be used for combined analysis. The meta-analysis effect size of irAEs was RR = 4.29, 95% CI = 1.73–10.61, and $P = 0.002$, indicating that the incidence of irAEs in "ICIs+ChT" was significantly increased compared with that in chemotherapy alone (Figure 11).

From the perspective of trAEs, the three most common trAEs of "ICIs + ChT" were neutropenia (26.64%), an increase in serum glutamic-oxalacetic transaminase (AST, 11.86%), and anemia (11.20%); however, compared with "ChT", the incidence of these trAEs did not significantly increase (Figure 12A). From the perspective of irAEs, the three most common irAEs were arthralgia (11.86%), an increase in alanine aminotransferase (10.73%), and an increase in aspartate aminotransferase (9.60%). Although the incidence of single immune-related adverse events was not statistically significant, the combined incidence of irAEs showed significant differences (Figure 12B).

3.9. Analysis for bias and heterogenicity

The publication bias funnel plots for OS and PFS are shown in Figures 13A, B. Begg's test suggests that the funnel plots for OS (z = 0.75, $P = 0.452$) and PFS (z = 1.13, $P = 0.260$) were basically symmetric, indicating no publication bias (Figures 13C, D). Radial plots were used to evaluate

Quality assessment							No of patients		Effect		Quality	Importance
No of studies	Design	Risk of bias	Inconsistency	Indirectness	Imprecision	Other considerations	PD-1 / PD-L1 inhibitor combined with chemotherapy	Chemotherapy alone	Relative (95% CI)	Absolute		
Overall survival for SCLC (follow-up 1-32 months; assessed with: Survival analysis)												
6	randomised trials	no serious risk of bias[1]	no serious inconsistency	no serious indirectness	no serious imprecision	strong association[2]	1341/1341 (100%)	1297/1297 (100%)	HR 0.800 (0.731 to 0.876)	200 fewer per 1000 (from 124 fewer to 269 fewer)	⊕⊕⊕⊕ HIGH	CRITICAL
								0%		-		
Progression-free survival for SCLC (follow-up 1-29 months; assessed with: Survival analysis)												
6	randomised trials	serious[1]	no serious inconsistency	no serious indirectness	no serious imprecision	strong association[2]	1341/1341 (100%)	1297/1297 (100%)	HR 0.815 (0.757 to 0.878)	185 fewer per 1000 (from 122 fewer to 243 fewer)	⊕⊕⊕⊕ HIGH	CRITICAL
								0%		-		
Objective Response Rate (assessed with: RECIST 1.1)												
6	randomised trials	serious[3]	serious[4]	no serious indirectness	no serious imprecision	reduced effect for RR >> 1 or RR << 1[5]	840/1310 (64.1%)	779/1264 (61.6%)	RR 1.06 (1.00 to 1.12)	37 more per 1000 (from 0 more to 74 more)	⊕⊕⊕O MODERATE	IMPORTANT
								46.25%		28 more per 1000 (from 0 more to 56 more)		
								65.68%		39 more per 1000 (from 0 more to 79 more)		
Disease control rate (assessed with: RECIST 1.1)												
5	randomised trials	serious[1]	serious[5]	no serious indirectness	no serious imprecision	none	3677/4595 (80%)	2861/3613 (79.2%)	OR 1.03 (0.78 to 1.35)	5 more per 1000 (from 44 fewer to 45 more)	⊕⊕OO LOW	IMPORTANT
								44.89%		7 more per 1000 (from 60 fewer to 75 more)		
								93.33%		2 more per 1000 (from 17 fewer to 16 more)		
Adverse events (assessed with: Medical records)												
5	randomised trials	no serious risk of bias	no serious inconsistency	no serious indirectness	no serious imprecision	none	593/1255 (47.3%)	513/1208 (42.5%)	OR 1.16 (0.97 to 1.39)	37 more per 1000 (from 7 fewer to 82 more)	⊕⊕⊕⊕ HIGH	IMPORTANT
								11.34%		16 more per 1000 (from 3 fewer to 38 more)		
								75.22%		27 more per 1000 (from 6 fewer to 56 more)		
Immune-related adverse events (assessed with: Medical records)												
5	randomised trials	no serious risk of bias	no serious inconsistency	no serious indirectness	no serious imprecision	none	259/1253 (20.7%)	72/1208 (6%)	OR 4.29 (1.73 to 10.61)	154 more per 1000 (from 39 more to 342 more)	⊕⊕⊕⊕ HIGH	CRITICAL
								0.9%		28 more per 1000 (from 6 more to 79 more)		
								24.49%		337 more per 1000 (from 115 more to 530 more)		

[1] There may be bias in allocation concealment.
[2] Hazard ratio is large with a small standard error.
[3] There may be bias in blinding of outcome assessment.
[4] The ORR effect size of SCLC were different and may be changed if clinical trials are added in the future.
[5] If clinical trials are added in the future, the results of DCR may be changed.

FIGURE 3
GRADE evidence profile for main outcomes.

heterogenicity, and the results are shown in Figures 13E, F. For both OS and PFS, all studies fell within the confidence interval of the radial plot, and the slope of the scatter plot is small, indicating no significant heterogenicity between different studies.

4. Discussion

The popularity of immunotherapy continues to rise, and it has become very effective in the field of tumor treatment, gaining widespread attention in various malignant tumors such

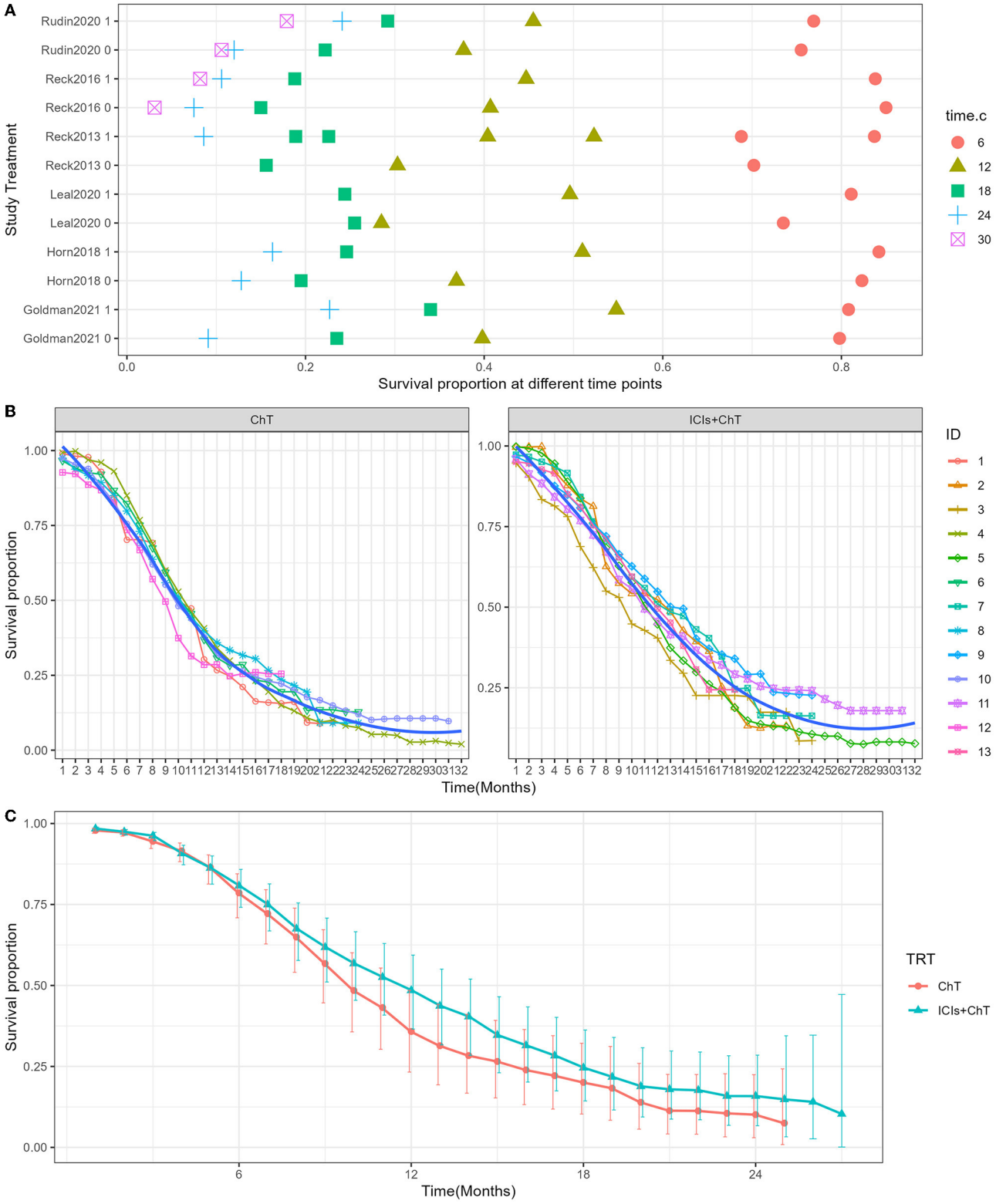

FIGURE 4
Meta-analysis results of overall survival for SCLC: **(A)** overall survival proportions distribution chart; **(B)** overall survival curves for SCLC paneled by different treatments (trts, ChT: chemotherapy, ICIs+ChT: immune checkpoint inhibitors+ chemotherapy); **(C)** grouped meta-analyzed overall survival curves with error bars.

TABLE 2 Grouped meta-analyzed survival proportions for SCLC (%).

Group	Time point (month)	OS (95% CI)	PFS (95% CI)
ChT	6	78.58% (95% CI = 70.89–84.47)	26.26% (95% CI = 15.57–38.24)
ICIs +ChT	6	80.75% (95% CI = 74.14–85.83)	35.95% (95% CI = 24.94–47.06)
ChT	12	35.8% (95% CI = 23.26–48.5)	4.82% (95% CI = 1.47–11.29)
ICIs +ChT	12	48.46% (95% CI = 36.55–59.38)	12.23% (95% CI = 5.77–21.25)
ChT	18	20.07% (95% CI = 10.29–32.17)	-
ICIs +ChT	18	24.57% (95% CI = 14.36–36.23)	-
ChT	24	10.12% (95% CI = 2.98–22.45)	-
ICIs +ChT	24	15.84% (95% CI = 6.7–28.48)	-

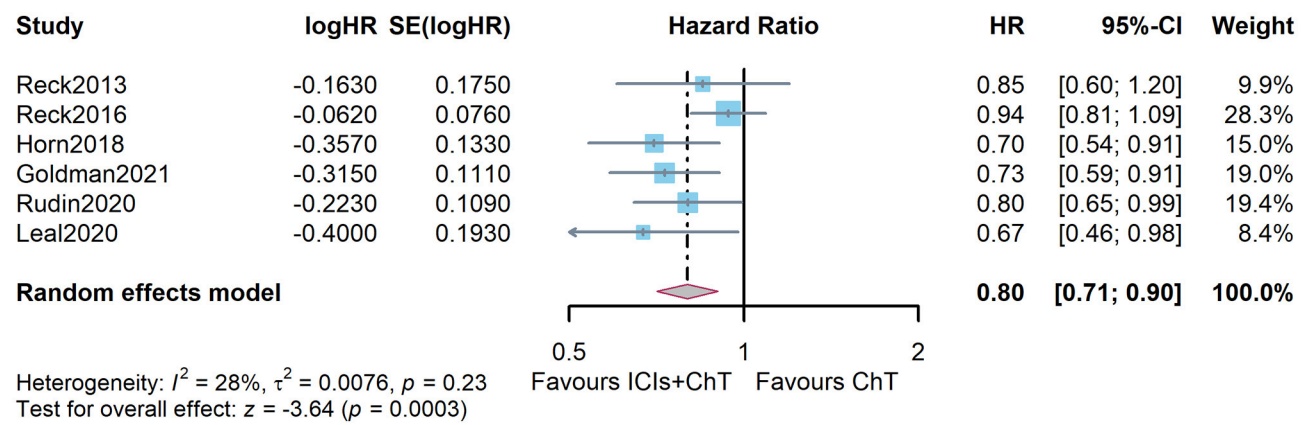

FIGURE 5
Comparison of overall survival (OS) between ICIs+ ChT and ChT based on the traditional hazard ratio model.

as melanoma, kidney cancer, lung cancer, and colorectal cancer. An exploratory study called CheckMate 026 showed that tumor mutational burden (TMB) was considered a predictive biomarker associated with the efficacy of ICIs (18). A previous genome-wide analysis of 110 SCLC specimens found that the SCLC genome was unstable and demonstrated a higher TMB (19–21). Theoretically, SCLC has higher tumor neoantigens on the surface and is more susceptible to immunotherapy. Therefore, many scholars have explored the efficacy of ICIs on SCLC in recent years (22).

Ipilimumab, a CTLA-4 inhibitor and the first immune-targeted drug used in SCLC, preliminarily showed good clinical activity in the treatment of patients with extensive-stage SCLC in the CA184-041 study (15). The CA184-041 study is a randomized, double-blind, multicenter phase II clinical trial exploring the efficacy of ipilimumab in combination with paclitaxel and carboplatin (CP) as first-line therapy in ES-SCLC (15). The results of CA184-041 showed that compared with CP alone, CP followed by ipilimumab had significantly improved immune-related PFS (irPFS; HR = 0.64, P = 0.03), but did not prolong PFS (6.4 months vs. 5.3 months, HR = 0.93, P = 0.37) and OS (12.9 vs. 9.9 months, HR = 0.75; P = 0.13) (15). Subsequently, based on the CA184-041 study, a number of clinical trials on the treatment of SCLC with ipilimumab were carried out. The CA184-156 (NCT10450761) study was the only phase III study to date to explore the efficacy of ipilimumab as first-line therapy in the treatment of ES-SCLC (10). However, this study found that adding ipilimumab to etoposide plus platinum was not beneficial in improving OS in patients with ES-SCLC (10).

Despite disappointing data from the trials of ipilimumab in ES-SCLC, three large trials targeting the PD-1/PD-L1 pathway were subsequently conducted to explore the role of PD-1/PD-L1 inhibitors in ES-SCLC patients, namely IMpower133 (6), CASPIAN (7, 8), and KEYNOTE-604 studies (16). Unlike the CTLA-4 inhibitors, PD-1/PD-L1 inhibitors seem to have better performance in ES-SCLC. IMpower133 study was the first phase III RCT exploring the efficacy of atezolizumab combined with standard chemotherapy in ES-SCLC globally and demonstrated that atezolizumab combined with chemotherapy can significantly prolong OS and PFS in ES-SCLC (6). Based on the excellent results of the IMpower133 study, atezolizumab combined with Etoposide + Cisplatin (EP) had been recommended as the standard first-line treatment for ES-SCLC (6). CASPIAN study is a phase III RCT of durvalumab combined with standard chemotherapy in the treatment of ES-SCLC, and it had proved that this regimen can also significantly prolong the OS and PFS of ES-SCLC, and ORR as well (7, 8). KEYNOTE-028 study demonstrated the anti-tumor activity of monotherapy with pembrolizumab, a PD-1 monoclonal antibody, in previously treated patients with ES-SCLC (23). A pooled analysis based on KEYNOTE-028 and KEYNOTE-158

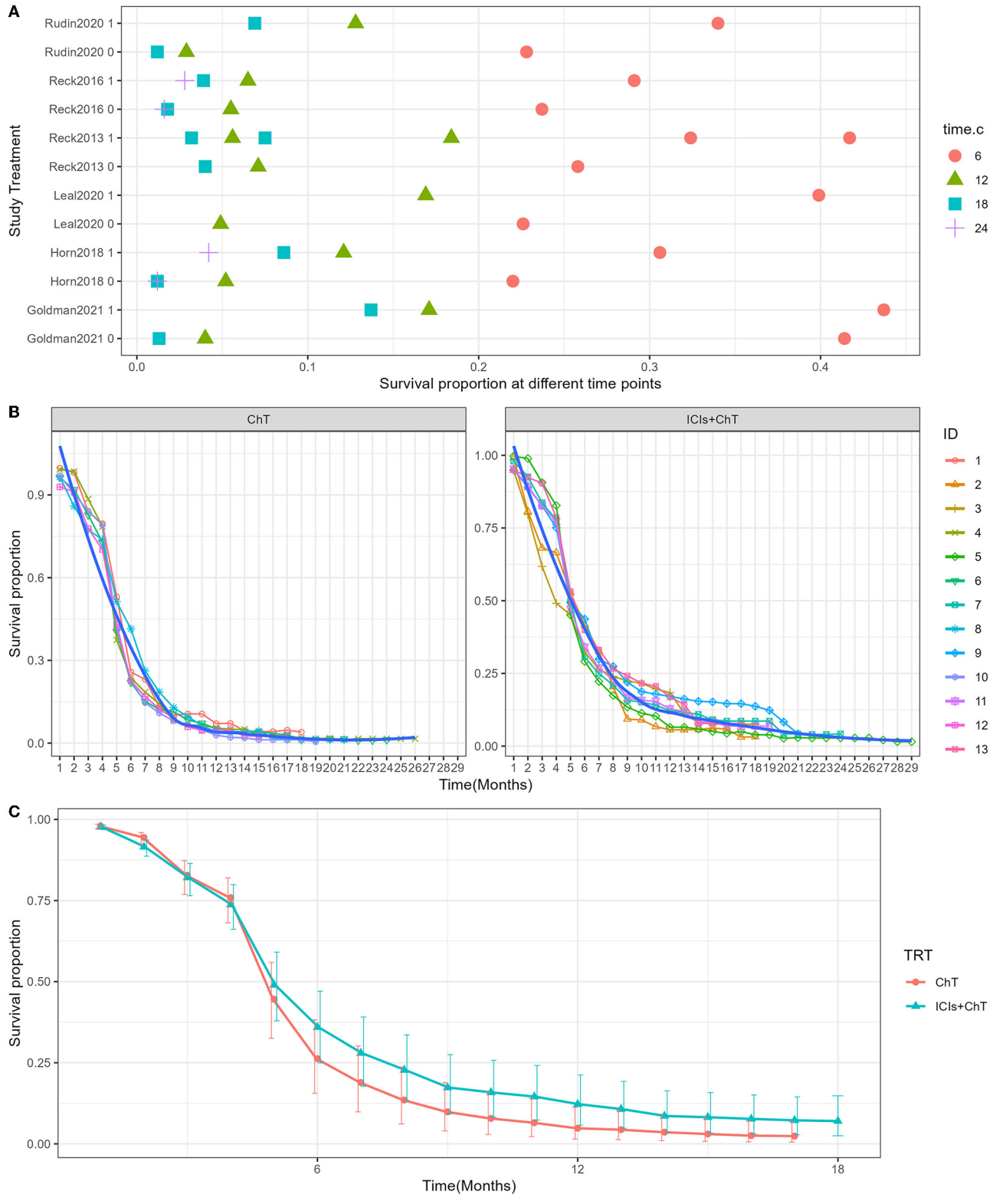

FIGURE 6
Meta-analysis results of progression-free survival for SCLC: **(A)** Progression-free survival proportions distribution chart; **(B)** Progression-free survival curves for SCLC paneled by different treatments (trts, ChT: chemotherapy, ICIs+ChT: immune checkpoint inhibitors+ chemotherapy); **(C)** grouped meta-analyzed progression-free survival curves with error bars.

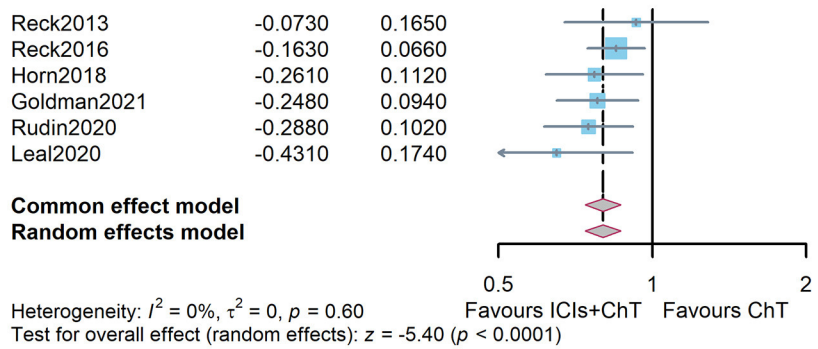

FIGURE 7
Comparison of progression-free survival (PFS) between ICIs+ChT and ChT in SCLC.

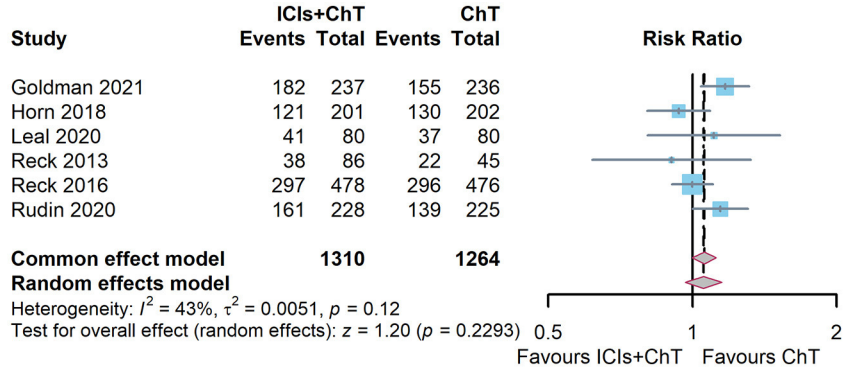

FIGURE 8
Comparison of objective response rate (ORR) between ICIs+ChT and ChT in SCLC.

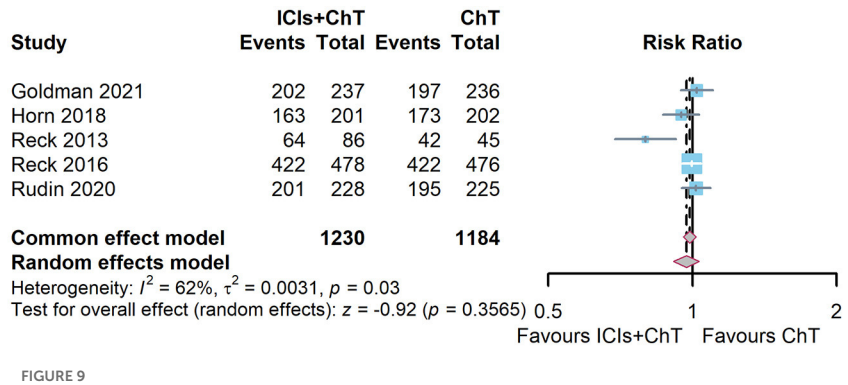

FIGURE 9
Comparison of disease control rate (DCR) between ICIs+ChT and ChT in SCLC.

studies showed that the ORR of pembrolizumab alone was 19.3% in patients with relapsed or metastatic SCLC who had received ≥2 lines of prior therapy; the incidence of grade 3–5 adverse events was 9.6%, and 67.7% of patients had sustained remission for ≥12 months (24). KEYNOTE-604 study (NCT03066778) further demonstrated that pembrolizumab combined with standard chemotherapy can significantly improve OS and PFS in the first-line treatment of ES-SCLC (16). ECOG-ACRIN EA5161 is a phase II randomized controlled clinical study comparing the efficacy of nivolumab combined with standard chemotherapy in the first-line treatment of ES-SCLC (17). Although the full report of this study has not yet been published, in view of the positive results of

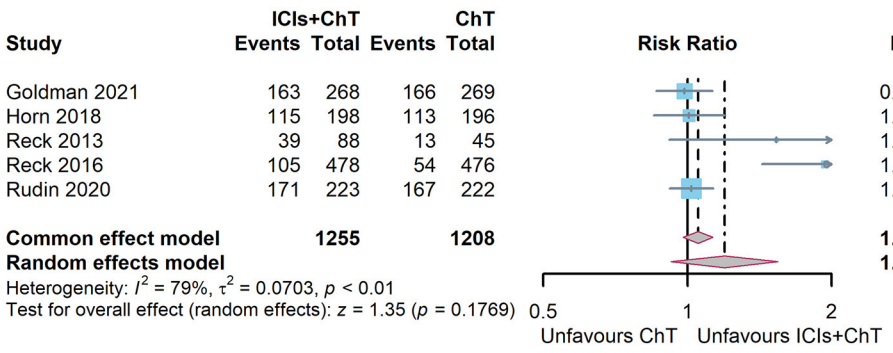

FIGURE 10
Comparison of grade 3–5 treatment-related adverse events between ICIs+ChT and ChT.

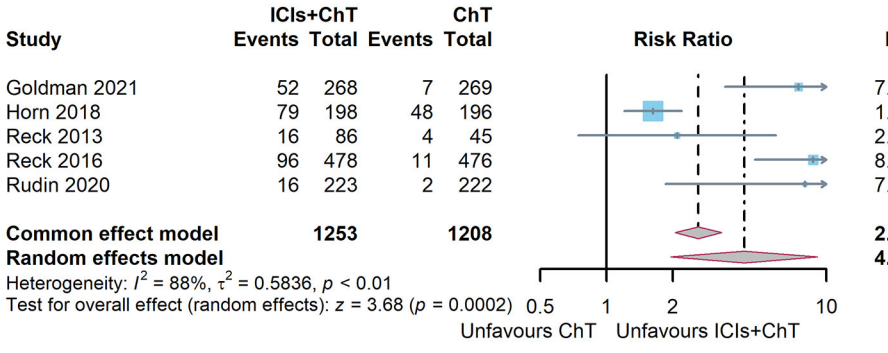

FIGURE 11
Comparison of grade 3–5 immune-related adverse events between ICIs+ChT and ChT.

nivolumab in this study, which has important clinical value, it is also included in this meta-analysis. This study also confirmed that nivolumab combined with standard chemotherapy in the first-line treatment of ES-SCLC can significantly improve OS and PFS.

Regarding the abovementioned studies, PD-1/PD-L1 inhibitors combined with standard chemotherapy can improve the efficacy of ES-SCLC. Although the abovementioned four RCTs found that ICIs combined with chemotherapy increased grade 3–5 irAEs, the overall safety and tolerability were acceptable, indicating that the regimen is safe and feasible. It can be seen from the six RCTs included in our study that CTLA-4 inhibitors and PD-1/PD-L1 inhibitors have different performances in the first-line combination therapy of ES-SCLC. However, there is no head-to-head comparative study comparing the efficacy of different PD-1/PD-L1 inhibitors as the first-line combination therapy in ES-SCLC. A recent network meta-analysis comparing the efficacy of atezolizumab, durvalumab, pembrolizumab, and nivolumab as the first-line treatment in patients with ES-SCLC found that atezolizumab, durvalumab, pembrolizumab, and nivolumab had no significant statistical difference in PFS or OS (25). However, durvalumab showed an ORR advantage compared to atezolizumab, but also a significantly higher risk of irAEs (25).

As demonstrated in the abovementioned RCTs, the combination of ICIs and chemotherapy as the first-line treatment for ES-SCLC is generally successful, and more and more ICIs have been approved, marking a new era of ICIs in anti-cancer treatment (26, 27). Our current study aimed to evaluate the efficacy and safety of ICIs combined with standard chemotherapy vs. chemotherapy alone in the first-line treatment of ES-SCLC *via* meta-analysis. At the same time, combined with the WHO-recommended Grades of Recommendations Assessment, Development and Evaluation (GRADE) system, an evidence-based evaluation of important outcomes was conducted, and possible treatment recommendations were elicited. A total of six RCTs were included in our study. Compared with chemotherapy alone, ICIs combined with standard chemotherapy as the first-line treatment in patients with ES-SCLC are more advantageous in prolonging OS and PFS. Apart from previously reported results (25, 28, 29), we presented the results of HR-based meta-analyses and mixed-effect model-based meta-analyses. The advantage of the mixed-effect model is that it makes full use of the survival information at different time points in the original study (14). Together with the sample size, it can achieve the same effect as individual patient data (IPD) meta-analysis, and the mixed-effect model can provide the estimated survival proportions at different time points; therefore, a combined survival curve can be drawn. As indicated in Table 2, the estimated 1- and 2-year OS rate in the "ICIs+ChT" and "ChT" group was 48.46% vs. 35.8%, and 15.84% vs. 10.12%, respectively. The estimated 6- and 12-month PFS rate in the "ICIs+ChT" and "ChT" group was 35.95% vs. 26.26%, and

10.3389/fmed.2023.1198950

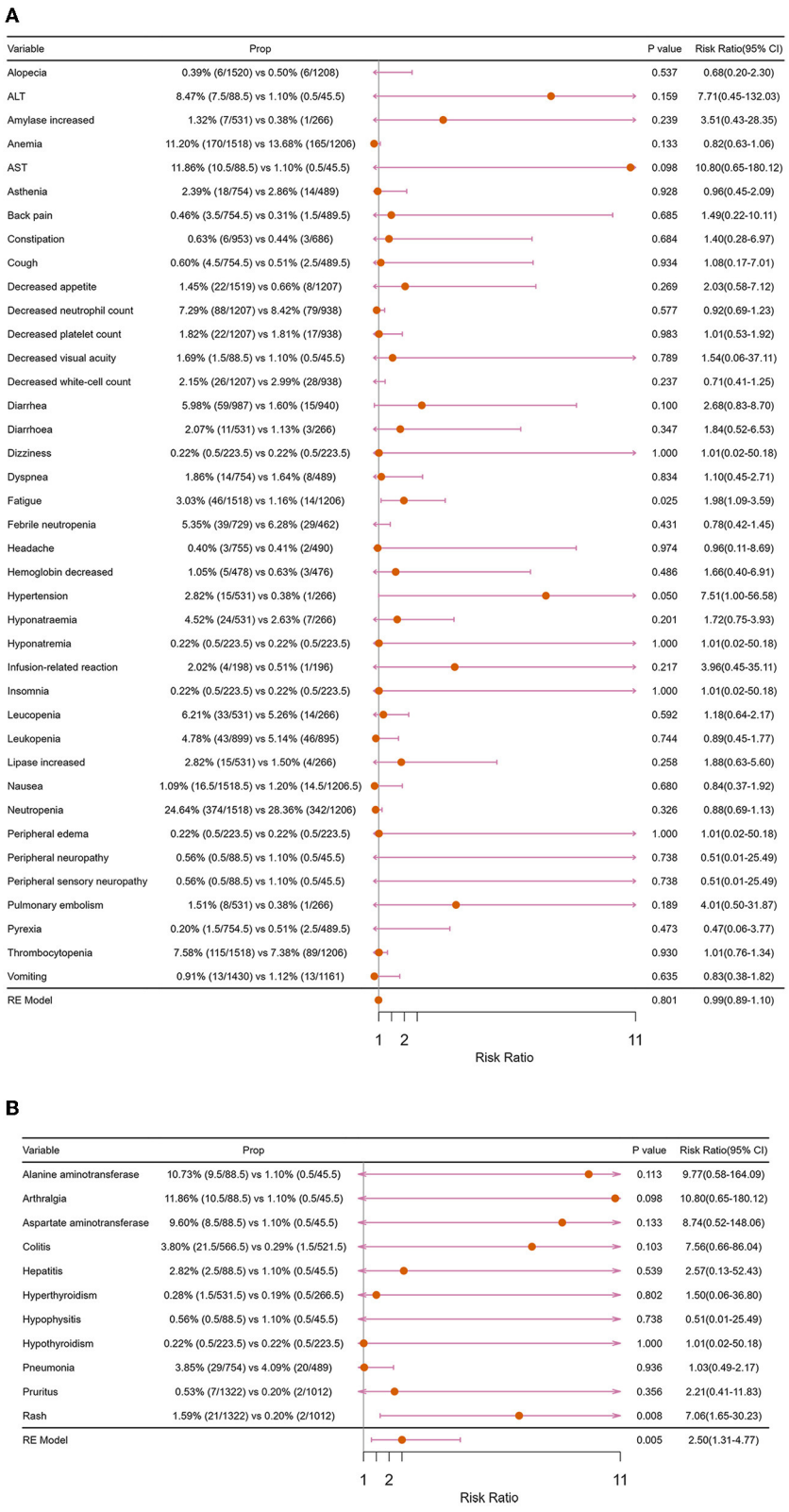

FIGURE 12
Forest plots of major adverse events: **(A)** treatment-related adverse events; **(B)** immune-related adverse events.

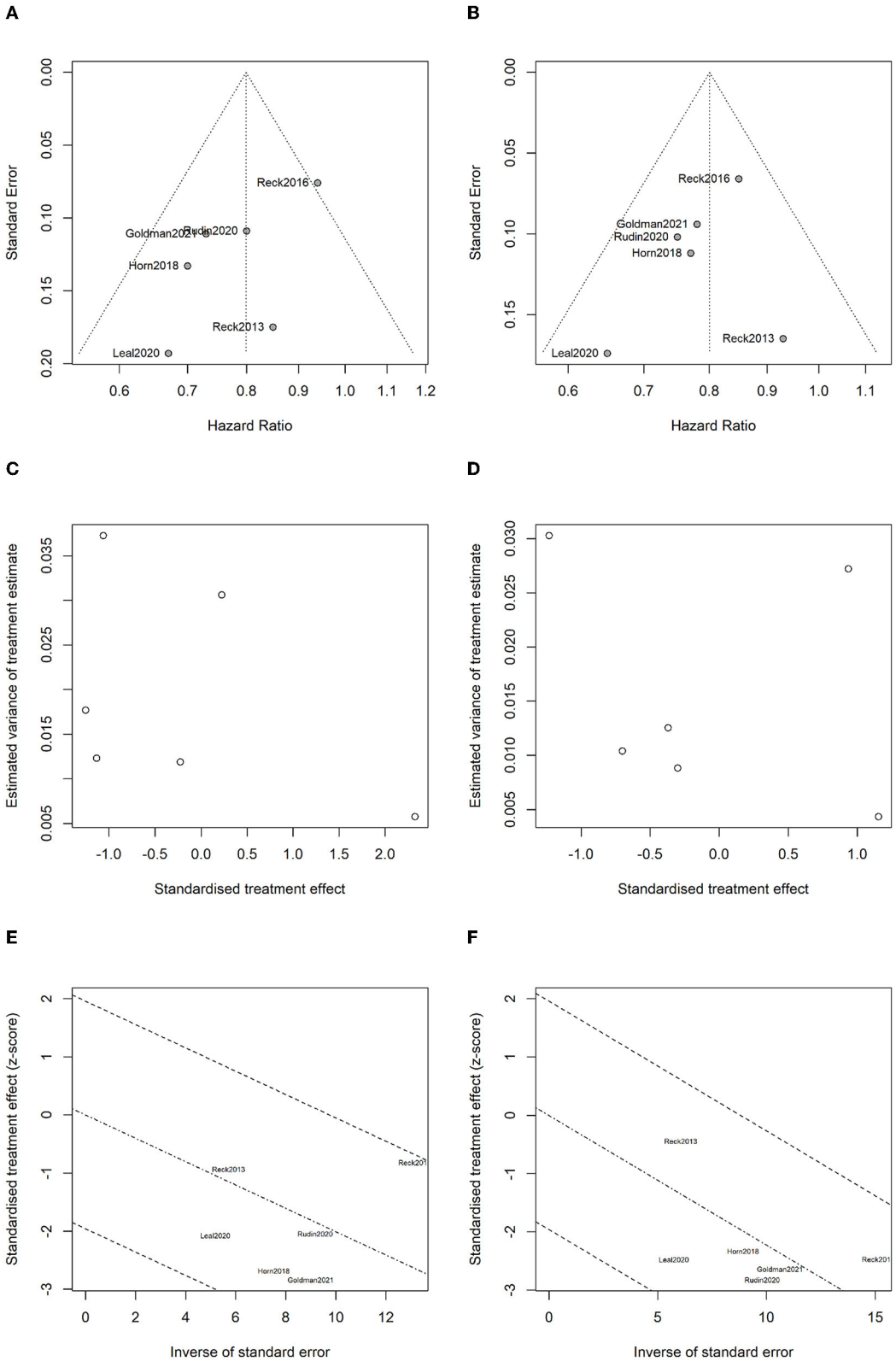

FIGURE 13
Analysis for bias and heterogenicity: **(A)** funnel plot of overall survival for evaluating publication bias; **(B)** funnel plot of progression-free survival for evaluating publication bias; **(C)** Begg's test results for overall survival; **(D)** Begg's test results for progression-free survival; **(E)** radial plot for overall survival to evaluate heterogenicity; and **(F)** radial plot for progression-free survival to evaluate heterogenicity.

12.23 % vs. 4.82%, respectively. A meta-analysis based on the mixed-effect model provided more direct survival information, and the survival curves for different treatments as well. Taken together, it can be concluded that compared with chemotherapy alone, ICIs combined with standard chemotherapy can reduce the risk of death in OS and PFS by 20% and 18.5%, respectively. However, no significant improvement in ORR and DCR had been observed. Only the CASPIAN study indicated that durvalumab combined with chemotherapy can significantly improve ORR (79.5% vs. 70.3%) (7, 8), while not in other studies. The underlying reason could probably be that SCLC was a chemotherapy-sensitive malignancy, and in the first-line treatment, chemotherapy could induce the greatest degree of tumor regression. Therefore, the combination treatment of ICIs could not significantly improve ORR and DCR. However, previous studies indicated that, unlike traditional treatments, immunotherapy can bring long-lasting immune responses and long-term survival benefits even after the patients had stopped using it, and in patients with stable disease (SD), which was known as the "smearing phenomenon". The specific mechanism of the "smearing effect" remains unclear. One view is that immunotherapy has a unique mechanism of action in the anti-tumor process, which can initiate or restart the cancer-tumor cycle in patients, and amplify the immune effect, but not cause an unlimited autoimmune response. Based on this superiority of anti-tumor immune responses, immune memory may provide long-term immune protection, thereby enabling long-term survival (30). The smearing effect in the survival curves could be found in many clinical trials with immunotherapy. In CheckMate 017/057 studies, patients treated with nivolumab continued to show a long-term OS benefit at 5 years compared with those with docetaxel, with a 5-year OS rate of 13.4% vs. 2.6%. Regardless of the histology of squamous cell carcinoma or non-squamous cell carcinoma, patients treated with nivolumab were five times more likely to survive more than 5 years compared with chemotherapy. Therefore, immunotherapy had greatly prolonged the survival of patients with advanced-stage cancer (31, 32). From the perspective of PFS and OS benefits, although ICIs combined with chemotherapy cannot improve the ORR and DCR of patients with ES-SCLC, the smearing effect of ICIs can still enable these patients to achieve long-term survival. In addition to factors related to the tumor itself, DCR and ORR also have certain inherent limitations as evaluation indicators. ORR is the sum of the ratios of complete response (CR) to partial response (PR), as the direct measurement of tumor response to anti-tumor drug, which can reliably reflect the anti-tumor activity of the drug. However, a simple ORR is not enough to explain the problem, and sufficient duration of response (DOR) is also needed to evaluate the effectiveness of tumor treatment (33). The longer the duration of the response, the more likely it is that an increase in ORR will bring clinical benefits. DCR is the proportion of patients with stable disease (SD) on top of ORR. However, it is also susceptible to the natural course of tumors and cannot reliably reflect the anti-tumor activity of drugs (34, 35).

The safety of ICIs combined with chemotherapy is another major concern (36, 37). Understanding the possible AEs is of vital importance in the application of immunotherapy (37). In this study, we analyzed the differences in the incidence of grade 3–5 trAEs and grade 3–5 irAEs between "ICIs+ChT" and "ChT". Compared with chemotherapy, "ICIs+ChT" as the first-line treatment in patients with ES-SCLC did not increase the incidence of grade 3–5 trAEs. However, the incidence of grade 3–5 irAEs was significantly increased. It has been reported that trAEs of ICIs were anemia, nausea, myalgia, decreased appetite, and neutropenia, while irAEs were rash, pneumonia, hepatitis, colitis, ophthalmia, and so on (38, 39). In the "ICIs+ChT" group, trAEs were more common in grades 1-2, and most of them could be alleviated with corresponding symptomatic treatment (38). According to previous reports, the incidence of grade 3–5 colitis and hepatitis in the "ICIs+ChT" group was higher than that in the chemotherapy group, and most irAEs could be controlled with a drug suspension and glucocorticoid administration (40, 41). In order to reduce the increased mortality caused by irAEs, the overall management principles are early detection, early evaluation, and early treatment (38, 42). It should be noted that approximately 10% of SCLC patients have paraneoplastic syndrome (PNS), and PNS in the nervous system is considered an autoimmune sequela. The presence of PNS may lead to a worse prognosis, and given the possibility of self-mimetic activation, attention should be paid to the increased incidence of PNS caused by immunotherapy (43). Fortunately, no significant increase in PNS was observed in patients receiving ICIs in combination with chemotherapy in IMPower133 or CASPIAN studies (1).

Compared with several previous meta-analyses on ICIs combined with chemotherapy vs. chemotherapy alone in the first-line treatment of ES-SCLC (25, 28, 29), the following advantages and innovations could be found in our articles: (1) the largest number of original studies were included, and two CTLA-4 inhibitor studies and four PD-1/PD-L1 inhibitor studies were also included. (2) Using innovations in meta-analysis methodologies, we not only adopted the traditional inverse variance meta-analysis method with HR as the effect value but also gave the results of the meta-analysis based on the mixed-effect model. We used the mixed-effect model proposed by Arends et al. to perform a meta-analysis on the survival proportions information in the survival curve (14) and granted the meta-analysis results in higher precision. We presented not only the forest plot but also the survival curves reconstructed by the meta-analysis, which was very valuable to the evidence users. (3) To the best of our knowledge, there is currently no evidence recommendation based on the GRADE system for ICIs combined with chemotherapy in the first-line treatment of ES-SCLC. In the GRADE system, although evidence based on RCTs is initially rated as high quality, confidence in the relevant evidence may be downgraded due to five important factors (44). According to the GRADE methodological quality evaluation, among the six indicators in this meta-analysis, four outcomes (OS, PFS, incidence of trAEs, and irAEs) were considered as high-grade evidence, while ORR and DCR were judged to be low-grade evidence. The main reasons for low-grade evidence are as follows: ① The full text of ECOG-ACRIN EA5161 has not been reported (17), and there is a lack of availability information of DCR, a risk of "incomplete outcome data" bias was assigned to the assessment; ② there is obvious heterogeneity between six studies, and the results of the meta-analysis are negative, limiting the generalization of the evidence. In addition, because the effect

size is borderline, it is possible to change the statistical results of ORR by adding studies. Due to the need to sign the informed consent form for treatment, it is difficult to achieve double-blinding of patients and interventionists, so allocation concealment and blinding in this study were not used as an important evidence basis for consideration. In this study, we set OS, PFS, and the incidence of irAEs as the main "key" outcome indicators. Given the overall high quality of the original studies, the wide sample population with different ethnicities, and the obvious effect value of key indicators, the authenticity of the conclusions is reliable and the extrapolation is good. Therefore, we set the evidence recommendation level of these indicators as "strong recommendation" (1). However, as the summary effect value of trAEs was not significant, the level of evidence recommendation was set to be "weak recommendation" (2). Similarly, the level of evidence recommendation is set to be "weak recommendation" (2) due to the low level of evidence for ORR and DCR.

Immune checkpoint-blocking drugs represented by PD-1/PD-L1 antibodies have achieved surprising results in the treatment of various cancers, but the overall effectiveness is a key drawback (45). The heterogeneity of tumors and the diversity of the immune microenvironment are the main factors limiting efficacy (46). Inevitably, there is also a problem of drug resistance in anti-PD-1/PD-L1, which has attracted the attention of scholars (47). The combination scheme based on PD-1/PD-L1 antibodies is expected to address the shortcomings of low efficiency and susceptibility to drug resistance in a single target, making it a frontier in international research (47). With further research on the mechanism of signaling pathways of PD-1/PD-L1 and TGFR2/TGF- β in tumors, bifunctional anti-PD-L1/TGF-βRII agents have shown that it can simultaneously block PD-1/PD-L1 and TGFR2/TGF-β signal pathway, promote the activation of effector T cells, regulate the tumor microenvironment, reverse immunosuppression and fibrosis, and show better anti-tumor effect than PD-L1 monoclonal antibody in a variety of mouse tumor-bearing models (48). The bifunctional agent bintrafusp alfa (previously named M7824), comprising the extracellular domain of human TGFβRII (TGFβ Trap) linked to the C-terminus of the human anti-PD-L1 heavy chain (αPD-L1), has been developed in an attempt to address this issue (49). Recently, some novel anti-TGF-beta/PD-L1 bispecific antibodies such as YM101 (50) and SHR-1701 (46) have been developed, which effectively overcome anti-PD-1/PD-L1 resistance in some cold tumors (51). Anyway, immunotherapy has broad application prospects for small-cell lung cancer.

Although we had made a comprehensive summary of the existing studies, the following limitations still exist in our study. First, our analysis included only RCTs; however, phase III registration trials are often highly case-selective, and subjects in RCTs are not fully representative of real-world clinical patients. In RCTs, elderly and/or frail ES-SCLC patients, especially patients with comorbidities and worse performance status (PS $\geq$ 2), are often excluded from registration trials. Whether those patients can also benefit from ICIs treatment, no strong conclusions can be drawn (52). A current study based on real-world data suggested that the benefits of combination therapy with ICIs are comparable to clinical trials after adjusting for age and PS score (53). Whether ICIs are recommended for patients with pre-existing autoimmune disease, organ transplantation, or chronic viral infection (e.g., hepatitis B) is still debatable. For these patients, a multidisciplinary discussion should be adhered to decide whether to administer ICIs or not (54). Second, the studies included were all published in English. Third, the efficacy of ICIs may be related to some clinical factors such as gender, age, race, smoking history, and chemotherapy regimens. Our study did not further analyze the influence of these factors. Previously published meta-analyses had been conducted for subgroup analyses of these factors (25, 28, 29). Finally, as more and more ICIs are developed and applied clinically, it is still debatable whether these novel drugs can achieve the same clinical benefits as the existing ICIs.

5. Conclusion

Our meta-analysis has affirmed the clinical benefit of "ICIs+ChT" as the first-line treatment for patients with ES-SCLC with solid evidence. Compared with conventional chemotherapy, although "ICIs+ChT" had increased the incidence of grade 3–5 irAEs, ICIs combined with chemotherapy significantly improved OS and PFS in ES-SCLC patients, and their trAEs were acceptable. Therefore, ICIs combined with chemotherapy can be used as the first-line treatment for patients with ES-SCLC.

Data availability statement

The original contributions presented in the study are included in the article/supplementary material, further inquiries can be directed to the corresponding authors.

Author contributions

JZ and YD: conception and design and provision of study materials or patients. JZ and BH: collection and assembly of data. JZ and XC: data analysis and interpretation. JZ, YD, BH, and XC: manuscript writing and editing. All authors contributed to the manuscript and approved the submitted version.

Funding

This study was supported in part by Joint Funds for the Innovation of Science and Technology, Fujian Province (Grant No. 2020Y9036 to XC), the Fujian Research and Training Grants for Young and Middle-aged Leaders in Healthcare (to XC), the National Clinical Key Specialty Construction Program (Grant No. 2021), the Fujian Provincial Clinical Research Center for Cancer Radiotherapy and Immunotherapy (Grant No. 2020Y2012), Fujian Provincial Natural and Scientific Foundation (Grant No: 2023J011255 to XC), the Fujian Provincial Health Technology Project (Youth Scientific Research Project, 2019-1-50 to JZ), the Nursery Fund Project of the Second Affiliated Hospital of Fujian Medical University (Grant No: 2021MP05 to JZ), and Fujian Education and Research Grants for Young and Middle-aged Teachers (Grant No: JAT220083 to YD).

Acknowledgments

This study was registered in the PROSPERO International Prospective Register of Systematic Reviews (CRD42022348496).

Conflict of interest

The authors declare that the research was conducted in the absence of any commercial or financial relationships that could be construed as a potential conflict of interest.

Publisher's note

References

1. Iams WT, Porter J, Horn L. Immunotherapeutic approaches for small-cell lung cancer. *Nat Rev Clin Oncol.* (2020) 17:300–12. doi: 10.1038/s41571-019-0316-z

2. Pelosi G, Bianchi F, Hofman P, Pattini L, Strobel P, Calabrese F, et al. Recent advances in the molecular landscape of lung neuroendocrine tumors. *Expert Rev Mol Diagn.* (2019) 19:281–97. doi: 10.1080/14737159.2019.1595593

3. Rossi A, Di Maio M, Chiodini P, Rudd RM, Okamoto H, Skarlos DV, et al. Carboplatin- or cisplatin-based chemotherapy in first-line treatment of small-cell lung cancer: the COCIS meta-analysis of individual patient data. *J Clin Oncol.* (2012) 30:1692–8. doi: 10.1200/jco.2011.40.4905

4. Melosky B, Cheema PK, Brade A, McLeod D, Liu G, Price PW, et al. Prolonging survival: the role of immune checkpoint inhibitors in the treatment of extensive-stage small cell lung cancer. *Oncologist.* (2020) 25:981–92. doi: 10.1634/theoncologist.2020-0193

5. Koinis F, Kotsakis A, Georgoulias V. Small cell lung cancer (SCLC): no treatment advances in recent years. *Transl Lung Cancer Res.* (2016) 5:39–50. doi: 10.3978/j.issn.2218-6751.2016.01.03

6. Horn L, Mansfield AS, Szczesna A, Havel L, Krzakowski M, Hochmair MJ, et al. First-line atezolizumab plus chemotherapy in extensive-stage small-cell lung cancer. *N Engl J Med.* [2018] 379:2220–9. doi: 10.1056/NEJMoa1809064

7. Goldman JW, Dvorkin M, Chen Y, Reinmuth N, Hotta K, Trukhin D, et al. Durvalumab, with or without tremelimumab, plus platinum-etoposide versus platinum-etoposide alone in first-line treatment of extensive-stage small-cell lung cancer (CASPIAN): updated results from a randomised, controlled, open-label, phase 3 trial. *Lancet Oncol.* (2021) 22:51–65. doi: 10.1016/S1470-2045(20)30539-8

8. Paz-Ares L, Dvorkin M, Chen Y, Reinmuth N, Hotta K, Trukhin D, et al. Durvalumab plus platinum-etoposide versus platinum-etoposide in first-line treatment of extensive-stage small-cell lung cancer (CASPIAN): a randomised, controlled, open-label, phase 3 trial. *Lancet.* (2019) 394:1929–39. doi: 10.1016/S0140-6736(19)32222-6

9. Ortega-Franco A, Ackermann C, Paz-Ares L, Califano R. First-line immune checkpoint inhibitors for extensive stage small-cell lung cancer: clinical developments and future directions. *ESMO Open.* (2021) 6:100003. doi: 10.1016/j.esmoop.2020.100003

10. Reck M, Luft A, Szczesna A, Havel L, Kim SW, Akerley W, et al. Phase III randomized trial of ipilimumab plus etoposide and platinum versus placebo plus etoposide and platinum in extensive-stage small-cell lung cancer. *J Clin Oncol.* (2016) 34:3740–8. doi: 10.1200/JCO.2016.67.6601

11. Moher D, Liberati A, Tetzlaff J, Altman DG, Group P. Preferred reporting items for systematic reviews and meta-analyses: the PRISMA statement. *J Clin Epidemiol.* (2009) 62:1006–12. doi: 10.1016/j.jclinepi.2009.06.005

12. Atins D, Best D, Briss P. Grading quality of evidence and strength of recommendations. *BMJ.* (2004) 328:1490. doi: 10.1136/bmj.328.7454.1490

13. Parmar MK, Torri V, Stewart L. Extracting summary statistics to perform meta-analyses of the published literature for survival endpoints. *Stat Med.* (1998) 17:2815–34. doi: 10.1002/(sici)1097-0258(19981230)17:24<2815::aid-sim110>3.0.co;2-8

14. Arends LR, Hunink MG, Stijnen T. Meta-analysis of summary survival curve data. *Stat Med.* (2008) 27:4381–96. doi: 10.1002/sim.3311

15. Reck M, Bondarenko I, Luft A, Serwatowski P, Barlesi F, Chacko R, et al. Ipilimumab in combination with paclitaxel and carboplatin as first-line therapy in extensive-disease-small-cell lung cancer: results from a randomized, double-blind, multicenter phase 2 trial. *Ann Oncol.* (2013) 24:75–83. doi: 10.1093/annonc/mds213

16. Rudin CM, Awad MM, Navarro A, Gottfried M, Peters S, Csoszi T, et al. Pembrolizumab or placebo plus etoposide and platinum as first-line therapy for extensive-stage small-cell lung cancer: randomized, double-blind, phase III KEYNOTE-604 study. *J Clin Oncol.* (2020) 38:2369–79. doi: 10.1200/jco.20.00793

17. Leal T, Wang Y, Dowlati A. Randomized phase II clinical trial of cisplatin/carboplatin and etoposide (CE) alone or in combination with nivolumab as frontline therapy for extensive-stage small cell lung cancer (ES-SCLC): ECOG-ACRIN EA5161. *J Clin Oncol.* (2020) 38:9000. doi: 10.1200/jco.2020.38.15_suppl.9000

18. Peters S, Creelan B, Hellmann MD, Socinski MA, Reck M, Bhagavatheeswaran P, et al. Abstract CT082: Impact of tumor mutation burden on the efficacy of first-line nivolumab in stage iv or recurrent non-small cell lung cancer: an exploratory analysis of CheckMate 026. *Cancer Res.* (2017) 77:CT082-CT. doi: 10.1158/1538-7445.Am2017-ct082

19. Rudin CM, Durinck S, Stawiski EW, Poirier JT, Modrusan Z, Shames DS, et al. Comprehensive genomic analysis identifies SOX2 as a frequently amplified gene in small-cell lung cancer. *Nat Genet.* (2012) 44:1111–6. doi: 10.1038/ng.2405

20. Peifer M, Fernández-Cuesta L, Sos ML, George J, Seidel D, Kasper LH, et al. Integrative genome analyses identify key somatic driver mutations of small-cell lung cancer. *Nat Genet.* (2012) 44:1104–10. doi: 10.1038/ng.2396

21. George J, Lim JS, Jang SJ, Cun Y, Ozretić L, Kong G, et al. Comprehensive genomic profiles of small cell lung cancer. *Nature.* (2015) 524:47–53. doi: 10.1038/nature14664

22. Hellmann MD, Callahan MK, Awad MM, Calvo E, Ascierto PA, Atmaca A, et al. Tumor mutational burden and efficacy of nivolumab monotherapy and in combination with ipilimumab in small-cell lung cancer. *Cancer Cell.* (2018) 33:853–61.e4. doi: 10.1016/j.ccell.2018.04.001

23. Ott PA, Elez E, Hiret S, Kim DW, Morosky A, Saraf S, et al. Pembrolizumab in patients with extensive-stage small-cell lung cancer: results from the phase Ib KEYNOTE-028 study. *J Clin Oncol.* (2017) 35:3823–9. doi: 10.1200/jco.2017.72.5069

24. Chung HC, Piha-Paul SA, Lopez-Martin J, Schellens JHM, Kao S, Miller WH, et al. Pembrolizumab after two or more lines of previous therapy in patients with recurrent or metastatic SCLC: results from the KEYNOTE-028 and KEYNOTE-158 studies. *J Thorac Oncol.* (2020) 15:618–27. doi: 10.1016/j.jtho.2019.12.109

25. Chen J, Wang J, Xu H. Comparison of atezolizumab, durvalumab, pembrolizumab, and nivolumab as first-line treatment in patients with extensive-stage small cell lung cancer: A systematic review and network meta-analysis. *Medicine (Baltimore).* (2021) 100:e25180. doi: 10.1097/md.0000000000025180

26. Saleh K, Khalife-Saleh N, Kourie HR. Finally, after decades, immune checkpoint inhibitors dethroned the standard of care of small-cell lung cancer. *Immunotherapy.* (2019) 11:457–60. doi: 10.2217/imt-2019-0010

27. Schmid S, Fruh M. Immune checkpoint inhibitors and small cell lung cancer: what's new? *J Thorac Dis.* (2018) 10:S1503–S8. doi: 10.21037/jtd.2018.01.113

28. Chen HL, Tu YK, Chang HM, Lee TH, Wu KL, Tsai YC, et al. Systematic review and network meta-analysis of immune checkpoint inhibitors in combination with chemotherapy as a first-line therapy for extensive-stage small cell carcinoma. *Cancers (Basel).* (2020) 12:12. doi: 10.3390/cancers12123629

29. Landre T, Chouahnia K, Des Guetz G, Duchemann B, Assie JB, Chouaid C. First-line immune-checkpoint inhibitor plus chemotherapy versus chemotherapy alone for extensive-stage small-cell lung cancer: a meta-analysis. *Ther Adv Med Oncol.* (2020) 12:1758835920977137. doi: 10.1177/758835920977137

30. Wu S, Li D, Chen J, Chen W, Ren F. Tailing effect of PD-1 antibody results in the eradication of unresectable multiple primary lung cancer presenting as ground-glass opacities: a case report. *Ann Palliat Med.* (2021) 10:778–84. doi: 10.21037/apm-20-2132

31. Horn L, Spigel DR, Vokes EE, Holgado E, Ready N, Steins M, et al. Nivolumab versus docetaxel in previously treated patients with advanced non-small-cell lung cancer: two-year outcomes from two randomized, open-label, phase III trials (CheckMate 017 and CheckMate 057). *J Clin Oncol.* (2017) 35:3924–33. doi: 10.1200/JCO.2017.74.3062

32. Borghaei H, Gettinger S, Vokes EE, Chow LQM, Burgio MA, de Castro Carpeno J, et al. Five-year outcomes from the randomized, phase III trials CheckMate 017 and 057: nivolumab versus docetaxel in previously treated non-small-cell lung cancer. *J Clin Oncol.* (2021) 39:723–33. doi: 10.1200/JCO.20.01605

33. Baggerly K. Experimental design, randomization, and validation. *Clin Chem.* (2018) 64:1534–5. doi: 10.1373/clinchem.2017.273334

34. Sharon E, Foster JC. Design of phase II oncology trials evaluating combinations of experimental agents. *J Natl Cancer Inst.* (2023) 115:613–8. doi: 10.1093/jnci/djad052

35. Zhou J, Jiang X, Xia HA, Wei P, Hobbs BP. Predicting outcomes of phase III oncology trials with Bayesian mediation modeling of tumor response. *Stat Med.* (2022) 41:751–68. doi: 10.1002/sim.9268

36. Pavan A, Attili I, Pasello G, Guarneri V, Conte PF, Bonanno L. Immunotherapy in small-cell lung cancer: from molecular promises to clinical challenges. *J Immuno Ther Cancer.* (2019) 7:205. doi: 10.1186/s40425-019-0690-1

37. Huang W, Chen J-J, Xing R, Zeng Y-C. Combination therapy: future directions of immunotherapy in small cell lung cancer. *Transl Oncol.* (2021) 14:100889. doi: 10.1016/j.tranon.2020.100889

38. Darnell EP, Mooradian MJ, Baruch EN, Yilmaz M, Reynolds KL. Immune-related adverse events (irAEs): diagnosis, management, and clinical pearls. *Curr Oncol Rep.* (2020) 22:39. doi: 10.1007/s11912-020-0897-9

39. Myers G. Immune-related adverse events of immune checkpoint inhibitors: a brief review. *Curr Oncol.* (2018) 25:342–7. doi: 10.3747/co.25.4235

40. Haanen J, Carbonnel F, Robert C, Kerr KM, Peters S, Larkin J, et al. Management of toxicities from immunotherapy: ESMO Clinical Practice Guidelines for diagnosis, treatment and follow-up. *Ann Oncol.* (2017) 28:iv119–iv42. doi: 10.1093/annonc/mdx225

41. Ru CH, Zhuang YB. Efficacy and safety of addition of anti-pd1 to chemotherapy in treatment of non-small cell lung cancer. *Comb Chem High Throughput Screen.* (2018) 21:711–7. doi: 10.2174/1386207322666190125150921

42. Thompson JA. New NCCN guidelines: recognition and management of immunotherapy-related toxicity. *J Natl Compr Canc Netw.* (2018) 16:594–6. doi: 10.6004/jnccn.2018.0047

43. Iams WT, Shiuan E, Meador CB, Roth M, Bordeaux J, Vaupel C, et al. Improved prognosis and increased tumor-infiltrating lymphocytes in patients who have SCLC with neurologic paraneoplastic syndromes. *J Thorac Oncol.* (2019) 14:1970–81. doi: 10.1016/j.jtho.2019.05.042

44. Guyatt GH, Oxman AD, Vist GE, Kunz R, Falck-Ytter Y, Alonso-Coello P, et al. GRADE: an emerging consensus on rating quality of evidence and strength of recommendations. *BMJ.* (2008) 336:924–6. doi: 10.1136/bmj.39489.470347.AD

45. Gulley JL, Schlom J, Barcellos-Hoff MH, Wang XJ, Seoane J, Audhuy F, et al. Dual inhibition of TGF-β and PD-L1: a novel approach to cancer treatment. *Mol Oncol.* (2022) 16:2117–34. doi: 10.1002/1878-0261.13146

46. Liu D, Zhou J, Wang Y, Li M, Jiang H, Liu Y, et al. Bifunctional anti-PD-L1/TGF-βRII agent SHR-1701 in advanced solid tumors: a dose-escalation, dose-expansion, and clinical-expansion phase 1 trial. *BMC Med.* (2022) 20:408. doi: 10.1186/s12916-022-02605-9

47. Yi M, Wu Y, Niu M, Zhu S, Zhang J, Yan Y, et al. Anti-TGF-β/PD-L1 bispecific antibody promotes T cell infiltration and exhibits enhanced antitumor activity in triple-negative breast cancer. *J Immunother Cancer.* (2022) 10:12. doi: 10.1136/jitc-2022-005543

48. Khalili-Tanha G, Fiuji H, Gharib M, Moghbeli M, Khalili-Tanha N, Rahmani F, et al. Dual targeting of TGF-β and PD-L1 inhibits tumor growth in TGF-β/PD-L1-driven colorectal carcinoma. *Life Sci.* (2023) 2023:121865. doi: 10.1016/j.lfs.2023.121865

49. Knudson KM, Hicks KC, Luo X, Chen JQ, Schlom J, Gameiro SR. M7824, a novel bifunctional anti-PD-L1/TGFβ Trap fusion protein, promotes anti-tumor efficacy as monotherapy and in combination with vaccine. *Oncoimmunology.* (2018) 7:e1426519. doi: 10.1080/2162402x.2018.1426519

50. Yi M, Niu M, Wu Y, Ge H, Jiao D, Zhu S, et al. Combination of oral STING agonist MSA-2 and anti-TGF-β/PD-L1 bispecific antibody YM101: a novel immune cocktail therapy for non-inflamed tumors. *J Hematol Oncol.* (2022) 15:142. doi: 10.1186/s13045-022-01363-8

51. Lind H, Gameiro SR, Jochems C, Donahue RN, Strauss J, Gulley JM, et al. Dual targeting of TGF-β and PD-L1 via a bifunctional anti-PD-L1/TGF-βRII agent: status of preclinical and clinical advances. *J Immunother Cancer.* (2020) 8:1. doi: 10.1136/jitc-2019-000433

52. Xue L, Chen B, Lin J, Peng J. Anti-PD-L1 immune checkpoint inhibitors in combination with etoposide and platinum for extensive-stage small cell lung cancer: a case report. *Ann Palliat Med.* (2021) 10:828–35. doi: 10.21037/apm-20-2574

53. Mencoboni M, Ceppi M, Bruzzone M, Taveggia P, Cavo A, Scordamaglia F, et al. Effectiveness and safety of immune checkpoint inhibitors for patients with advanced non small-cell lung cancer in real-world: review and meta-analysis. *Cancers (Basel).* (2021) 13:6. doi: 10.3390/cancers13061388

54. Califano R, Gomes F, Ackermann CJ, Rafee S, Tsakonas G, Ekman S. Immune checkpoint blockade for non-small cell lung cancer: What is the role in the special populations? *Eur J Cancer.* (2020) 125:1–11. doi: 10.1016/j.ejca.2019.11.010

frontiers | Frontiers in Medicine

TYPE Original Research
PUBLISHED 25 September 2023
DOI 10.3389/fmed.2023.1273406

OPEN ACCESS

EDITED BY
Zheng Wang,
Shanghai Jiao Tong University, China

REVIEWED BY
Ruo Wang,
Shanghai Jiao Tong University, China
Dongxiao Zhang,
Capital Medical University, China
Jiayu Sheng,
Shanghai University of Traditional Chinese Medicine, China

*CORRESPONDENCE
Hongfeng Chen
✉ fenhong674chen@yeah.net
Meina Ye
✉ yepangmi@163.com

†These authors have contributed equally to this work

RECEIVED 06 August 2023
ACCEPTED 31 August 2023
PUBLISHED 25 September 2023

CITATION
Zhou Y, Wu J, Ma L, Wang B, Meng T, Chen H and Ye M (2023) Differences and significance of peripheral blood interleukin-6 expression between patients with granulomatous lobular mastitis and those with benign breast tumors. *Front. Med.* 10:1273406.
doi: 10.3389/fmed.2023.1273406

Differences and significance of peripheral blood interleukin-6 expression between patients with granulomatous lobular mastitis and those with benign breast tumors

Yue Zhou†, Jingjing Wu†, Lina Ma, Bing Wang, Tian Meng, Hongfeng Chen* and Meina Ye*

Department of Breast Surgery (Traditional), Longhua Hospital Affiliated to Shanghai University of Traditional Chinese Medicine, Shanghai, China

Objective: It is unclear whether the mechanism of the interleukin (IL)-6 signaling pathway is similar between granulomatous lobular mastitis (GLM) and benign breast tumors. This study aimed to explore the differences and significance of peripheral blood IL-6 and related cytokines, routine blood test results, and C-reactive protein (CRP) levels between patients with GLM and benign breast tumors.

Methods: Seventy-three inpatients with GLM who underwent surgery and 60 patients with benign breast tumors diagnosed based on pathological findings between November 2022 and May 2023 were included. The white blood cell (WBC) and neutrophil (NEU) counts were determined using an automatic blood cell analyzer, the CRP level was determined by an immunoturbidimetric assay, and serum IL-6 and related cytokine levels were determined by an enzyme-linked immunosorbent assay.

Results: The WBC, NEU, and CRP values in patients with GLM were significantly higher than those in patients with benign breast tumors ($P < 0.01$). Serum IL-6 levels were significantly higher in patients with GLM than in those with benign breast tumors ($P < 0.01$). There were no significant differences in the serum concentrations of IL-1β, IL-7, and interferon (IFN)-γ between patients with GLM and those with benign breast tumors ($P > 0.05$), but the tumor necrosis factor (TNF)-α level was higher in patients with GLM than in those with benign breast tumors ($P < 0.01$). In patients with GLM, the Pearson correlation analysis showed that the IL-6 level was positively correlated with NEU, NEU%, CRP, IL-17, and TNF-α values ($P < 0.01$). Additionally, the IL-6 level was weakly positively correlated with WBC and IFN-γ values. Conversely, in patients with benign breast tumors, the IL-6 level was not significantly correlated with the aforementioned indicators in routine blood tests but was positively correlated with IL-17, IFN-γ, and TNF-α values ($P < 0.01$).

Conclusions: IL-6, NEU, NEU%, and CRP values were significantly elevated in patients with GLM compared to those with benign breast tumors, indicating that IL-6 plays an important role in the development and onset of GLM. The correlation between these cytokines and the development and progression of benign breast

tumors needs to be further explored, as cytokines such as IL-6 may provide effective markers for the treatment of GLM.

KEYWORDS

cancer-associated inflammatory cytokines, interleukin-6 (IL-6), breast benign tumor, granulomatous lobular mastitis, correlation analysis

1. Introduction

Granulomatous lobular mastitis (GLM) is a rare, chronic, non-specific inflammatory disease of the breast that has seen an increasing incidence in recent years (1). Although GLM is an inflammatory disease, its clinical characteristics are complex and diverse, especially at the mass stage, making it difficult to distinguish between benign breast tumors and breast cancer. The etiology of this disease remains unclear. However, antibiotics and hormones have poor effects on GLM. It easily suppurates and ulcerates repeatedly, forming sinuses, fistulas, or ulcers, thus resulting in breast disfiguration, which seriously affects the patient's quality of life (2). This disease is difficult to treat clinically, and its clinical and radiographic features can simulate breast cancer. Current clinical studies have suggested that the pathogenesis of GLM includes inflammation, immune reactions, apoptosis, tissue damage, and gene polymorphisms. However, its etiology remains controversial (3). Therefore, it is of great importance and value to explore the etiology and pathogenesis of GLM.

Interleukin (IL)-6 is a pleiotropic cytokine that is both an inflammatory cytokine and a cancer-associated cytokine (4). In an inflammatory tumor microenvironment, IL-6 has demonstrated the ability to induce pro- and anti-inflammatory responses using three mechanisms of signal transduction (classical signaling, transsignaling, and cluster signaling), interact with a diversity of target cells, and induce endocrine effects in an autocrine/paracrine manner (5). Studies have shown that the IL-6/Janus tyrosine family kinase (JAK)/signal transducer and the activator of the transcription 3 (STAT3) signaling pathway is closely related to plasma cell mastitis (6, 7) and idiopathic granulomatous mastitis (8). However, the in-depth pathogenesis of GLM has not been reported. Existing studies have confirmed that the IL-6/JAK/STAT3 signaling pathway is crucial for the proliferation and survival of tumor cells (9); however, it is unclear whether this pathway plays a similar role in GLM formation and whether its mechanism is similar to that in benign breast tumor. No studies have investigated whether the IL-6 signaling pathway is involved in the formation of GLM. In our previous study, we quantitatively analyzed the difference in protein expression in GLM lesion tissues and healthy breast tissues adjacent to the lesion using tandem mass tag (TMT) quantitative proteomics technology and found that the expression of the STAT3 protein in GLM lesion tissues was significantly higher than that in healthy breast tissues. Based on this finding, this study aimed to further explore the differences and significance of IL-6 in the development of GLM and benign breast tumors to provide new ideas and bases for clinical diagnosis and treatment.

2. Materials and methods

2.1. Patients

This study included 73 operative inpatients with GLM and 60 operative inpatients with benign breast tumors (excluding breast cysts or benign breast tumors with inflammation) from the Department of Breast Surgery (Traditional), Longhua Hospital Affiliated to Shanghai University of Traditional Chinese Medicine, who were diagnosed based on pathological findings between November 2022 and May 2023.

2.2. Laboratory data

This study was a retrospective trial. Serum samples were collected from patients with GLM and those with benign breast tumors. A total of 5 ml of fasting venous blood was obtained from each patient on the day of hospital admission, placed in an ethylenediaminetetraacetic acid anticoagulant tube, and sent to the Clinic Laboratory of Longhua Hospital within 2 h for routine blood testing and for determining the C-reactive protein (CRP) and cytokine levels. The white blood cell (WBC) count, neutrophil (NEU) count, and neutrophilic granulocyte percentage (NEU %) were detected using an automatic hematology analyzer. CRP was detected by immunoturbidimetry, and serum cytokines were detected by an enzyme-linked immunosorbent assay.

2.3. Statistical analysis

Continuous variables were reported as mean (±standard deviation). The independent *t*-test was performed to analyze normally distributed values, and the Pearson's method was employed to perform correlation analysis. To predict the IL-6 levels in patients with GLM, the logistic regression model was employed, and the independent variables of time since the appearance of masses ($\leq$3 months = 0, >3 months = 1), mass size (<10 cm = 0, $\geq$10 cm = 1), antibiotic use, and glucocorticoid use for treating this disease were integrated. SPSS software (version 27.0; IBM Corp.) was used to analyze all data. All the *p*-values reported were two-sided, and *p*-values < 0.05 were considered statistically significant.

3. Results

3.1. Patient characteristics

Clinical characteristics of the 133 inpatients are shown in Table 1. Specific clinical characteristics of patients with benign

TABLE 1 Clinical characteristics of the 133 inpatients.

Characteristics		Group	
		Granulomatous lobular mastitis ($n = 73$)	Benign breast tumor ($n = 60$)
Age, years, mean (SD)		33.38 (4.86)	32.32 (6.52)
BMI, mean (SD)		23.56 (4.2)	21.25 (2.39)
Childbearing history, *N* (%)	o	1 (1.4%)	24 (40.0%)
	1	60 (82.2%)	30 (50.0%)
	2	12 (16.4%)	6 (10.0%)
Elevated prolactin level, *N* (%)		24 (32.9%)	6 (10.0%)
Elevated cholesterol level, *N* (%)		19 (26.0%)	18 (30.0%)
Elevated triglycerides level, *N* (%)		14 (19.2%)	2 (3.3%)
Breast surgery history, *N* (%)		5 (6.8%)	7 (11.7%)

TABLE 2 Clinical characteristics of the 60 inpatients with benign breast tumors.

Characteristics		*N* (%)
Pattern	Unilateral	25 (41.7%)
	Bilateral	35 (58.3%)
Number of tumors	1	12 (20%)
	2–5	36 (60%)
	≥5	12 (20%)
Time since tumors appearing	<1 year	23 (38.3%)
	1–5 years	28 (46.7%)
	≥5 years	9 (15.0%)
Breast imaging reporting and data system (BI-RADS)	Unknown	2 (3.3%)
	3	44 (73.3%)
	3–4a	9 (15.0%)
	4a	5 (8.3%)
Family history of breast tumors	Benign tumor	2 (3.3%)
	Breast cancer	1 (1.7%)

TABLE 3 Clinical characteristics of the 73 inpatients with granulomatous lobular mastitis.

Characteristics		*N* (%)
Pattern	Unilateral	67 (91.8%)
	Bilateral	6 (8.2%)
Time since the appearance of lumps	<1 month	2 (2.7%)
	1–3 months	27 (40.0%)
	>3 months	44 (60.3%)
Size of the lumps (palpation)	<5 cm	2 (2.7%)
	5–10 cm	44 (60.3%)
	≥10 cm	27 (37.0%)
Extent of lesions (MRI)	≤2 quadrants	42 (57.5%)
	>2 quadrants	31 (42.5%)
Lesions involving the areola		69 (94.5%)
Nipple inversion		26 (35.6%)
Erythema nodosum		17 (23.3%)
Antibiotic use		37 (50.1%)
Glucocorticoid use		12 (16.4%)
History of GLM		5 (6.8%)

breast tumors and those with GLM are presented in Tables 2, 3, respectively. All patients were women with an average age of 32.90 ± 5.67 (range, 20–45) years. The average ages of patients with GLM and those with benign breast tumors were 33.38 ± 4.86 years and 32.32 ± 6.52 years, respectively, without a significant difference between the two groups ($P > 0.05$). None of the patients had immune system diseases, and they were not treated with immunosuppressants.

3.2. Comparisons of routine blood test results and the CRP level

Based on routine blood tests of the 73 patients with GLM, the average WBC count was 7.91 ± 2.31 × 10^9/L and 17 of the patients (23.3%) had a higher WBC count than the upper limit of normal value (9.5 × 10^9/L). The average NEU count was 5.64 ± 2.03 × 10^9/L; 22 patients (30.1%) had an NEU count higher than the upper limit of normal value (6.3 × 10^9/L). The average NEU% was 68.70 ± 13.23%; 41 patients (56.2%) had an NEU% higher than the upper limit of normal value (70%). The average CRP level was 4.45 ± 5.85 mg/L; 19 patients (24%) had a CRP level higher than the upper limit of normal value (5 mg/L).

Based on routine blood tests of the 60 patients with breast benign tumors, the average WBC count was 5.75 ±

TABLE 4 Comparison of routine blood test results and CRP levels between patients with GLM and benign breast tumors ($\bar{X} \pm s$).

Variable		WBC ($\times 10^9$/L)	NEU ($\times 10^9$/L)	NEU% (%)	CRP (mg/L)
Group	GLM ($n = 73$)	7.91 ± 2.31	5.64 ± 2.03	68.70 ± 13.23	4.45 ± 5.85
	Benign tumor ($n = 60$)	5.75 ± 1.42	3.69 ± 1.38	62.76 ± 9.91	0.49 ± 0.50
***P*-value**		0.001	0.009	0.966	<0.001

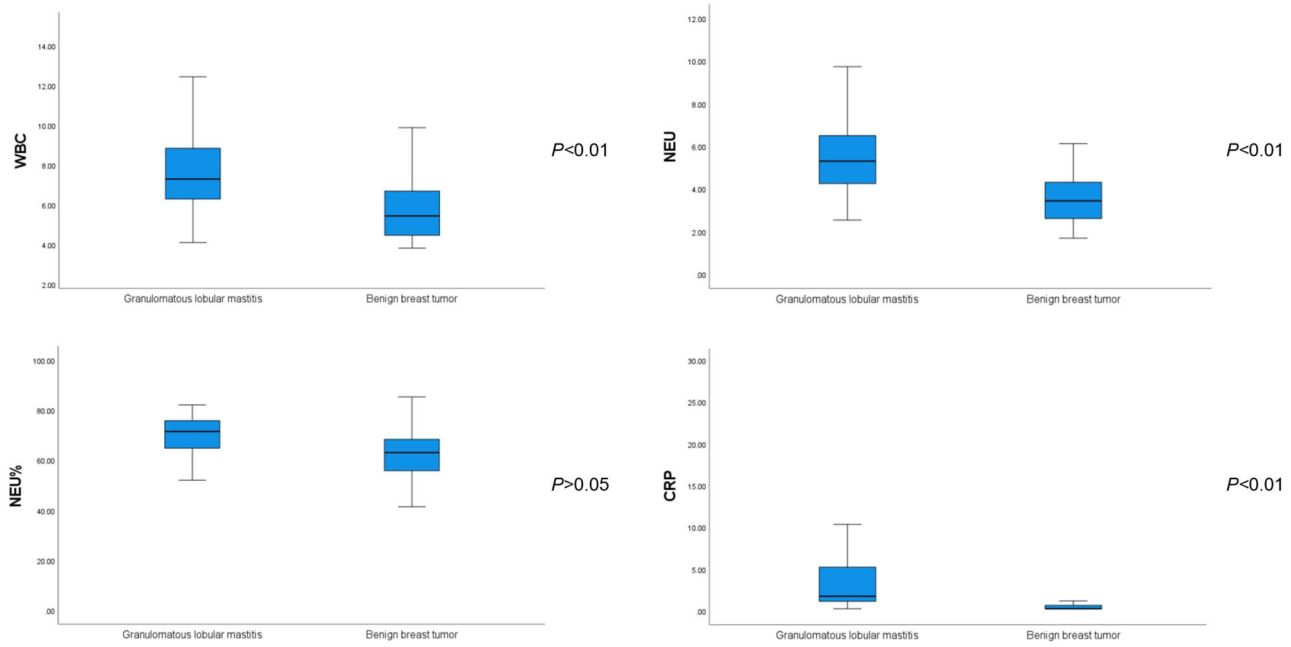

FIGURE 1
Comparison of white blood cell, neutrophil, neutrophilic granulocyte percentage, and C-reactive protein values between patients with GLM and those with benign breast tumors.

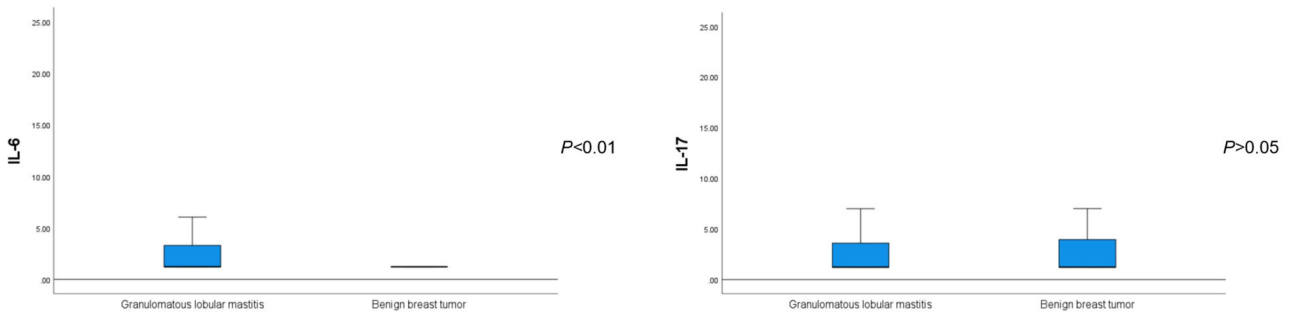

FIGURE 2
Comparison of serum IL-6 and IL-17 levels between patients with GLM and those with benign breast tumors.

TABLE 5 Comparison of serum cytokine levels between patients with GLM and those with benign breast tumors ($\bar{X} \pm s$).

Variable		IL-6 (pg/ml)	IL-1β (pg/ml)	IL-17 (pg/ml)	IFN-γ (pg/ml)	TNF-α (pg/ml)
Group	GLM ($n = 73$)	2.99 ± 3.35	3.30 ± 4.53	6.91 ± 9.57	2.89 ± 2.10	1.69 ± 1.74
	Benign tumor ($n = 60$)	1.25 ± 0.20	2.66 ± 2.17	5.46 ± 5.78	2.26 ± 1.71	1.36 ± 0.65
***P*-value**		<0.001	0.097	0.108	0.053	0.009

1.42 × 10^9/L. One of the patients (1.7%) had a WBC count higher than the upper limit of normal value. The average NEU count was 3.69 ± 1.38 × 10^9/L; 3 patients (5%) had an NEU count higher than the upper limit of normal value. The average NEU% was 62.76 ± 9.91%; 12 patients (20.0%) had an NEU% higher than the upper limit of normal value. The average CRP level was 0.49 ± 0.50 mg/L; no patients had a CRP level higher than the upper limit of normal value.

The WBC, NEU, and CRP values were significantly higher in patients with GLM than in those with benign breast tumors ($P < 0.01$). However, there was no significant difference in the NEU% between the groups ($P > 0.05$), as shown in Table 4 and Figure 1.

3.3. Comparisons of serum cytokine levels

The average serum IL-6 concentration in patients with GLM was 2.99 ± 3.34 pg/ml, which was significantly higher than that in patients with benign breast tumors ($P < 0.01$). Regarding other inflammatory and tumor-associated cytokines, there was no significant difference in the serum IL-17 concentration between patients with GLM and those with benign breast tumors ($P > 0.05$) (Figure 2). IL-β1 and IFN-γ concentrations were not significantly different between the two groups ($P < 0.1$), whereas serum TNF-α concentrations in patients with GLM were significantly higher than those in patients with benign breast tumors ($P < 0.01$), as shown in Table 5.

3.4. Correlation analysis of IL-6 levels and inflammatory indicators

In patients with GLM, the Pearson correlation analysis showed that IL-6 levels were positively correlated with NEU, NEU%, CRP, IL-17, and TNF-γ values ($P < 0.01$) but weakly positively correlated with WBC and IFN-γ values ($P < 0.1$). In patients with benign breast tumors, the IL-6 level was not significantly correlated with the aforementioned indicators in routine blood tests ($P > 0.05$), but it was positively correlated with IL-17, TNF-α, and IFN-γ levels ($P < 0.01$), as shown in Tables 6, 7, respectively.

3.5. Logistic regression analysis of factors associated with IL-6 levels in patients with GLM

Binary logistic regression analysis revealed that the time since the appearance of masses [odds ratio (OR) = 0.293, $P < 0.05$), mass size (OR = 3.602, $P < 0.05$), and glucocorticoid use (OR = 5.690, $P < 0.05$) were individual predictors of IL-6 levels in patients with GLM (Table 8). The correlation between the time since the appearance of masses and mass size with IL-6 levels is shown in Figure 3.

TABLE 6 Correlation analysis between IL-6 levels and inflammatory indicators in patients with GLM.

Variable	WBC		NEU		NEU%		CRP		IL-1β		IL-17		IFN-γ		TNF-α	
IL-6	*r*-value	*P*-value	*r*-value	*P*-value	*r*-value	*P*-value	*r*-value	*P*-value	*r*-value	*P*-value	*r*-value	*P*-value	*r*-value	*P*-value	*r*-value	*P*-value
	0.212	0.071	0.305	0.009	0.302	0.009	0.506	<0.001	0.147	0.215	0.300	0.010	0.204	0.084	0.325	0.005

10.3389/fmed.2023.1273406

TABLE 7 Correlation analysis between IL-6 and inflammatory indicators in patients with benign breast tumor.

Variable	WBC		NEU		NEU%		CRP		IL-1β		IL-17		IFN-γ		TNF-α	
IL-6	*r*-value	*P*-value	*r*-value	*P*-value	*r*-value	*P*-value	*r*-value	*P*-value	*r*-value	*P*-value	*r*-value	*P*-value	*r*-value	*P*-value	*r*-value	*P*-value
	0.011	0.935	0.004	0.974	0.011	0.933	−0.062	0.636	−0.096	0.464	0.377	0.003	0.372	0.003	0.673	<0.001

4. Discussion

4.1. GLM is a rare, chronic, non-specific inflammatory disease

GLM mainly involves the mammary lobules and is characterized by non-caseating granulomas centered on the mammary lobules (10). It is an independent and peculiar disease of the breast that, although benign, is insensitive to routine anti-inflammatory therapy and may relapse even after repeated surgical treatments. Since a breast mass is the most common initial symptom, GLM is difficult to diagnose clinically in the early stage of the disease and is easily misdiagnosed as a benign or malignant breast tumor. If misdiagnosed as a tumor, it cannot be treated with appropriate methods at the right time, resulting in the spread and protracted course of the disease (11). Therefore, it poses a challenge in the breast surgery field.

In addition, the etiology and pathogenesis of GLM are unclear, although internal experts and those abroad have unanimously recognized the following as etiologies: (1) Deposit and blockage of the lactiferous duct by laticifer secretions: Breast duct obstruction and secretion accumulation can develop for various reasons, and then, the congested substances can stimulate the duct wall, causing the wall to produce inflammatory cells and promote fibroplasia, resulting in intense inflammatory reactions and (2) autoimmune reactions caused by the overflow of substances in the duct: Breast duct obstruction can cause duct dilation, which, to a certain extent, can lead to atrophy of the epithelium of the duct wall, and the accumulation of lipids and epithelial cell debris can corrode the duct wall, resulting in duct wall damage and thereby leading to autoimmune response (12).

Most scholars believe that GLM is an aseptic inflammatory disease, whereas others believe that it is related to infections caused by specific bacteria. However, the positivity rate in bacterial cultures of GLM samples is low; therefore, its pathogenesis is controversial (13). Clinical studies have shown that inflammatory indicators, such as the WBC count, CRP level, and erythrocyte sedimentation rate; autoimmune indicators, such as lymphocytes, immunoglobulin, and antinuclear antibody profiles; and endocrine indicators, such as prolactin, which are related to the disease, are less significant in making a definite diagnosis (14). Similarly, in this study, we observed that the proportion of patients with hyperprolactinemia was higher in the GLM group (32.9%) than in the benign breast tumor group (10.0%; $P < 0.01$). Interestingly, the body mass index was higher in patients with GLM than in those with benign breast tumors ($P < 0.05$), suggesting that obesity may be related to the pathogenesis of GLM.

In our previous study, we quantitatively analyzed the difference in protein expression in GLM lesion tissues and healthy breast tissues adjacent to the lesion using TMT quantitative proteomics technology and found that the expression of STAT3 protein in GLM lesion tissues was significantly higher than that in healthy breast tissues. In the present study, we further investigated the differences in the peripheral blood inflammatory indicator IL-6 and other cytokines in patients with GLM and those with benign breast tumors, which provided an innovative idea for exploring the pathogenesis, clinical diagnosis, and treatment of GLM.

TABLE 8 Logistic regression analysis of factors associated with IL-6 levels in patients with GLM.

	β-value	*P*-value	*OR*-value	95% CI
Time since the appearance of masses	−1.228	0.033	0.293	0.095∼0.906
Mass size (palpation)	1.282	0.024	3.602	1.179∼11.004
Antibiotics use	0.427	0.437	1.533	0.522∼4.505
Glucocorticoids use	1.739	0.017	5.690	1.163∼27.838

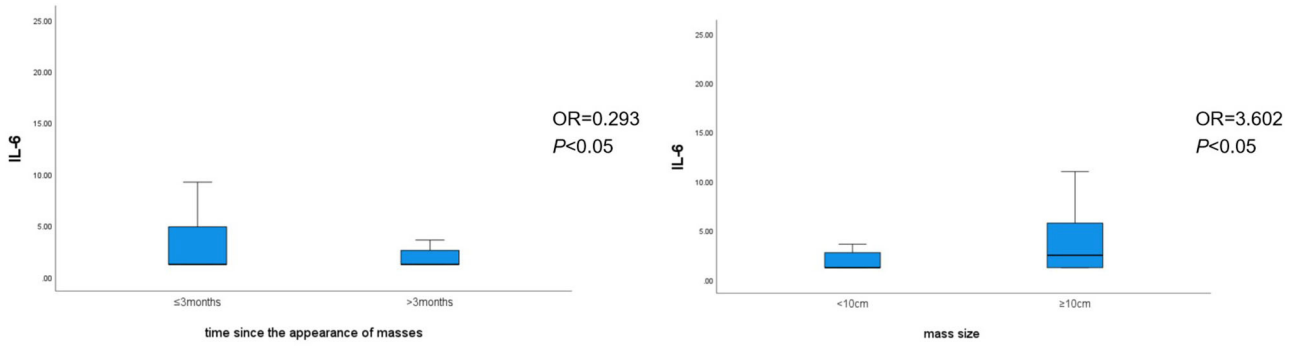

FIGURE 3
Correlation between the time since the appearance of masses and mass size with IL-6 levels.

4.2. Role of IL-6 in inflammatory reactions and the tumor microenvironment

IL-6 is an inflammatory cytokine that is closely related to inflammatory reactions and is a cancer-associated inflammatory factor. Pleiotropic cytokine TNF-α produced by macrophages, endothelial cells, and smooth muscle cells can stimulate smooth muscle cells to produce IL-6, together with IL-β1 and IFN-γ. IL-6 is a central regulator of inflammatory reactions that can stimulate the release of vasoactive substances and induce fibrinogen secretion and CRP production (15). The involvement of IL-6 in the pathophysiology of inflammatory diseases makes it an important target for the treatment of these diseases (16). In the tumor microenvironment, IL-6 can be produced by various cells, including tumor-associated macrophages, granulocytes, and tumor cells, which are its main sources. T-cells and myeloid-derived suppressor cells can also contribute to elevated IL-6 levels in tumors (17). IL-6 is released by tumor and stromal cells in an autocrine or paracrine manner and infiltrates the local area of solid tumors. The inhibition and activation of IL-6 may be involved in the development and progression of tumors by regulating the expression of inflammatory cytokines. They can promote tumor cell proliferation and inhibit apoptosis through transduction of the JAK signal and transcription of the STAT (18, 19), phosphoinositol 3-kinase, mitogen-activated protein kinase, and extracellular signal-regulated kinase 1/2 pathways, altering the tumor microenvironment and the immune response and thus affecting the growth, invasion, and metastasis of tumors (20). Recent studies have compiled evidence indicating that the IL-6 cytokine family (soluble factors) may be used for early and more precise breast cancer diagnosis and for designing targeted therapy to treat or even prevent metastasis development (21).

STAT3 signal transduction, mediated by IL-6, is an important signaling pathway that has recently been discovered. This pathway, stimulated and activated by cytokines, plays a crucial role in many important biological processes such as cell proliferation, differentiation, apoptosis, and immune response regulation (22). As an important intracellular signaling pathway, the IL-6/JAK2/ STAT3 pathway plays an important role in cell proliferation and differentiation by affecting the activation status of various downstream effector molecules. Excessive release of IL-6 under inflammatory stimulation is an effective activator of the JAK2/STAT3 signaling pathway, and IL-6 may promote the process of epithelial-mesenchymal transition by activating this pathway to exert its pro-inflammatory effect (23). In the tumor microenvironment, continuous stimulation with IL-6 can activate JAK2, resulting in STAT3 phosphorylation and thereby promoting tumor growth, drug resistance, and metastasis. Activation of the IL-6/JAK2/STAT3 signaling pathway is involved in the development and progression of tumors and contributes to the formation of the tumor inflammatory microenvironment (24).

Although some studies have shown that the IL-6/JAK2/STAT3 signaling pathway is related to non-puerperal mastitis, such reports are few. Our previous study showed that STAT3 protein expression was significantly higher in GLM lesion tissues than in healthy breast tissues. As the STAT3 protein is a key transcriptional regulatory factor in the IL-6 signaling pathway, whether this finding suggests that IL-6 is involved in the formation of GLM and benign breast tumors and whether there is a difference in the roles of IL-6 in these two diseases were the main objectives of the present study.

4.3. Difference and significance of peripheral blood IL-6 expression in patients with GLM and those with benign breast tumors

It is difficult to explain the poor effects of antibiotics and glucocorticoids in treating GLM. Few studies have examined the association between biomarkers and clinical outcomes. In this study, we observed that WBC, NEU, and CRP values were higher in patients with GLM than in those with benign breast tumors, but WBC, NEU, NEU%, and CRP values were not elevated in most patients with GLM, which explains the poor effect of antibiotics and glucocorticoids in the treatment of this disease.

It is of great importance to examine whether serum IL-6 expression differs between patients with GLM and those with benign breast tumors and to explore the correlation between IL-6 and traditional inflammatory indicators, such as WBC, NRU, and CRP values, as GLM is an inflammatory disease and IL-6 is a pleiotropic cytokine. This study's results showed that the serum IL-6 level was significantly higher in patients with GLM than in those with benign breast tumors. Concerning the other inflammatory and tumor-associated cytokines, the serum TNF-α level was significantly higher in patients with GLM than in those with benign breast tumors; IL-β1 and IFN-γ levels were slightly higher in patients with GLM than in those with benign breast tumors; and elevation of the IL-17 level did not show any significant difference between the two diseases. Additionally, binary logistic regression analysis revealed that serum IL-6 levels may be elevated early because of the presence of breast masses (within <3 months) and large masses (>1 cm).

In patients with GLM, further correlation analysis showed that the IL-6 level was positively correlated with NEU, NEU%, CRP, IL-17, and TNF-α values, but it was weakly positively correlated with WBC and IFN-γ values. In contrast, in patients with benign breast tumors, the IL-6 level was not significantly correlated with the aforementioned indicators in routine blood tests but was positively correlated with cytokines IL-17, IFN-γ, and TNF-α. The correlation between IL-6 and TNF-α was more significant in patients with benign breast tumors than in those with GLM patients, which is worth noting and requires further research.

5. Conclusions

Serum levels of IL-6, TNF-α, and other inflammatory and cancer-associated cytokines, as well as WBC, NEU, and CRP values, have a certain correlation with the development and progression of GLM; thus, they can reflect the disease to a certain extent. However, current treatments for GLM, such as surgery and antibiotic and glucocorticoid, immunosuppressant, and prolactin inhibitor therapies, are ineffective and lack validation.

Therefore, it is hoped that the exploration of cytokines such as IL-6 can provide effective markers for the treatment of GLM. With further research, over-activation of the STAT3 protein is receiving more attention, and increasing evidence suggests that the IL-6/STAT3 signaling pathway plays an important role in the inflammation, development, and progression of tumors. Specific interventions targeting the related proteins and enzymes in this pathway may provide new ideas for the treatment of inflammation and tumors. It is also hoped that this signaling pathway can serve as a reference for the investigation of the mechanism and design of drugs, thereby becoming one of the directions for the study of treatment for GLM.

Data availability statement

The datasets presented in this study can be found in online repositories. The names of the repository/repositories and accession number(s) can be found in the article/supplementary material.

Ethics statement

The studies involving humans were approved by the Longhua Hospital Affiliated to Shanghai University of Traditional Chinese Medicine. The studies were conducted in accordance with the local legislation and institutional requirements. The participants provided their written informed consent to participate in this study.

Author contributions

HC: Supervision, Writing—review and editing. MY: Funding acquisition, Writing—review and editing. YZ: Funding acquisition, Writing—original draft, Writing—review and editing. JW: Resources, Writing—review and editing, Supervision. LM: Data curation, Writing—review and editing. BW: Methodology, Writing—review and editing. TM: Methodology, Writing—review and editing.

Funding

This study was supported by Longhua Hospital Affiliated to Shanghai University of Traditional Chinese Medicine, Clinical Technology Training Plan (PY2022016). It was also supported by "Longhua Hospital-Minhang" Chinese medicine specialty (special disease) Alliance (2021-2023) Construction projects (LM05).

Conflict of interest

The authors declare that the research was conducted in the absence of any commercial or financial relationships that could be construed as a potential conflict of interest.

The reviewer JS declared a shared parent affiliation with the authors to the handling editor at the time of review.

Publisher's note

References

1. Zhang CJ, Hu JH, Zhao X. Hunan expert consensus on diagnosis and treatment of granulomatous lobular mastitis (2021 edition). *Chin J Gen Surg.* (2021) 30:1257–73. doi: 10.7659/j.issn.1005-6947.2021.11.001

2. Wang Q, Yu HJ. Precision diagnosis and treatment of granulomatous mastitis. *Chin J Breast Dis*. (2017) 11:129–31. doi: 10.3877/cma.j.issn.1674-0807.2017.03.001

3. Tan QT, Tay SP, Gudi MA, Nadkarni NV, Lim SH, Chuwa EWL. Granulomatous mastitis and factors associated with recurrence: an 11-year single-Centre study of 113 patients in Singapore. *World J Surg.* (2019) 43:1737–45. doi: 10.1007/s00268-019-05014-x

4. Li P, Liu X, Liu HL, Wang XC. The cancer-associated inflammatory cytokine IL-6 plays roles in tumor microenvironment. *Modern Oncol.* (2017) 25:3174–7. doi: 10.3969/j.issn.1672-4992.2017.19.038

5. Ene CV, Nicolae I, Geavlete B, Geavlete P, Ene CD. IL-6 signaling link between inflammatory tumor microenvironment and prostatic tumorigenesis. *Anal Cell Pathol.* (2022) 5:5980387. doi: 10.1155/2022/5980387

6. Liu Y, Zhang J, Zhou YH, Zhang HM, Wang K, Ren Y, et al. Activation of the IL-6/JAK2/STAT3 pathway induces plasma cell mastitis in mice. *Cytokine.* (2018) 110:150–8. doi: 10.1016/j.cyto.2018.05.002

7. Liu Y, Sun Y, Zhou Y, Tang X, Wang K, Ren Y, et al. Sinomenine hydrochloride inhibits the progression of plasma cell mastitis by regulating IL-6/JAK2/STAT3 pathway. *Int Immunopharmacol.* (2020) 81:106025. doi: 10.1016/j.intimp.2019.106025

8. Huang YM, Lo C, Cheng CF, Lu CH, Hsieh SC, Li KJ. Serum C-reactive protein and interleukin-6 levels as biomarkers for disease severity and clinical outcomes in patients with idiopathic granulomatous mastitis. *J Clin Med.* (2021) 10:2077. doi: 10.3390/jcm10102077

9. Li YF, Huo D, Luan SJ, Ma N, Gao X, Han D. The role of the IL-6/JAK2/STAT3 signaling pathway in tumors. *Chem Life.* (2021) 41:535–40. doi: 10.13488/j.smhx.20200650

10. Wan H, Lu DM. *Non-Puerperal Mastitis.* Shanghai: Shanghai Science and Technology Press (2022).

11. Wei LG, Han M. Diagnosis and treatment of non-puerperal mastitis: a systematic literature review. *The J Prac Med.* (2022) 38:1161–5. doi: 10.3969/j.issn.1006-5725.2022.09.022

12. Liu WL, Niu XH. *Surgical Glandology Chinese and Western Integrative Medicine*. Beijing: China Traditional Chinese Medicine Press (2021), 284.

13. Tu DL, Zhen LL, Li Z, Zhao RP, Liu MM, Li Z. Advances in etiology of non-lactation mastitis. Chin J Breast Dis. (2018) 12: 55–9. doi: 10.3877/cma.j.issn.1674-0807.2018.01.011

14. Goulabchand R, Hafidi A, Van de Perre P, Millet I, Maria ATJ, Morel J, et al. Mastitis in autoimmune diseases: review of the literature, diagnostic pathway, and pathophysiological key players. *J Clin Med*. (2020) 9: 958. doi: 10.3390/jcm9040958

15. Kumari N, Dwarakanath BS, Das A, Bhatt AN. Role of interleukin-6 in cancer progression and therapeutic resistance. *Tumour Biol.* (2016) 37:11553–72. doi: 10.1007/s13277-016-5098-7

16. Kaur S, Bansal Y, Kumar R, Bansal G. A panoramic review of IL-6: structure, pathophysiological roles and inhibitors. *Bio Org Med Chem.* (2020) 28:115327. doi: 10.1016/j.bmc.2020.115327

17. Gyamfi J, Eom M, Koo J-S, Choi J. Multifaceted roles of interleukin-6 in adipocyte-breast cancer cell interaction. *Transl Oncol.* (2018) 11:275–85. doi: 10.1016/j.tranon.2017.12.009

18. Meraviglia-Crivelli D, Villanueva H, Zheleva A, Villalba-Esparza M, Moreno B, Menon AP, et al. IL-6/STAT3 signaling in tumor cells restricts the expression of frameshift-derived neoantigens by SMG1 induction. *Mol Cancer*. (2022) 21:211. doi: 10.1186/s12943-022-01679-6

19. Kuo I-Y, Yang Y-E, Yang P-S, Tsai Y-J, Tzeng H-T, Cheng H-C, et al. Converged Rab37/IL-6 trafficking and STAT3/PD-1 transcription axes elicit an immunosuppressive lung tumor microenvironment. *Theranostics*. (2021) 11:7029–44. doi: 10.7150/thno.60040

20. Karakasheva TA, Lin EW, Tang Q, Qiao E, Waldron TJ, Soni M, et al. IL-6 mediates cross-talk between tumor cells and activated fibroblasts in the tumor microenvironment. *Cancer Res*. (2018) 78:4957–70. doi: 10.1158/0008-5472.CAN-17-2268

21. Felcher CM, Bogni ES, Kordon EC. IL-6 cytokine family: a putative target for breast cancer prevention and treatment. *Int J Mol Sci.* (2022) 23:1809. doi: 10.3390/ijms23031809

22. Akanda MR, Nam H-H, Tian W, Islam A, Choo B-K, Park B-Y. Regulation of JAK2/STAT3 and NF-κB signal transduction pathways; Veronica polita alleviates dextran sulfate sodium- induced murine colitis. *Biomed Pharmacother*. (2018) 100:296–303. doi: 10.1016/j.biopha.2018.01.168

23. Singh AK, Bhadauria AS, Kumar U, Raj V, Rai A, Kumar P, et al. Author correction: novel indole-fused benzo- oxazepines (IFBOs) inhibit invasion of hepatocellular carcinoma by targeting IL-6 mediated JAK2/STAT3 oncogenic signals. *Sci Rep*. (2020) 10:2391. doi: 10.1038/s41598-020-59134-9

24. Thomas SJ, Snowden JA, Zeidler MP, Danson SJ. The role of JAK/STAT signalling in the pathogenesis, prognosis and treatment of solid tumours. *Br J Cancer*. (2015) 113:365–71. doi: 10.1038/bjc.2015.233

frontiers | Frontiers in Oncology

TYPE Original Research
PUBLISHED 05 December 2023
DOI 10.3389/fonc.2023.1267626

OPEN ACCESS

EDITED BY
John Varlotto,
Marshall University Chief of Radiation Oncology, United States

REVIEWED BY
Eric Chi-ching Ko,
University of Massachusetts Medical School, United States
Steven N. Seyedin,
University of California, Irvine, United States

*CORRESPONDENCE
Johnny Kao
johnnykaomd@gmail.com

RECEIVED 01 August 2023
ACCEPTED 10 November 2023
PUBLISHED 05 December 2023

CITATION
Kao J, Sahagian M, Gupta V, Missios S and Sangal A (2023) Long-term disease-free survival following comprehensive involved site radiotherapy for oligometastases. *Front. Oncol.* 13:1267626. doi: 10.3389/fonc.2023.1267626

Long-term disease-free survival following comprehensive involved site radiotherapy for oligometastases

Johnny Kao[1,2,3]*, Michelle Sahagian[1,2], Vani Gupta[1,2], Symeon Missios[3,4] and Ashish Sangal[3]

[1]Department of Radiation Oncology, Good Samaritan University Hospital, West Islip, West Islip, NY, United States, [2]New York Institute of Technology College of Osteopathic Medicine, Old Westbury, NY, United States, [3]Cancer Institute, Good Samaritan University Hospital, West Islip, NY, United States, [4]Long Island Brain and Spine, West Islip, NY, United States

Introduction: Despite recent advances in drug development, durable complete remissions with systemic therapy alone for metastatic cancers remain infrequent. With the development of advanced radiation technologies capable of selectively sparing normal tissues, patients with oligometastases are often amenable to comprehensive involved site radiotherapy with curative intent. This study reports the long-term outcomes and patterns of failure for patients treated with total metastatic ablation often in combination with systemic therapy.

Materials and methods: Consecutive adult patients with oligometastases from solid tumor malignancy treated by a single high volume radiation oncologist between 2014 and 2021 were retrospectively analyzed. Oligometastases were defined as 5 or fewer metastatic lesions where all sites of active disease are amenable to local treatment. Comprehensive involved site radiotherapy consisted of stereotactic radiotherapy to a median dose of 27 Gy in 3 fractions and intensity modulated radiation therapy to a median dose of 50 Gy in 15 fractions. This study analyzed overall survival, progression-free survival, patterns of failure and toxicity.

Results: A total of 130 patients with 209 treated distant metastases were treated with a median follow-up of 36 months. The 4-year overall survival, progression-free survival, local control and distant control was 41%, 23%, 86% and 29%. Patterns of failure include 23% alive and free of disease (NED), 52% distant failure only, 9% NED but death from comorbid illness, 7% both local and distant failure, 4% NED but lost to follow-up, 4% referred to hospice before restaging, 1% local only failure, 1% alive with second primary cancer. Late grade 3+ toxicities occurred in 4% of patients, most commonly radionecrosis.

Conclusion: Involved site radiotherapy to all areas of known disease can safely achieve durable complete remissions in patients with oligometastases treated in the real world setting. Distant failures account for the majority of treatment failures and isolated local failures are exceedingly uncommon. Oligometastases represents a promising setting to investigate novel therapeutics targeting minimal residual disease.

KEYWORDS

oligometastases, radiation therapy, minimal residual disease, palliative care, stereotactic body radiation therapy

1 Introduction

There is great enthusiasm for advances in drug development targeting distant metastases from solid tumors in the mainstream media (1). Despite significant progress, metastatic cancer remains largely incurable and results in approximately 90% of cancer deaths (2, 3). Following treatment with either immunotherapy or molecularly targeted systemic therapies alone, responses are uncommon benefiting less than 13% of all cancer patients (4, 5). Published evidence dating to the late 2000's established the long-term curative potential of radiation therapy to all areas of known disease for patients with oligometastases (6–8). Two randomized trials demonstrated improved progression-free survival and overall survival when comprehensive local consolidative therapy is added to systemic therapy alone for patients with oligometastases from non-small cell lung cancer or mixed primary tumors (9, 10). By contrast, adding stereotactic radiation to some but not all distant metastases fails to improve outcomes compared to immunotherapy alone (11–13).

In the real world setting, patients with less than 5 distant metastases represent approximately 30% of patients requiring radiation therapy for metastatic disease (14). While much of the published evidence of radiation therapy for extracranial oligometastases focused narrowly on stereotactic body radiation therapy for well selected patients, real world patients include clinical presentations requiring alternative modes of radiation therapy including stereotactic radiosurgery for brain metastases or intensity modulated radiation therapy for a bulky primary tumor and regional nodes (9, 15, 16). We hypothesized that the development of advanced radiation technologies capable of sparing normal tissues at risk along with appropriate risk stratification would allow for the safe and effective application of comprehensive involved site radiation for a broader group of patients with oligometastases seen in the context of a busy community hospital practice (17).

2 Materials and methods

2.1 Patient selection

This study was approved by the Good Samaritan University Hospital IRB #16-016 with waiver of informed consent. The study population included consecutive patients ≥18 years of age with pathologically confirmed solid tumor malignancy with oligometastases referred to a single high volume radiation oncologist. Oligometastases were defined as 5 or fewer active metastatic lesions on whole body imaging where all sites of active disease, including the primary tumor and involved regional lymph nodes, were amenable to treatment. For patients with metachronous metastases, the primary tumor was controlled with prior local therapy. Whole body imaging included PET/CT, CT chest, abdomen and pelvis, bone scan or MRI of the brain or spine as per National Comprehensive Cancer Network guidelines for specific primary tumors.

Relevant baseline patient characteristics include ECOG performance status, primary tumor and histology, pre-treatment serum albumin, ESTRO/EORTC oligometastatic disease classification, age, gender, metastasis site, number of metastases treated, cumulative GTV volume, radiation dose and number of fractions for each treatment site, whether the primary tumor was also treated and systemic therapy (18). Diverse radiation dose schedules to primary tumor and metastases were converted to a biological equivalent dose (BED) using the formula BED = D x [1+d/(α/β)] where D is total dose delivered, d is dose per fraction and α/β=10 for malignant tumors. This information was extracted from retrospective EPIC and Aria chart review.

2.2 Treatment and follow-up

Patient immobilization was highly personalized based on location. All patients underwent CT simulation and contouring and external beam radiotherapy treatment planning was performed on Eclipse. When appropriate, MRI, PET or CT with contrast was imported and fused to assist with accurate target delineation. Depending on location, volume and organs at risk, intensity modulated radiation therapy, stereotactic body radiotherapy or stereotactic radiosurgery was prescribed with PTV expansions as appropriate. The GTV (or ITV for tumors with organ motion) received ≥100% of the prescribed dose and the PTV received a minimum of ≥95% of the prescribed dose. When conflicting, organ at risk dose limits were prioritized over PTV coverage. Image-guided radiation therapy was delivered on the Varian TrueBeam or Varian Edge equipped with a 6-degree of freedom robotic couch and cone beam CT. Brachytherapy planning was performed on Oncentra and delivered using Nucleotron high dose rate brachytherapy. A small subset of patients underwent surgery (most commonly craniotomy) or interventional radiology ablation in addition to radiotherapy.

Systemic therapy was administered at the discretion of the treating medical oncology and/or urologist. Prior to radiation, 68% were not actively receiving systemic therapy while 32% received systemic therapy with diverse treatment regimens (Supplementary Table 1). During or following radiation, 74% received systemic therapy and 26% received no systemic therapy. Systemic treatment regimens included 18% chemotherapy alone, 15% hormonal therapy with or without androgen receptor inhibitor or CDK4/6 inhibitor, 12% immunotherapy alone, 10% chemotherapy combined with biologically targeted therapy, 9% biologically targeted therapy alone, 9% chemoimmunotherapy and 2% hormonal therapy with chemotherapy or targeted therapy.

During radiotherapy, patients were assessed weekly. Following radiotherapy, patients were followed by radiation oncology and medical oncology using EPIC and supplemented by tumor imaging and blood work. In the community hospital setting, follow-up is quite robust with scheduled outpatient follow-up supplemented by a daily inpatient huddle jointly attended by both medical oncology and radiation oncology.

2.3 Outcomes

The primary endpoints were overall survival and progression-free survival using the Kaplan Meier method measured from date of consultation until death or most recent follow-up. Potential predictors of survival were assessed using the log-rank test using cutpoints validated in the published literature. Variables with a p value of <0.10 were entered into Cox multivariable regression analysis. Treatment failures were further classified to estimate local control and distant control on a per patient basis. Patient and treatment characteristics were reported with median and interquartile ranges (IQR) for continuous variables. Acute and late toxicities were scored using the Common Terminology Criteria for Adverse Events (CTCAE) version 5.0. Statistical analysis was performed using Stata version 13.1.

3 Results

3.1 Patient and treatment characteristics

Between 1/2014 and 12/2021, a total of 130 patients with 209 targeted distant metastases were treated by a single radiation oncologist. Patient and disease characteristics were summarized in Table 1. The most common primary tumors were lung (35%), prostate (12%) and breast (9%). The median follow-up among surviving patients was 35.2 months (IQR 19.5 to 64.1 months).

Radiation technique included stereotactic radiation for 69 patients to a median dose of 27 Gy (IQR 27 to 33 Gy) in a median of 3 fractions (IQR 3 to 4). Image-guided radiation therapy was administered to 84 patients to a median dose of 50 Gy (IQR 45 to 59.4 Gy) in a median of 15 fractions (IQR 10 to 28 fractions). Brachytherapy was delivered to 2 patients to a median dose of 24 Gy in a median of 4 fractions. Treatment of the primary tumor ± regional lymph nodes was administered to 47% of patients. The median cumulative GTV volume was 44.1 cc (IQR 14.1 to 117.1 cc). An example of the treatment technique and follow-up is shown in Figure 1.

3.2 Survival outcomes and patterns of recurrence

The median overall survival is 36.1 months with a 4-year overall survival of 41.1% (95% CI 30.6-50.5) (Figure 2A). The median progression-free survival was 12.5 months with a 4-year progression-free survival of 23.1% (95% CI, 15.3-31.9) (Figure 2B). The 4-year local control was 85.7% (95% CI, 73.9-92.5) and the 4-year distant control was 28.6% (95% CI, 19.3-38.5) (Figures 2C, D). On univariable and multivariable analysis, the only significant predictors of overall survival were age, performance status, favorable primary site (defined as breast, prostate and kidney) and pre-treatment serum albumin (Table 1, Supplementary Table 2). The only predictors of progression-free survival on univariable and multivariable analysis were albumin and melanoma (Supplementary Tables 2, 3).

Patterns of failure include 23% alive and free of disease (NED), 52% distant failure only, 9% NED but death from comorbid illness, 7% both local and distant failure, 4% NED but lost to follow-up, 4% referred to hospice before restaging, 1% local only failure, 1% alive with second primary cancer. Specific causes of comorbid death are listed in Supplementary Table 4. Among the 30 patients who remain alive and NED, 8 patients did not receive systemic therapy and the most common primary tumors were 9 patients with non-small cell lung cancer, 5 patients with prostate adenocarcinoma and 5 patients with breast adenocarcinoma.

3.3 Toxicity

Toxicities for all patients are summarized in Table 2. Grade 1 to 2 acute toxicities were recorded in 38% of patients. High grade acute toxicities included 1 patient with grade 3 skin toxicity and 1 patient with esophageal cancer and distant lymph node metastases who experienced grade 5 cardiac complications following esophagectomy with pathologic complete response (Table 2). Late grade 2 toxicities included 2 patients with radionecrosis, 1 patient with grade 2 vaginal stenosis, 1 patient with grade 2 pneumonitis, 1 patient with grade 2 erectile dysfunction and 1 patient with grade 2 urinary toxicity. Late grade ≥3 toxicities included 3 cases of grade 3 radionecrosis requiring surgery, 1 case of orthopedic screw fixation fracture and 1 case of grade 3 rectal bleeding (Table 2). The 4-year cumulative incidence of late grade ≥3 toxicity rate was 5% (95% CI, 2-12) (Figure 2E).

4 Discussion

The concept of curative intent radiation therapy to all areas of known metastatic disease was first proposed by Hellman and Weichselbaum in 1994 (19). By safely irradiating all areas of known disease, usually in combination with systemic therapies, a small but reproducible minority of previously incurable patients achieve long-term complete remissions (3, 10, 20). In this large single physician experience of comprehensively treating 130 patients with limited metastatic disease from 2014 to 2021, 30 patients are not only alive but without evidence of disease. While prior studies focused on the treatment of extracranial oligometastases treated with stereotactic body radiotherapy, this large real world experience included patients with oligometastases requiring treatment of the primary site, regional nodes and brain metastases (15).

In the authors' opinion, this study better represents the entire spectrum of oligometastases in the context of patients with distant metastases referred to radiation oncology. Despite using lower biologically equivalent doses than prior studies that focused exclusively on stereotactic body radiotherapy, involved site radiation achieved durable targeted metastasis control in 86% of

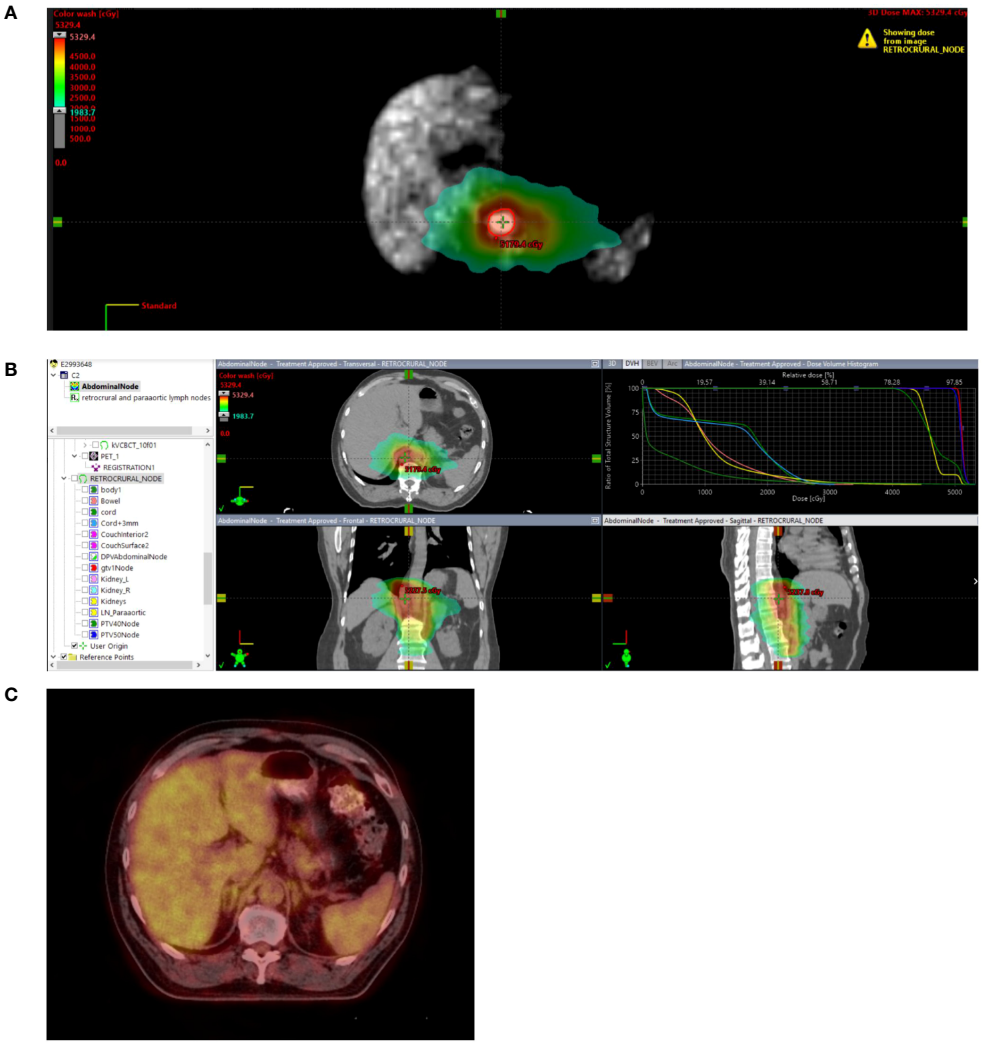

FIGURE 1
Stage IIIB rectal cancer initially treated with total neoadjuvant therapy followed by sphincter-sparing surgery with pathologic complete response followed by 2 additional cycles of adjuvant FOLFOX. While on surveillance, the patient presented with an elevated CEA of 18.3. PET/CT demonstrated a new 3.5 cm retrocrural node with a SUVmax of 3.5 without additional areas of FDG avid disease. Biopsy confirmed metastatic rectal adenocarcinoma. **(A)** Treated with involved site radiotherapy to 50 Gy in 10 fractions to the PET positive node while covering PET negative prominent paraaortic nodes to 40 Gy in 10 fractions. **(B)** Radiation plan demonstrating selective sparing of uninvolved bowel, liver, kidneys and spinal cord. **(C)** Restaging 6 month PET/CT negative. Remains on surveillance off therapy more than 3 years after treatment with a recent CEA 1.3, undetectable circulating tumor DNA and negative CT and MRI.

patients with oligometastases with an acceptable toxicity profile. Prior studies reported 63 to 87% local control at 3 to 5 year follow-up although comparisons across studies are unreliable due to heterogeneity (10, 21–24). The Duke University group reported ~90% tumor metastasis control at a median follow-up of 2 years for oligometastasis patients treated to 50 Gy in 10 fractions (16). Taken together, these data expand access to effective local oligometastasis treatment for the many clinical presentations not amenable to stereotactic body radiotherapy including those with bulky disease immediately adjacent to organs at risk. The median GTV treated in this series was 44.1 cc vs. 8.2 cc in a large multi-institutional oligometastasis database focused exclusively on stereotactic body radiotherapy (25).

While drug development continues to progress for many solid tumors, systemic therapy alone for distant metastases is generally not curative and may induce therapy-resistant genomic driver mutations (26, 27). In this series, the majority of treatment failures were the result of the development of new metastatic tumors despite advances in systemic therapy. Since isolated local failures are exceedingly rare, oligometastases may be an appropriate population to test novel therapeutics targeting either minimal residual disease or dormant micrometastases (3). Immune checkpoint inhibitors appear more effective against primary tumors and micrometastases compared to macrometastases (26). Durvulamab as consolidative treatment for stage III lung cancer following chemoradiation improves long-term overall survival and represents a potential model for this drug development strategy (28). Systematically combining comprehensive involved site radiotherapy with more effective systemic therapies represents a highly promising alternative to drug therapy alone for patients with

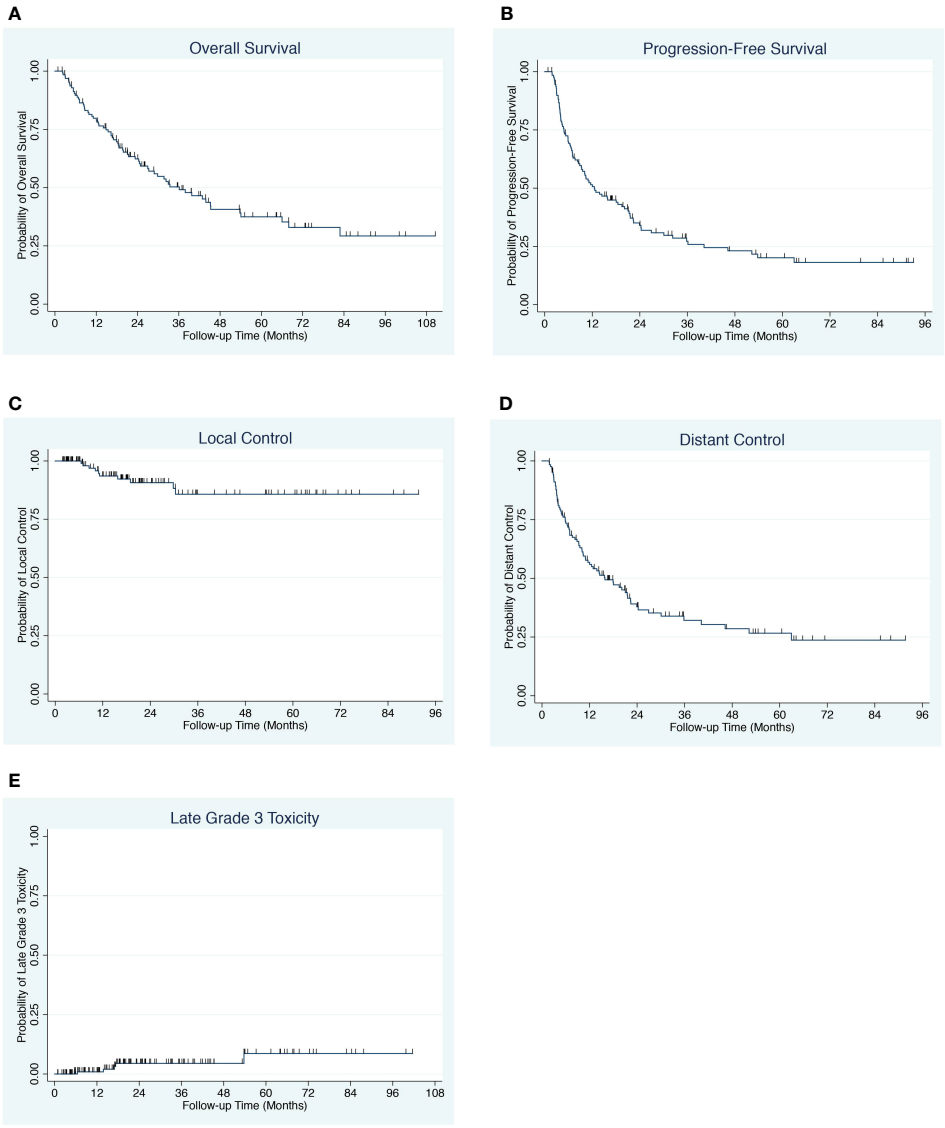

FIGURE 2
(A) Overall survival for patients with oligometastases. **(B)** Progression-free survival for patients with oligometastases. **(C)** Local control for patients with oligometastases. **(D)** Distant control for patients with oligometastases. **(E)** Late Grade ≥3 Toxicity for patients with oligometastases.

oligometastases. Systemic therapy alone remains the standard approach for patients with >5 distant metastases with radiotherapy reserved for palliation of symptoms since subtotal metastatic ablation does not appear to alter the natural history of polymetastases (11–13).

As a single institution retrospective series of oligometastases, the patient population is inherently heterogeneous and the sample size is relatively small. The small sample size undoubtedly contributed to the inability to disprove the null hypothesis with potential predictors of progression-free survival and overall survival with radiation dose intensity, cumulative GTV volume, adjuvant systemic therapy, synchronous vs. metachronous metastases and number of metastases (Table 1, Supplementary Table 2). For the majority of these variables, there was a large numerical difference in progression-free survival but this failed to reach statistical significance. Additionally, hepatobiliary primary tumors appears to be an unfavorable primary site but did not reach statistical significance on multivariable analysis. There was no systemic therapy alone control arm so it is possible that the long-term disease-free survival and overall survival would have been similar with systemic therapy alone. Generalizability and scalability are always valid critiques of any single physician experience. On the other hand, it is well established that including opinions from a diverse group improve decision making by avoiding groupthink and the perspective of the community practitioner in academic discourse should not be ignored (29).

Although single institution and particularly single physician series are not currently in vogue, this study design has counterintuitive strengths. In contrast to large academic centers, radiation oncologists in community practice are generalists that

TABLE 1 Characteristics of 130 patients with oligometastases.

Variable	Percent (number)	Median Overall Survival (months)	P value
Age, Median (range)	71 (28 to 96)		0.02
<70	45% (58)	66.0	
≥70	55% (72)	27.0	
Gender			0.26
Male	54% (70)	45.3	
Female	46% (60)	28.9	
ECOG performance status			0.003
0	23% (30)	Not reached	
1	48% (63)	28.9	
2	22% (28)	18.6	
3 or 4	7% (9)	12.8	
Category of oligometastatic disease			0.98
Synchronous oligometastases	40% (52)	42.8	
Metachronous oligorecurrence or oligoprogression	37% (48)	36.1	
Other (induced or repeat oligorecurrence oligoprogression oligopersistence)	23% (30)	31.7	
Primary tumor			
Lung	35% (45)	43.9	0.92
Prostate	12% (15)	67.9	0.03
Breast	9% (12)	82.9	0.56
Colorectal	8% (10)	42.8	0.88
Endometrial	8% (10)	31.7	0.56
Melanoma	5% (6)	24.6	0.08
Occult primary	5% (6)	7.1	0.07
Hepatobiliary and pancreatic	4% (5)	15.5	<0.01
Other *	16% (21)	33.4	0.41
Favorable primary tumor			0.02
Breast, prostate or kidney		67.9	
All others		28.9	
Metastasis location	209 tumors		
Bone	31% (40)	36.1	0.46
Brain	30% (39)	28.9	0.49
Lung	22% (28)	39.8	0.71
Distant Lymph Nodes	19% (25)	45.2	0.80
Liver	10% (13)	9.9	0.15
Adrenal	3% (4)	12.2	0.64
Albumin			<0.001
≥3.4	66% (86)	45.2	
<3.4	28% (33)	15.5	
Unknown	8% (11)	31.7	
Number of metastases treated			0.43
0	7% (9)	31.7	
1	56% (72)	36.1	
2 to 5	36% (47)	32.3	
Cumulative GTV in cm^3, median (range)	44.1 (0.1 to 562.6)		0.25
<27.7 cc	39% (51)	43.9	
≥27.7 cc	61% (79)	31.7	
Primary tumor BED			0.51
<75 Gy	25% (33)	31.7	
≥75 Gy	22% (28)	54.1	
Primary tumor not treated	53% (69)	33.4	
Average metastasis BED			0.73
<75 Gy	61% (79)	36.1	
75 to 99.9 Gy	22% (28)	28.9	
≥100 Gy	18% (23)	42.8	
Adjvuant systemic therapy			0.32
Yes	74% (96)	36.1	
No	26% (34)	43.9	

*Other primary sites include ovary 3%, gastroesophageal 3%, non-melanoma skin 3%, renal 2%, sarcoma 2%, cervix 2%, thyroid 1%.

result in practical advantages for treatment and follow-up for patients with oligometastases. High volume general radiation oncologists are facile at safely and effectively administering radiation therapy throughout the body so there is no fragmentation of care between anatomic sites (30). Since distance travelled is reduced for patients choosing care at the community setting, these suburban patients are more likely present to their local hospital rather than the urban academic medical center for acute hospitalization thus enhancing the completeness of follow-up in the context of distant metastases (31). In the specific case of specialized cancer specific hospitals, there may not be an associated emergency room and they generally will not share a common electronic medical record platform with the local primary care provider or other non-oncology specialists (32). While retrospective series are not typically associated with complete and deep record keeping, as a single physician series, these patients are extremely well known to the physician over a period of years (33). It seems likely that follow-up quality will be more complete than multi-institutional databases

TABLE 2 Toxicity Following Comprehensive Involved Site Radiotherapy for Oligometastases.

Toxicity	Acute Grade 1-2% (n)	Acute Grade ≥3 % (n)	Late Grade 1-2 % (n)	Late Grade ≥3% (n)
Gastrointestinal	13% (17)	0% (0)	2% (2)	1% (1)
Genitourinary	4% (5)	0% (0)	2% (3)	0% (0)
Neurologic	0% (0)	0% (0)	3% (4)	2% (3)
Pulmonary	2% (3)	0% (0)	2% (3)	0% (0)
Skin	16% (21)	1% (1)	1% (1)	0% (0)
Orthopedic	0% (0)	0% (0)	2% (2)	1% (1)
Fatigue	10% (13)	0% (0)	1% (1)	0% (0)
Cardiac	0% (0)	1% (1)	0% (0)	0% (0)

reflecting the experience of a large number of providers (34). Finally for this radiation oncologist with extensive experience with treatment distant metastases, selection of curative intent comprehensive metastatic ablation was informed not only by technical feasibility but also by prognosis using a validated model to supplement clinical intuition (17, 35).

In conclusion, involved site radiotherapy to all areas of known disease can safely achieve durable complete remissions in >20% of patients with oligometastases treated in the real world setting. Distant failures account for the majority of treatment failures and isolated local failures are exceedingly uncommon. Oligometastases represent a promising setting to investigate novel therapeutics targeting minimal residual disease.

Data availability statement

The raw data supporting the conclusions of this article will be made available by the authors, without undue reservation.

Ethics statement

The studies involving humans were approved by Good Samaritan University Hospital IRB #16-016. The studies were conducted in accordance with the local legislation and institutional requirements. Written informed consent for participation was not required from the participants or the participants' legal guardians/next of kin in accordance with the national legislation and institutional requirements.

Author contributions

JK: Writing – original draft, Writing – review & editing. MS: Writing – original draft, Writing – review & editing. VG: Writing – original draft, Writing – review & editing. SM: Writing – original draft, Writing – review & editing. AS: Writing – original draft, Writing – review & editing.

Funding

The author(s) declare that no financial support was received for the research, authorship, and/or publication of this article.

Acknowledgments

The authors acknowledge the invaluable contributions of Dr. Leonidas Salichos for biostatistical support, Ms. Lauren Alexander for data acquisition and Mr. Caleb Kao for data acquisition and data analysis.

Conflict of interest

JK served on Advisory Boards for Astra Zeneca and previously led an educational webinar for Varian; SM previously led an educational webinar for Varian.

The remaining authors declare that the research was conducted in the absence of any commercial or financial relationships that could be construed as a potential conflict of interest.

Publisher's note

Supplementary material

The Supplementary Material for this article can be found online at: https://www.frontiersin.org/articles/10.3389/fonc.2023.1267626/full#supplementary-material

References

1. Pickert K. Is a revolution in cancer treatment within reach? *New York Times* (2023) 6.

2. Lambert AW, Pattabiraman DR, Weinberg RA. Emerging biological principles of metastasis. *Cell* (2017) 168(4):670–91. doi: 10.1016/j.cell.2016.11.037

3. Gerstberger S, Jiang Q, Ganesh K. Metastasis. *Cell* (2023) 186(8):1564–79. doi: 10.1016/j.cell.2023.03.003

4. Haslam A, Gill J, Prasad V. Estimation of the percentage of US patients with cancer who are eligible for immune checkpoint inhibitor drugs. *JAMA Netw Open* (2020) 3(3):e200423. doi: 10.1001/jamanetworkopen.2020.0423

5. Prasad V. Perspective: The precision-oncology illusion. *Nature* (2016) 537(7619): S63. doi: 10.1038/537S63a

6. Kao J, Packer S, Vu HL, Schwartz ME, Sung MW, Stock RG, et al. Phase 1 study of concurrent sunitinib and image-guided radiotherapy followed by maintenance sunitinib for patients with oligometastases: acute toxicity and preliminary response. *Cancer* (2009) 115(15):3571–80. doi: 10.1002/cncr.24412

7. Milano MT, Katz AW, Muhs AG, Philip A, Buchholz DJ, Schell MC, et al. A prospective pilot study of curative-intent stereotactic body radiation therapy in patients with 5 or fewer oligometastatic lesions. *Cancer* (2008) 112(3):650–8. doi: 10.1002/cncr.23209

8. Salama JK, Hasselle MD, Chmura SJ, Malik R, Mehta N, Yenice KM, et al. Stereotactic body radiotherapy for multisite extracranial oligometastases: final report of a dose escalation trial in patients with 1 to 5 sites of metastatic disease. *Cancer* (2012) 118(11):2962–70. doi: 10.1002/cncr.26611

9. Gomez DR, Tang C, Zhang J, Blumenschein GR Jr., Hernandez M, Lee JJ, et al. Local consolidative therapy vs. Maintenance therapy or observation for patients with oligometastatic non-small-cell lung cancer: long-term results of a multi-institutional, phase II, randomized study. *J Clin Oncol* (2019) 37(18):1558–65. doi: 10.1200/JCO.19.00201

10. Palma DA, Olson R, Harrow S, Gaede S, Louie AV, Haasbeek C, et al. Stereotactic ablative radiotherapy for the comprehensive treatment of oligometastatic cancers: long-term results of the SABR-COMET phase II randomized trial. *J Clin Oncol* (2020) 38(25):2830–8. doi: 10.1200/JCO.20.00818

11. Kim S, Wuthrick E, Blakaj D, Eroglu Z, Verschraegen C, Thapa R, et al. Combined nivolumab and ipilimumab with or without stereotactic body radiation therapy for advanced Merkel cell carcinoma: a randomised, open label, phase 2 trial. *Lancet* (2022) 400(10357):1008–19. doi: 10.1016/S0140-6736(22)01659-2

12. McBride S, Sherman E, Tsai CJ, Baxi S, Aghalar J, Eng J, et al. Randomized phase II trial of nivolumab with stereotactic body radiotherapy versus nivolumab alone in metastatic head and neck squamous cell carcinoma. *J Clin Oncol* (2021) 39(1):30–7. doi: 10.1200/JCO.20.00290

13. Schoenfeld JD, Giobbie-Hurder A, Ranasinghe S, Kao KZ, Lako A, Tsuji J, et al. Durvalumab plus tremelimumab alone or in combination with low-dose or hypofractionated radiotherapy in metastatic non-small-cell lung cancer refractory to previous PD(L)-1 therapy: an open-label, multicentre, randomised, phase 2 trial. *Lancet Oncol* (2022) 23(2):279–91. doi: 10.1016/S1470-2045(21)00658-6

14. Kao J, Farrugia MK, Frontario S, Zucker A, Copel E, Loscalzo J, et al. Association of radiation dose intensity with overall survival in patients with distant metastases. *Cancer Med* (2021) 10(22):7934–42. doi: 10.1002/cam4.4304

15. Lehrer EJ, Singh R, Wang M, Chinchilli VM, Trifiletti DM, Ost P, et al. Safety and survival rates associated with ablative stereotactic radiotherapy for patients with oligometastatic cancer: A systematic review and meta-analysis. *JAMA Oncol* (2021) 7 (1):92–106. doi: 10.1001/jamaoncol.2020.6146

16. Shenker RF, Price JG, Jacobs CD, Palta M, Czito BG, Mowery YM, et al. Comparing outcomes of oligometastases treated with hypofractionated image-guided radiotherapy (HIGRT) with a simultaneous integrated boost (SIB) technique versus metastasis alone: A multi-institutional analysis. *Cancers (Basel)* (2022) 14(10):2403. doi: 10.3390/cancers14102403

17. Zucker A, Tsai CJ, Loscalzo J, Calves P, Kao J. The NEAT predictive model for survival in patients with advanced cancer. *Cancer Res Treat* (2018) 50(4):1433–43. doi: 10.4143/crt.2017.223

18. Guckenberger M, Lievens Y, Bouma AB, Collette L, Dekker A, deSouza NM, et al. Characterisation and classification of oligometastatic disease: a European Society for Radiotherapy and Oncology and European Organisation for Research and Treatment of Cancer consensus recommendation. *Lancet Oncol* (2020) 21(1):e18–28. doi: 10.1016/S1470-2045(19)30718-1

19. Hellman S, Weichselbaum RR. Oligometastases. *J Clin Oncol* (1995) 13(1):8–10. doi: 10.1200/JCO.1995.13.1.8

20. Kao J, Chen CT, Tong CC, Packer SH, Schwartz M, Chen SH, et al. Concurrent sunitinib and stereotactic body radiotherapy for patients with oligometastases: final report of a prospective clinical trial. *Target Oncol* (2014) 9(2):145–53. doi: 10.1007/s11523-013-0280-y

21. Baker S, Jiang W, Mou B, Lund CR, Liu M, Bergman AM, et al. Progression-free survival and local control after SABR for up to 5 oligometastases: an analysis from the population-based phase 2 SABR-5 trial. *Int J Radiat Oncol Biol Phys* (2022) 114(4):617–26. doi: 10.1016/j.ijrobp.2022.05.033

22. Chalkidou A, Macmillan T, Grzeda MT, Peacock J, Summers J, Eddy S, et al. Stereotactic ablative body radiotherapy in patients with oligometastatic cancers: a prospective, registry-based, single-arm, observational, evaluation study. *Lancet Oncol* (2021) 22(1):98–106. doi: 10.1016/S1470-2045(20)30537-4

23. Hong JC, Ayala-Peacock DN, Lee J, Blackstock AW, Okunieff P, Sung MW, et al. Classification for long-term survival in oligometastatic patients treated with ablative radiotherapy: A multi-institutional pooled analysis. *PloS One* (2018) 13(4):e0195149. doi: 10.1371/journal.pone.0195149

24. Sutera P, Clump DA, Kalash R, D'Ambrosio D, Mihai A, Wang H, et al. Initial results of a multicenter phase 2 trial of stereotactic ablative radiation therapy for oligometastatic cancer. *Int J Radiat Oncol Biol Phys* (2019) 103(1):116–22. doi: 10.1016/j.ijrobp.2018.08.027

25. Cao Y, Chen H, Sahgal A, Erler D, Badellino S, Biswas T, et al. Volumetric burden of metastatic lesions drives outcomes in patients with extracranial oligometastatic disease. *Cancer Med* (2021) 10(22):8091–9. doi: 10.1002/cam4.4332

26. Ganesh K, Massague J. Targeting metastatic cancer. *Nat Med* (2021) 27(1):34–44. doi: 10.1038/s41591-020-01195-4

27. Martinez-Jimenez F, Movasati A, Brunner SR, Nguyen L, Priestley P, Cuppen E, et al. Pan-cancer whole-genome comparison of primary and metastatic solid tumours. *Nature* (2023) 618(7964):333–41. doi: 10.1038/s41586-023-06054-z

28. Antonia SJ, Villegas A, Daniel D, Vicente D, Murakami S, Hui R, et al. Overall survival with durvalumab after chemoradiotherapy in stage III NSCLC. *N Engl J Med* (2018) 379(24):2342–50. doi: 10.1056/NEJMoa1809697

29. Boulware LE, Corbie G, Aguilar-Gaxiola S, Wilkins CH, Ruiz R, Vitale A, et al. Combating structural inequities - diversity, equity, and inclusion in clinical and translational research. *N Engl J Med* (2022) 386(3):201–3. doi: 10.1056/NEJMp2112233

30. Tsai CJ, Gomez DR, Yang TJ. Metastatic disease as a distinct discipline in radiation oncology. *JAMA Oncol* (2021) 7(1):21–2. doi: 10.1001/jamaoncol.2020.1824

31. Lamont EB, Hayreh D, Pickett KE, Dignam JJ, List MA, Stenson KM, et al. Is patient travel distance associated with survival on phase II clinical trials in oncology? *J Natl Cancer Inst* (2003) 95(18):1370–5. doi: 10.1093/jnci/djg035

32. Merkow RP, Yang AD, Pavey E, Song MW, Chung JW, Bentrem DJ, et al. Comparison of hospitals affiliated with PPS-exempt cancer centers, other hospitals affiliated with NCI-designated cancer centers, and other hospitals that provide cancer care. *JAMA Intern Med* (2019) 179(8):1043–51. doi: 10.1001/jamainternmed.2019.0914

33. Kao J, Zucker A, Urso M, Karwowski P, Jain N, Jain S, et al. Improving survival prognostication in patients with metastatic cancer through clinical judgment. *Anticancer Res* (2022) 42(3):1397–401. doi: 10.21873/anticanres.15609

34. Siddiqui S, Rowland L, Copel E, Sangal A, Soni V, Eckardt P, et al. Personalized palliative and survivorship care for patients with metastatic cancer treated with radiation therapy. *Anticancer Res* (2023) 43(4):1387–95. doi: 10.21873/anticanres.16287

35. Kao J, Gold KD, Zarrili G, Copel E, Silverman AJ, Ramsaran SS, et al. Clinical predictors of survival for patients with stage IV cancer referred to radiation oncology. *PloS One* (2015) 10(4):e0124329. doi: 10.1371/journal.pone.0124329

Frontiers in Medicine

Translating medical research and innovation into improved patient care

A multidisciplinary journal which advances our medical knowledge. It supports the translation of scientific advances into new therapies and diagnostic tools that will improve patient care.

Discover the latest Research Topics

See more →

Frontiers

Avenue du Tribunal-Fédéral 34
1005 Lausanne, Switzerland
frontiersin.org

Contact us

+41 (0)21 510 17 00
frontiersin.org/about/contact